NMR studies of the BamA complex proteins at high resolution

Inauguraldissertation

zur

Erlangung der Würde eines Doktors der Philosophie

vorgelegt der

Philosophisch-Naturwissenschaftlichen Fakultät

Der Universität Basel

von

Jean-Baptiste Hartmann

aus Frankreich

Basel, 2019

Genehmigt von der Philosophisch-Naturwissenschaftlichen Fakultät

auf Antrag von

Prof. Dr. S. Hiller, Prof. Dr. T. Maier.

Basel, 16.10.2018

Prof. Dr. M. Spiess, Dean of the Faculty

Abstract

The β-barrel assembly machinery (BAM) complex is essential for the biogenesis of outer membrane proteins (OMPs) in Gram-negative bacteria, with the membrane protein BamA acting as a catalyst for folding of OMPs in the outer membrane. Recently, structures of the BAM complex have been solved, displaying the molecular organization of the five proteins of the complex (BamABCDE). However, the mechanism by which BamA completes its insertase role is unclear. This PhD thesis focuses on the optimization of sample preparation and backbone assignment of the BamA β-barrel domain for solution NMR spectroscopy. Initial NMR spectra of the BamA β-barrel showed broad peaks with a low signal-to-noise ratio. This was likely due to a dynamic nature of the gate-region, as revealed by cysteine-scanning experiments. Therefore, as a first step to obtain a sample of BamA β-barrel suitable for NMR spectroscopy, buffer conditions were optimized. Then, in order to reduce the dynamics of the BamA β-barrel, a construct was designed with a C-terminal extension by nine residues. In addition to this extension, the G433A mutation in the gate-region was identified as to improve the quality of the NMR spectra. At that point, a combination of specific isotopic labeling and unlabeling in auxotrophic strains, triple-resonance experiments and 3D NOESY experiments allowed to obtain sequence-specific NMR resonance assignments of a large portion of the BamA β-barrel in LDAO micelles. The assignments revealed that some residues of the BamA β-barrel were found in different conformations that can be stabilized by the formation of a disulfide bond or by the C-terminal extension. Moreover, the crystal structure of the extended BamA β-barrel was determined, revealing a longer, and therefore more stable β-strand formed between the first and last strand of the barrel, explaining the stabilizing effect observed in its NMR spectrum. Additional work was performed on the soluble proteins of the BAM complex (BamBCDE). The expression and purification of BamB, BamC BamD and BamE was optimized and NMR spectra were recorded. BamD was found to be unstable once purified, and quickly precipitated, preventing to reach a molar concentration suitable for NMR spectroscopy. As a way to circumvent this issue, a hybrid construct of BamCD was prepared. The protein was able to reach high concentrations while keeping its stability. The fingerprint spectrum of BamCD was recorded and the peaks belonging to BamD overlapped with the peaks measured from a sample of individual BamD. This stabilized sample opens the possibility to obtain the sequence-specific assignments of BamD. Overall, this work resulted in the assignment of a large portion of the BamA β-barrel. As BamA is a potential target for new antibiotics, this assignment opens a way to perform NMR studies on BamA with substrates and ligands and understand the mechanical implications of their binding. Additionally, the dynamic nature of the BamA β-barrel

was demonstrated by observing multiple conformations with solution-state NMR spectroscopy. In combination with the available assignment, it will be possible to observe the effects of binding molecules, mutations, or of the molecular environment on the conformational ensemble of BamA.

Table of content

Chapter 1: Nuclear magnetic resonance applied to biological macromolecules

Introduction

In 1937, Isidor Isaac Rabi in Columbia University measured the magnetic moment of lithium chloride, lithium fluoride, and dilithium using an oscillatory radio-frequency field (Rabi et al., 1939). Using the same method, they discovered that the proton momentum was 2.785±0.02 nuclear magneton instead of the theory that predicted a value of 1. They also measured that the magnetic moment of the deuteron was 0.855±0.006 nuclear magneton (Kellogg et al., 1939). Those experiments founded the Nuclear Magnetic Resonance (NMR) field and Isidor Isaac Rabi was rewarded with the Nobel Prize in physics in 1944.

Nuclear magnetic resonance spectroscopy is a method to measure the magnetic properties of atomic nuclei. American physicist Edward Purcell at Harvard University and Swiss physicist Felix Bloch at Stanford University first reported about NMR of bulk materials in 1946 (Bloch, 1946, Purcell et al., 1946). For this groundwork, they were awarded with the Nobel Prize in physics in 1952.

In the beginning NMR, spectrometers used continuous-wave spectroscopy (CW). This method consists of keeping the frequency of the electromagnetic field constant and varying the strength of the magnetic field. CW spectroscopy sweeps through all individual frequencies in succession, at a slow rate, to avoid the distortion of the lines.

Swiss physicist Richard Ernst introduced a faster technique known as Fourier transformed NMR to process acquired data from free induction decay experiments (Ernst and Anderson, 1966). This innovation allowed to apply radiofrequency pulse sequences to a range of frequencies instead of a single line, drastically reducing the time required to achieve the same sensitivity with CW-NMR. Complex molecules with many resonances, were now in the range of the capabilities of NMR and the length of the pulses could be optimized to measure chemical reactions of various durations. For its achievements, Richard Ernst was awarded with the Nobel Prize in chemistry in 1991. Since then, NMR has expanded as a major method used to analyze chemical products, a way to probe physical properties of materials, image the human body (MRI), and a technique to unveil structures and mechanisms of biological molecules at atomic resolution, among many other disciplines were it proved to be a breakthrough discovery.

As of September 2018, the protein data bank (PDB, Berman et al., 2000) contains 12374 NMR structures out of 144682 entries, which accounts for 8.6% of the depositions. As an essential experiment to the field of protein NMR, heteronuclear single quantum coherence spectroscopy

(HSQC) started with the work from Geoffrey Bodenhausen and D.J Ruben in 1980 (Bodenhausen and Ruben, 1980) and allowed to record two-dimensional spectra of ^{1}H proton coupled with ^{15}N nitrogen or ^{13}C carbon. Unfortunately, the use of liquid-state NMR for the structure determination of proteins of higher molecular mass is limited because of increased transverse relaxation. The linewidth of the peaks is broader and the complexity of the spectrum is increased with a greater number of residues. The molecular-weights limitation of NMR were pushed forward as 3D-HSQC experiments (Ikura et al., 1990), perdeuteration techniques (Gardner and Kay, 1998), transverse optimized spectroscopy experiments (Pervushin et al., 1997), isotope incorporation (McIntosh and Dahlquist, 1990), methyl sidechain labeling (Kerfah et al., 2015) and labeling of specific amino acids (Ellman et al., 1992) were developed. On the side of the spectrometer, increases in the strength of the fields allowed for more sensitivity and the use of cryo-probe raised the signal to noise ratio of acquisitions. Even more challenging to study with NMR are membrane proteins which account for only 110 structures solved for α-helical proteins and 30 structures for β-barrel proteins, represented in the PDB. However, solution NMR can be used to study membrane proteins in native-like membrane mimetics such as nanodiscs

1.1 NMR Spectroscopy principles

Nuclei in a magnetic field can absorb electromagnetic radiation and re-emit it. The frequency at which the radiation is absorbed and emitted depends of the strength of the magnetic field and on the intrinsic magnetic properties of the nuclei. Isotopes with an odd mass number possess a half integer nuclear spin quantum number I. Nuclei with a spin quantum number greater than ½ have an electric quadrupole moment created from a distribution of nuclear charges that is not spherical. Therefore their magnetic state is much shorter lived than nuclei of I=½. Their resonance lines are broader. Liquid-state NMR focuses then on spin with I=½. Biomolecules spins of interest are mainly ^{1}H, ^{13}C, ^{15}N, ^{19}F and ^{31}P.

Spin I interacts with the magnetic field and gives rise to two energy levels which are characterized by the magnetic quantum number m. The correlation between spin angular momentum and magnetic quantum number is given by:

$$I_z = \hbar m \qquad (1)$$

Where $\hbar$ is Planck's constant divided by 2π and m is the magnetic quantum number, which has 2I+1 values:

$$m = I, I-1, I-2, \ldots, -I+1, -I \qquad (2)$$

Therefore a nucleus with spin half has a magnetic quantum number m=±½

In the absence of an external magnetic field, the quantum states for the 2I+1 values of m have the same energy.

The spin quantum number gives rise to nuclear spin angle momentum which further gives rise to a nuclear magnetic moment μ:

$$\mu_z = \gamma I_z = \gamma \hbar m \qquad (3)$$

Where γ is the gyromagnetic ratio of the nuclei (**Table 1.1**).

Nucleus	I	γ/2π (Hz · T^{-1})	Natural abundance %
^{1}H	½	42.6 ·10^{6}	99.9885
^{2}H	1	6.5 ·10^{6}	0.0115
^{13}C	½	10.7 ·10^{6}	1.07
^{14}N	½	3.1 ·10^{6}	99.632
^{15}N	½	-4.3 ·10^{6}	0.368
^{19}F	½	40.1 ·10^{6}	100
^{31}P	½	17.2 ·10^{6}	100

Table 1.1 Gyromagnetic ratios, nuclear spin quantum numbers and the relative natural abundance found on earth for isotopes of interest for biomolecular NMR.

For a spin half, in the absence of external magnetic field, there are two energy levels which are equally populated (degenerate). When placed under an external magnetic field, the degeneracy is lifted and the energies from the spin states of the nucleus are given by:

$$\mathrm{E} = -\vec{\mu} \cdot \vec{\mathrm{B}} \qquad (4)$$

Where $\vec{\mathrm{B}}$ is the magnetic field vector applied. When we apply a magnetic field B_0 to the spins, which is by convention directed toward the z-axis, we can write the following equation describing the energy of the system.

$$\mathrm{E} = -\gamma \mathrm{I}_z \mathrm{B}_0 = -\mathrm{m}\hbar\gamma \mathrm{B}_0 \qquad (5)$$

In the presence of this magnetic field, the nuclei can either align parallel or anti-parallel to B_0. The energy difference between those two levels can be defined as:

$$\Delta E = \hbar\gamma B_0 \qquad (6)$$

Transitions between those levels can be stimulated by applying electromagnetic radiations. The amount of energy necessary for this stimulation is proportional to the strength of the static magnetic field.

In the case of a single nucleus with a spin quantum number I=½ under a static magnetic field B_0, two nuclear spin states are possible. Their energy levels are separated by the Zeeman transition (**Figure 1.1**). We refer of the spin with m=½ as the α state and the one with m=-½ as the β state. Depending on the sign of the gyromagnetic ratio the energy difference sign is negative or positive.

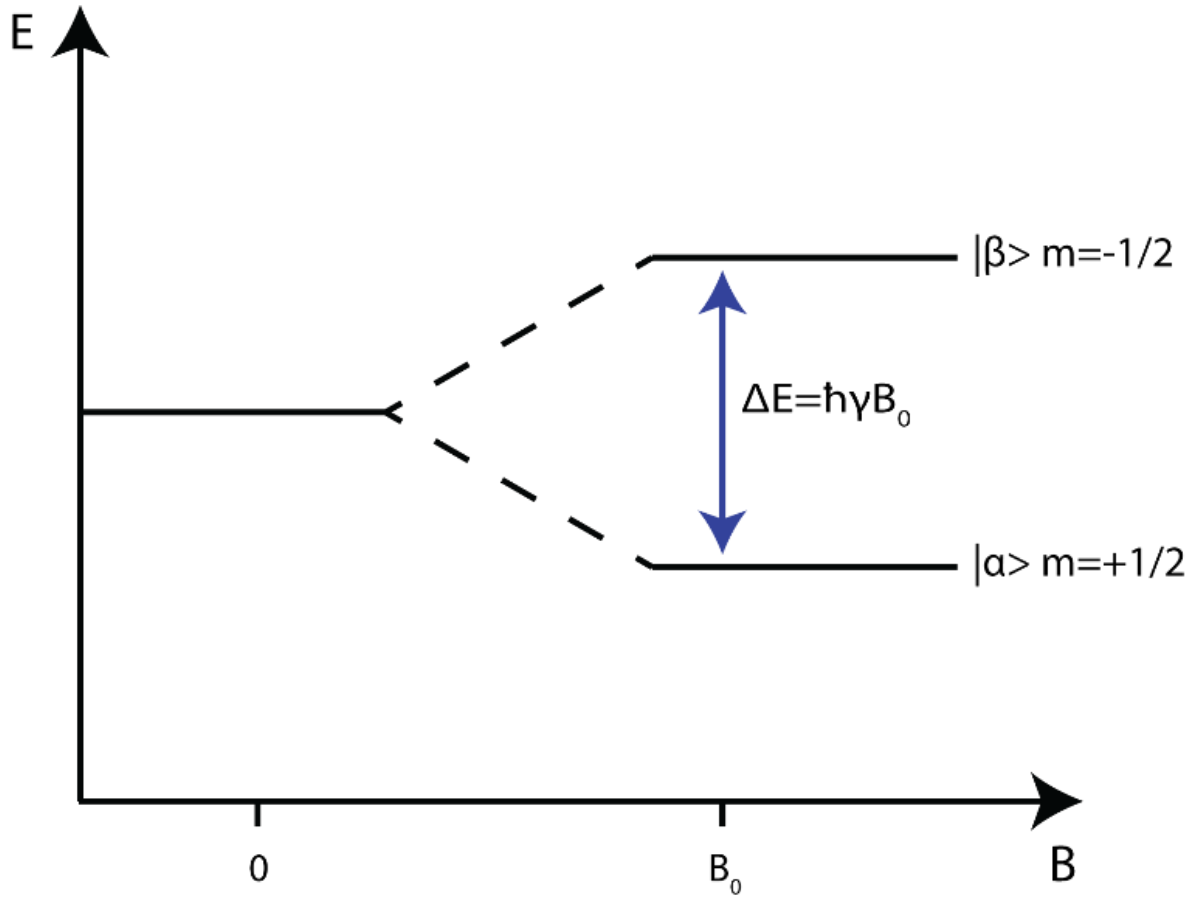

Figure 1.1 Diagram representing the Zeeman transition between the two energy levels α and β.

At thermal equilibrium, Boltzman equations allows to calculate the population of both α and β states using the equation:

$$\frac{n_\beta}{n_\alpha} = e^{(-\frac{\hbar\gamma B_0}{k_B T})} \qquad (7)$$

For a ^{1}H nucleus measured in a 900 MHz spectrometer at 310.15 K, this ratio is equal to 0.999807. This tiny difference in the state population yields observable signal by NMR.

1.2 Bloch equations

In a static magnetic field of B_0 amplitude, the Larmor frequency is the precessional frequency of the spin around the magnetic field:

$$\omega_0 = -\gamma B_0 \qquad (8)$$

The Larmor frequency depends on the strength of the magnetic field as well as on the gyromagnetic ratio of the spin. Spectrometers are commonly referenced by their proton Larmor frequency (i.e. a 900 MHz spectrometer).

Felix Bloch set up a formalism to describe the evolution of the magnetization over time with relaxation times T_1 (longitudinal relaxation time) and T_2 (transverse relaxation time), in the form of the Bloch equations (Bloch., 1946).

$$\frac{dM_x(t)}{dt} = \gamma\,(M(t) \times B(t))_x - \frac{M_x(t)}{T_2} \qquad (8)$$

$$\frac{dM_y(t)}{dt} = \gamma\,(M(t) \times B(t))_y - \frac{M_y(t)}{T_2}$$

$$\frac{dM_z(t)}{dt} = \gamma\,(M(t) \times B(t))_z - \frac{M_z(t) - M_0}{T_1}$$

Where $M_x(t)$, $My(t)$ and $M_z(t)$ are the x, y and z-components of the nuclear magnetization as a function of time and $B_x(t)$, $B_y(t)$, $B_z(t)$ the x, y and z-components of the magnetic field B.

In a case of precession without relaxation Bloch equations solutions are:

$$M'_x = M_x \cos(\omega t) + M_y \sin(\omega t) \qquad (9)$$

$$M'_y = M_y \cos(\omega t) - M_x \sin(\omega t)$$

However, in all systems, spin-lattice and spin-spin relaxation occur, and can be considered as first order process with T_1 and T_2 times respectively. After a magnetic perturbation and because of the relaxation processes the magnetization components on the z-axis, and in the transverse plane returns to equilibrium. The z-axis relaxation equation is given by:

$$M_z(t) = M_0 - [M_0 - M_z(0)] \exp(-R_1 t) \qquad (10)$$

$M_z(0)$ is the z-axis component magnetization at t=0. R_1 is the spin-lattice relaxation rate constant. M_0 is the equilibrium magnetization on the z-axis. The transverse components of magnetization relax following equations:

$$M_x(t) = M_x(0)\exp(-R_2 t) \qquad (11)$$

$$M_y(t) = M_y(0)\exp(-R_2 t)$$

R_2 is the spin-spin relaxation rate constant. $M_x(0)$ and $M_y(0)$ are the transverse components of magnetization at t=0.

1.3 1D-NMR experiment

At thermal equilibrium, the spins of a sample, or bulk magnetization M_0, are parallel to the static field. By applying an on-resonance pulse B_1 on the bulk magnetization (**Figure 1.2 A**), flipping of the vector of the bulk magnetization $\overrightarrow{M_0}$ occurs with a desired angle depending on the power and the duration of the pulse. A 90° pulse flips the bulk magnetization in the transverse plane (**Figure 1.2 B)**. After the 90° pulse is discontinued, the bulk magnetization starts to approach its thermal equilibrium in the form of free induction decay (FID), following Bloch equations (**Figure 1.2 C)**. The FID is acquired and Fourier-transformed (**Figure 1.2 D**).

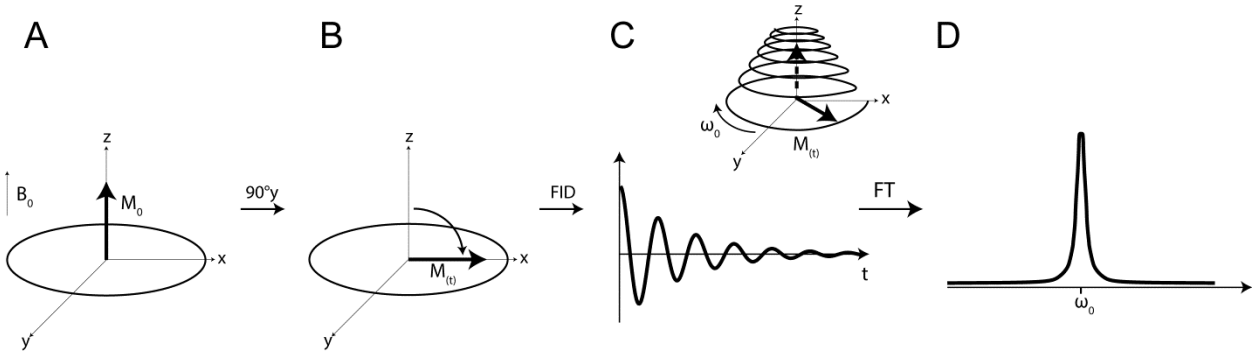

Figure 1.2 A) After the 90° pulse along the y-axis, bulk magnetization is flipped to the transverse plane **(B)**. **C)** Over time, magnetization returns to thermal equilibrium and detected as FID as a function of time and Fourier-transformed as a function of frequency **(D)**.

1.4 Chemical shifts

The electrons surrounding the nucleus generate a magnetic field of their own, which affect the local magnetic experienced by the nucleus known as nuclear shielding. The magnetic field experienced by a nucleus is thus depending on both primary and secondary magnetic fields. Therefore, the frequency of the pulse required to achieve resonance of the nuclei depends on its electronic environment. In biomolecular NMR, the amino acids of a protein will experience different electronic environments depending on surrounding amino acids and other atoms. We can differentiate the residues of a protein according to the local variations in their electronic environment by measuring their chemical shifts.

The shielding of a nucleus can be described as:

$$\omega = -\gamma(1-\sigma)B_0 \qquad (12)$$

Where σ is the average shielding constant for the nucleus. Resonance frequencies are dependent on the strength of the magnetic field B_0. In order to simplify data comparison measured with different spectrometers, the chemical shifts are expressed in parts per million (ppm/ δ) relatively to the resonance signal of a reference chemical.

$$\delta = \frac{\Omega - \Omega_{\mathrm{ref}}}{\omega_0} \cdot 10^6 = (\sigma_{\mathrm{ref}} - \sigma) \cdot 10^6 \qquad (13)$$

Where Ω and Ω_{ref} are the offset frequencies of the measured signal and of the reference.

When a protein is in a random-coil conformation, its amino acids present little difference in their chemical shifts. Those values are specific for each amino-acid type and represent an average of the chemical shifts for the conformations sampled by the residues in an unstructured state. The characteristics chemical shifts values of residues in the random-coil conformation have been measured as references. Comparing the chemical shifts of a protein, to those references, allow to determine the secondary chemical shift of a residue. For example, in α-helices, C_α atoms will tend to present positive secondary shifts while they will tend to have negative secondary chemical shifts in β-strands.

In biomolecular NMR, the secondary chemical shift of a residue is the difference between its measured and its expected chemical shift.

$$\Delta\delta = \delta_{\mathrm{measured}} - \delta_{\mathrm{random\ coil}} \qquad (14)$$

Variations in the protein structure can be monitored by the change in chemical shifts due to the change in local environment known as chemical shift perturbations (CSPs). Events such as binding another protein or ligand, will affect the chemical shift environment of the residues involved in the interaction. In a two-dimensional proton-nitrogen correlation spectrum, each residue is represented by a peak. Upon binding of a partner, the coordinates of the peak will shift in the proton ($\Delta\delta(^1\mathrm{H})$) and nitrogen ($\Delta\delta(^2\mathrm{H})$) dimension.

The chemical shift perturbation in this frame is calculated as:

$$\mathrm{CSP} = \sqrt{(\Delta\delta(\,^{1}\mathrm{H}))^2 + (\frac{1}{5}(\Delta\delta(^{15}\mathrm{N}))^2} \qquad (15)$$

CSP is a tool to study surface protein-protein or protein-ligand interactions (Goldflam et al., 2012; Thompson et al., 2015; Vinogradova and Qin, 2012), the unfolding of proteins (Mielke and Krishnan, 2009) and other experiments where residues are experiencing a transition in their electronic environments.

1.5 Scalar couplings

Covalent bonds are chemical bonds that involve two atoms sharing electrons pairs. In NMR spectroscopy these covalent bonds give rise to the splitting of the resonance signals of the nucleus into multiplets (**Figure 1.3**) (Ramsey and Purcell, 1952). This effect is called the scalar coupling (Gutowsky et al., 1951). The two spins involved are usually denoted as I and S, and the constants which define the strength of the coupling is termed $^{n}J_{IS}$ (Hz) where n is the number of covalents bonds separating the two nuclei. In biomolecular NMR, a typical example would be to study two spins of spin ½ separated by one bond. In such a system, resonance frequencies ω_I and ω_S :

$$\omega_I = -\gamma_I B_0(1-\sigma_I),\ \omega_s = -\gamma_s B_0(1-\sigma_S) \qquad (16)$$

Each spin having one magnetic quantum number m_I and m_S, the two-spin system has four energy levels, formed by all the possible combinations between m_I and m_S (**Table 1.2**).

Spin state	Total magnetic quantum number
αα	1
αβ	0
βα	0
ββ	-1

Table 1.2 Possible energy states in a two-spin system, transitions between those states must only change by one unit.

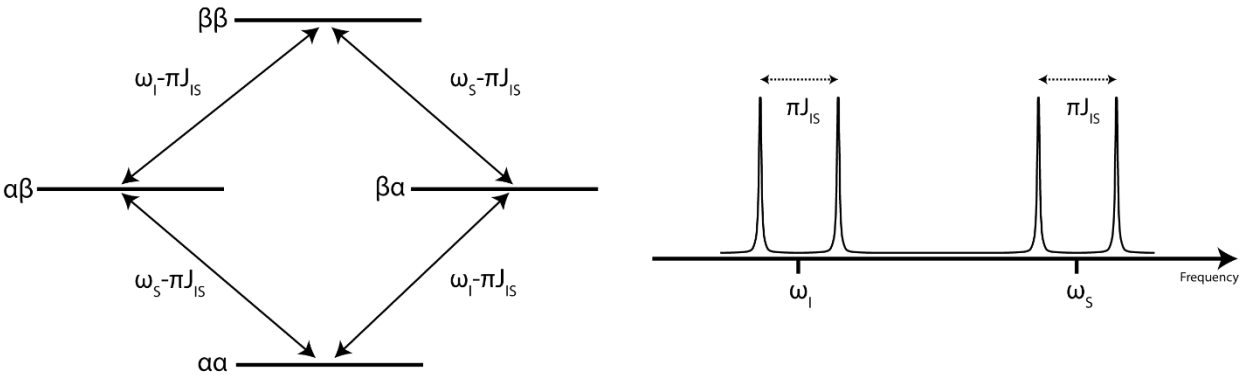

Figure 1.3 Transition diagram between energy levels in a in a two spin system (left). Possible transitions between the four states (αα, αβ, βα, ββ) are represented by arrows. In the Fourrier transformed NMR spectrum (right), the peaks are coupled by the scalar constant J_{IS}. The multiplets are centered on the Larmor frequency of the respective spins. Image adapted from (Cavanagh et al., 2007).

1.6 Chemical exchange

As shown before, nuclei can experience modifications of their electronic environment in a dynamic protein or when another molecule binds. In such a system, the protein population has a distribution of members which have different conformations. The chemical rate constant k, represents the rate of exchange between those conformations. In a simple case, where a nucleus samples two conformations A and B, the ratio between the chemical rate constant k and the resonance frequency difference between those two conformations Δν will determine the exchange regime (**Figure 1.4**). If $k << \Delta\nu$ then the exchange is in "slow regime" in the NMR timeframe. We can observe the two individual conformations as two separate peaks. As the chemical rate constant increases, the nucleus exchanges conformations faster. This means that the two frequencies modulate each other and lose coherence. The peaks broaden and start to merge. In intermediate exchange, $k \approx \Delta\nu$, the peaks are coalesced and their broadening can prevent them to be detectable in the spectrum. In the fast exchange, $k >> \Delta\nu$, one peak is measured, whose chemical shift is the mean of the two conformations.

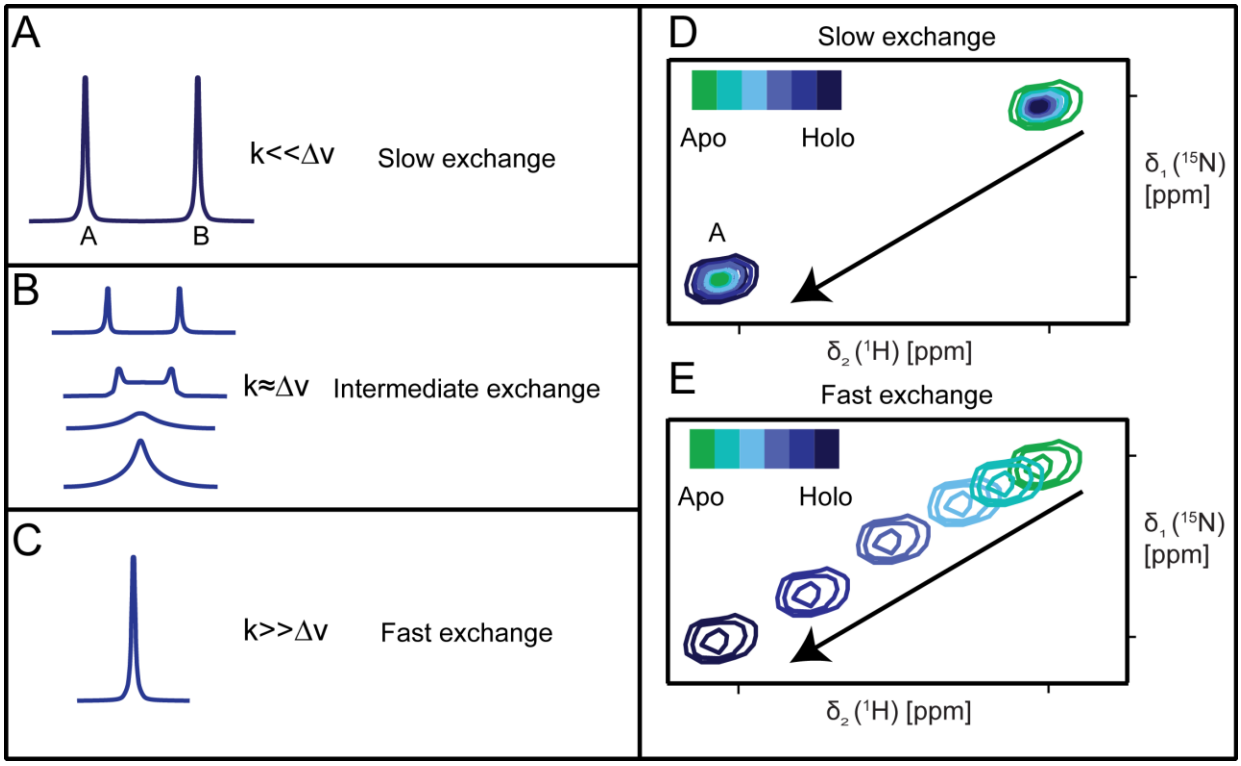

Figure 1.4. **A, B, C)** 1D-NMR peaks of a proton exchanging between two conformations A and B in slow, intermediate and fast exchange regimes. **D, E)** [^{15}N,^{1}H]-HSQC chemical shift of a residue exchanging between two conformations A and B in slow and fast exchange regime upon binding of a partner.

1.7 Relaxation

The relaxation phenomenon is the process that cause the return to equilibrium of a population of spin after a radiofrequency pulse has been applied. At equilibrium, spin populations are described by the Boltzmann distribution. In a two-state system, the equilibrium magnetization is proportional to the difference between the spins populating each of the energy state α and β.

$$M_z \propto (n_\alpha - n_\beta) \qquad (17)$$

Transitions between energy states displace population from α to β and reciprocally, until the states are populated according to the Boltzman distribution. Assuming the process is of first order with a rate constant of W. The rate of change in the population α:

$$\frac{dn_\alpha}{dt} = -Wn_\alpha + Wn_\beta, \frac{dn_\beta}{dt} = -Wn_\beta + Wn_\alpha \qquad (18)$$

We previously saw that when the bulk magnetization is flipped in the transverse plane by a 90° pulse, it relaxes over time and returns to zero. This relaxation process can be described as two component: the loss in xy-plane magnetization is called transverse relaxation (or spin-spin relaxation) and the z-magnetization component of the relaxation is called longitudinal (spin-lattice) relaxation. Transitions between energy states displace population from α to β and reciprocally.

$$\frac{dM_z}{dt} = \frac{d(n_\alpha - n_\beta)}{dt} = -2W(M_z - M_z^0) \quad (18)$$

$M_z^0 = (n_\alpha^0 - n_\alpha^0)$ is the equilibrium magnetization on the z-axis. W is termed the transition rate constant.

The relaxation time T_1 is related to the relaxation rate W:

$$T_1 = \frac{1}{R_1} = \frac{1}{2W} \quad (19)$$

Integrating the equation yields:

$$M_z(t) = [M_z(0) - M_z^0]e^{-\frac{t}{T_1}} + M_z^0 \quad (20)$$ **(Figure 1.5)**

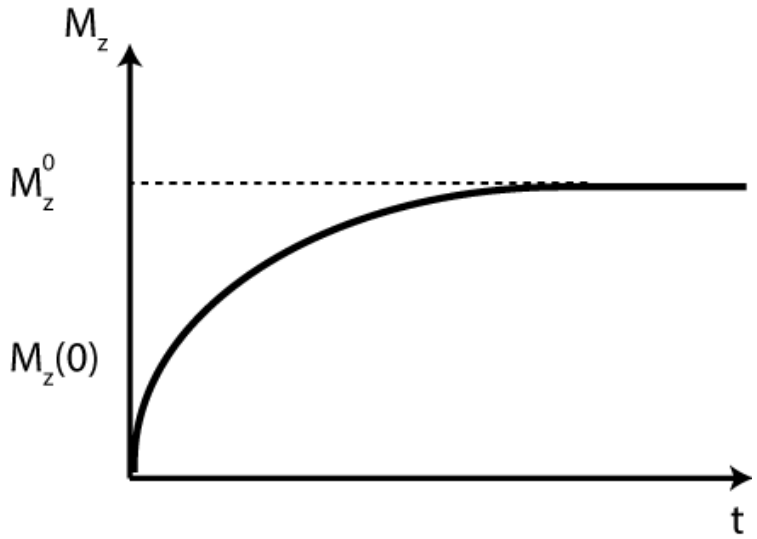

Figure 1.5. Evolution of the z-magnetization relaxation for α to β state transition in a spin ½ system following an exponential curve. M_z^0 is the z-component of the magnetization at equilibrium and $M_z\ (0)$ the magnetization at t=0. Figure adapted from (Keeler., 2002).

In solution, the spectral density function describes the probability to find motions at the defined angular frequency ω. The quantity of molecular motions found at a frequency depends on the size of the molecule, and therefore, on τ_c, which is the rotational correlation time of the molecule.

$$J(\omega) = \frac{2\tau_c}{1+(\omega\tau_c)^2} \quad (21)$$

Likewise, relaxations times T_1 and T_2 also depends on τ_c. (**Figure 1.6**).

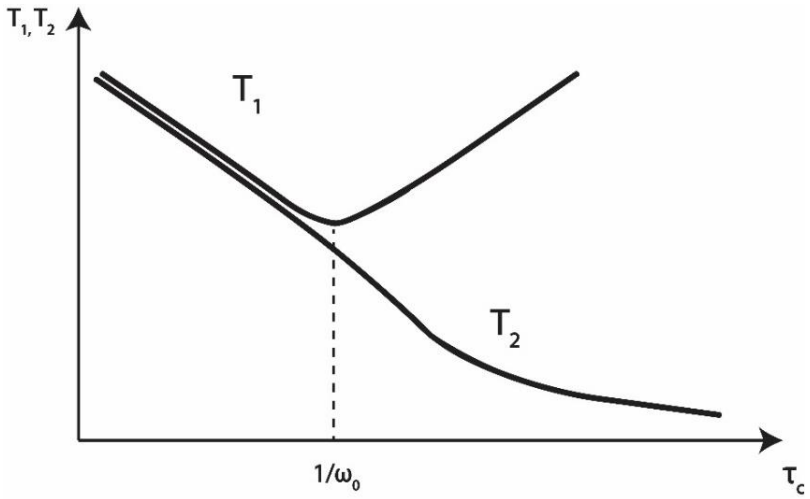

Figure 1.6 Effects of the T_1 and T_2 on τ_c. Larger molecules have higher rotational correlation times and their relaxation is dominated by the T_2 relaxation time constant. Image adapted from Reich, H.J., 2016.

As T_1 depends on τ_c and $T_1 = \frac{1}{2W}$, the spectral density function is proportional to the relaxation rate constant W.

$$J(\omega) \propto W \quad (22)$$

The transverse relaxation describes the decay of the transverse magnetization over time.

$$M_{xy}(t) = M_{xy}(0)e^{-\frac{t}{T_2}} \quad (23)$$

Where $M_{xy}(0)$ is the transverse equilibrium magnetization. T_2 is the transverse relaxation time constant and $R_2 = \frac{1}{T_2}$ the transverse relaxation rate constant.

The Bloembergen-Purcell-Pound theory describes the relaxation through dipole-dipole interactions (which is the dominant relaxation mechanism in liquids, and is therefore relevant for water and liquid-state NMR) (Bloembergen et al., 1948). In 1955, Solomon, build a model to explain T_1 and T_2 for two protons relaxing through dipole-dipole interactions.

$$\frac{1}{T_1} = \frac{6}{20} \cdot \frac{\hbar^2 \gamma^4}{r^6} \cdot \left[\frac{\tau_c}{1+\omega^2 \tau_c^2} + \frac{4\tau_c}{1+4\omega^2 \tau_c^2}) \right] \quad (24)$$

$$\frac{1}{T_2} = \frac{3}{20} \cdot \frac{\hbar^2 \gamma^4}{r^6} \cdot \left[3\tau_c + \frac{\tau_c}{1+\omega^2 \tau_c^2} + \frac{4\tau_c}{1+4\omega^2 \tau_c^2}) \right] \quad (25)$$

As we see, the relaxations time constants are proportional to the inverse of the power of six of the distance between the spins, and on the power of four of the gyromagnetic ratio of the spins.

For large molecules, R_2 is dominated by the first term of the equation (**Figure 1.7**). For those molecules, the relaxation time constant keep decreasing with the size. The linewidth of the peaks for a system are given by the full width at mid height (FWMH) which is represented by the following equation:

$$\Delta_\nu = \frac{1}{\pi T_2} \quad (26)$$

This means that for larger molecules, a loss in resolution is to be expected, as the peaks are getting broader with the increase in size. Additionally the broadening, diminishes the peak signal to noise ratio, as the integrals of the peaks stay the same.

1.8 Solomon equation

In NMR, the vector model of magnetization cannot describe systems of more than one spin. To describe more complex systems, the products operators are used. Operators represent measurable quantities, like the magnetization, the angular momentum and the energy. A spin in orbit around an axis of rotation have an angular momentum. The axis components of the spin angular momentum are represented by the operators I_x, I_y, I_z. During equilibrium, only the z-component of magnetization is present.

The Solomon equations describe the dipolar relaxation of a two spin system (Solomon, 1955).

Let the first spin be noted I and the second spin S. The rate constants are termed W_I and W_s for allowed I and S spins transitions (**Figure 1.7**). For forbidden transitions, zero quantum transition is denoted W_0 and double quantum transition W_2.

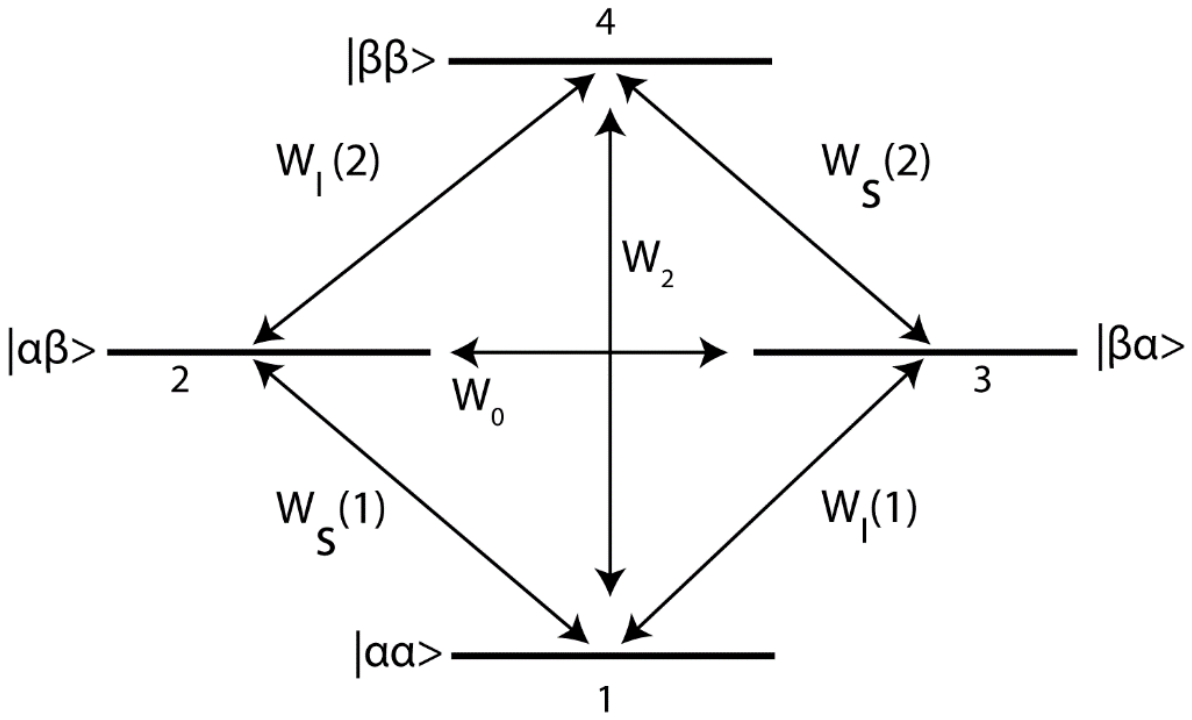

Figure 1.7 Scheme describing the transitions between different energy states of a two-spin system.

We can write the variations of spin population over time with the differential equation, summing the variations of the other populations of spins:

$$\frac{dn_1}{dt} = -W_S(1)n_1 - W_I(1)n_1 - W_2n_1 + W_S(1)n_2 + W_I(1)n_3 + W_2n_4 \quad (27)$$

$$\frac{dn_2}{dt} = -W_S(1)n_2 - W_I(2)n_2 - W_0n_2 + W_S(1)n_2 + W_I(2)n_4 + W_0n_3$$

$$\frac{dn_3}{dt} = -W_I(1)n_3 - W_S(2)n_3 - W_0n_3 + W_I(1)n_1 + W_S(2)n_4 + W_0n_2$$

$$\frac{dn_4}{dt} = -W_S(2)n_4 - W_I(2)n_4 - W_2n_4 + W_S(2)n_3 + W_I(2)n_2 + W_2n_1$$

The z-component of the magnetization of the I spin, can be calculated from the population difference involved in the two I spin transitions $W_I(1)$, (n_1-n_3) and $W_2(1)$, (n_2-n_4).

$$I_z = n_1 - n_3 + n_2 - n_4 \quad (28)$$

The same is done for the S spin:

$$S_z = n_1 - n_2 + n_3 - n_4 \quad (29)$$

The operator $2I_ZS_Z$ represents the population difference between the two I spin transitions.

$$2I_zS_z = n_1 - n_3 - n_2 + n_4 \quad (30)$$

The Solomon equation gives us the evolution of those operators over time:

$$\frac{dI_z}{dt} = -(W_2 - W_0)S_z - (W_I^1 - W_I^2)2I_zS_z \quad (31)$$

$$\frac{dS_z}{dt} = -(W_2 - W_0)I_z - (W_S^1 - W_S^2 + W_2 + W_0)S_z - (W_S^1 - W_S^2)2I_zS_z$$

$$\frac{d2I_zS_z}{dt} = -(W_I^1 - W_I^2 + W_S^1 + W_S^2)2I_zS_z$$

The change of magnetization of I_z over time is not only dependent on itself but also on S_z and $2I_ZS_Z$. The z-component of the magnetization of the spin I_z is dependent of the z-component magnetization of the spin S.

$(W_2 - W_0)$ is termed the cross-relaxation rate constant (σ_{12})

$(W_I^1 + W_I^2 + W_2 + W_0)$ is termed the self-relaxation rate constant of spin I ($R_Z^{(I)}$)

$(W_s^1 + W_S^2 + W_2 + W_0)$ is termed the self-relaxation rate constant of spin S ($R_Z^{(S)}$)

$(W_I^{(1)} - W_I^{(2)})2I_zS_z$ describes the transfer of I_ZS_Z to I spin magnetization.

The operator $2I_ZS_Z$ self-relaxes with the following rate constant:

$$R_{IS} = (W_I^{(1)} + W_S^{(1)} + W_S^{(2)}) \quad (31)$$

1.9 Nuclear Overhauser effect

The nuclear Overhauser effect (NOE, Overhauser, 1953) applied to NMR (Kaiser, 1963) , is a transfer of magnetization between two dipolar-coupled spins by a cross-relaxation effect through space.

If the S spin magnetization changes from equilibrium, the I spin will be affected with a rate proportional to the cross relaxation rate (σ_{IS}) and with how much the S spin deviates from equilibrium. This variation in the I spin magnetization will be reflected by an intensity change in the spectrum. When the S spin magnetization changes, the I spin intensity will reflect this perturbation.

From the Solomon equation we see that:

$$\frac{d(I_z - I_z^0)}{dt} = -R_I(I_z - I_z^0) - \sigma_{IS}(S_z - S_Z - S_Z^0) \qquad (31)$$

We can write the cross-relaxation rate constant as:

$$\sigma_{IS} = (W_2 - W_0) = 2\gamma_I^2\gamma_S^2\hbar^2 \frac{1}{r_{IS}^6}[\, J(\omega_{W_2}) - J(\omega_{W_0})] \qquad (32)$$

Where $J(\omega)$ is the spectral density function at the frequency ω which describes the amount of molecular motions at this frequency.

$$J(\omega) = \frac{2\tau_c}{1+\omega^2\tau_c^2} \propto W \qquad (33)$$

We see that the cross relaxation rate constant sign can be positive or negative depending on the rotational correlation constant (τ_c) (**Figure 1.8**), hence on the size of the molecule. When W_2=W_0, $\sigma_{IS} = 0$, the NOE enhancement is null.

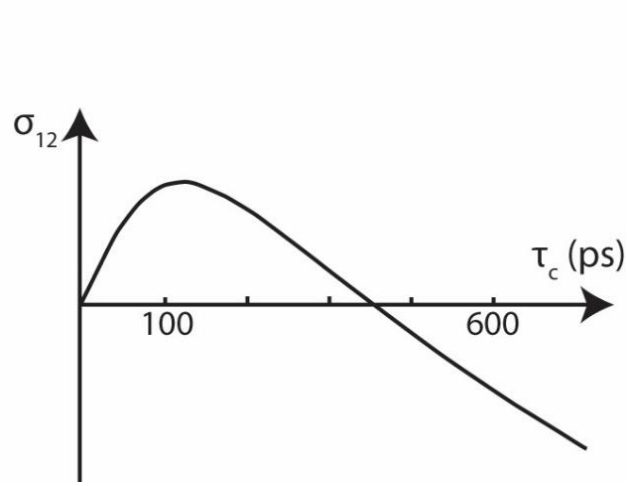

Figure 1.8 Dependency of the cross-relaxation rate constant on the rotational correlation time for a 500 MHz Larmor frequency.

The NOE contain information about the distance r between the spins represented by $\frac{1}{r_{IS}^6}$ in equation (32). The closer the spins are in space, the higher will be the magnetization transfer between the spin.

For a two-spin system I and S, where S is irradiated with a radiofrequency field that does not affect I. Before the mixing time, magnetization on the I and S spins are represented by the following equations:

$$S_z(0) = -\cos\Omega_S t_1 S_z^0,\ I_z(0) = -\cos\Omega_I t_1 I_z^0 \qquad (34)$$

Where the offset $\Omega=\omega_0 - \omega_{rf}$, ω_{rf} is the transmitter frequency. It is the difference between the Larmor frequency of the spin and the transmitter frequency.

The equation for the evolution on the magnetization of S is:

$$\frac{dS_z(\tau_m)}{dt}_{initial} = \sigma_{IS}(I_z(t) - I_z^0) - R_s(S_z(t) - S_z^0) \qquad (35)$$

Solving the equation yields:

$$S_z(\tau_m) = \sigma_{IS}\tau_m I_z^0 + R_S\tau_m S_z^0 \qquad (a) \qquad (36)$$

$$+\cos\Omega_1 t_1[\sigma_{IS}\tau_m]I_z^0 \qquad (b)$$

$$+\cos\Omega_S t_1[R_S\tau_m - 1]S_z^0 \qquad (c)$$

After the mixing time, the z-component of spin S magnetization is rotated by a 90° pulse to be measured (**Figure 1.9**). The magnetization on spin S will precess at Ω_S during t_2. The NOESY spectrum will contain peaks represented by the terms (a), (b) and (c) (**Figure 1.10**).

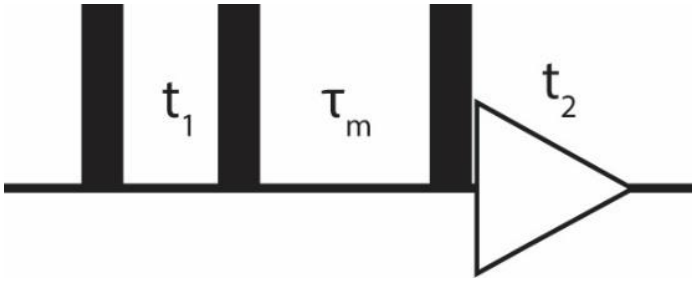

Figure 1.9 A simple NOESY pulse sequence. Full bars represent 90° pulses. The white arrow represent the acquisition.

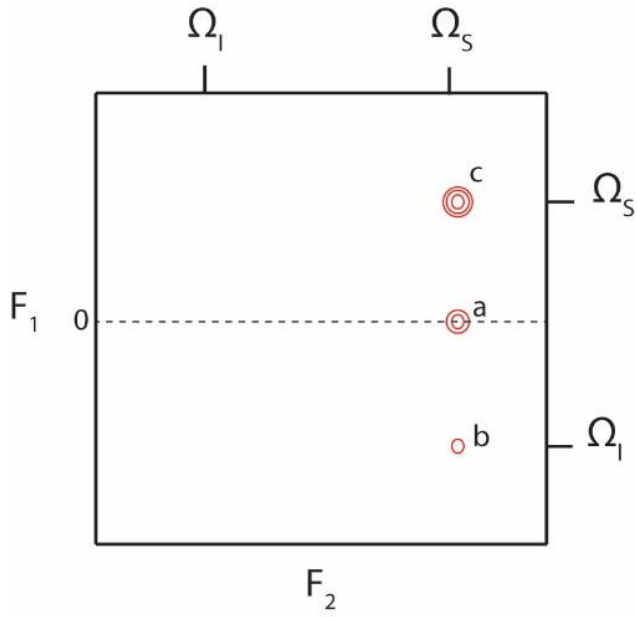

Figure 1.10 Example spectrum of a 2D-NOESY experiment. Term (a) do not evolve with t_1, in t_2 it evolves at Ω_S. The peak coordinate will therefore be $\{F_1, F_2\} = \{0, \Omega_S\}$. It is an axial peak. Term (b) is a cross peak. It evolves during t_1 and t_2 at Ω_I and Ω_S respectively. We see that the intensity is proportional to the cross correlation rate constant and to the mixing time. Its coordinates are $\{F_1, F_2\} = \{\Omega_I, \Omega_S\}$.Term (c) is a diagonal peak of coordinates $\{F_1, F_2\} = \{\Omega_S, \Omega_S\}$ that evolves during t_1 and t_2 at Ω_S and Ω_I respectively. This peak is negative as $R_S\tau_m - 1 \ll 0$ in the initial rate and goes back to zero with the mixing time, with a R_S rate. When R_I and $R_S > 0$, σ_{IS} can be positive or negative. When $\sigma_{IS} > 0$, the diagonal and cross peaks will have opposite signs. When $\sigma_{IS} < 0$, all the peaks will have the same sign.

1.10 Heteronuclear NMR of proteins

We already saw that one-dimensional NMR is able to detect the protons of the proteins. For structural and functional studies, it becomes necessary to use additional nuclei that are found within those macromolecules. In a 1D-experiment, the signal is acquired as a function of one variable of time and Fourier transformed to yield a spectrum. The spectrum is a function of frequency. In a 2D-experiment, the experiment is recorded as a function of two variables of time t_1 and t_2 (**Figure 1.11 A**). First, a series of 1D experiments are recorded with different t_2 times and Fourier transformed (**Figure 1.11 B)**, then a second Fourier transform with time t_1 yields the 2D-spectrum. The 2D spectrum is then a function of two frequencies (**Figure 1.11 C**).

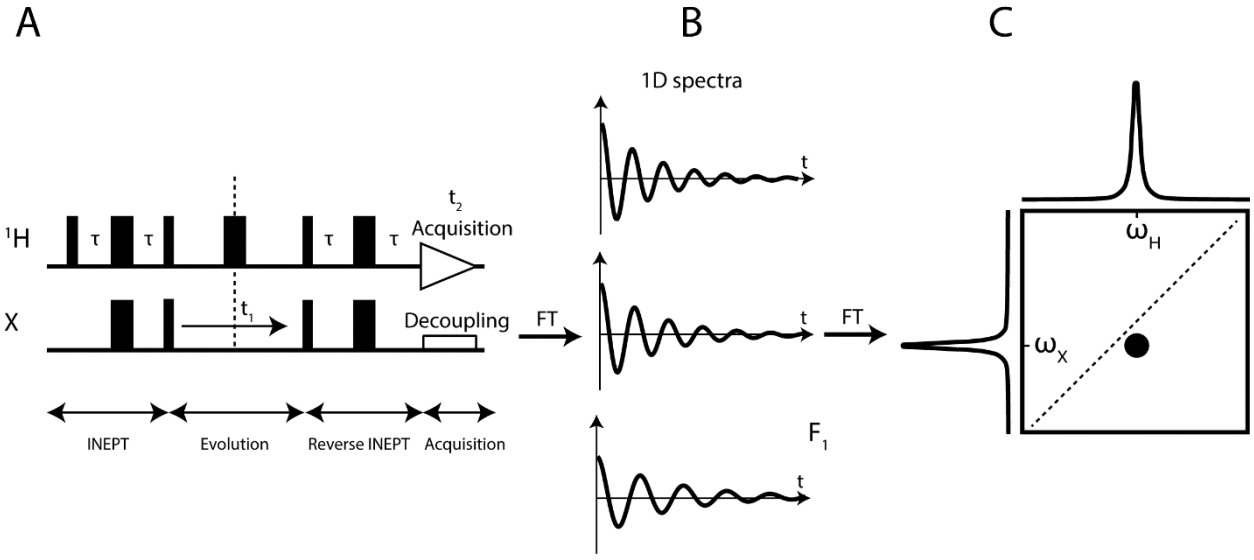

Figure 1.11 A) Scheme of a 2D-HSQC experiment, the experiment is recorded with variables t1 and t2 times. Pulses of 90° are represented by thin bars and 180° pulses by thick bars. **B)** The acquired data are processed by two successive Fourier-transform. **C)** The result 2D-spectra contains peaks which are described by two frequencies.

As we remember, the gyromagnetic ratio of the proton is the highest of any nuclei. A very sensitive experiment is to transfer the magnetization from ^{1}H to ^{15}N (2D [^{15}N, ^{1}H]-HSQC). This experiment yields what is called a “fingerprint” spectrum where every peptide bond is represented as a peak. NH_2-containing side chains (asparagine and glutamine) are represented as a doublet of peak on the top right side of the spectrum.

In the 2D-HSQC experiment, the first insensitive nuclei enhanced by polarization transfer (INEPT)(Morris and Freeman, 1979) pulse train transfer magnetization from the proton to the other nuclei. Its first 90° converts H_z magnetization to $-H_y$, the following 180° pulse after time τ is

to evolve the coupling between the two nuclei while without evolving the proton magnetization. The magnetization is then $-H_yX_z$. At the end of the INEPT, 90° pulse on both channels transfer the magnetization to H_zX_y. Then, the antiphase magnetization of the X nucleus evolves during t_1. Heteronuclear couplings between proton and X nuclei are refocused in the middle of the evolution time with a 180° pulse of the proton. A reverse INEPT transfers the magnetization from the X spin to in-phase proton magnetization. Acquisition starts along with the use of a composite pulse decoupling (CPD) scheme to prevent magnetization arising from the coupling of the proton-X nuclei. τ length is equal to $\frac{1}{4}(J_{HX})$. With no decoupling, the experiments would yield four peaks **(Figure 1.12 A**) for each H-X bond at frequencies of $\omega_H \pm \frac{\pi J_{HX}}{2}$ and $\omega_X \pm \frac{\pi J_{HX}}{2}$.

The refocusing 180° pulse during t_1 allows for the decoupling of the proton during X nuclei evolution. The decoupling of the X nuclei during proton acquisition is performed by CPD scheme. With those decouplings active, the spectrum is simplified to only one peak per H-X bond (**Figure 1.12 B**).

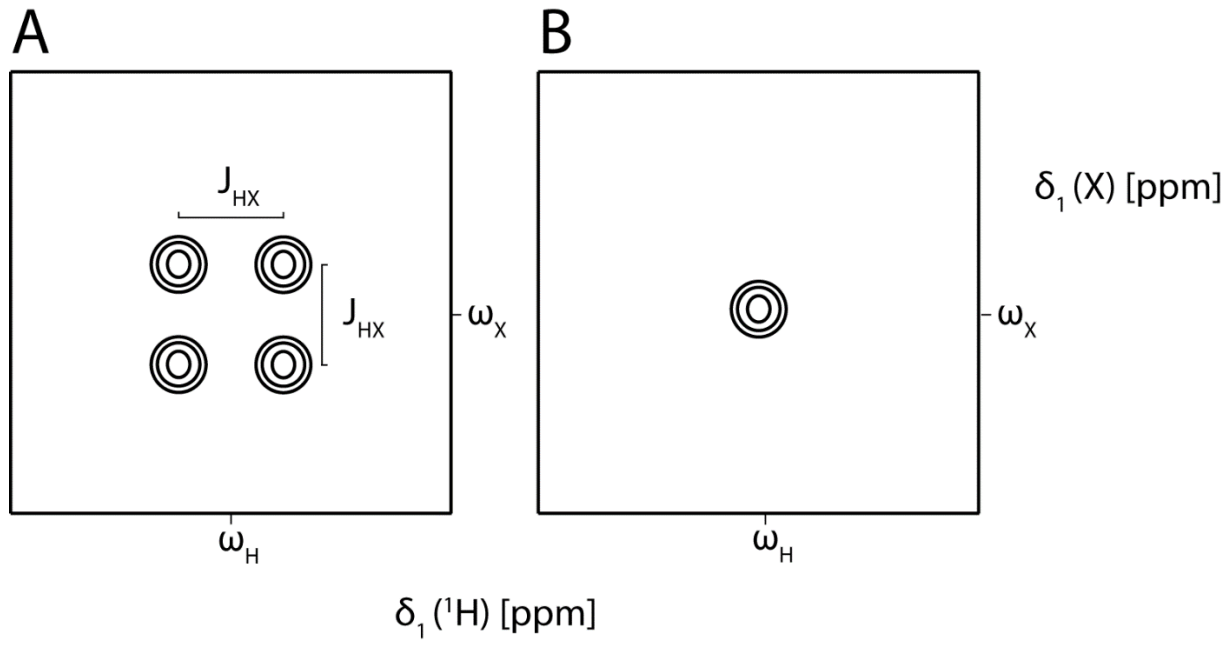

Figure 1.12 H-X HSQC spectrum. **A)** Undecoupled spectrum, four peaks are present for one H-X bond. They are separated by the scalar coupling J_{HX} on both dimensions. They are centered on coordinates [ω_H, ω_X]. **B)** With active decoupling, only one peak is present. Its coordinates are [ω_H, ω_X].

1.11 Transverse Relaxation-Optimized Experiments.

Liquid-state NMR spectroscopy is able to measure proteins of limited size because of fast transverse relaxation of the nuclei by dipole-dipole (DD) coupling and chemical shift anisotropy (CSA). The idea behind Transverse-relaxation-optimized spectroscopy (Pervushin et al., 1997) is to reduce transverse relaxation by compensating dipole-dipole and chemical shift anisotropy components of relaxation. Chemical shift anisotropy (CSA) is due to the chemical environment around a spin (Saitô et al., 2010). Electrons around a nucleus can shield this nucleus from the main magnetic field B_0. As such, the local magnetic field is different for every spin, this is the reason why we can measure chemical shifts. If the chemical shifts of the molecule varies along different directions, then the chemical shift tensor describing the electric field around the nucleus is asymmetric. Nucleus with a half spin and a large chemical shift range are relaxing faster due to CSA effects and display broader peaks. In fast tumbling systems, the CSA relaxation mechanisms are averaged out. For larger molecules, the rotational correlation time (τ_c) becomes longer, increasing the transversal relaxation contribution. Dipole-dipole coupling depends on the distance between nuclei and the angle between the internuclear vector and the magnetic field. As the molecule tumble in solution, the dipoles are generating an oscillating magnetic field which contributes to the relaxation of nearby spins. The TROSY-type experiment uses constructive interference between DD coupling and CSA to reduce the transverse relaxation (**Figure 1.13**). TROSY-type experiments allow to measure spectra of proteins of higher molecular weight (**Figure 1.14**).

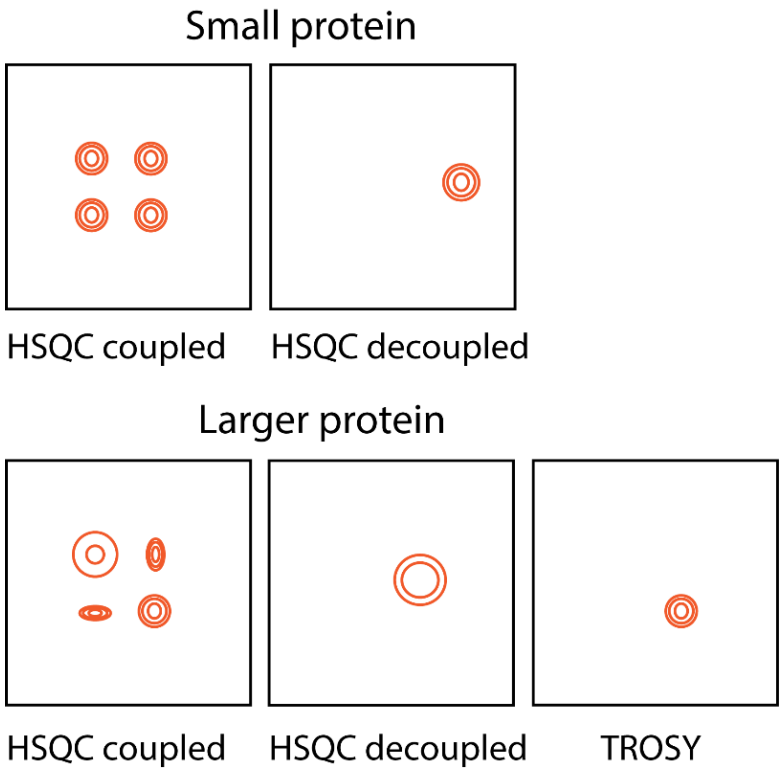

Figure 1.13 In the undecoupled HSQC experiment, multiplets are present because of the scalar couplings. For larger proteins, the components of those multiplets have different widths because they relax with different rates. The TROSY experiment aims at selecting only the component for which CSA and DD relaxation have cancelled each other out. TROSY experiments are well-suited to increase the signal to noise ratio and the linewidth for spectra of large molecules.

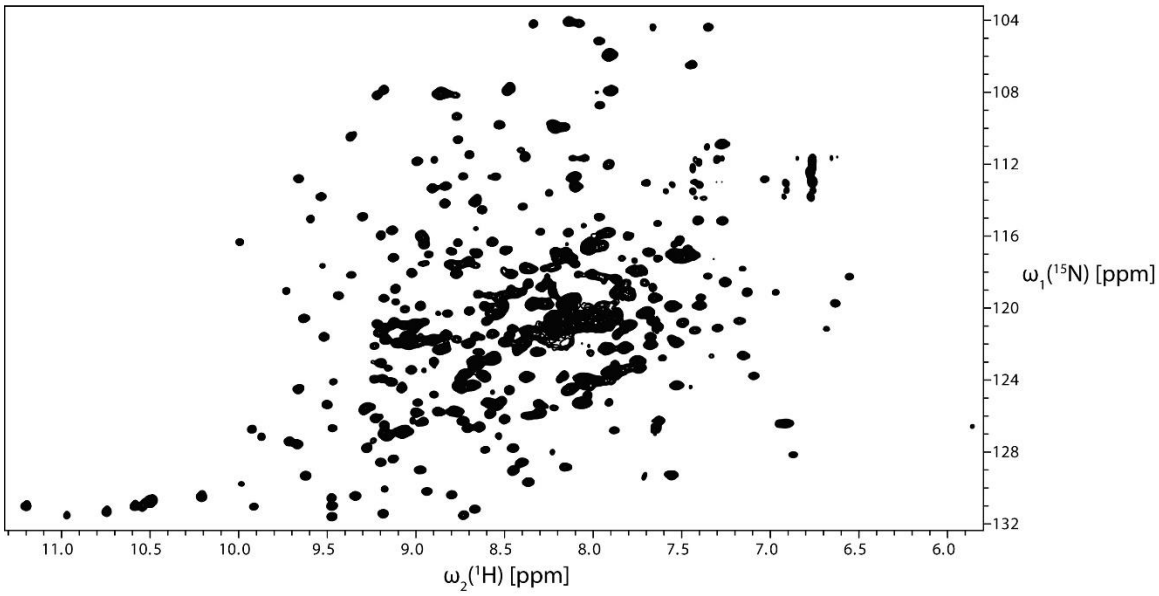

Figure 1.14 Example of a 2D [^{15}N,^{1}H]-TROSY-HSQC experiment of the BamA β-barrel protein in solution. Each peak represents the backbone ^{1}H-^{15}N bond of a residue.

1.12 Descriptions of experiments for the assignment of proteins

3D-HNCA

For large proteins isotopically labeled with ^{15}N and ^{13}C the use of three-dimensional experiments is necessary to perform the sequential assignment the backbone of the molecule (Ikura et al., 1990). The assignment aims at identifying the residues to which the peaks belong, opening a way to study function and structure at atomic resolution. For the HNCA experiment (Kay et al., 1990; Salzmann et al., 1999), magnetization starts on the amide proton and is then transferred to ^{15}N via the J_{NH} using an INEPT pulse sequence, and then to the $^{13}C_{\alpha}/^{13}C_{\alpha-1}$ with the $J_{NC\alpha}$ with another INEPT and then back to ^{15}N and ^{1}H with reverse-INEPT pulse sequence (**Figure 1.15**).

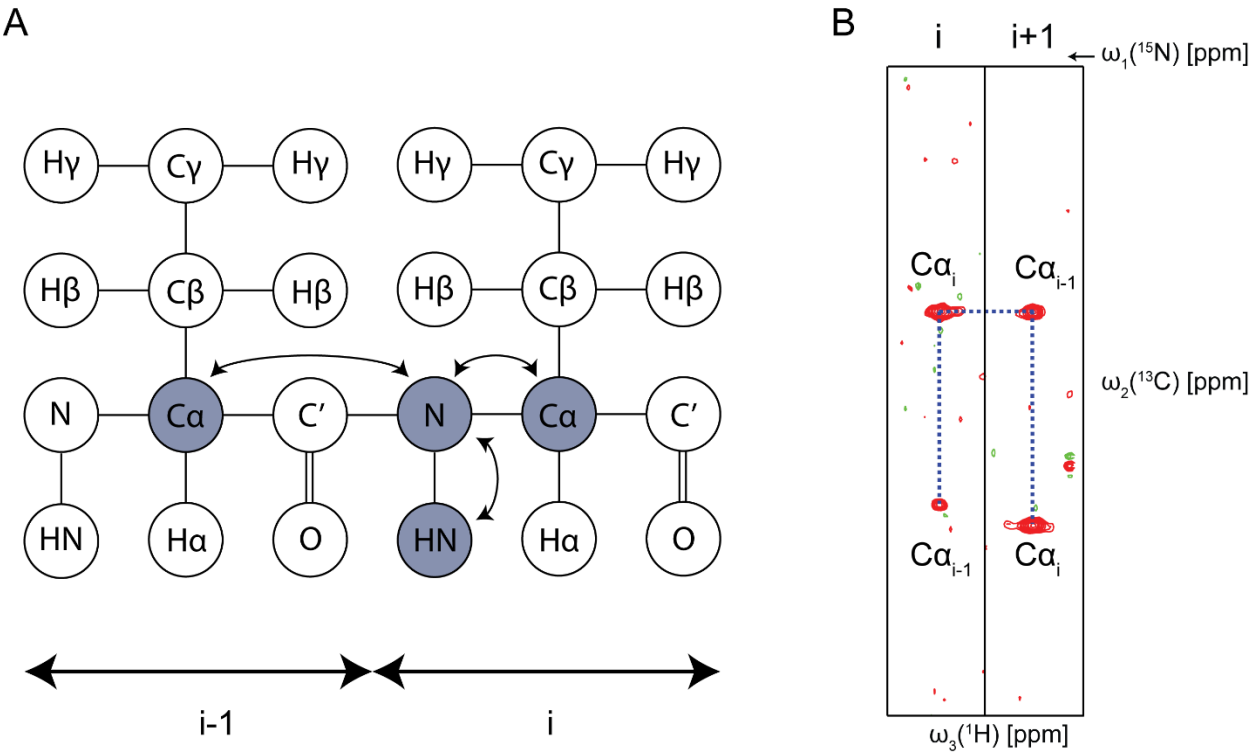

Figure 1.15 A) Representation of the transfer of magnetization in the HNCA experiment (adapted from Victoria A. Higman, http://www.protein-nmr.org.uk). **B)** Example of HNCA strips of the BamA β-barrel protein in solution. Consecutive residues in the backbone are connected as the successor residue sees the $C\alpha_{-1}$ of the predecessor.

The magnetization is evolved on the ^{1}H amide nuclei as well as on ^{15}N amide and $^{13}C_{\alpha}$, yielding a 3D experiment. Once calibrated onto the 2D [^{15}N-^{1}H]-HSQC experiment, each [^{1}H-^{15}N] peak will show two peaks in the carbon dimension. The coupling between ^{15}N and $^{13}C_{\alpha}$ is stronger than the ^{15}N $^{13}C_{\alpha-1}$ coupling, the most intense peak usually belongs to the C_{α} of the observed residue and

the least intense to the previous residue. We can therefore use the HNCA to sequentially assign the backbone of the protein. However in larger proteins, ambiguities start to arise as many different successors for one residue are possible. It is to be noted that proline do not have an amide proton and cannot be assigned using this experiment.

3D-HNCO

The HNCO (**Figure 1.16**) (Grzesiek and Bax, 1992; Kay et al., 1990) is the most sensitive 3D experiment, it correlates the CO-N-HN of the backbone and can be used with the HN(CA)CO experiment (Clubb et al., 1992) to perform sequential assignment. The 2D-HNCO version, can be used in specific amino acid isotopic labeling samples to detect the successor of a residue which is ^{13}C labeled. The CO chemical shifts can also be used to predict the secondary chemical shifts. The HNCO experiment transfers magnetization from the proton to the nitrogen of the amide group then to the carbonyl of the previous residue.

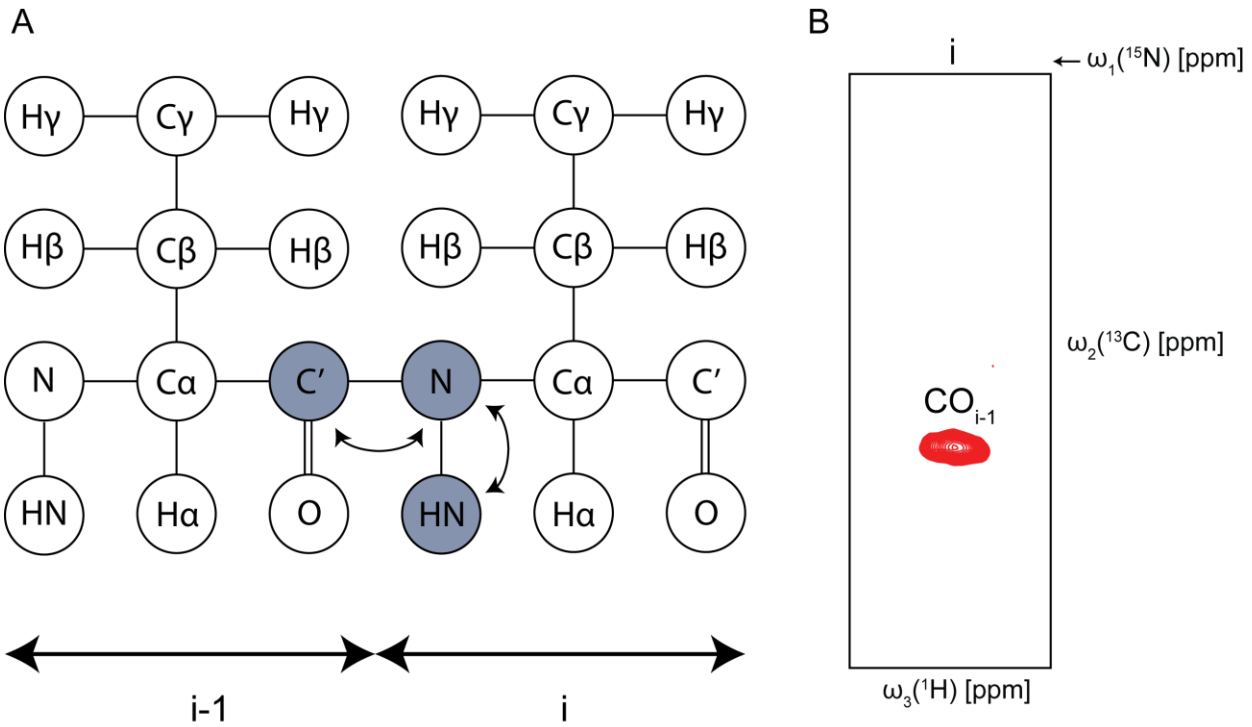

Figure 1.16 A) Representation of the transfer of magnetization in the HNCO experiment (adapted from Victoria A. Higman, http://www.protein-nmr.org.uk).**B)** Example of HNCO strip of the BamA β-barrel protein in solution. The visible chemical shift comes from the CO of the predecessor residue

3D-HNCACB

The HNCACB experiment (**Figure 1.17**) (Grzesiek and Bax, 1992; Salzmann et al., 1999) is a three-dimensional experiment for which magnetization is transferred from the amide proton to the amide ^{15}N via the J_{HN} coupling with an INEPT. Then it is transferred from the ^{15}N to the $^{13}C_{\alpha}$ using the scalar coupling $J_{NC\alpha}$. The magnetization is partially transferred to $^{13}C_{\beta}$ using an INEPT block. Afterwards, the magnetization is evolved for a t_1 time. Magnetization is transferred back to $^{13}C_{\alpha}$ and ^{15}N using reverse INEPTs and the ^{15}N is evolved for a t_2 time. On the last step, polarization is transferred back to the amide proton where it is evolved as the acquisition starts for a t_3 time. The time t_1, t_2, t_3 are varied by increments to form the three dimensions of the experiment.

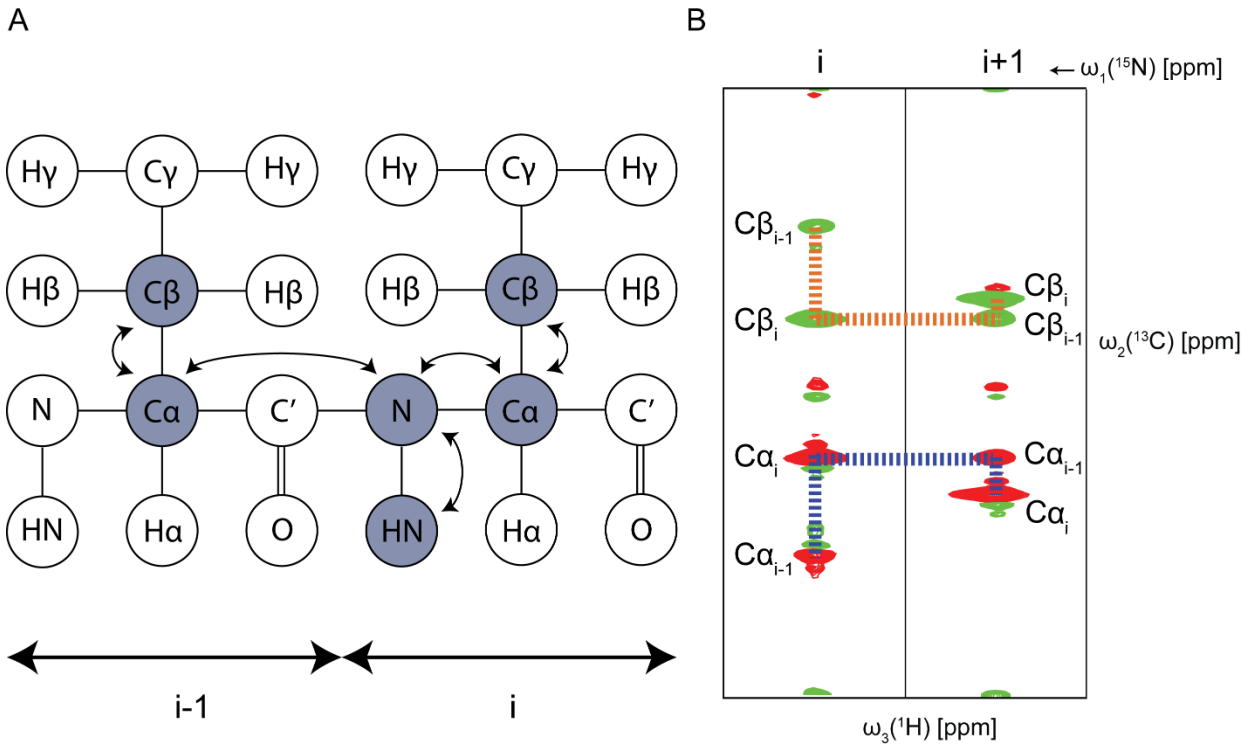

Figure 1.17 A) Representation of the transfer of magnetization in the HNCACB experiment (adapted from Victoria A. Higman, http://www.protein-nmr.org.uk). **B)** Example of HNCACB strips of the BamA β-barrel protein in solution. Four peaks are visible for each strip. C_{α} and $C_{\alpha-1}$ are present, as well as C_{β} and $C_{\beta-1}$. This experiment is less sensitive as the HNCA but allows to solve ambiguous connections as the C_{β} brings additional information about the connectivity.

^{15}N-NOESY-HSQC

In the ^{15}N-NOESY-HSQC experiment (**Figure 1.18**) (Fesik and Zuiderweg, 1988; Marion et al., 1989; Talluri and Wagner, 1996) the magnetization starts on the protons and is then exchanged to all the close protons, then it is transferred to ^{15}N and back to proton for detection. This experiment is performed to acquire data about space proximity of protons which are coupled to ^{15}N nuclei. The intensity of the crosspeaks in proportional to $\frac{1}{r_{HH}{}^{-6}}$ where r_{HH} is the distance between the two protons. As such, the experiments can be performed to acquire restrains for structure calculation. It can also be used in combination with atomic resolution knowledge of the structure to help assignment of the protein.

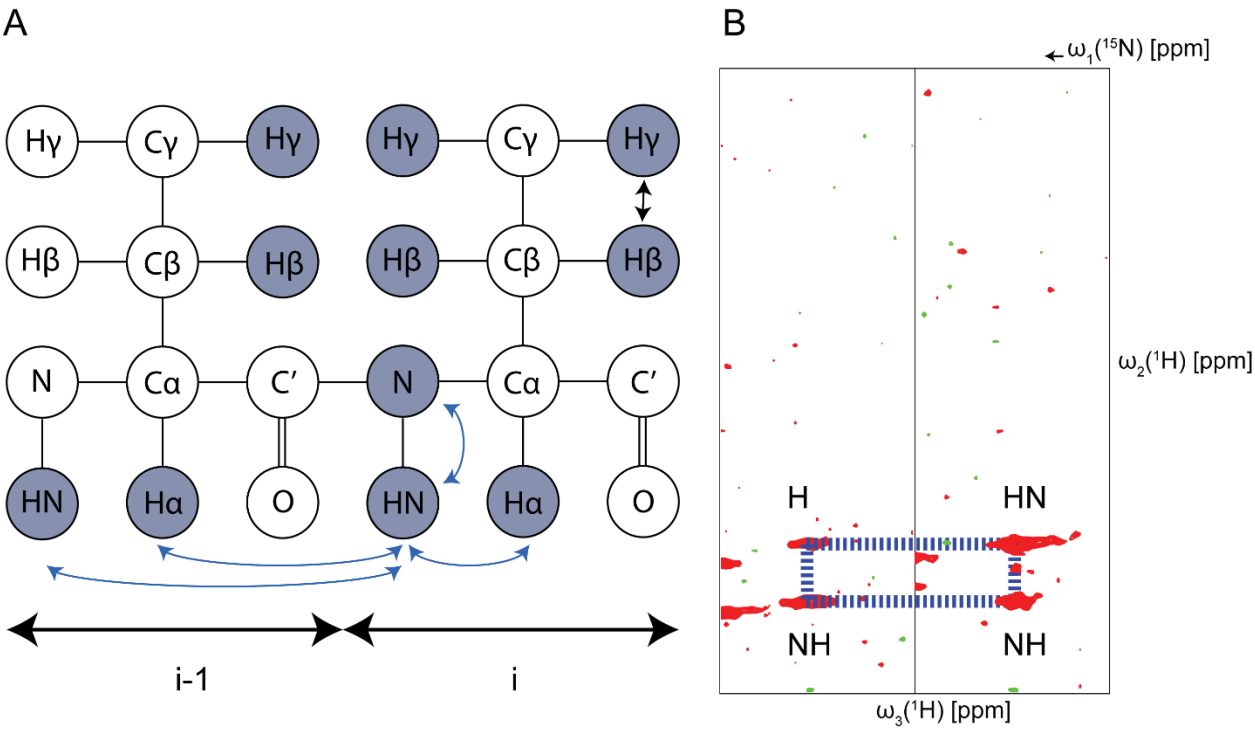

Figure 1.18 A) Representation of the transfer of magnetization in the ^{15}N-NOESY-HSQC experiment (adapted from Victoria A. Higman, http://www.protein-nmr.org.uk). **B)** Example of ^{15}N-NOESY-HSQC strips of the BamA β-barrel protein in solution. Crosspeaks exist for protons that are close in space and that correlate to the backbone ^{15}N amide. In the example strips, two residues are facing in a β-sheet and form a hydrogen bond. As they are close in space, the protons exchange magnetization during the mixing time and correlate to each of the backbone ^{15}N.

^{13}C-HMQC

In the ^{13}C-HMQC experiment (**Figure 1.19**), magnetization starts on the proton and is transferred on the ^{13}C and back to the proton for acquisition. This is the ^{13}C counterpart of the ^{15}N-HSQC. In the scope of assigning the methyl groups of the sidechains, this experiment is performed at high resolution in order to pick the peaks in the spectra (**Figure 1.20**).

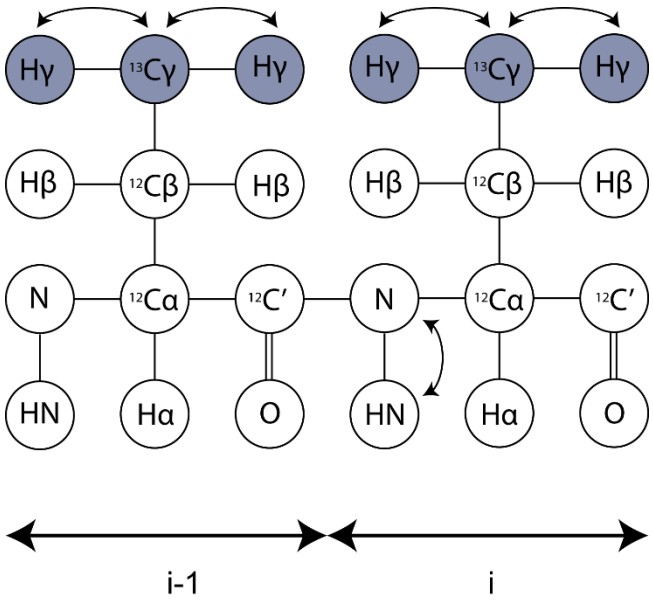

Figure 1.19 Representation of the transfer of magnetization in the HMQC experiment for a sample ^{13}C labeled on the methyl sidechains.

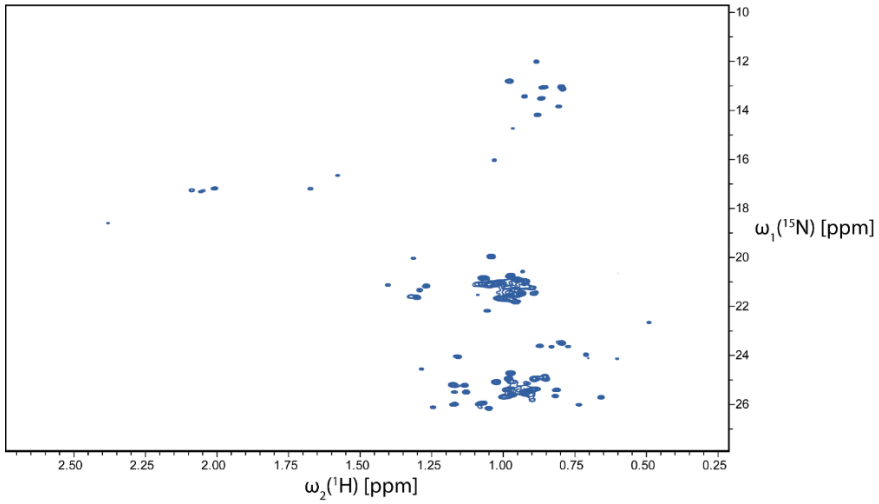

Figure 1.20 Example of a [^{1}H-^{13}C]-HMQC experiment of the BamA β-barrel protein in solution. Each peak represents a ^{1}H-^{13}C bond. In that case the sample is ^{13}C labeled on the methyl of the side chains.

13C-NOESY-HMQC

In the ^{13}C-NOESY-HMQC experiment (**Figure 1.21**), the magnetization is transferred from ^{1}H to ^{13}C by scalar coupling and back to the proton. It is then exchanged during close by protons during the mixing time and the signal is acquired. This experiment can be used to assign sidechains when combined with available structural information.

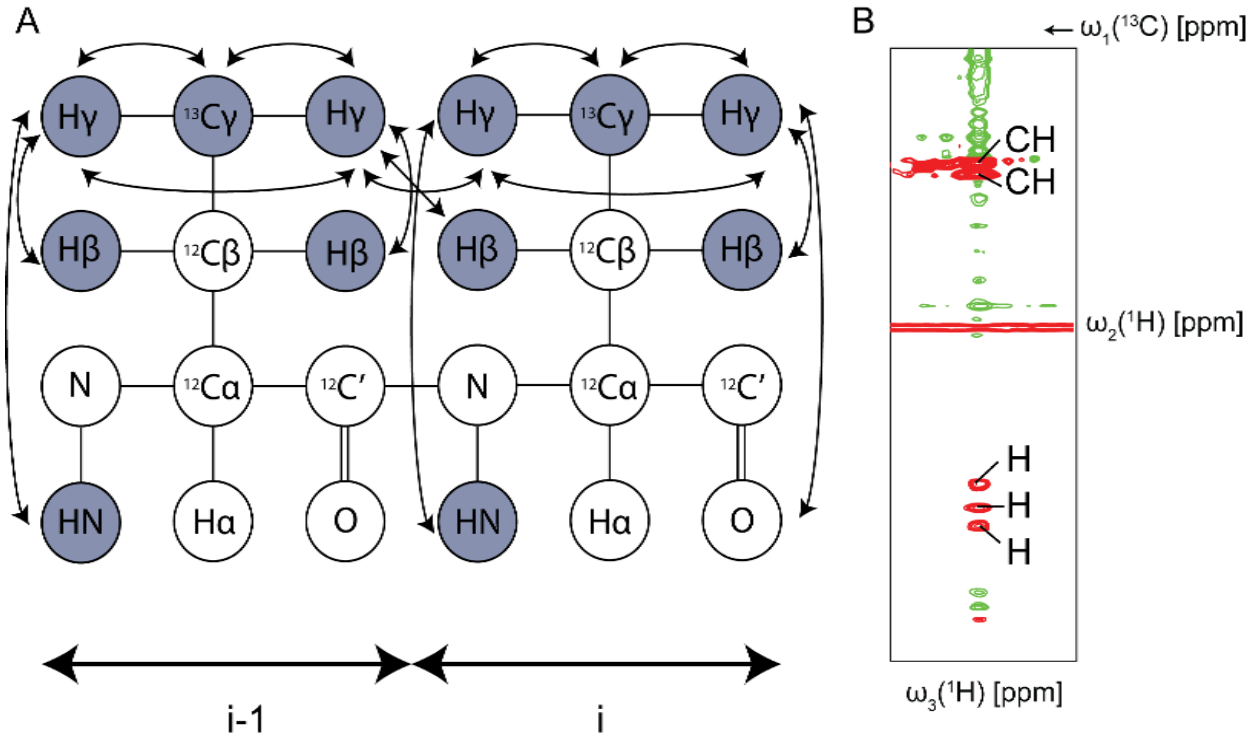

Figure 1.21 A) Representation of the transfer of magnetization in the 3D-NOESY-HMQC experiment for a sample ^{13}C labeled on the methyl sidechains. **B)** Example of ^{15}N-NOESY-HMQC strip of the BamA β-barrel protein in solution.

Chapter 2: Study of the BamBCDE associated lipoproteins

I carried all the work presented in this chapter.

2.1 Introduction to the Bam complex

Gram-negative bacteria possess an inner membrane, composed of phospholipids, spanned by α-helical proteins and an outer membrane, asymmetrical and composed of phospholipids, lipopolysaccharides (LPS) (Nikaido and Vaara, 1985), spanned by β-barrel proteins. Those integral outer membrane proteins are playing important roles in the cell (Koebnik et al., 2000; Nikaido, 2003). Outer membrane proteins are translated by the ribosome, their signal sequence (Sjöström et al., 1987) is then recognized by the SecYEG complex which translocate them to the periplasm. From that point they are stabilized by chaperones (Korndörfer et al., 2004; Schiffrin et al., 2017; Thoma et al., 2015; Zhong et al., 2013) who help them to reach the β-barrel assembly machinery complex (BAM). In order for cells to adapt to external conditions, they are required to be inserted readily into the outer membrane. Proteins of the Omp85 family, including the BamA complex (**Figure 2.1**), are highly conserved and essential for outer membrane biogenesis in bacteria and mitochondria (Gentle et al., 2004; Hagan and Kahne, 2011; Knowles et al., 2009a; Ricci et al., 2012; Robert et al., 2006; Rossiter et al., 2011; Voulhoux et al., 2003). BamA, the main protein of the Bam complex, is a 16-stranded β-barrel prolonged by five periplasmic polypeptide transport domains (POTRA) (Sánchez-Pulido et al., 2003). Whereas the POTRA domains assist proteins coming from the periplasm to fold in the outer membrane (Patel and Kleinschmidt, 2013), only POTRA5 is essential (Bos et al., 2007).

The barrel is associated in a complex with four solubles lipoproteins BamB, BamC, BamD and BamE (Sklar et al., 2007; Wu et al., 2005) that are anchored on the inner leaflet of the outer membrane. Structures of the BamA barrel with POTRA5 in *E. coli* (Albrecht et al., 2014), with its fifth periplasmic POTRA domains in *N. gonorrhoeae* (Noinaj et al., 2013) as well as its complex with the BamB, BamC, BamD and BamE associated lipoproteins in *E.coli* (Bakelar et al., 2016; Gu et al., 2016; Han et al., 2016, Iadanza et al., 2016) have been resolved (**Figure 2.2**). BamB is a ring-like protein formed by an eight-bladed β-propeller fold (Dong et al., 2012; Kim and Paetzel, 2011; Noinaj et al., 2011). Each blade formed by four antiparallel β-sheet. The blades are organized around a pseudo-eight-fold axis. This donut-like organization shows homology to proteins with WD40 domains, which are proteins that build scaffold with other proteins to form complexes (Kim and Paetzel, 2011; Neer et al., 1994; Noinaj et al., 2011). BamB binds to BamA on its POTRA 2 and 3 domains on one side of the complex (Gu et al., 2016). BamC is made of two-domains separated by a long liker. The N–terminal domain has two α-helices sitting against an anti-parallel β-sheet composed of five strands while the C-terminal domain possess a six-stranded antiparallel β-sheet, three α-helices and a 3_{10}-helix (Kim et al., 2011a; Warner et al.,

2011). BamE is formed by two N-terminal antiparallel α-helices and a C-terminal twisted antiparallel β-sheet composed of three β-strands (Kim et al., 2011b; Knowles et al., 2010, 2011). On one side of the barrel sits the BamCDE subcomplex, with interactions between the C-terminal domain of BamD and the POTRA5 domain of BamA. On the other side, BamB interacts with the POTRA3 domain. Finally, BamE, mainly interacts with BamD, but also shows contacts with BamC, and BamA, at the interface between BamA and BamD (Gu et al., 2016).

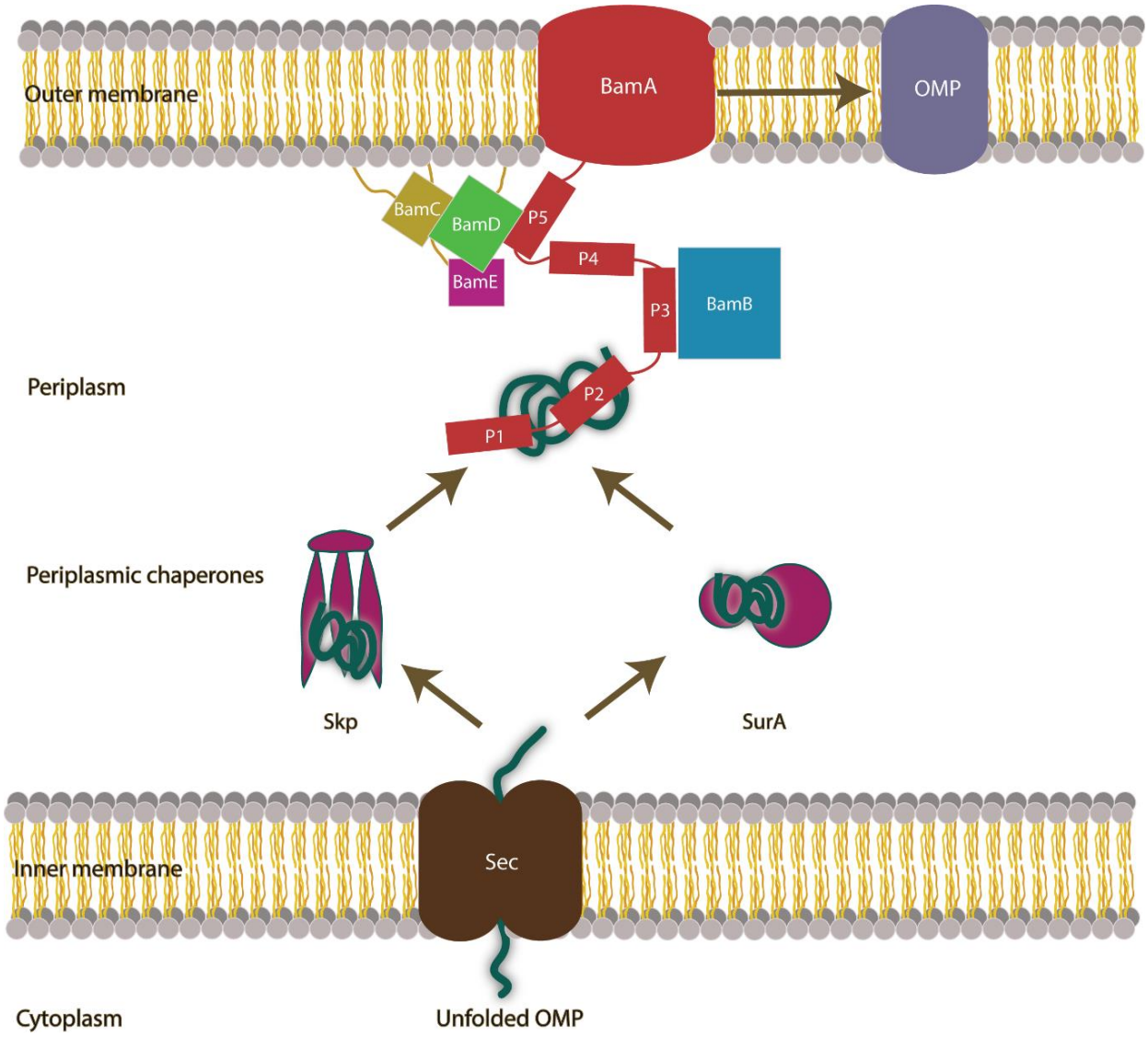

Figure 2.1 Representation of the OMP pathway. OMPs are translated by the ribosome in the cytoplasm and brought to the SEC machinery by chaperones (Trigger factor and SecB). After translocation by the SEC complex, polypeptide chains of the OMPs are protected by periplasmic chaperones (Skp and SurA) and transported to the Bam complex to be inserted into the outer membrane.

BamA and BamD are the only proteins from the complex essential for the biogenesis of outer membrane proteins (Malinverni et al., 2006; Rossiter et al., 2011; Wu et al., 2005). Functional studies have started to unveil the roles of the BamA associated lipoproteins. BamD was shown to bind to unfolded OmpA and BamA (Hagan et al., 2013), it was also demonstrated that a peptide constituted from a fragment of a substrate OMP protein, was able to bind BamD and inhibits the β-barrel assembly by interfering with the BamD/OMP interaction (Hagan et al., 2015). Additionally BamD and BamE where shown to control loop 6 of BamA conformation by the BamD/POTRA5 interaction by respectively increasing and decreasing loop 6 exposure (Rigel et al., 2013). BamC backbone assignment was made available and its liquid-state NMR structure was determined (Knowles et al., 2009b). BamE backbone assignment was determined (Knowles et al., 2010). BamB was shown to be capable of binding unfolded substrates (Hagan et al., 2013). BamD and BamB might help to bind and localize the unfolded OMPs to the membrane (Hagan et al., 2013).

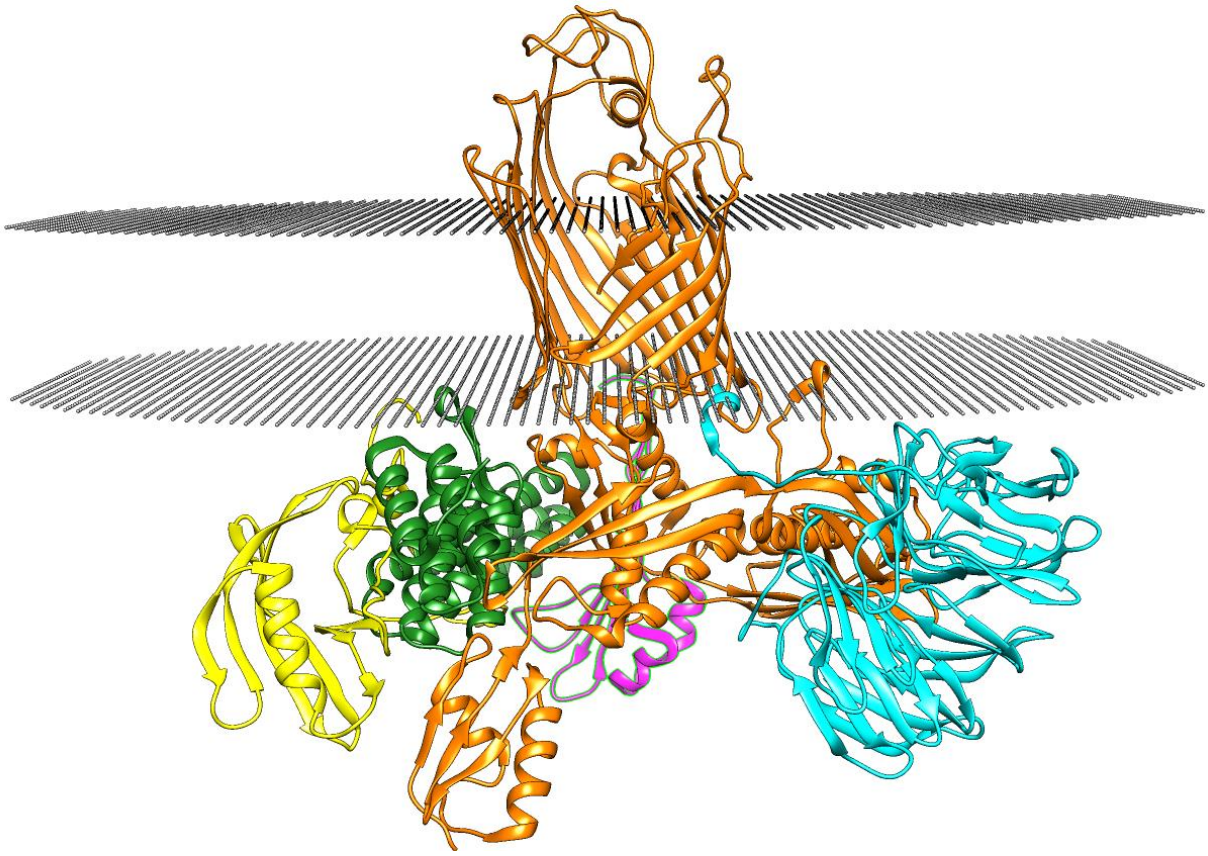

Figure 2.2 Cryo-EM structure of the Bam complex (Iadanza et al., 2016, PDB: 5LJO), represented in a simulated membrane, with the PPM server (PPM server, Lomize et al., 2012). The BamA barrel is in the open conformation represented in orange, BamB is in blue, BamC in yellow, BamD in green and BamE in magenta.

While it had been shown that the Bam complex catalyze the folding of β-barrels in vitro (Hagan and Kahne, 2011; Plummer and Fleming, 2015). The mechanism by which BamA β-barrel catalyzes the folding of OMPs is still under investigation. The argument that the BamA β-barrel holds parts of its function by thinning the surrounding bilayer (Fleming, 2015) and that defects in the bilayer facilitate unfolded OMPs insertion (Danoff and Fleming, 2015) are backed by observations than the hydrophobic belt of the barrel is substantially reduced on the C-terminal side of the barrel (Noinaj et al., 2013), but it is not the only feature to account for the folding mechanism. A structural property from the BamA-barrel, is the loose closing between its first and last strand (Noinaj et al., 2013) that was also observed in its homolog TamA (Gruss et al., 2013). Forming a disulfide bridge in the gate-region of the barrel was shown to be lethal in vivo (Noinaj et al., 2014), demonstrating that the opening of this region is required for the function. Disulfide crosslinking of the gate-region in different registers proved this region to be very dynamic (Doerner and Sousa, 2017) and MD simulations previewed the opening of the barrel (Noinaj et al., 2013) that was later observed by cryo-electron microscopy (Iadanza et al., 2016,) and X-ray crystallography (Gu et al., 2016) (**Figure 2.3)**. The β1-β16 region was proposed to act as a template for β-augmentation, by recognizing, binding and serving as a guide to fold the incoming substrate, forming an hybrid-barrel between BamA and the folding OMP. The proposed hybrid-barrel model (Gruss et al., 2013) was also suggested by experiments with homolog protein TtOmp85 (Estrada Mallarino et al., 2015; Henke et al., 2016). A recent paper about mitochondrial SAM50, lends toward this model, localizing OMP precursors in the lateral-gate with disulfide cross-linking experiments (Höhr et al., 2018), this work also showed the recognition of the β-signal sequence by the first strand of TtOmp85, a conserved motif across outer membrane proteins which is also specifically recognized by BamA (Robert et al., 2006). Despite those advances, there is still to witness a BamA-substrate complex at atomically resolution, a difficult challenge, as the complex is probably transient.

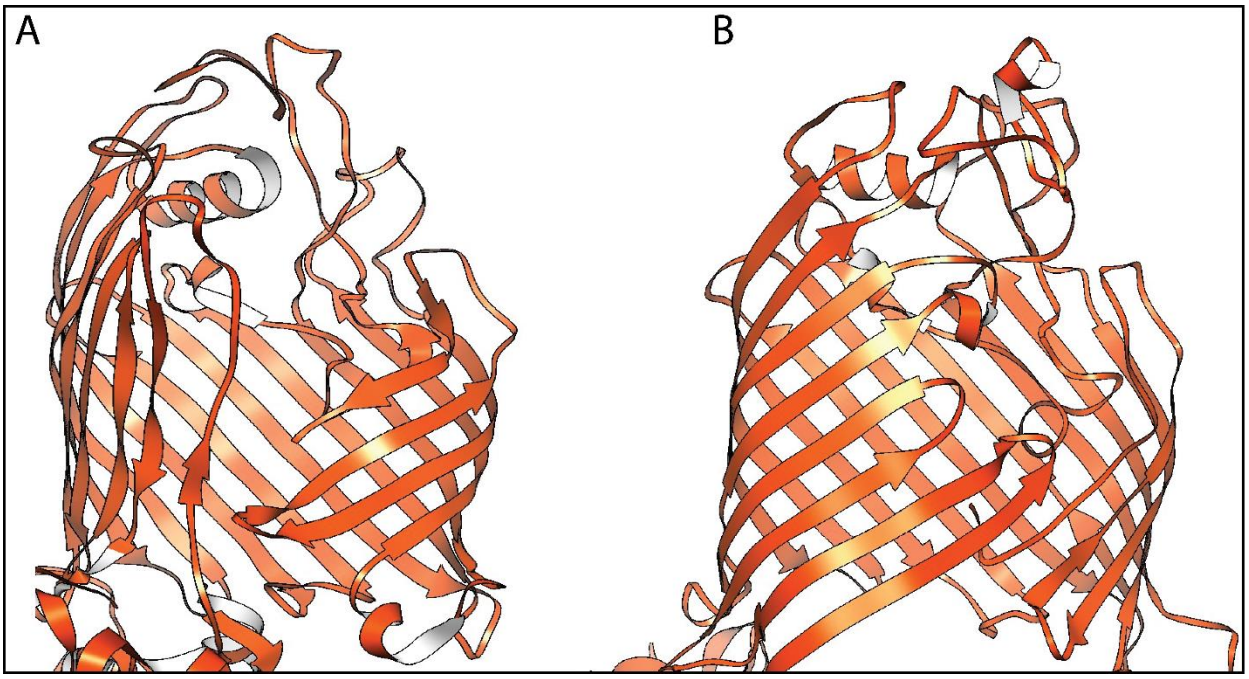

Figure 2.3 The BamA barrel in the open **(A)** and closed **(B)** conformations within the BamA complex, respectively from (Iadanza et al., 2016, Gu et al., 2016;).

As essential proteins with the ability to bind unfolded OMP substrates, BamA and BamD are considered a potential target for the development of new antibiotics (Hagan et al., 2015; Mori et al., 2012). In order to investigate protein/ligand interaction as high resolution, liquid-state NMR spectroscopy is a powerful tool in the arsenal of structural biology, however chemical shift assignments are required to obtain atomical resolution information the binding. While, BamC and BamE were previously assigned (Knowles et al., 2009b, 2010), BamB, BamD and BamA assignments are unavailable, because of limitations in the quality of the sample for NMR-spectroscopy and size-restrictions. A milimolar concentrated sample of protein is usually required for triple-resonance backbone experiments for assignment, but BamD, had been found to be unstable and precipitate at high concentrations (Albrecht and Zeth, 2010) and BamA spectral quality decreased with concentration (Morgado et al., 2015). Additionally, BamA constitutes a pinnacle in the limitations for backbone assignment of membrane proteins because of its mass (43 kDa) and molecular crowding (389 residues).

2.2 Summary

To investigate the interaction of BamD with unfolded substrate at atomic resolution, assignment of at least part of the protein for NMR spectroscopy is essential. However, the preparation of a BamD sample suitable for assignment was limited by its intrinsic instability. The protein was found to precipitate when concentrated despite many buffer conditions tested, implying that the surface of BamD must interact with a partner to be stable. The interaction of BamC with BamD was studied by NMR titration of the full-length [U-^{2}H-^{15}N]-BamC with BamD. Signals from the N-terminus of BamC dwindled upon adding BamD, showing that the N-terminus region of BamC is involved with the binding of BamD. A microscale thermophoresis experiment was performed and characterized the affinity constant K_d to be 17 µM between the two partners. It was hypothesized that BamD required to bind the N-terminus of BamC to keep to protein soluble at higher concentrations and a hybrid construct was designed, encompassing the N-terminus of BamC and BamD, separated by a flexible linker in order to maintain the protein soluble at higher concentrations. After optimizing the buffer conditions, it was found that the hybrid protein requires an absence of salt for its concentration to be able to reach 620 µM and yield a NMR spectrum with a quality suitable for triple resonance backbone assignment experiments.

2.3 Results

The expression and purification of BamB, BamC, BamD and BamE was performed using previously established protocols (Kim and Paetzel, 2011; Kim et al., 2011a, 2011b; Knowles et al., 2011; Neer et al., 1994; Noinaj et al., 2011b; Warner et al., 2011). BamB, BamC, BamD and BamE were expressed and purified for NMR spectroscopy and 2D [^{1}H, ^{15}N]-TROSY experiments were recorded (**Figure 2.4 to Figure 2.7**). During the purification process of BamC, the protein was found to be sensitive to proteases, and the samples were supplemented with protease inhibitors. During BamD purification, it was noticed that the protein is unstable and degrades swiftly. Moreover, wild-type BamD could not be concentrated above 150 µM without precipitating. We however noticed that a concentration of 1 M Urea allowed to concentrate BamD up to 250 µM while reducing the precipitation process. We therefore attempted to record 3D experiment in order to start the backbone assignment of BamD for NMR spectroscopy. Unfortunately, the combination of protein precipitation over the course of the HNCA and HN(CA)CB experiments, and the relatively low concentration, yielded only a limited amount of C_α and C_β peaks and was not enough to assign any portion of the protein.

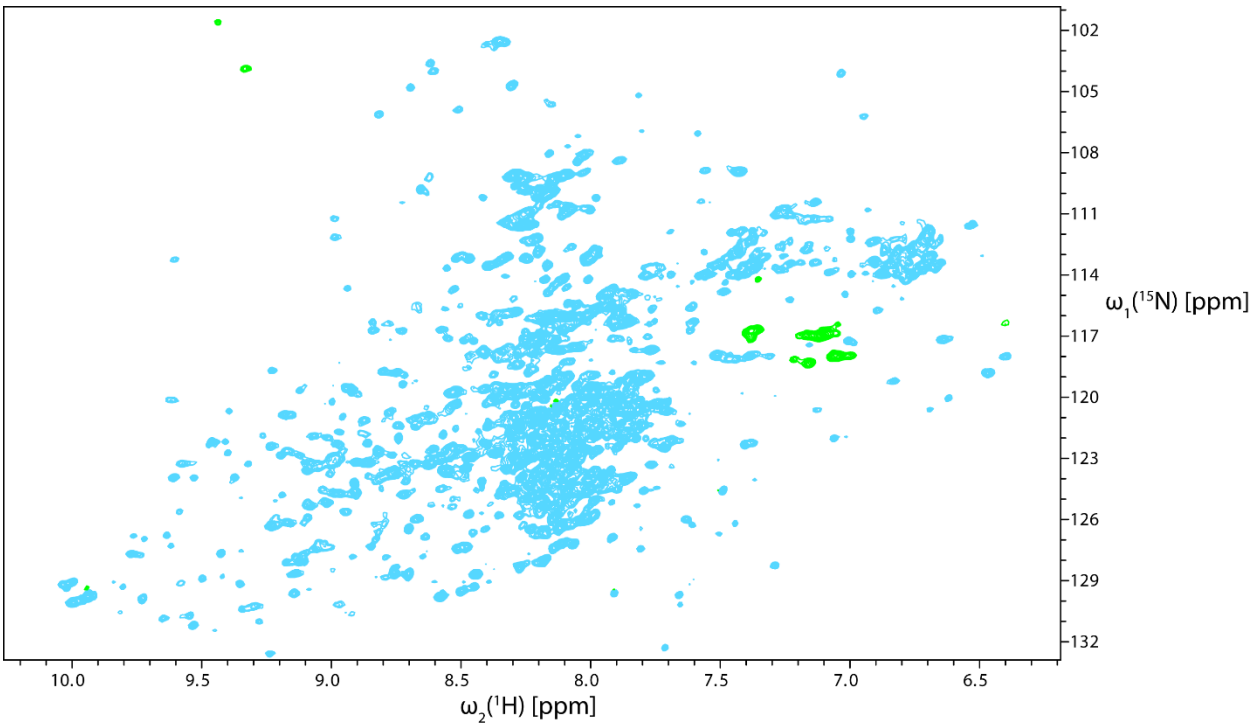

Figure 2.4 2D [^{15}N, ^{2}H]-TROSY of [U-^{2}H,^{15}N]-BamB at 50 µM in 0.05 M NaPi ,50 mM NaCl pH 6 at 30 °C. BamB has 373 residues. The spectral quality is poor. No assignment of this protein is available.

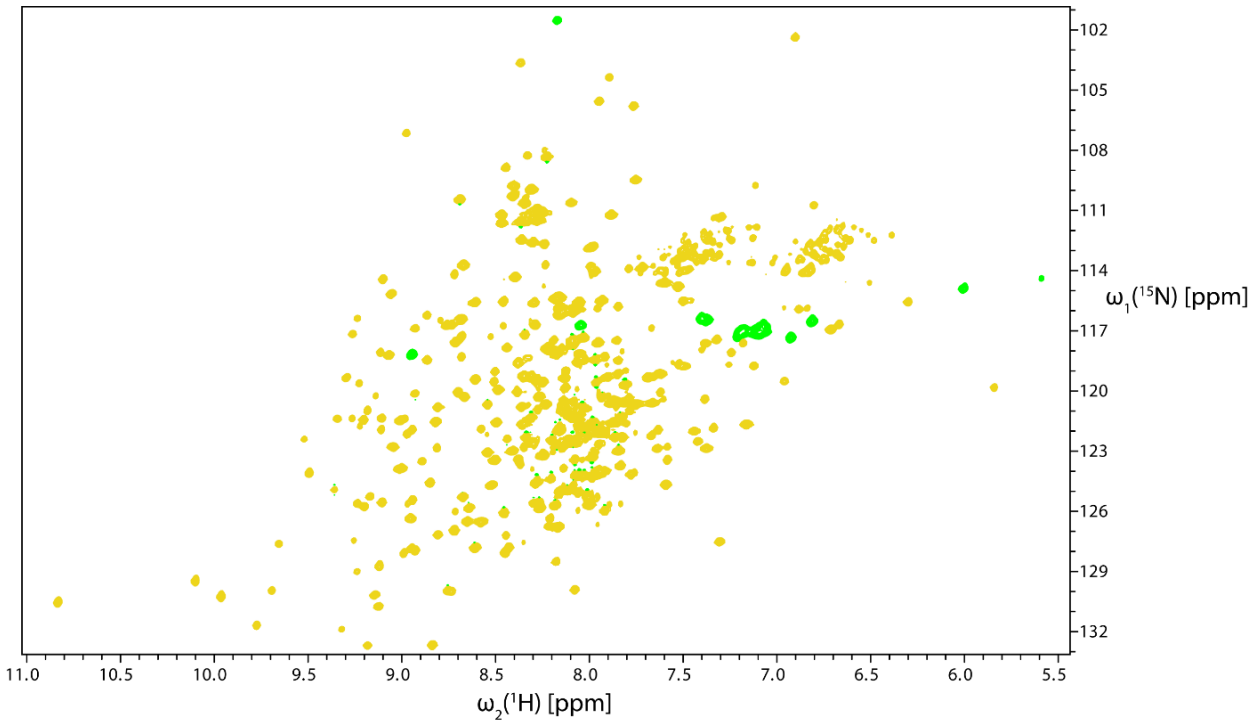

Figure 2.5 2D [^{1}H,^{15}N]-TROSY of [U-^{2}H,^{15}N]-BamC at 150 µM in 0.05 M NaPi 50 mM NaCl pH 6 at 30 °C. The assignment is available (Knowles et al., 2009).

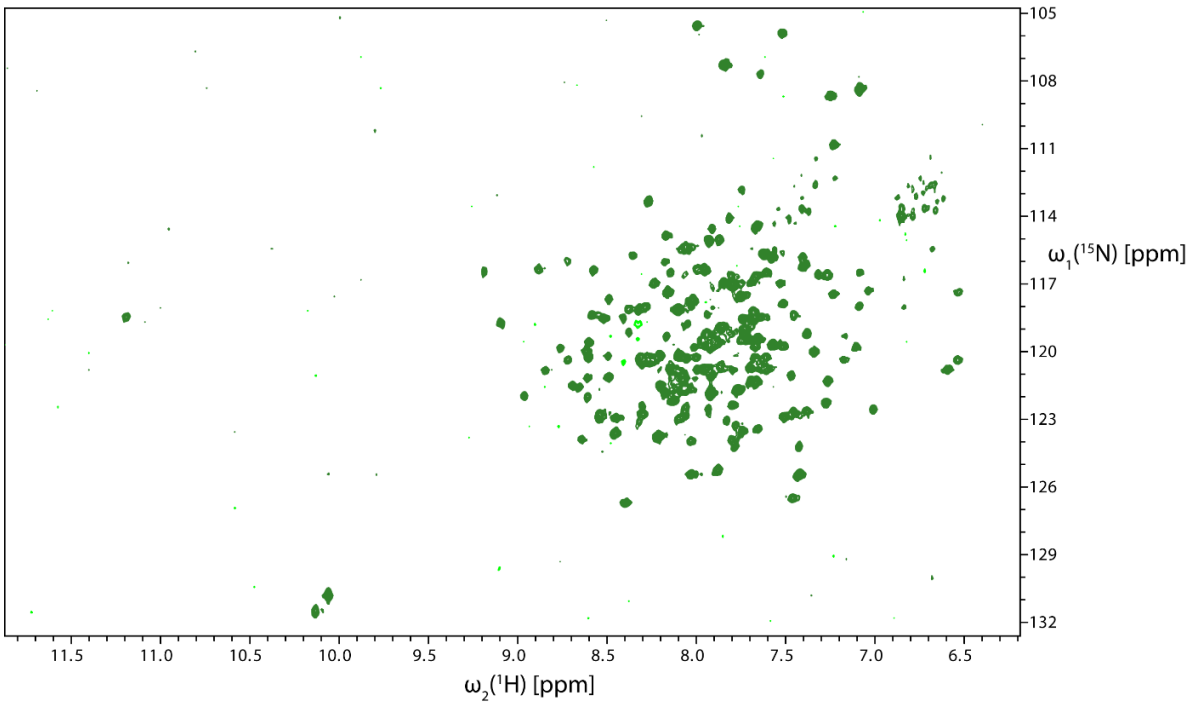

Figure 2.6 2D [^{1}H,^{15}N]-TROSY of [U-^{2}H,^{15}N]-BamD at 80 µM in 20 mM Tris pH 8, 150 mM NaCl at 30°C. Unlike BamC and BamD, the assignment of BamD is unavailable, due to its instability.

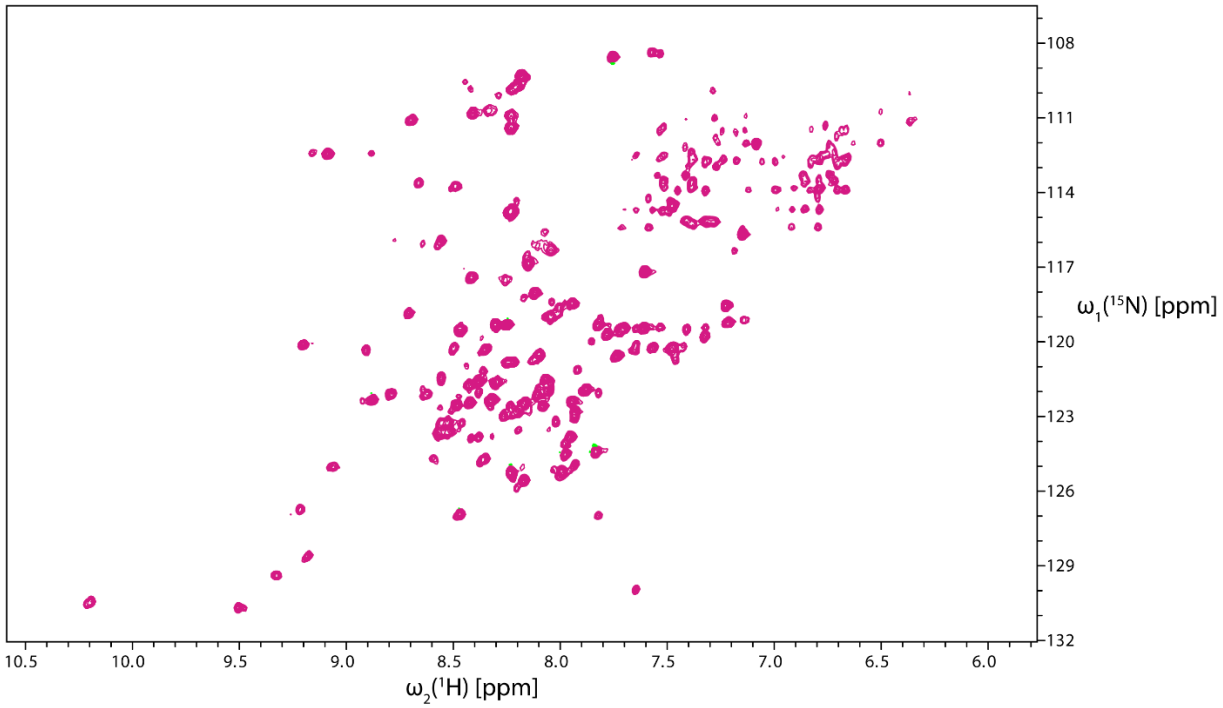

Figure 2.7 2D [^{1}H,^{15}N]-TROSY of monomeric [U-^{2}H,^{15}N]-BamE at 40 µM in 50 mM NaPi pH 7, 50 mM NaCl at 30 °C. The monomer of BamE was selected by SEC chromatography. The assignment is available (Knowles et al. 2010).

The titration of a 80 µM sample of [^{2}H,^{15}N]-BamC in the absence and presence of 150 µM of [^{1}H, ^{14}N]-BamD (**Figure 2.8 A**) was performed. The data was analyzed using the available assignment of BamC (Knowles et al., 2009b). No significant chemical shift difference (CSD) was observed. However, the signal to noise ratio diminished for the peaks of BamC located in the N-terminus region (**Figure 2.8 B**), showing that the binding occur in the intermediate exchange (Kleckner and Foster, 2011) and that the N-terminus of BamC is involved in the interaction with BamD. Because no assignment of BamD is available, it was not possible to analyze the titration of [^{2}H,^{15}N]-BamD and unlabeled BamC with NMR spectroscopy. The residues of BamC involved in the interaction with BamD are colored in red on the structure of the BamABCDE complex (**Figure 2.8 C**).

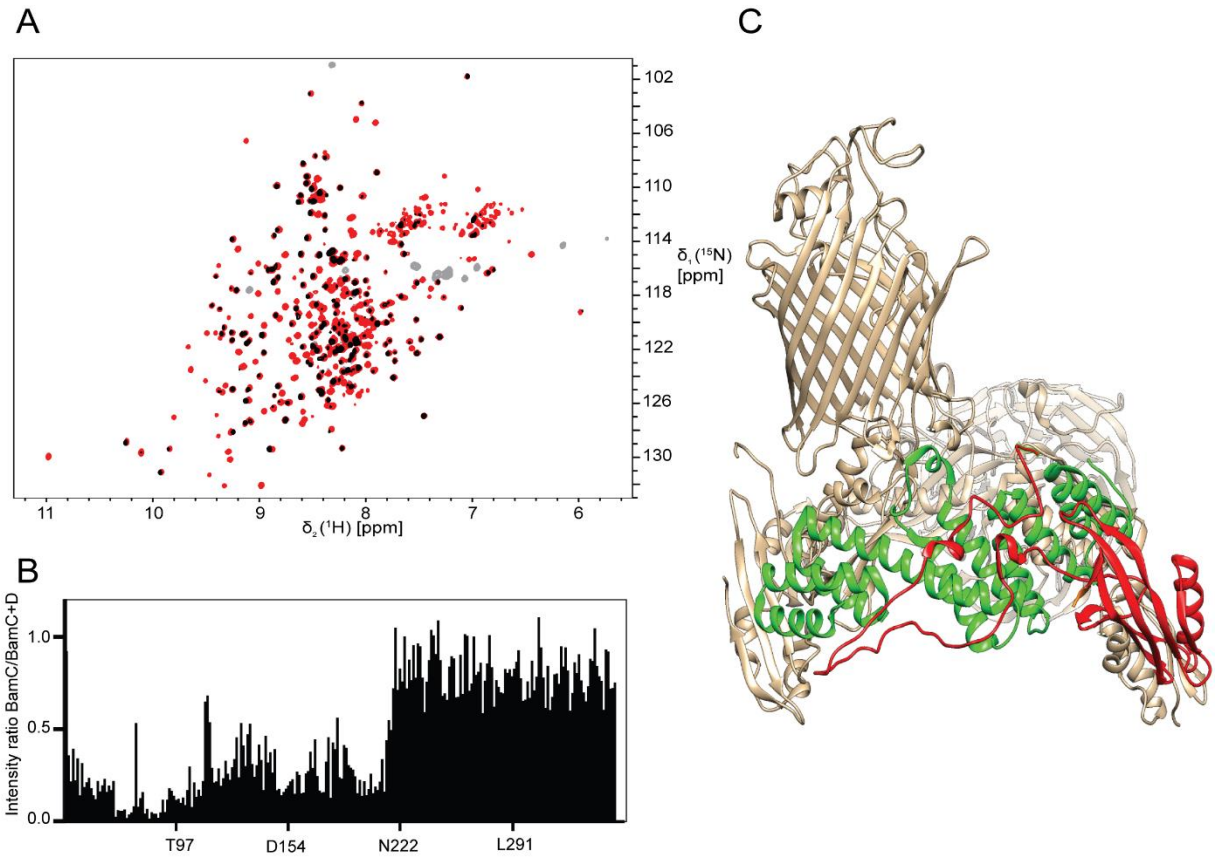

Figure 2.8 A) 2D [^{1}H,^{15}N]-TROSY of [U-^{2}H,^{15}N]-BamC at 80 µM in the absence (red) and presence (black) of 150 µM of [^{1}H, ^{14}N]-BamD in 50 mM NaPi pH 6, NaCl 50 mM at 30 °C. **B**) Intensity ratio of the peaks were calculated for the free form and the bound form of BamC and plotted. Upon the addition of BamD, peak intensities of BamC are drastically reduced in its N-terminus region showing that the N-terminus domain of BamC binds to BamD. **C**) Crystal structure of the BamABCDE complex (Iadanza et al., 2016). BamC residues that interact with BamD are colored in red.

When looking at the crystal structure of the BamABCDE complex (Iadanza et al, 2016), there is no electron density for the C-terminus region of BamC. The authors confirmed the presence of

the full-length BamC in the preparation to be crystallized. The absence of electron density in the structure was explained by the flexibility of the N-terminus region of BamC.

Afterwards, microscale thermophoresis (MST) (Jerabek-Willemsen et al., 2014), was used to measure the affinity of binding between BamC and BamD (**Figure 2.9**). The dissociation constant was found to be 17 µM.

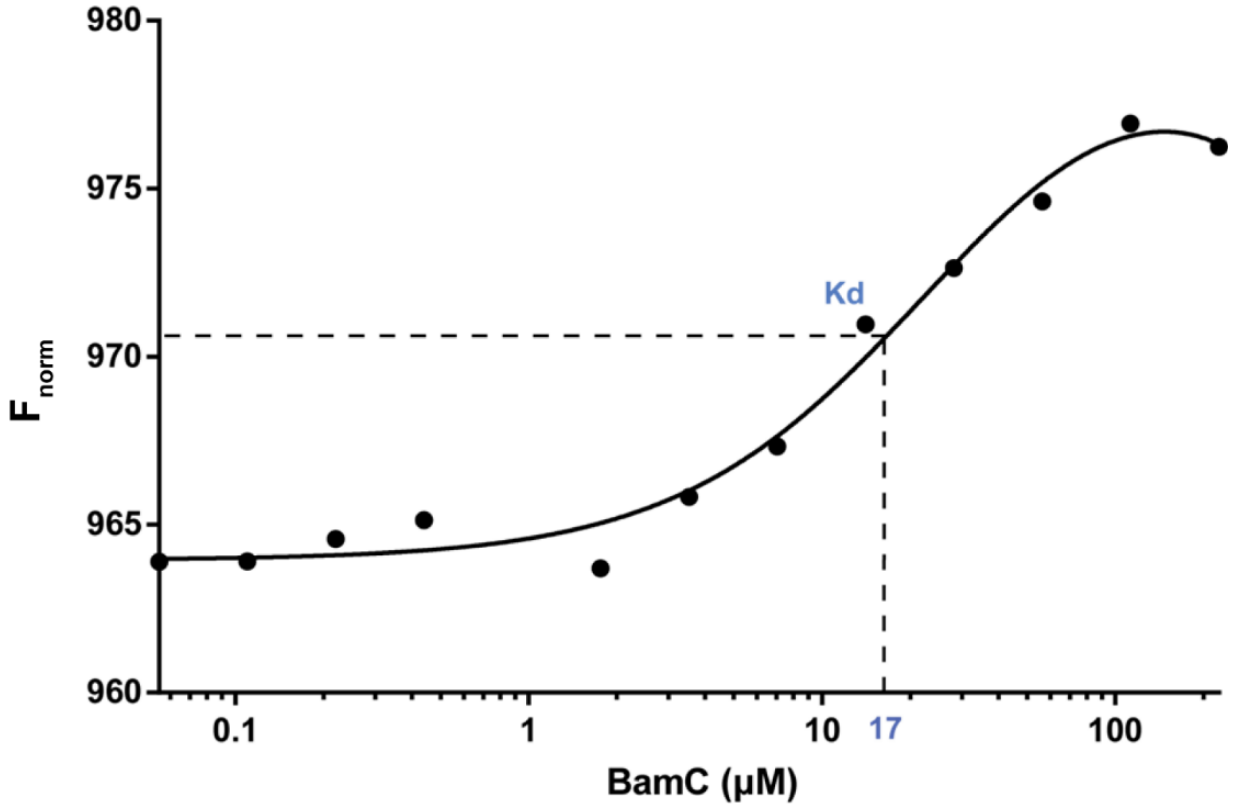

Figure 2.9 Plot of the BamC titration with BamD performed by microscale thermophoresis in buffer 20 mM Tris pH 8, 100 mM NaCl. BamD binds on BamC N-terminus with a micromolar affinity.

After establishing the BamC-BamD interaction, it was realized that the BamD instability might be caused by its BamC binding surface being unoccupied. To circumvent this issue, a construct designed to encompass BamD (29-245) and the N-ter of BamC (26-217) separated by a flexible linker (GGGSGG) was fused in a single protein (refer to appendix). The flexible linker still allows for structural flexibility between the two domains while avoiding artificial constrains of distance or orientation between the proteins. Purification of the hybrid protein was performed without degradation or precipitation, showing the necessity for BamC N-ter to protect the surface of BamD from self-interactions. The sample of the hybrid protein could be concentrated up to 2 mM, but the quality of the NMR spectrum was rapidly degrading when over 150 µM which is insufficient for backbone assignment experiments. Dynamic light scattering (DLS) is a method to measure

the size and size distribution of molecules in solution (Stetefeld et al., 2016; Yu et al., 2013). The Brownian motions of proteins in solution yield fluctuations in the intensity of laser light, scattered by the sample. The BamC-BamD hybrid protein sample was measured with DLS to evaluate its monodispersity at various concentrations. As visible in **Figure 2.10**, the size distribution increased with the concentration, indicating the formation of soluble aggregates.

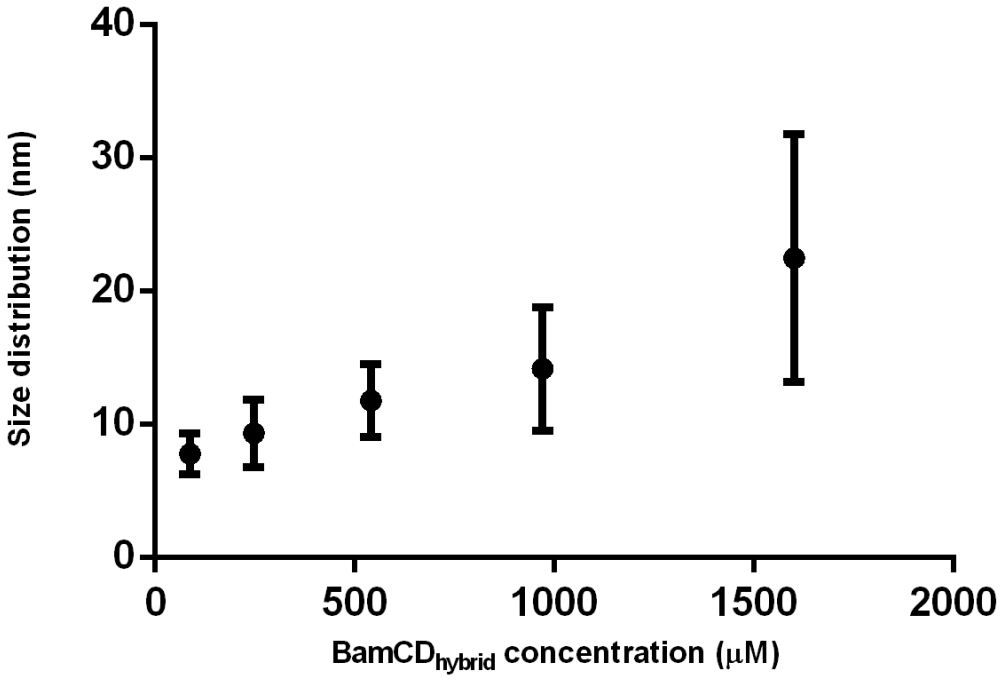

Figure 2.10 Plot of the size distribution measured from samples of various concentrations of the fused BamC$_{Nter}$-BamD protein by dynamic light scattering in 20 mM Tris pH 8, 150 mM NaCl. The size distribution increases with the concentration, indicating the formation of soluble aggregates.

As was reported in the literature, some proteins are more soluble with the least amount of salt possible, or even in pure water (Song, 2009). After a buffer optimization procedure, a salt-free buffer with a very low concentration of buffer and low pH (4 mM MES pH 4.6) allowed the protein to be concentrated to 620 µM yielding a high quality NMR-spectrum suitable for NMR triple-labeled backbone experiments (**Figure 2.11**). To evaluate the importance of the pH on the spectrum, a sample was recorded at pH 8, and displayed a poor quality (**Figure 2.12**).

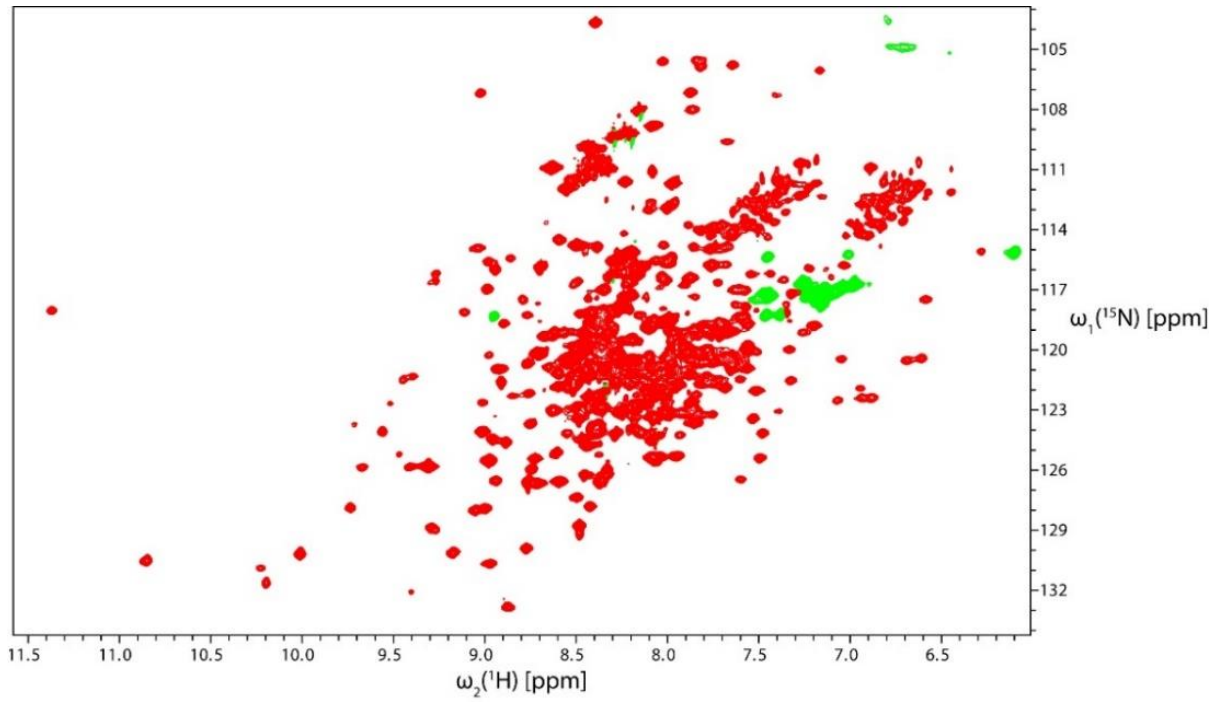

Figure 2.11 2D [^{1}H,^{15}N]-TROSY of [U-^{2}H,^{15}N]-(Nter)-BamC-GGGSGG-BamD at 620 µM in 4 mM MES pH 4.6 at 37°C.

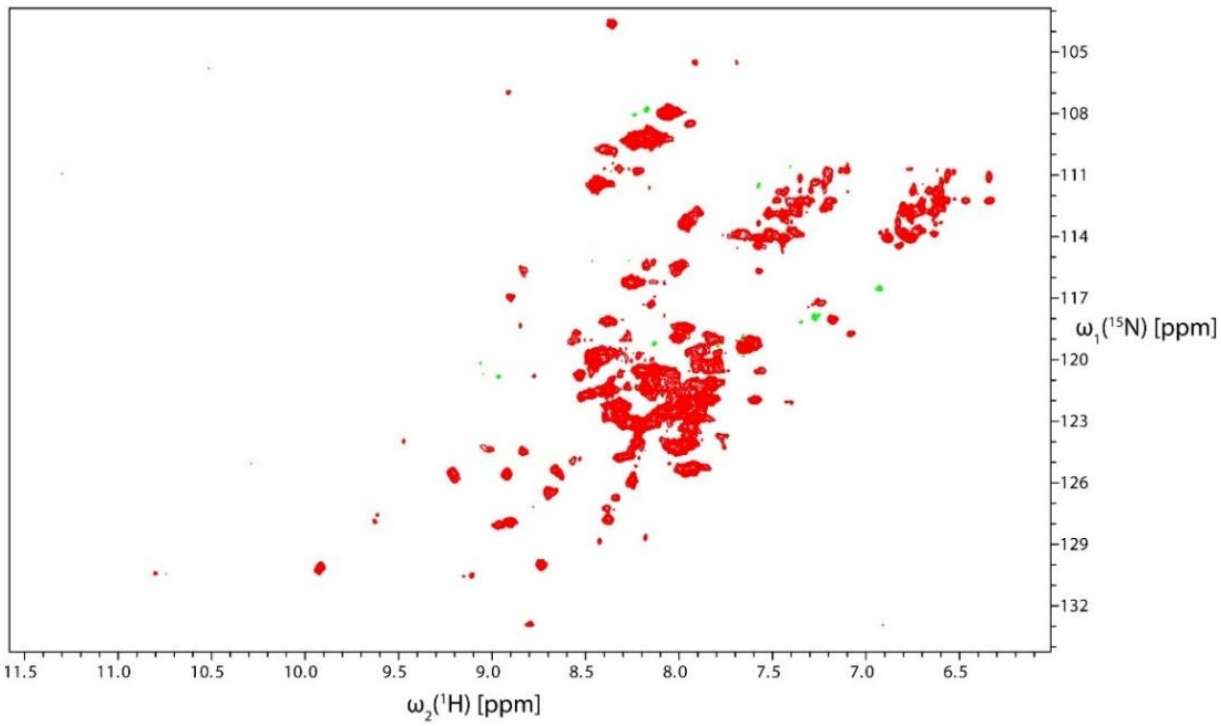

Figure 2.12 2D [^{1}H,^{15}N]-TROSY of [U-^{2}H,^{15}N]-(Nter)-BamC-GGGSGG-BamD at 620 µM in 4 mM Tris pH 8 at 30 °C.

An overlay between the spectra of BamD and the BamC-BamD hybrid protein shows that the chemical shifts belonging to the BamD protein are very well overlapping, demonstrating the possibility to assign the backbone residues belonging to BamD by recording 3D experiments on this construct (**Figure 2.13**).

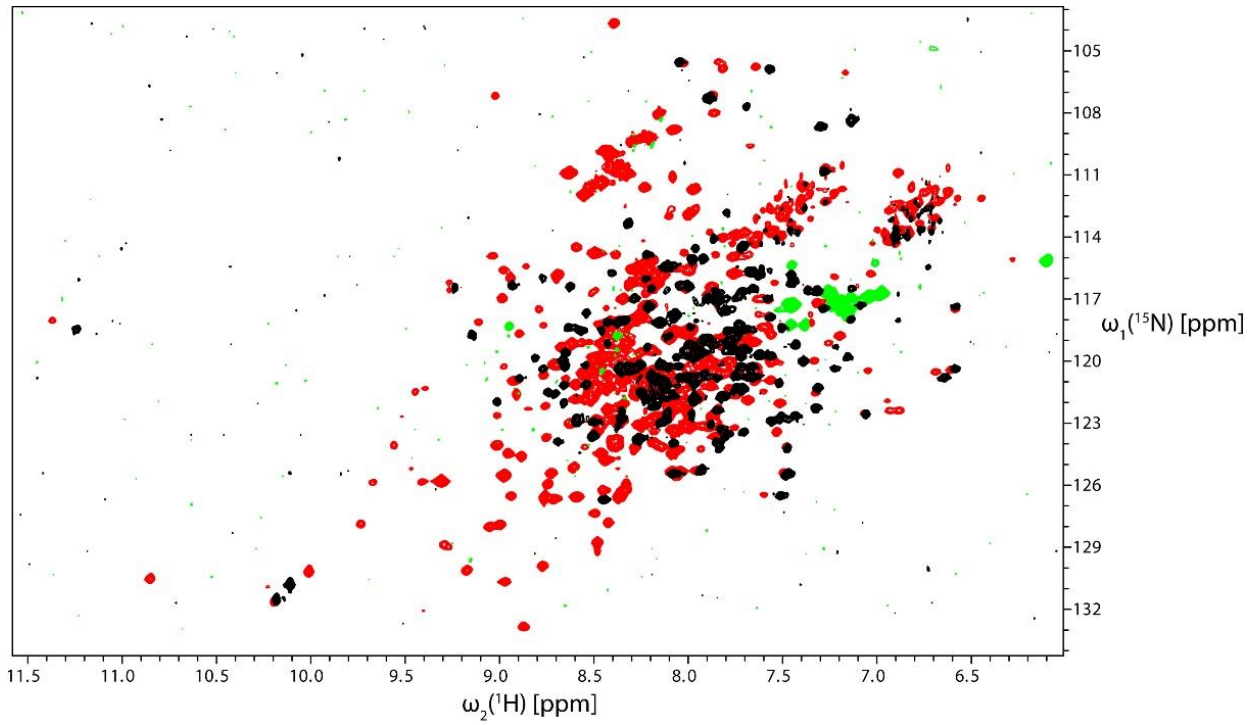

Figure 2.13 2D [^{1}H,^{15}N]-TROSY of [U-^{2}H,^{15}N]-(Nter)-BamC-GGGSGG-BamD at 620 µM in 4 mM MES pH 4.6 at 37 °C in red and [U-^{2}H,^{15}N]-BamD at 80 µM in 20 mM Tris pH 8, 150 mM NaCl at 30 °C in black. BamD contains 217 residues.

It was shown that BamD binds to unfolded OMPs substrates in vitro, including OmpA and BamA (Hagan et al., 2013). The β-signal is a conserved motif of OMPs which is recognized by assembly machineries, including the Bam complex (Robert et al., 2006). A peptide containing this β-sequence was shown to inhibit the β-barrel assembly machinery in vivo by binding with BamD (Hagan et al., 2015). In order to verify this potential binding, a peptide containing the β-signal of BamA was designed with the sequence SAGIALQWMS. A titration of [U-^{2}H,^{15}N]-BamD with an equimolar amount of peptide was performed. No CSD or intensity was observed upon addition of peptide (**Figure 2.14**).

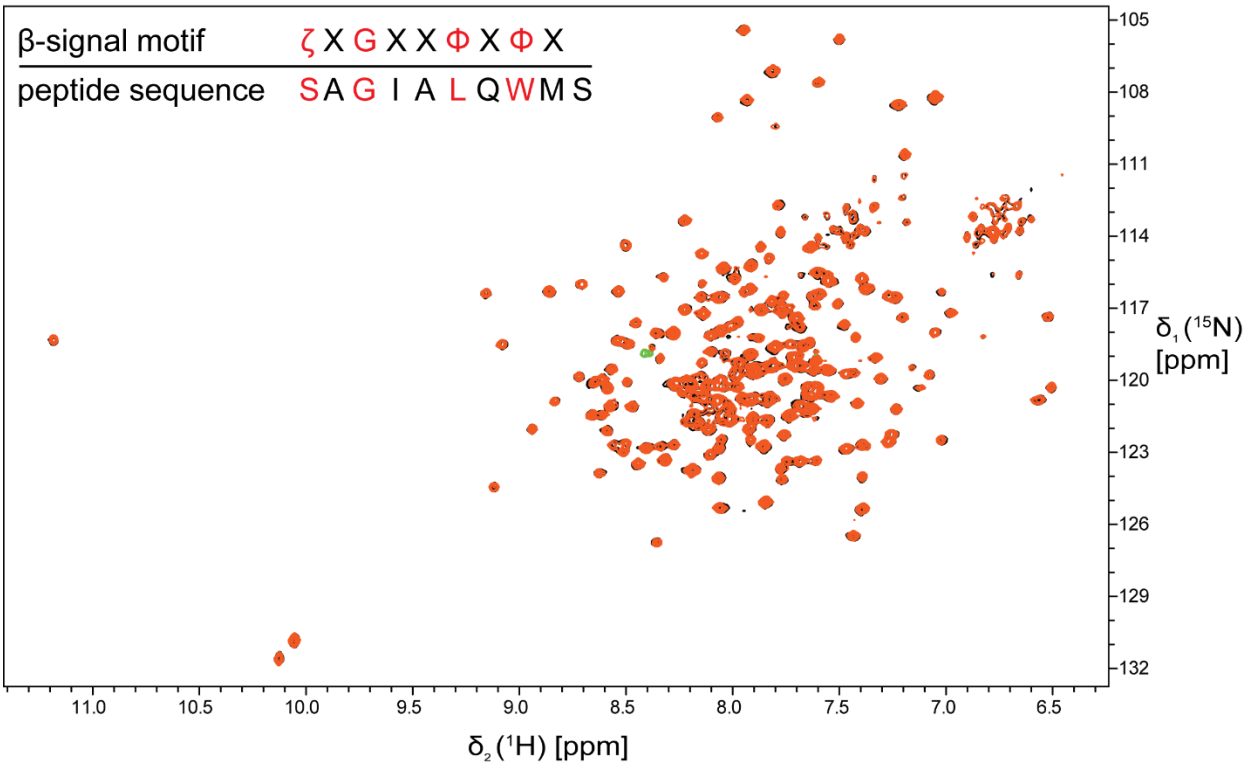

Figure 2.14 2D [^{1}H,^{15}N]-TROSY of [U-^{2}H,^{15}N]-BamD at 60 µM in 20 mM Tris pH 8, 300 mM NaCl, 6% DMSO at 30 °C in black and [U-^{2}H,^{15}N]-BamD at 60 µM + SAGIALSWMS peptide at 60 µM in 20 mM Tris pH 8, 300 mM NaCl, 6% DMSO at 30°C in orange.

2.4 Discussion

As a conclusion, the BamB, BamC BamD and BamE were expressed, purified and measured by NMR spectroscopy. The binding of BamD with the N-terminus domain of BamC was demonstrated with NMR spectroscopy. Their affinity constant was determined to be 17 µM with MST and it was discovered that BamD stability is conditioned by its interaction with BamC. As a result of this observation, a hybrid construct formed of BamD and $BamC_{Nter}$ was designed. In order to enable the possibility of assigning the backbone of BamD, the buffer conditions were optimized to keep the hybrid protein sample monodisperse and aggregation-free at high concentrations. In the spectrum of this hybrid protein, we can identify the peaks belonging to BamD. Because the backbone assignment of $BamC_{Nter}$ is available, the remaining peaks in the spectrum are belonging to BamD. The next steps will be to record triple-labeled experiments (HNCA, HNCACB…) to perform the sequential assignment of the BamD protein. This will set a plateform to study the function and interactions of BamD by liquid-state NMR spectroscopy at atomic resolution. As a

follow-up strategy, it would be useful to obtain the assignment of the methyl side-chains of BamD, as a mean to study its role within a reconstituted Bam complex. The titration of BamD with a potential binding peptide was tried without success.

2.5 Materials and methods

Expression and purification

BamB was expressed and purified according to Kim and Paetzel, 2011. Cells were grown in M9 media supplemented with $^{15}NH_4Cl$ and 99.9 % D_20. The size-exclusion chromatography step was performed in the NMR buffer (50 mM NaPi pH 6, 50 mM NaCl). The protein was concentrated to 50 µM and the sample was supplemented with 5 % D_2O prior to NMR spectroscopy. BamC was expressed and purified according to Albrecht and Zeth, 2010. The his-tag was not cleaved off. For NMR spectroscopy, cells were grown in M9 media supplemented with $^{15}NH_4Cl$ and 99.9 % D_2O, otherwise they were grown in LB. The size-exclusion chromatography step was performed in the NMR buffer (0.05 M NaPi pH 6, 50 mM NaCl). The protein was concentrated to 150 µM and the sample was supplemented with 5 % D_2O prior to NMR spectroscopy. BamD was expressed and purified according to Albrecht and Zeth, 2010. The his-tag was not cleaved off. For NMR spectroscopy, cells were grown in M9 media supplemented with $^{15}NH_4Cl$ and 99.9 % D_20, otherwise they were grown in LB. The size-exclusion chromatography step was performed in the NMR buffer (20 mM Tris pH 8, 150 mM NaCl). For NMR, the protein was concentrated to 80 µM and the sample was supplemented with 5 % D_2O. BamD was noticed to be unstable over time and precipitate. BamE was expressed and purified according to Albrecht and Zeth, 2010. The his-tag was not cleaved off. Cells were grown in M9 media supplemented with $^{15}NH_4Cl$ and 99.9 % D_2O. The size-exclusion chromatography step was performed in the NMR buffer (50 mM NaPi pH 7, 50 mM NaCl). Like Kim et al., 2011b, the BamE protein eluted as a mixture of monomer and dimer from the size exclusion column. The fraction corresponding to the monomer was pooled and concentrated to 40 µM and the sample was supplemented with 5% D_2O prior to NMR spectroscopy. (Nter)-BamC- GGGSGG–BamD hybrid plasmid was transformed in BL21 (LEMO) strain. Cells were grown in M9 media supplemented with $^{15}NH_4Cl$ and 99.9 % D_2O until OD_{600} reached 0.6 and induced with 0.4 mM IPTG. Protein was expressed O/N at 20 °C. Cells were resuspended in 20 mM Tris pH 8, 150 mM NaCl (Buffer A) supplemented with 20 mM imidazole and supplemented with EDTA-free complete protease inhibitor cocktail, DNase I and lysozyme. Cells were broken by sonicating on ice and centrifuged. The soluble fraction was passed on a HisTrap HP 5mL column. The column was washed with 10 CV of Buffer A, 10 CV of Buffer A +

50 mM Imidazole and eluted with 5 CV of Buffer A + 500 mM Imidazole. The protein was concentrated with a 30 kDa cut-off Vivaspin concentrator and injected into a Superdex S75 100/300 GL column for size exclusion chromatography with 4 mM MES pH 4.6. The protein was concentrated to 620 µM for NMR spectroscopy. For storage, proteins were flash frozen in liquid nitrogen and conserved in a -80 °C freezer.

MST

In a temperature gradient, molecules movement depends on their size, charge and hydration shell (Duhr and Braun, 2006). When binding to another protein, those parameters can vary, changing the way the protein moves along the gradient. Fluorescence is monitored over time. As, the laser heat up the capillary, fluorescence decreases because of the fluorophore quantum yield decreasing with temperature, after that point, fluorescence decrease is driven by thermophoresis effects. After 30 s the laser is turned off. Fluorescence values are measured before the laser is turned off for all the titrations points and are corrected for the fluorescence decrease caused by the quantum yield effect. Points are plotted as normalized fluorescence values over the partner concentration to calculate the K_d.

Purified BamD was dialyzed in a 0.5 mL Slide-A-Lyzer cassette with a 10 kDa MWCO and dialyzed against 1.25 L of 0.1 M NaPi pH 6.6, 0.15 M NaCl at 4 °C. After 4 h of dialysis, the buffer pool was replaced, four times in total. The protein was then incubated 1 h at 4°C with a ten-fold molar excess of DyLight 488 NHS-Ester fluorescent dye. The sample was then dialyzed O/N at 4 °C in a 0.5 mL Slide-A-Lyzer cassette with a 10 kDa cut-off against 2L of 20 mM Tris, 100 mM NaCl. The buffer pool was changed two times for two additional steps of dialysis of 4 H. BamC (26-344) was eluted from the S75 size exclusion chromatography column with 20 mM Tris, 100 mM NaCl buffer. Samples were measured on a nanoTemper monolith instrument. The concentration of labeled BamD was set at 40 nM and titrated with a range of BamC concentrations (225 µM, 112 µM, 56 µM, 28 µM, 14 µM, 7 µM, 3.5 µM, 1.75 µM, 440 nM, 220 nM, 110 nM, 55 nM). The curve was fitted and the K_d was determined at the concentration of half of the normalized fluorescence response.

DLS

The (Nter)-BamC- GGGSGG–BamD hybrid protein was concentrated to 1.6 mM in 20 mM Tris pH8, 150 mM NaCl. A series of samples was prepared at different concentrations (1.6 mM, 0.97 mM, 0.54 mM, 0.27 mM, 87 µM). Experiments were measured on a nanoTemper monolith,

Malvern Instruments Zetasizer Nano ZS Dynamic Light Scattering Instrument. The size distribution was plotted against the concentration.

NMR spectroscopy

The 50 µM sample of [U-^{2}H, ^{15}N]-BamB in buffer 0.05 M NaPi ,50 mM NaCl pH 6.5 was measured with a 2D [^{1}H,^{15}N]-TROSY HSQC at 30 °C experiment on a 700 MHz spectrometer and 32 scans. The transmitter frequency offset was set on 4.74 ppm for the proton and 117 ppm for the ^{15}N with spectral widths of 16 ppm and 32 ppm respectively and recorded with 256 points for the indirect dimension and 2048 points for the direct dimension. The 150 µM sample of [U-^{2}H, ^{15}N] BamC in buffer 0.05 M NaPi, 50 mM NaCl pH 6 was measured with a 2D [^{1}H,^{15}N]-TROSY HSQC at 30 °C experiment on a 700 MHz spectrometer and 166 scans. The transmitter frequency offset was set on 4.7 ppm for the proton and 117 ppm for the ^{15}N with spectral widths of 16 ppm and 32 ppm respectively and recorded with 256 points for the indirect dimension and 2048 points for the direct dimension. The 80 µM sample of [U-^{2}H, ^{15}N] BamD in buffer 20 mM Tris pH 8, 150 mM NaCl was measured with a 2D [^{15}N, ^{1}H]-TROSY HSQC at 30 °C experiment on a 700 MHz spectrometer and 48 scans. The transmitter ^{15}N frequency offset was set on 4.7 ppm for the proton and 117 ppm for the ^{15}N with spectral widths of 16 ppm and 32 ppm respectively and recorded with 256 points for the indirect dimension and 2048 points for the direct dimension. The 40 µM sample of [U-^{2}H, ^{15}N] BamE in buffer 50 mM NaPi pH 7, 50 mM NaCl was measured with a 2D [^{1}H,^{15}N]-TROSY HSQC at 30 °C experiment on a 700 MHz spectrometer and 48 scans. The transmitter frequency offset was set on 4.7 ppm for the proton and 117 ppm for the ^{15}N with spectral widths of 16 ppm and 32 ppm respectively and recorded with 256 points for the indirect dimension and 2048 points for the direct dimension.

For the titration of BamC with BamD, a 2D [^{15}N, ^{1}H]-TROSY of [U-^{2}H,^{15}N]-BamC at 80 µM in the absence and presence of 150 µM of [^{1}H, ^{14}N]-BamD was measured in 50 mM NaPi pH 6, NaCl 50 mM at 30 °C with a 700 MHz spectrometer. 230 scans were acquired for the two experiments. The transmitter frequency offset was set on 4.7 ppm for the proton and 117 ppm for the ^{15}N with spectral widths of 16 ppm and 32 ppm respectively and recorded with 256 points for the indirect dimension and 2048 points for the direct dimension. The chemical shift difference and intensity ratio between the two spectra were plotted against the sequence of BamC to determine the binding domain.

For hybrid construct between the C-ter of BamC and BamD, a 2D [^{1}H,^{15}N]-TROSY of [U-^{2}H,^{15}N]-(Nter)-BamC-GGGSGG-BamD at 620 µM was measured in 4 mM MES pH 4.6 at 37 °C with a 700 MHz spectrometer and 24 scans. The transmitter frequency offset was set on 4.7 ppm for the proton and 117 ppm for the ^{15}N with spectral widths of 16 ppm and 32 ppm respectively and recorded with 256 points for the indirect dimension and 2048 points for the direct dimension.

For the titration of BamD with the SAGIALQWMS peptide, a 2D [^{1}H,^{15}N]-TROSY of [U-^{2}H,^{15}N]-BamD was measured at 60 µM in buffer 20 mM Tris pH8, 300 mM NaCl, supplemented with 6% DMSO, a second sample was prepared with 60 µM of [U-^{2}H,^{15}N]-BamD and 60 µM peptide in buffer 20 mM Tris pH8, 300 mM NaCl, supplemented with 6% DMSO . Samples were measured at 30°C with a 700 MHz spectrometer and 80 scans. The transmitter frequency offset was set on 4.7 ppm for the proton and 117 ppm for the ^{15}N with spectral widths of 16 ppm and 32 ppm respectively and recorded with 256 points for the indirect dimension and 2048 points for the direct dimension.

All the NMR samples contained 5 % D_2O. All spectrometers were equipped with cryo-probes. For all experiments the interscan delay was set to 1 s. The spectra were processed in TopSpin and analyzed in CARA.

Chapter 3: Conformational stability of the BamA β-barrel for NMR spectroscopy and crystallization.

Michael Zahn crystallized and solved the structure of the BamA β-barrel C-terminally stabilized with 9 residues of OmpX. Leonor Morgado cloned some of the BamA constructs used in this chapter (as listed in the appendix). Irena Burmann optimized the buffer conditions for NMR measurements of the BamA-OmpX B7B8 construct, and recorded the HNCA experiment to assign the C-terminal unfolded residues of BamA-OmpX B7B8. All other work was carried by me.

3.1 Summary

As the project started, the quality of the BamA β-barrel sample was poor and did not permit to plan for an extensive assignment strategy. BamA expression, refolding and purification was optimized to obtain the best possible sample but many peaks were broad or with low signal-to-noise. The BamA β-barrel is a dynamic protein that can sample a vast conformational ensemble. To address the issue of the quality of the BamA sample for NMR spectroscopy, several strategies were employed to increase the stability of the BamA β-barrel.

In order to study the possible hybrid-barrel mechanism, several constructs were prepared, where the sixteenth strand of the BamA barrel was extended with two additional strands from one of its OMP substrate. To our surprise, the construct formed by the BamA β-barrel and the last hairpin of OmpX, led to see a high quality single spectrum by solution NMR spectroscopy. We assigned the residues from the OmpX portion with a 3D-HNCA experiment, and found that many of them when located in the unstructured region of the spectrum (proton coordinate around 8 ppm). Step by step truncations and NMR spectroscopy allowed to find the required residues to improve the barrel steadiness, allowing us to crystallize and solve the structure of the minimally C-ter extended BamA β-barrel. The structure shows that four additional hydrogen bonds are formed in the gate region, explaining the stabilization effect observed in the NMR spectrum. A point mutation scanning of the gate region was performed and the G433A mutant proved to stabilize the barrel even further, increasing the signal-to-noise of the sample up to 700 µM. However, adding the POTRA3-5 domains to the already stabilized BamA-OmpX B7B8 construct, reduced the stability of the protein, and yielded a spectra of lesser quality. While the goal of this work was to obtain an observable hybrid-barrel protein for NMR spectroscopy, it instead opened the doors for the backbone assignment of the BamA β-barrel.

3.2 Results

Previous work (Morgado et al., 2015) compared the effect of different membrane mimetics on the BamA-POTRA5 by NMR spectroscopy. It was found that the detergent N,N-Dimethyldodecylamine N-oxide (LDAO) yielded a better spectral quality over DMPC:DiC7PC bicelles and MSP1D1:DMPC nanodiscs. The optimal LDAO ratio was determined to stand between 1:200 and 1:300 BamA:LDAO. After several optimizations steps, the best buffer and temperature conditions were found to be NaPi 20 mM NaCl 150 mM at pH 7.5 0.1% LDAO and 310,15 K. At this point, the spectral quality was however not sufficient to achieve a more complete assignment of the BamA β-barrel (**Figure 3.1**) and only a portion of the loop 6 and POTRA5 was assigned.

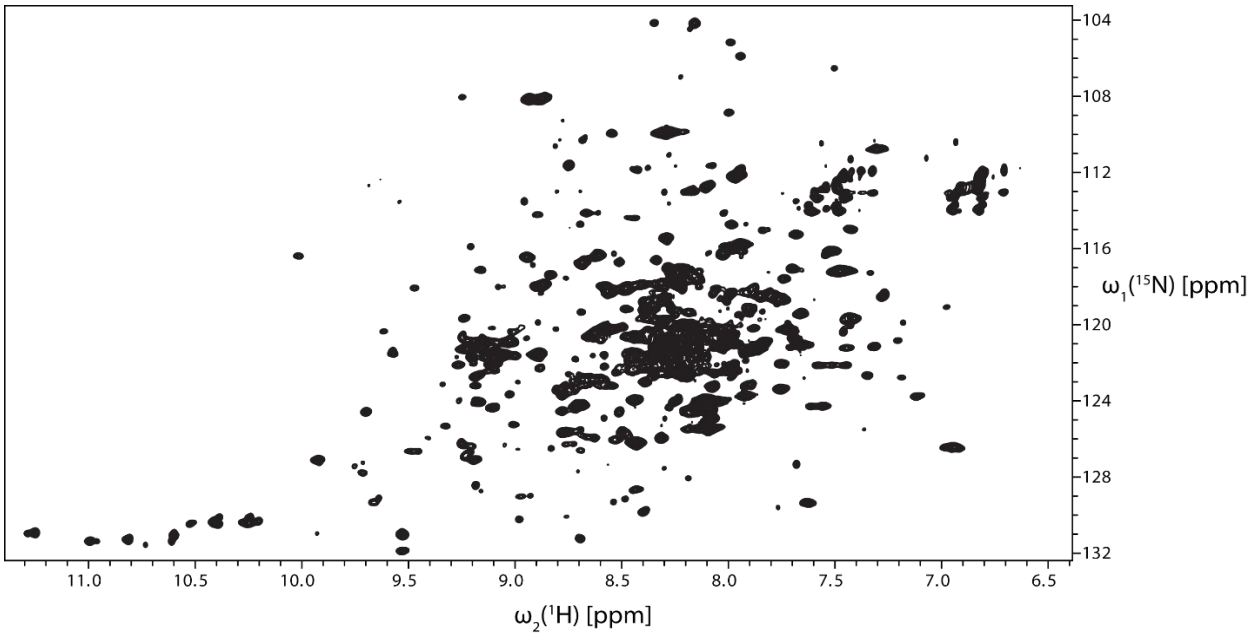

Figure 3.1 [^{15}N, ^{1}H]-TROSY-HSQC of a [U-^{2}H, ^{15}N] 500 µM sample of BamA β-barrel measured at 37 °C on a 700 MHz Bruker spectrometer in 20 mM NaPi pH7.5, 150mM NaCl 0.1 % LDAO. As visible from the figure, the distribution of intensities within the spectra is not homogeneous and some peaks are broadened. This sample was not suitable for NMR assignment. An explanation to the poor quality of the spectra is that the protein samples different conformations in solution.

The mechanism by which BamA catalyzes the insertion of OMPs into the outer membrane is still elusive. The hybrid barrel mechanism hypothesis proposes that the BamA-barrel is capable of opening to sequentially accommodate the hairpins of folding substrates by beta augmentation interaction (Remaut et al., 2006), to form a larger barrel. This hybrid barrel would progressively increase in size and diameter until no longer stable. BamA and the newly formed barrel would separate to release the OMP into the outer membrane (**Figure 3.2**).

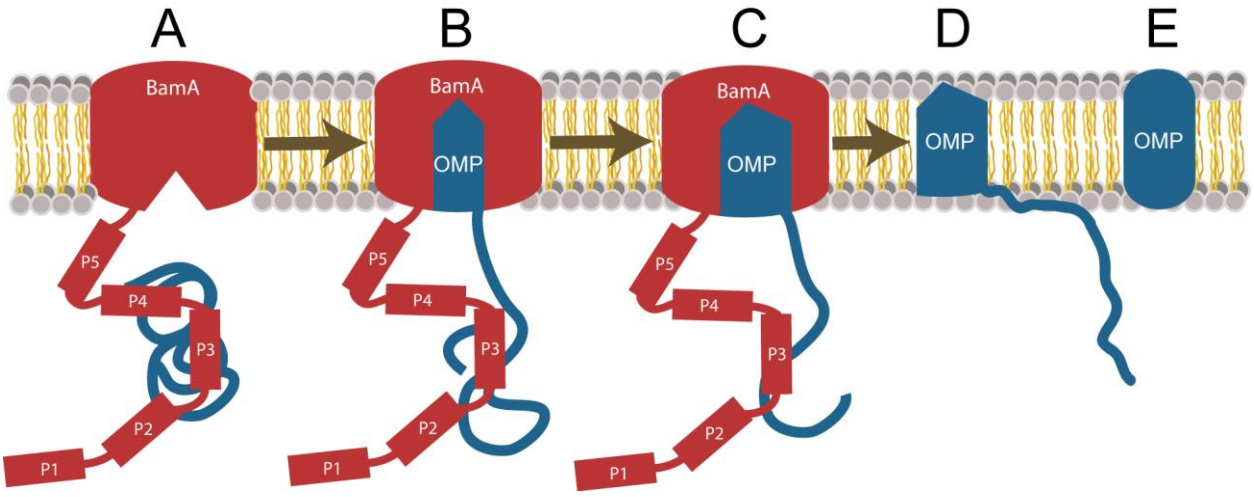

Figure 3.2 Scheme of the substrate assembly by hybrid-barrel formation mechanism. **A)** The gate region of BamA is dynamic and the BamA β-barrel can open and close. **B)** BamA recognizes the OMP substrate by its β-signal sequence and helps the folding of the first hairpin by beta augmentation interaction. **C)** The subsequent hairpins of the OMP fold. **D)** When the assembly reaches its stability threshold, the substrate is released into the outer-membrane. **E)** The substrate finishes its folding into the outer-membrane.

Following this idea, we wanted to create this hybrid by designing a protein encompassing both the BamA β-barrel, as well as a two-hairpin extension from various outer membrane proteins. Constructs containing the BamA β-barrel, followed by the two last β-strands from either of the OmpX (**Figure 3.3**), LamB or OmpF membrane protein were cloned by Leonor Morgado. Those proteins behaved very similarly to the bare BamA β-barrel during expression, refolding and purification. The [^{15}N, ^{1}H]-TROSY-HSQC spectra of those hybrid proteins were recorded. Surprisingly, the construct containing the BamA β-barrel followed by the two last β-strands of OmpX (BamA-OmpX B7B8) showed a spectrum with a much more homogeneous distribution of intensities (**Figure 3.4**). In this spectrum, many double peaks from the barrel-only construct, were singled out. Moreover, in the BamA barrel-only spectrum, many expected peaks were absent but when observing the C-terminally extended construct, chemical shifts appeared and the overall broadening of the peaks was reduced. Those observations led to the conclusion that the BamA β-barrel sample was in a dynamic state, which was hindering our ability to observe its peaks with

NMR spectroscopy and that the additional residues at the end of the barrel, stabilized one of the conformation over the other ones.

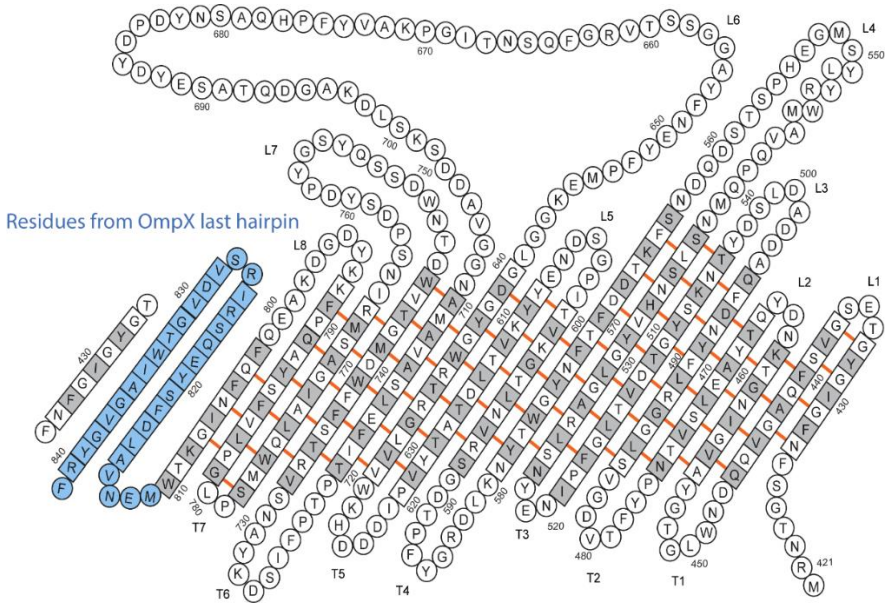

Figure 3.3 Diagram of the BamA extended β-barrel. The end of the barrel is elongated with the last hairpin from the OmpX protein. This scheme represents the hypothetical case in which the extra hairpin is folded.

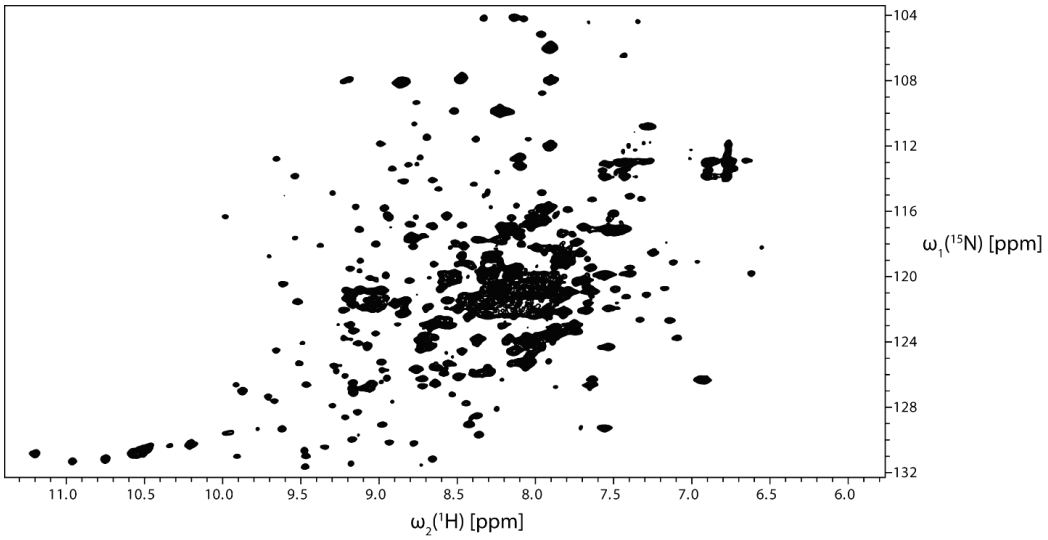

Figure 3.4 2D-[^{15}N, ^{1}H]-TROSY-HSQC of a [U-^{2}H, ^{15}N] 500 µM sample of BamA stabilized with the last hairpin of OmpX measured at 37°C on a 700 MHz Bruker spectrometer in 20 mM NaPi pH 7.5, 150 mM NaCl 0.1 % LDAO. As the BamA β-barrel is elongated with extra residues, its spectral quality drastically improves. Many peaks become visible, and the intensity distribution of the peaks is more homogeneous.

Extensive crystallization attempts of the BamA β-barrel were led without success but the increase in quality of the spectrum of the BamA-OmpX B7B8 construct provided confidence that the sample was more stable that the unextended barrel, and therefore easier to crystallize.

However, a HNCA experiment of the BamA-OmpX B7B8 protein was recorded by Irena Burmann **(Figure 3.5 A)**, and a portion of residues from the OmpX substrate was assigned. We located those assigned peaks around 8 ppm in the proton dimension, indicating those residues to be in an unstructured region of the protein. It was then clear that those amino acids did not contribute to the observed stabilization of the BamA β-barrel. Unfolded tails are known to hamper crystallization, but the exact sequence of residues to promote the stabilization was unknown. Several constructs were designed with the end of the extended barrel truncated at various positions **(Figure 3.5 B)** and measured by NMR spectroscopy **(Figure 3.6)** in order to find the minimal number of residues responsible for the stabilization effect. To accurately determine the spectral quality of those different constructs, the intensity of each peak was measured and the intensity distribution was compared for each spectrum **(Figure 3.7)**. For the peaks of the BamA β-barrel the distribution is widely spread between large and low intensities. On the other hand, for the BamA-OmpX B7B8 protein, the distribution is narrower with a much higher average intensity indicating a higher signal-to-noise over a larger number of residues.

Then, we compared the distribution of intensities of the constructs where the C-terminal extension was iteratively shorter. The distribution of intensities for the construct BamA-OmpX B7B8 A815stop was similar to the one of the BamA β-barrel, whereas the distribution from the constructs BamA-OmpX B7B8 Y820stop, BamA-OmpX B7B8 S827stop and BamA-OmpX B7B8 T832stop was similar to the construct BamA-OmpX B7B8. The conclusion was that only nine additional residues from OmPX were required at the C-terminus of BamA β-barrel to stabilize it.

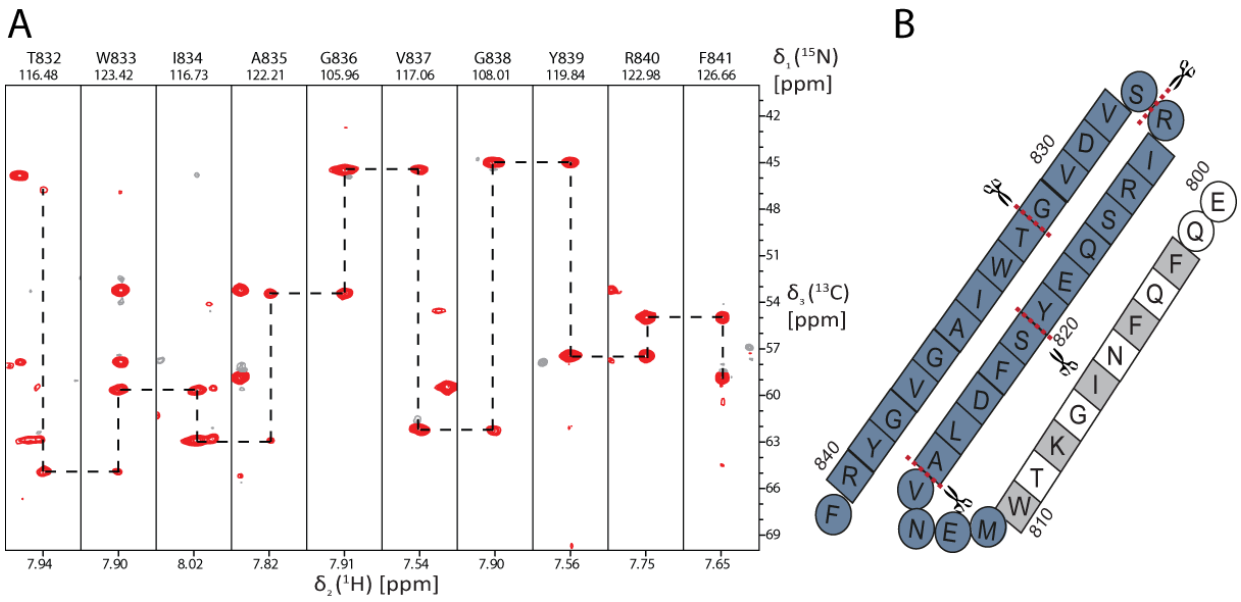

Figure 3.5 A) Strips of the 3D-HNCA experiment recorded on the BamA barrel extended with the last hairpin of OmpX. Those peaks were found in the unfolded region of the spectrum, showing that the residues from OmpX were not forming an extra hairpin at the end of the barrel. **B)** Representation of the C-terminus of the BamA-barrel, four truncated constructs were measured to determine the minimal number of residues required to stabilize the BamA β-barrel.

In a collaboration with Michael Zahn, crystals of the minimally stabilized construct of BamA β-barrel C-terminally extended with MENVALDS in LDAO/C8E4 micelles were grew **(Figure 3.8)**. The crystals diffracted at 2.5 Å and the structure was solved **(Figure 3.9 A, B)**. It showed that the additional residues MENVALDFS were able to tighten the interaction between strand 1 and 16 by forming four additional hydrogen bonds. This construct would then require more energy in order to fully open its gate as compared to the non-extended version. It was then evident that the effects observed in the NMR spectrum of the extended construct were explained by the stabilization of its seam region. While the BamA β-barrel only is in a dynamic conformational ensemble, the formation of additional interactions between residues of the first and last strand in the extended construct, favors the closed conformation over the other ones, consequently improving the quality of the NMR spectrum.

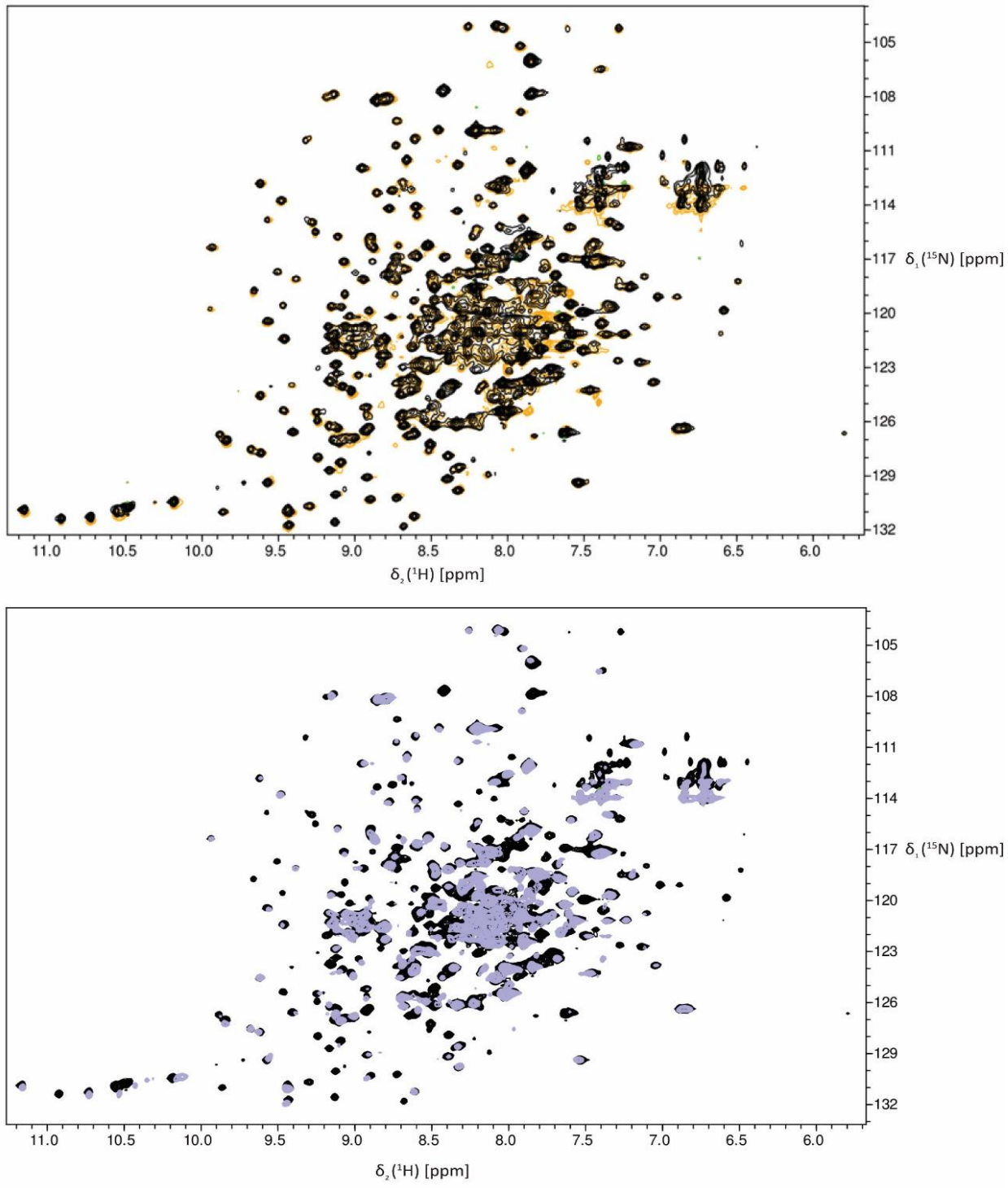

Figure 3.6 Top) [^{15}N, ^{1}H]-TROSY-HSQC of [U-^{2}H, ^{15}N]- BamA β-barrel stabilized with the last hairpin of OmpX (black) and [U-^{2}H, ^{15}N]-BamA β-barrel extended with 9 residues (MENVALDFS) of OmpX (orange). The spectra overlaps very well. **Bottom)** [^{15}N, ^{1}H]-TROSY-HSQC of [U-^{2}H, ^{15}N]-BamA stabilized with the last hairpin of OmpX (black) and [U-^{2}H, ^{15}N]-BamA β-barrel extended with 4 residues (MENV) of OmpX (purple).

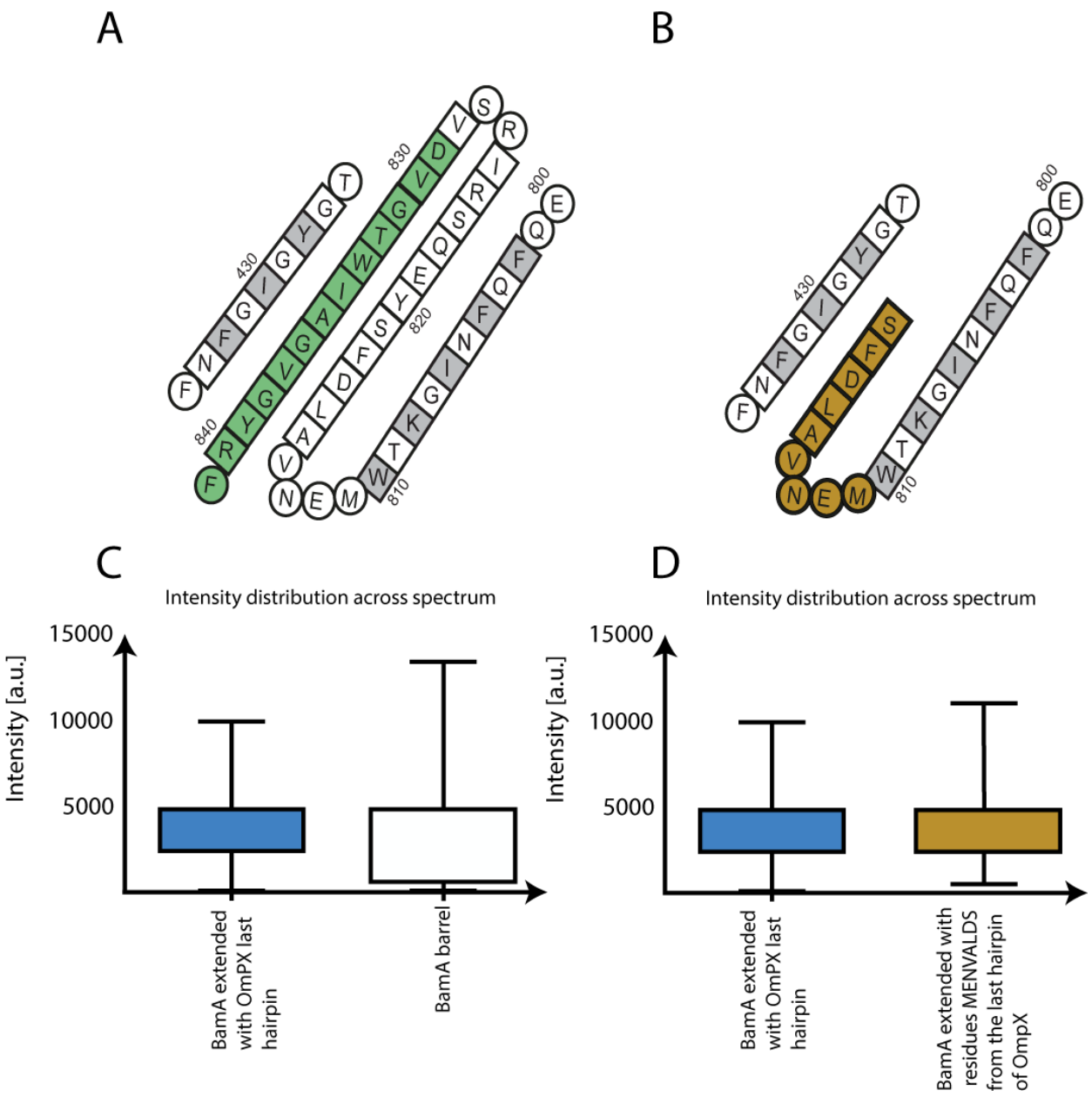

Figure 3.7 A) Assigned residues from the last hairpin of OmpX (green). **B**) C-terminus of BamA extended with 9 residues from OmpX (gold). **C)** Distribution of intensities in the spectrum of BamA-OmpX B7B8 (blue) and in the spectrum of the BamA β-barrel (white) **D)** Distribution of intensities in the spectrum of BamA-OmpX B7B8 (blue) and from the BamA β-barrel extended with 9 residues (MENVALDFS) from OmpX (gold). The distributions are very similar between the two spectra, showing that 9 residues are enough to yield a spectrum quality equal to the one brought by the two last strands of OmpX.

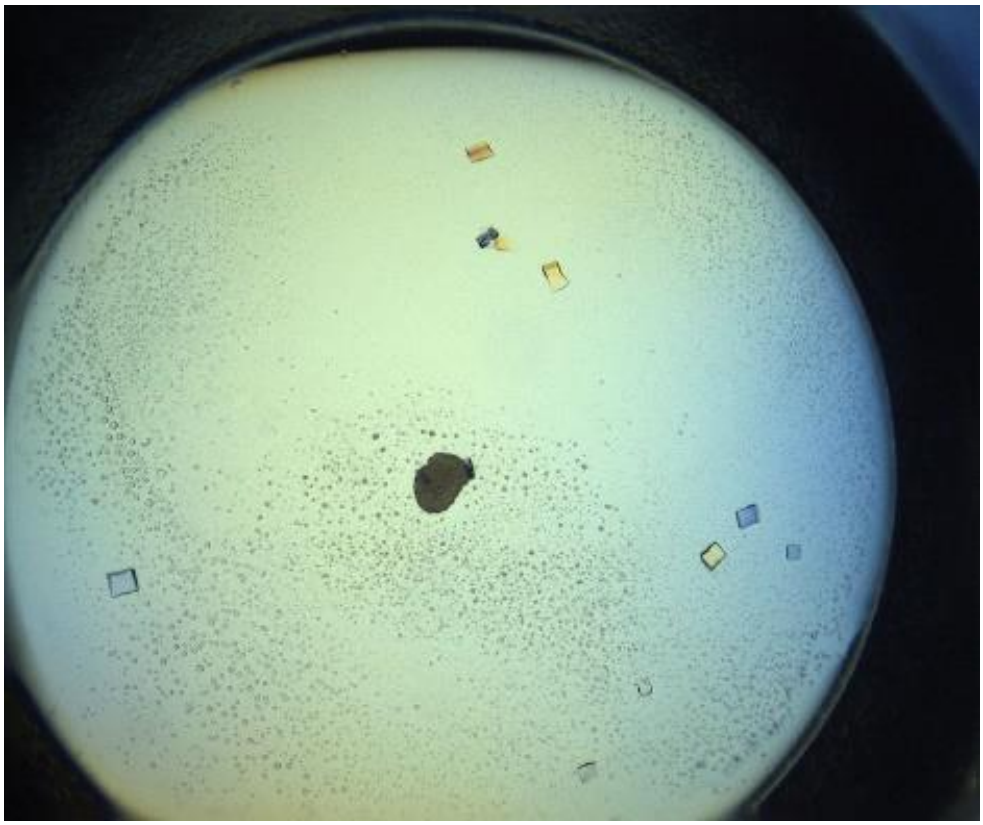

Figure 3.8 Crystals of BamA stabilized with 9 residues from OmpX. Crystallization condition: 22% (w/v) PEG 400, 0.07 M NaCl and 0.05 M sodium citrate pH 4.5.

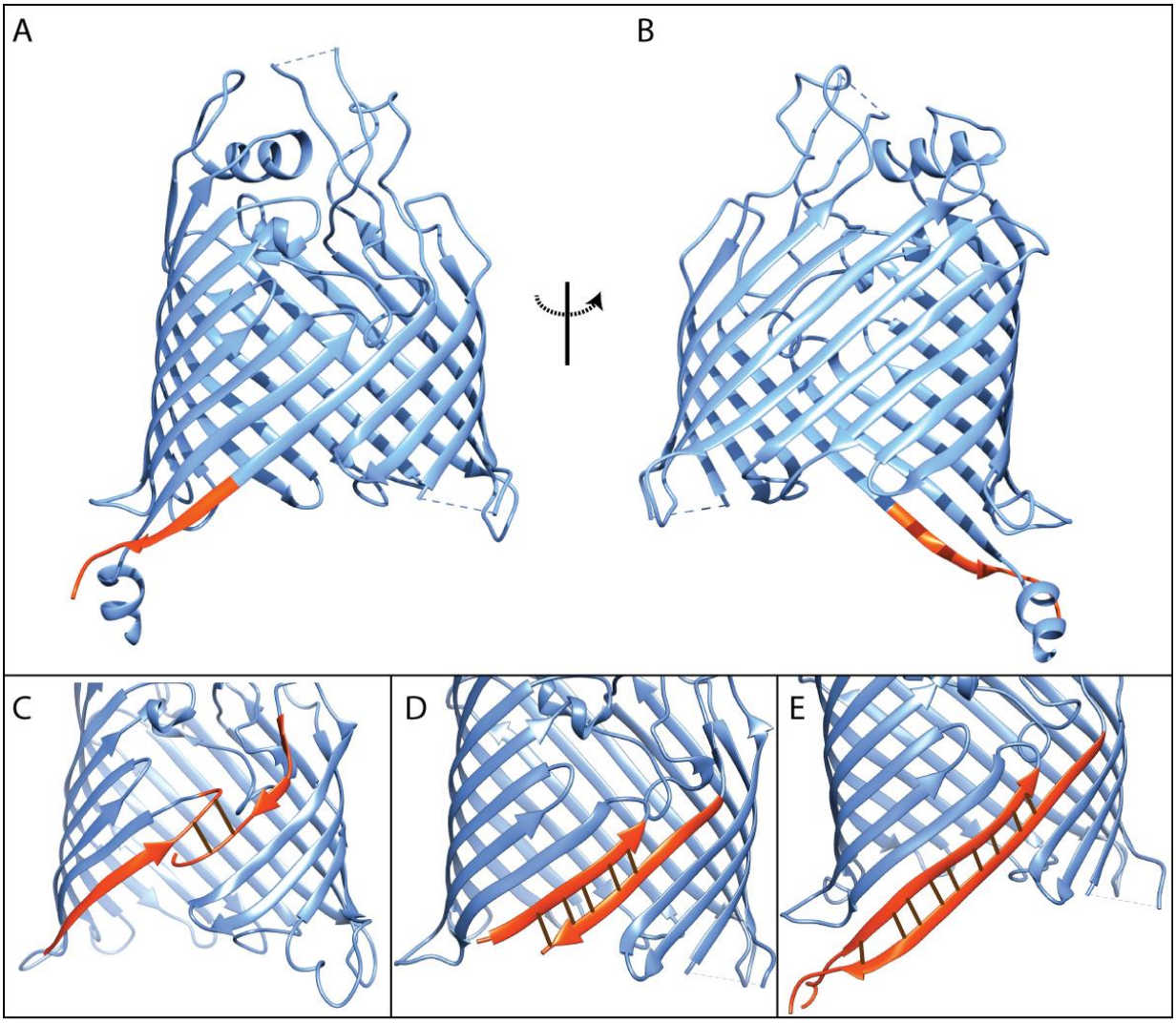

Figure 3.9 A) B) The crystal structure of BamA (in blue) extended with 9 residues of OmpX (in orange). **C)** Gate region from the 5AYW BamA complex structure. **D**) **E)** The residues from the C-terminal extension form four additional hydrogen bonds with the first strand of BamA, favoring the closure of the gate region.

The stabilized BamA β-barrel was measured at various concentrations and the signal-to-noise ratio did not increase for the peaks in the folded regions of the spectra over a molarity of 500 µM. This is still a challenging value to perform NMR backbone assignment for a membrane protein of this mass. To further stabilize the barrel and improve the quality of the sample for assignment, a point mutation screening was performed in the first and last strand of the BamA-OmpX B7B8 construct. The mutation G433A was found to improve the distribution of intensities across the spectrum compared to the BamA-OmpX B7B8 β-barrel (**Figure 3.10**). Additionally, 1D-experiments of the sample at different concentrations were measured to find that the signal-to-noise ratio of peaks in the folded region was increasing up to a sample concentration of 700 µM.

A possible explanation for this additional stability of the barrel might be explained by the mutation from a glycine to an alanine at the interface between the strand and the loop, reducing the conformational flexibility of the area.

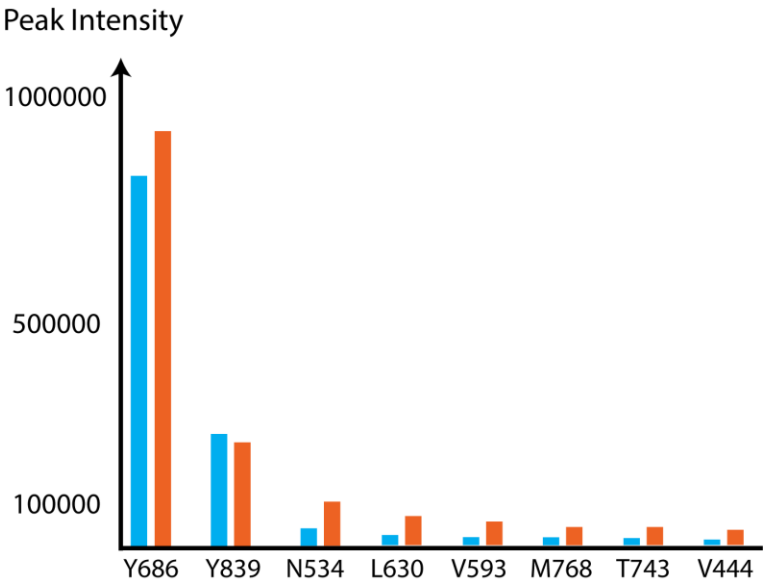

Residues	BamA-OmpXB7B8 $G_{433}A$/ BamA-OmpXB7B8 intensity ratio
Y686	1.16
Y839	0.90
N534	2.58
L630	2.28
V593	2.14
M768	2.39
T743	2.61
V444	2.34

Figure 3.10 Distribution of intensities of assigned residues for the BamA-OmpX B7B8 (blue) and BamA-OmpX B7B8 G433A mutation (orange) for samples of 500 µM [U-^{2}H, ^{15}N] proteins measured with a [^{15}N, ^{1}H]-TROSY-HSQC experiment and the same parameters of acquisition on a 600 MHz Bruker spectrometer. Y686 and Y839 residues are unstructured regions of BamA, the other residues are located in β-strand regions.

As compared to the BamA-OmpX B7B8 construct, an approximate gain of 2-fold the signal-to-noise was observed for residues of the BamA-OmpX B7B8 G433A construct in the β-strand region. The concentration at which the signal-to-noise was maximal peaked at 700 µM for the BamA-OmpX B7B8 G433A construct, as compared to 500 µM for the BamA-OmpX B7B8 construct. This is a 1.4 fold increase in the signal-to-noise ratio. With this mutation, we gained a 2.8-fold increase in the signal-to-noise ratio for the residues found in the β-strand region, which in turn, greatly improved the signal-to-noise of peaks acquired from 3D-experiments.

In order to evaluate the impact of the POTRA domains on the stability of the BamA-OmpX B7B8, a construct encompassing the BamA β-barrel with POTRA domains 3 to 5, and the two hairpins B7 and B8 of OmpX was prepared (**Figure 3.11**) and the NMR spectrum of this protein was recorded. As compared to the BamA-OmpX B7B8 construct, many peaks were still visible, indicating that the protein was folded but the presence of multiplets of low intensities in the spectrum and the broadening of the peaks led to think that the protein dynamics had increased due to the addition of the three POTRA domains.

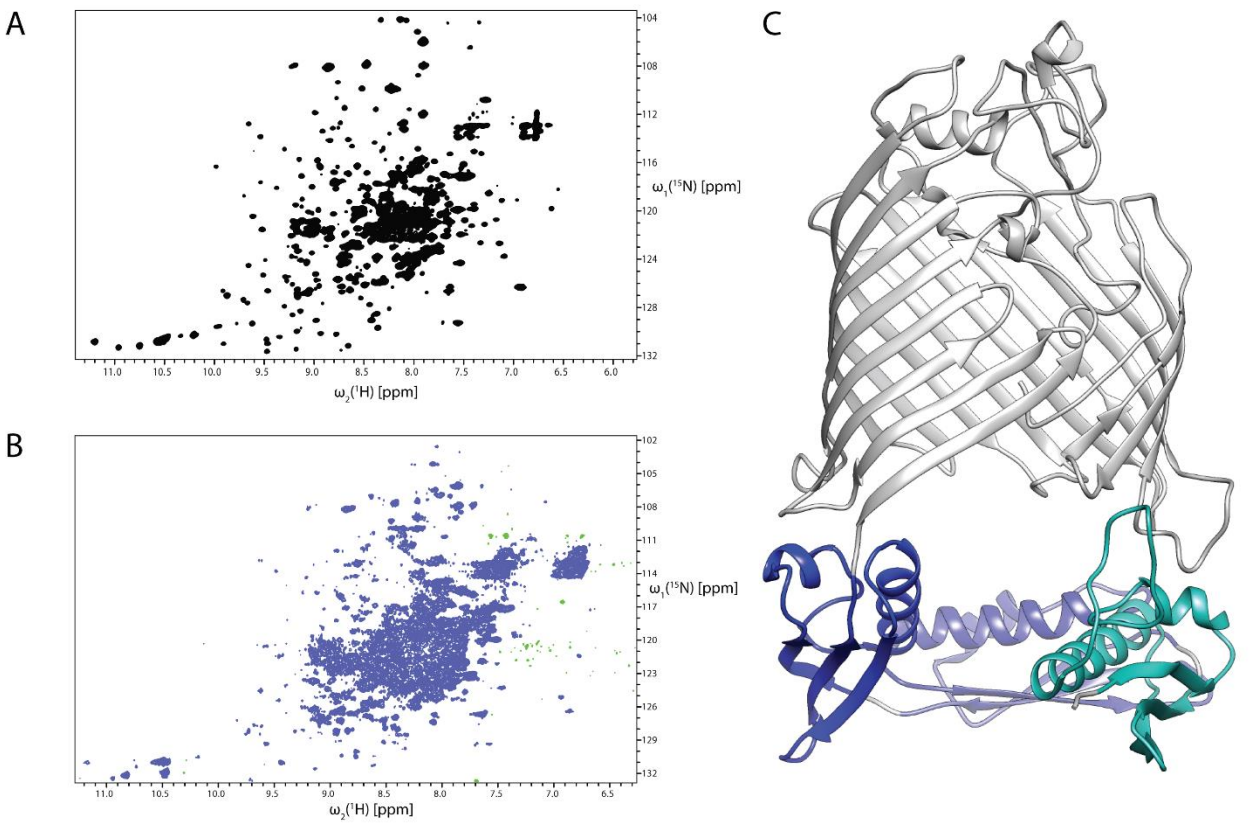

Figure 3.11 Effect on the POTRA3-5 domains the stability of the BamA-OmpX B7B8 protein in LDAO micelles. **A)** [^{15}N, ^{1}H]-TROSY-HSQC of [U-^{2}H, ^{15}N]- BamA C-terminally extended with the last hairpin of OmpX. **B)** [^{15}N, ^{1}H]-TROSY-HSQC of [U-^{2}H, ^{15}N]-BamA-POTRA3-5 C-terminally extended with the last hairpin of OmpX. **C)** Crystal structure of BamA with POTRA3-5, from PDB structure 5D0O (Gu, Y. et al., 2016).

3.3 Discussion

The BamA β-barrel was shown to be a very dynamic protein, resulting in an NMR sample that was not favorable for assignment as shown in the [^{15}N, ^{1}H]-TROSY-HSQC spectrum. Optimization of the conditions of buffer and temperature, and more importantly, the addition of nine extra residues from OmpX at the end of the barrel, allowed to greatly reduce the dynamics of the barrel. In combination with this extension, the screening of mutants in the gate region allowed to identify the G433A point mutation as having an important effect on the stability of the β-barrel. This point mutation permitted to reach a concentration of 700 µM with a 2.8-fold increase in the signal-to-noise ratio for folded residues over the non-mutated stabilized barrel. This jump in the quality of the sample enabled the possibility to acquire 3-dimensional experiments for backbone assignment. By obtaining the crystal structure of the BamA β-barrel C-terminally extended with nine residues from OmpX, we showed that the extension stabilized the gate-region by increasing the hydrogen bond count between the first and last strand. Hence, the stabilization of the gate-region triggered a global reduction dynamics in the entire BamA β-barrel. On the basis of the previously stabilized BamA OmpX B7B8 construct, the addition of three POTRA domains to the N-terminus seems to reverse the stabilization acquired from the extra C-terminal residues.

3.4 Materials and methods

Expression and purification

All the BamA constructs were expressed in inclusion bodies in *E.coli* BL21 (DE3) Lemo cells in LB media in the presence of 100 µg/ml ampicillin (pET15b). Cells were grown at 37° C until and OD600 of 0.8 and induced with 1 mM Isopropyl β-D-1-thiogalactopyranoside (IPTG). Cells were harvested after 5 h of expression and resuspended in buffer A (50 mM TRIS–HCl pH 8.0, 300 mM NaCl) in the presence of lysozyme, DNase I and EDTA-free complete protease inhibitor (Roche). Cells were lysed by sonication on ice and centrifuged for 30 min at 16,000 g. Inclusion bodies were solubilized in buffer A with 6 M guanidine hydrochloride. After 1 h of centrifugation at 16.000 g, supernatant was mixed with 5 mL of nickel-charged beads (Genescript) for 1 h at room temperature. Protein was eluted with buffer A supplemented of 6 M Gdm-HCl and 200 mM imidazole. Eluate was dialyzed against miliQ H_2O overnight with a snakeskin membrane of 3.5 kDa cutoff and precipitate was resupended in Buffer A + 6 M Gdm-Hcl. Bam A was diluted to 5 mg/mL and DTT was added to a final concentration of 10 mM prior to refolding.

Refolding was performed at 4° C by dropwise addition of 20 mL of the BamA solution to a final concentration of 1 mg/mL into 80 mL of the refolding buffer (50 mM Tris pH 8, 300 mM NaCl, 500 mM Arginine, 0.5 % LDAO, DTT 10 mM) while stirring the refolding solution. The solution stirred for 24 h and dialyzed against 20 mM Tris pH 8.0. BamA was applied to a HiTrap Q HP ion exchange column (GE). Buffer A: Tris pH 8.0, LDAO 0.1 %. Buffer B: Buffer A + 500 mM NaCl. The protein was eluted with a step gradient of buffer B (0 % B, 40 % B, 65 % B, 100 % B). Well-refolded protein eluted between 40-65 %B. When analyzed on a gel filtration column, the sample displayed a monodisperse profile.

NMR Spectroscopy

Samples were concentrated using a 30 kDa Vivaspin (Sartorius) concentrator and buffer exchanged to 0.02 M NaPi pH 6.5, 150 mM NaCl, LDAO 0.1 %, 5 % D2O (NMR buffer). Sample were either measured right away or flash frozen at -80° C and thawed prior to measurement. For samples with volumes below 500 µL, Shigemi tubes were used to measure experiment in the NMR spectrometer. Samples were measured on Bruker 600 MHz and 700 MHz spectrometers equipped with cryogenic triple-resonance probes. The temperature was set to 37 °C. The 2D [^{15}N, ^{1}H]-TROSY-HSQC experiment of the 500 µM [U-^{2}H, ^{15}N]-BamA-OmpX B7B8 extended construct was recorded in the NMR buffer with 2048 points on the ^{1}H dimension, 256 points on the ^{15}N dimension, with 8 scans. Transmitter offset was set on 4.7 ppm for the ^{1}H, 118 ppm for the ^{15}N. Sweep width was 16ppm for the ^{1}H and 30 ppm for the ^{15}N. Interscan delay was set to 1 s. The 2D [^{15}N, ^{1}H]-TROSY-HSQC experiment of the 150 µM [U-^{2}H, ^{15}N]-BamA-POTRA35-OmpX B7B8 construct was recorded in the NMR buffer with 2048 points on the ^{1}H dimension, 256 points on the ^{15}N dimension, with 96 scans. Transmitter offset was set on 4.7 ppm for the ^{1}H, 117 ppm for the ^{15}N. Sweep width was 16 ppm for the ^{1}H and 32 ppm for the ^{15}N. Interscan delay was set to 1 s. The 2D [^{15}N, ^{1}H]-TROSY-HSQC experiment of the 500 µM [U-^{2}H, ^{15}N]-BamA β-barrel construct was recorded in the NMR buffer with 2048 points on the ^{1}H dimension, 256 points on the ^{15}N dimension, with 96 scans. Transmitter offset was set on 4.7 ppm for the ^{1}H, 117 ppm for the ^{15}N. Sweep width was 16 ppm for the ^{1}H and 35 ppm for the ^{15}N. Interscan delay was set to 1 s. The 2D [^{15}N, ^{1}H]-TROSY-HSQC experiment of the 300 µM [U-^{2}H, ^{15}N]-BamA β-barrel construct C-terminally extended with 9 residues of OmpX (MENVALDFS) was recorded in the NMR buffer with 2048 points on the ^{1}H dimension, 256 points on the ^{15}N dimension, with 128 scans. Transmitter offset was set on 4.7 ppm for the ^{1}H, 117 ppm for the ^{15}N. Sweep width was 16 ppm for the ^{1}H and 32 ppm for the ^{15}N. Interscan delay was set to 1 s. The 2D [^{15}N, ^{1}H]-TROSY-HSQC experiment of the 270 µM [U-^{2}H, ^{15}N]-BamA β-barrel construct C-terminally extended with 4

residues (MENV) of OmpX was recorded in the NMR buffer with 2048 points on the ^{1}H dimension, 256 points on the ^{15}N dimension, with 152 scans. Transmitter offset was set on 4.7 ppm for the ^{1}H, 117 ppm for the ^{15}N. Sweep width was 16 ppm for the ^{1}H and 32 ppm for the ^{15}N. Interscan delay was set to 1 s. The 3D TROSY-HNCA experiment was recorded by Irena Burmann on a 500 µM sample of triple-labeled BamA-OmpX B7B8 extended construct with 2048 points on the ^{1}H, 100 points on the ^{13}C dimension and 88 points on the ^{15}N dimension with 52 scans. Transmitter offset was set on 4.72 ppm for the ^{1}H, 55 ppm for the ^{13}C and 118ppm for the ^{15}N. Interscan delay was set to 0.7 s. All experiments were processed with TopSpin (Bruker BioSpin) and analyzed with CARA. (Keller, Rochus, 2004).

Crystallization

Michael Zahn performed the crystallization of the BamA β-barrel including nine additional amino acids at the C-terminus (MENVALDFS). The protein buffer was exchanged by gel-filtration into 20 mM Tris pH 7.5, 150 mM NaCl, 0.05% LDAO and 0.35% C_8E_4. Initial crystallization trials were performed at 293 K by sitting-drop vapor diffusion using MemGold- and MemGold2-Screen from Molecular Dimensions with a Gryphon robot (Art Robin Instruments). The initial hits were optimized by fine-screening with larger drops by hanging drop vapor diffusion. Crystals in space group $P2_12_12$ were grown in 22 % (w/v) PEG 400, 0.07 M NaCl and 0.05 M sodium citrate pH 4.5. Crystals were directly flash-frozen in liquid nitrogen. A data set was collected at beamline X06DA (PXIII) at the Swiss Light Source (SLS, Paul Scherer Institute, Villigen, Switzerland). Phases were obtained by molecular replacement. The structure was deposited in the PDB with accession code 6FSU.

Chapter 4: Research publication

Johannes Thoma provided us with the double cysteine constructs used in the cysteine scanning experiments. Leonor Morgado cloned some of the BamA constructs used in this chapter (as listed in the the appendix). Irena Burmann optimized the buffer conditions for NMR measurements of the BamA-OmpX B7B8 construct, and recorded the HNCA experiment to assign the C-terminal unfolded residues of BamA-OmpX B7B8. Michael Zahn crystallized and solved the structure of the BamA β-barrel C-terminally stabilized with 9 residues of OmpX. Stefan Bibow assembled the BamA samples in nanodiscs and recorded the relaxation experiments. All other work was performed by me.

JACS
JOURNAL OF THE AMERICAN CHEMICAL SOCIETY
Article
pubs.acs.org/JACS

Sequence-Specific Solution NMR Assignments of the β-Barrel Insertase BamA to Monitor Its Conformational Ensemble at the Atomic Level

Jean-Baptiste Hartmann,[†] Michael Zahn,[†] Irena Matečko Burmann,[‡] Stefan Bibow, and Sebastian Hiller*

Biozentrum, University of Basel, Klingelbergstrasse 70, 4056 Basel, Switzerland

Supporting Information

ABSTRACT: β-barrel outer membrane proteins (Omps) are key functional components of the outer membranes of Gram-negative bacteria, mitochondria, and plastids. In bacteria, their biogenesis requires the β-barrel-assembly machinery (Bam) with the central insertase BamA, but the exact translocation and insertion mechanism remains elusive. The BamA insertase features a loosely closed gating region between the first and last β-strand 16. Here, we describe ∼70% complete sequence-specific NMR resonance assignments of the transmembrane region of the BamA β-barrel in detergent micelles. On the basis of the assignments, NMR spectra show that the BamA barrel populates a conformational ensemble in slow exchange equilibrium, both in detergent micelles and lipid bilayer nanodiscs. Individual conformers can be selected from the ensemble by the introduction of a C-terminal strand extension, single-point mutations, or specific disulfide cross-linkings, and these modifications at the barrel seam are found to be allosterically coupled to sites at the entire barrel circumference. The resonance assignment provides a platform for mechanistic studies of BamA at atomic resolution, as well as for investigating interactions with potential antibiotic drugs and partner proteins.

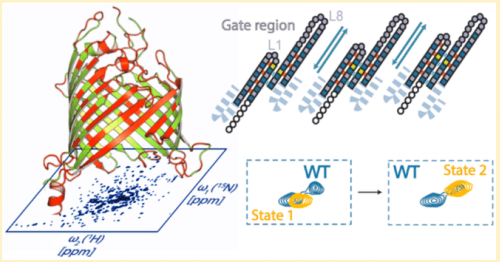

INTRODUCTION

Gram-negative bacteria possess an outer membrane, composed of an asymmetric lipid bilayer of phospholipids and lipopolysaccharides (LPS), which is spanned by β-barrel outer membrane proteins (OMPs). OMPs mediate key cellular functions as they mediate transport of metabolites across the membrane, act as receptors, or are involved in bacterial pathogenicity.[1−3] They are produced by the ribosome in the cytosol and then translocated by the SecYEG complex into the periplasm, where they are stabilized by molecular chaperones, such as SurA and Skp.[4−8] In *E. coli*, the biogenesis and folding of OMPs requires the Omp85 protein BamA, the central protein of the β-barrel assembly machinery (Bam) complex.[9−11] BamA consists of a 16-stranded C-terminal β-barrel domain and five N-terminal periplasmic polypeptide transport domains (POTRA).[12,13] POTRA5 is the only one required for cell survival.[14] BamA recognizes OMPs by their C-terminal β-sequence motif.[15] Moreover, BamA is associated in a complex with four other lipoproteins, BamB, BamC, BamD, and BamE,[16−30] that are anchored in the inner leaflet of the outer membrane. Crystal structures of *E. coli* BamA β-barrel domain,[31] full-length BamA of *N. gonorrheae*, and BamA lacking the first three POTRA domains in *H. ducreyi*,[32] as well as the full *E. coli* Bam complex with the barrel in opened and closed conformations and the homologue protein TamA have been determined.[33−37] The exact mechanism by which Bam catalyzes the insertion of the OMPs into the outer membrane is still unknown.[38−40] A special characteristic of the BamA barrel is the presence of a loose connection between its first and last β-strand. This weak barrel closure results in a highly dynamic region,[41] and the formation of a disulfide bridge between the strands of the gating region is lethal in vivo.[42] The dynamic behavior of the BamA barrel is therefore relevant to understand its function. Solution NMR spectroscopy is a method of choice for studying dynamic proteins in general and thus for the BamA protein in particular.

Here, we present the sequence-specific NMR assignment of approximately 70% of the transmembrane parts of the BamA β-barrel. Specific labeling and unlabeling methods were used in order to establish the assignment. A C-terminally extended BamA construct improved the NMR spectra quality substantially. The crystal structure of this construct reveals a stabilization of the barrel at the gating region which presumably reduces BamA dynamics. Based on the sequence-specific resonance assignment of the stabilized version, we

Received: March 28, 2018
Published: August 20, 2018

DOI: 10.1021/jacs.8b03220
J. Am. Chem. Soc. XXXX, XXX, XXX−XXX

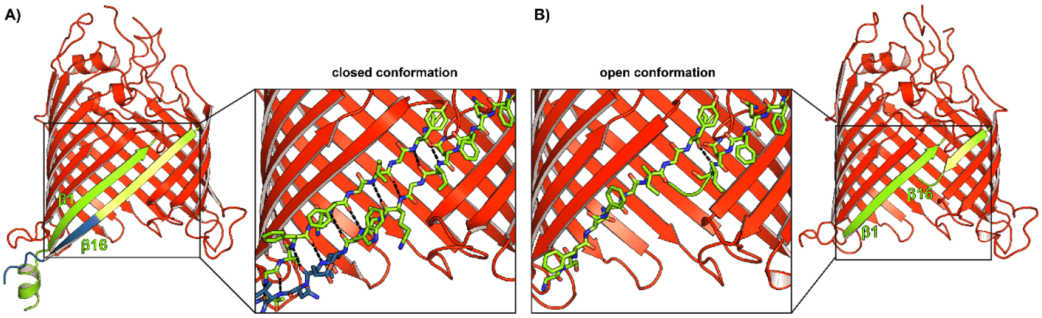

Figure 1. Design of a stabilized BamA variant. (A) Crystal structure of BamA^{+9} in detergent micelles. The barrel is locked in a closed conformation due to nine additional amino acids (blue) at the C-terminus of β-strand 16 (light green). (B) Crystal structure of wild-type BamA-barrel (PDB 5AYW),[35] showing the barrel-inward orientation of β-strand 16 (light green), which results in a loose barrel closure.

could then demonstrate that wild-type BamA barrel in detergent micelles switches between different conformational states at the gating region. Individual states can be isolated by a C-terminal strand extension, single point mutations, or locking the gating region with a disulfide bridge.

Sequence-Specific NMR Resonance Assignments of BamA. A prerequisite to enable atomic resolution studies of the BamA β-barrel in solution in detergent micelles is the sequence-specific resonance assignment of the protein. Backbone assignments of a 44 kDa membrane protein are particularly challenging, because the molecular weight of the detergent micelle adds to the protein, thereby increasing the nuclear spin relaxation rates. Previously published transverse relaxation-optimized heteronuclear single quantum coherence (TROSY-HSQC) spectra of the BamA barrel in different membrane mimetics had shown relatively poor spectra quality.[43] Relative to this starting point, the use of a new buffer condition (20 mM NaPi pH 7.5, 150 mM NaCl, 0.1% *N*,*N*-dimethyldodecylamine *N*-oxide (LDAO)) improved the spectral quality, but still, the spectrum of the wildtype protein featured inhomogeneous peak intensities and line widths, indicating the presence of conformational heterogeneity.

As a strategy to reach sequence-specific resonance assignments, we thus aimed at developing a stabilized version of the BamA barrel with high spectral quality and then to transfer these assignments back to the wildtype protein. By serendipity, we discovered such a construct in an attempt to create an insertion-transition-state-mimic, for which we added one β-hairpin of the protein OmpX to the BamA C-terminus. For this "BamA^{ext}" construct, a general improvement of the NMR spectral quality was observed, suggesting the presence of some kind of stabilizing effect arising from these 31 extra residues. Sequence-specific resonance assignments showed that the C-terminal portion of the extension was in a random-coli conformation, flexibly attached to the barrel (Figure S1). Then, we sequentially truncated residues from the C-terminal end of BamA^{ext}, until we found that the stabilizing effect was fully preserved in a construct with nine additional amino acids added to the BamA barrel (BamA^{+9}) but not with shorter extensions. We determined the crystal structure of this BamA^{+9} construct to a resolution of 2.6 Å (Table S1). The structure is virtually identical to the available structure of the wild-type barrel,[35] with the exception that the β-strand 16 with its C-terminal extension is forming multiple new backbone hydrogen bond contacts to the first β-strand, thereby closing the BamA lateral gate (Figure 1).

By testing some arbitrarily chosen glycine mutations in the gate region, we then also identified the mutation G433A to improve the experimental sensitivity further by about 2-fold. The mechanistic rationale behind this mutation effect remains unclear, perhaps the mutant protein favors even more a single conformation state. To check, if the mutation G433A or the C-terminal extensions influence the function of BamA in vivo, we carried out a complementation assay in living cells (Figure S2).[44] The data show that the mutation G433A has no detectable phenotype on *E. coli*, suggesting that the stabilization effect seen in the NMR spectrum has no significant consequences for BamA function. In contrast, however, any extensions of the C-terminus with more than one additional amino acid are not tolerated and result in a lethal phenotype (Figure S2).

Overall, the resulting BamA β-barrel construct (BamA^{ext}) consisting of residues 421 to 810, the C-terminal extension, and mutation G433A yielded a spectrum of remarkably high quality, opening the way for extensive sequence-specific resonance assignments (Figure 2A). As a reference point for a native-like lipidic environment, we also reconstituted BamA^{ext} in MSPΔH5 lipid bilayer nanodiscs, showing an overall well-dispersed spectrum (Figure 2B). We measured the rotational correlation time of BamA^{ext} and BamA^{+9} in LDAO micelles via TRACT and found a value in the range of τ_c = 50−60 ms (Figure S3).

Toward the assignment of the BamA^{ext} construct, we employed a structure-based assignment strategy. The strategy comprised (i) classical TROSY-type triple-resonance experiments,[45−48] (ii) amino-acid-selective labeled samples, and (iii) structure-guided nuclear Overhauser effect (NOE) interpretation. A 3D TROSY-HNCA experiment showed substantial amounts of intraresidual and sequential cross peaks and was used as the main experiment to connect backbone amide moieties (Figure S4). A 3D TROSY-HNCACB experiment in turn, which is intrinsically less sensitive, yielded detectable signals only for around 14% of the spin systems. In order to overcome ambiguities in sequential connectivities and to provide specific anchor points for the assignment, a total of 15 different BamA^{ext} samples were prepared with amino acid-specific labeling or unlabeling (Figure S5 and Table S2).

DOI: 10.1021/jacs.8b03220
J. Am. Chem. Soc. XXXX, XXX, XXX−XXX

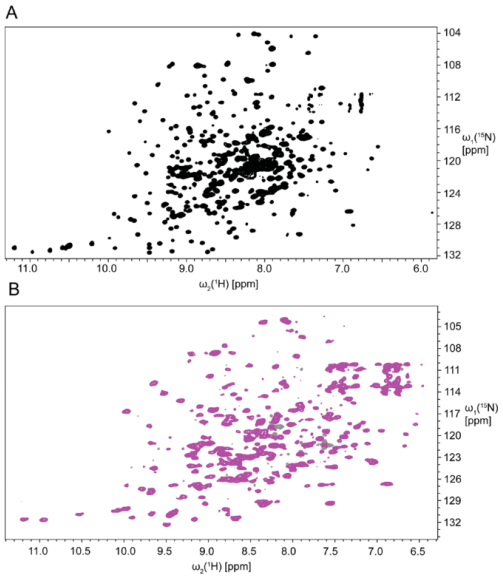

Figure 2. Solution NMR spectra of the BamA^{ext} barrel. (A) 2D [^{15}N, ^{1}H]-TROSY-HSQC of 500 μM a [U-^{2}H, ^{15}N]-BamA^{ext} in LDAO micelles. (B) 2D [^{15}N, ^{1}H]-TROSY spectra of 200 μM [U-^{2}H, ^{15}N]-BamA^{ext} in MSPΔH5 nanodiscs with the lipid 1,2-dimyristoyl-*sn*-glycero-3-phosphocholine (DMPC).

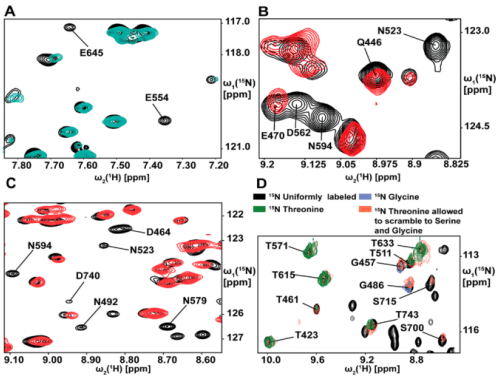

Figure 3. Amino-acid specific labeling and unlabeling of BamA^{ext}. Overlays of 2D [^{15}N, ^{1}H]-TROSY spectra of (A) [U-^{15}N]-labeled BamA^{ext} (black) and of selectively unlabeled glutamine/glutamic acid (turquoise). (B and C) [U-^{15}N] labeled BamA^{ext} (black) and with selectively unlabeled asparagine/aspartic acid (purple and red). (D) [U-^{15}N]-labeled BamA^{ext} (black) and selectively [^{15}N]-labeled for glycine (blue), threonine (green), and threonine with scrambling to serine and glycine (orange).

Initial trials with a more conventional specific labeling strategy in an *E. coli* BL21 expression strain, where additional amino acids were added to the medium to suppress scrambling,[49] yielded good results for some but not all amino acid types. We then switched to *E. coli* expression strains that are auxotrophic for one or several amino acids and obtained good protein expression in M9 medium.[50] These strains were used for both labeling as well as unlabeling schemes. For example, to uniformly unlabel glutamate and glutamine on a [U-^{15}N]-background, we expressed the protein in the strain ML17, which is auxotrophic for these two amino acids, in a growth medium prepared from ^{15}N-labeled algal extract (Isogro) and a large excess of unlabeled glutamine.

Isogro lacks the four amino acids cysteine, glutamine, asparagine, and tryptophan. Because glutamine is interconverted to glutamate and because the backbone amide group of tryptophan is synthesized in *E. coli* from glutamine, the resulting sample is unlabeled for tryptophan, glutamate, and glutamine, as well as partially for aspartate and asparagine (Figure 3A). In combination with selectively labeled samples for either tryptophan or aspartate/asparagine, we could then identify the peaks of glutamate and glutamine residues. Similarly, for the selective unlabeling of aspartate and asparagine we expressed BamA^{ext} in strain RF4 (auxotrophic for aspartate, phenylalanine and tyrosine) in a medium containing ^{15}N-labeled Isogro and unlabeled aspartate. The resulting sample was completely unlabeled in aspartate and asparagine and did not show scrambling toward other amino acids, so that these residues could be identified (Figure 3B,C). Information about serine and glycine residues in turn was obtained by considering the difference between two samples prepared with the auxotrophic strain RF2, where in one sample threonine was allowed to scramble into serine, and in the other sample, scrambling was suppressed by addition of unlabeled serine and glycine to the medium (Figure 3D). Because the identity of threonine and glycine peaks was known from other samples, the remaining scrambled peaks were identified as serines. In total, 16 different amino acids types could be assigned by specific labeling, thus immensely reducing the connection possibilities in the 3D HNCA and 3D HNCACB experiments.

Finally, our knowledge of the wild-type BamA and BamA^{+9} crystal structures combined with a 3D ^{15}N-resolved-[^{1}H,^{1}H]-NOESY experiment[51] allowed us to specifically connect the pairs of residues that are facing each other in two adjacent β-strands, connected by a pair of hydrogens bonds between the respective backbone amide and carboxyl groups (Figure S6). In a β-barrel protein, these residue pairs typically give rise to very intense NOE crosspeaks, in intensity often of at least 10% magnitude of the diagonal peak.

Taken together, by combining the information from triple resonance experiments, selective labeling and structure-guided NOE interpretation, around 70% of the transmembrane parts of the BamA barrel could be unambiguously assigned (Figures 4, S7, and S8). The BamA^{ext} construct has 422 amino acids, out of which 391 belong to BamA and 31 arise from the engineered strand extension. The transmembrane region (β-strands without loops and turns) comprises 182 nonproline residues, out of which 127 were assigned (70%). The loops and turns comprise a total of 191 nonproline residues, out of which 61 were assigned. Overall, a total of 352 resonances are observed in the 2D [^{15}N,^{1}H]-TROSY spectrum (Figure S7). Compared to the 373 nonproline residues, this means that at least 21 residues of BamA^{ext} are not detectable, presumably due to intermediate exchange. We expect that a majority of these residues are located in the loop and turn regions, based on the experience with other β-barrel membrane proteins. An analysis of the assignments with Talos-N showed that all available

DOI: 10.1021/jacs.8b03220
J. Am. Chem. Soc. XXXX, XXX, XXX−XXX

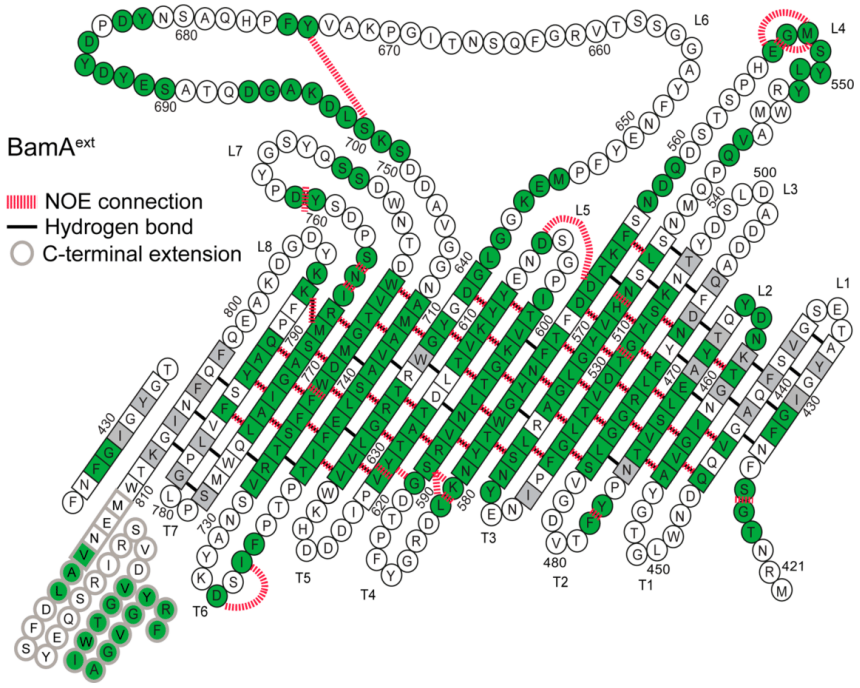

Figure 4. Sequence-specific resonance assignment of BamA^{ext}. Unambiguously assigned residues are colored in green, and experimentally observed NOE connections between amino acids are displayed with red dashed lines. The C-terminal extension is outlined in gray.

secondary chemical shifts match the structure of BamA (Figure S9).[52]

Monitoring the Conformational Ensemble of BamA. In the 2D [^{15}N, ^{1}H]-TROSY spectrum of wild-type BamA barrel in LDAO detergent micelles, multiple residues feature two or more resonance peaks in slow exchange. With the sequence-specific resonance assignment at hand, we thus aimed to monitor in atomic detail how individual conformational states contribute to the conformational ensemble of wild-type BamA. Importantly, wild-type BamA reconstituted in MSPΔH5 nanodiscs with the lipid DMPC showed very similar peak doubling patterns as in detergent, indicating that the BamA conformational equilibria are similar in the two environments (Figures 6A, S13, and S14). The LDAO micelle thus appears a suitable membrane mimetic to study the conformational equilibrium. Based on our assignment, we monitored different preparations of BamA by NMR fingerprint spectra, including the C-terminal extension BamA^{ext}, single point mutations in the gate region, and disulfide cross-linking of the gate region that stabilize individual register shifts at the gating region of BamA. To this end, double cysteine mutants of BamA were designed with two cysteines facing each other across a β-strand pair in different registers (Figures 5A and S10). Disulfide formation was confirmed by a thermoshift experiment, where all double cysteine BamA mutants were unfolded by a temperature gradient, allowing free cysteines to bind a fluorescent dye.[53,54] As a control experiment at a neutral site, the formation of disulfide bridges between β-strands 9 and 10 lead only to a disulfide bridge formation in register 0 mutants but not in registers +1 or −1 (Figure 5B). In contrast, at the gating region of BamA, cysteines facing each other in the registers −2, −1, 0, +1, and +2 were all found to form disulfide bridges (Figure 5C,D). These observations were further confirmed by SDS-PAGE, showing the presence of two close bands for all register mutants (Figure S11), and by mass spectrometry, which identified fragments linked by disulfide bonds for registers −2 to +1 from those purified lower bands (Figure S12). These results show that the gating region is able to sample different registers in agreement with published data.[41]

We then monitored the conformations of the cross-linked registers −1, 0, +1 and also the respective reduced forms of these BamA variants by solution NMR fingerprint spectra, along with the single-point mutation BamA(G431C) and the construct BamA^{ext} that is stabilized in register 0 (Figures 6 and S14). For multiple residues where the assignment could be transferred from BamA^{ext}, we found that the multiple conformations present in wild-type BamA are singled out in certain of these preparation. In particular, in the cross-linked mutants and in BamA^{ext}, only a single resonance is left for all peaks, indicating the selection of a single state, while in the reduced forms of the single or double cysteine mutants only a subset of the resonance peaks singled out (Figure 6A−C). Notably, the stabilized residues are localized all across the barrel circumference (Figure 6D). The reduction of multiple states into a single one is exemplified by residues D569 and T571 that show peak doublings in wild type BamA, but only one of these peaks when locked in register −1 or 0 and only

DOI: 10.1021/jacs.8b03220
J. Am. Chem. Soc. XXXX, XXX, XXX−XXX

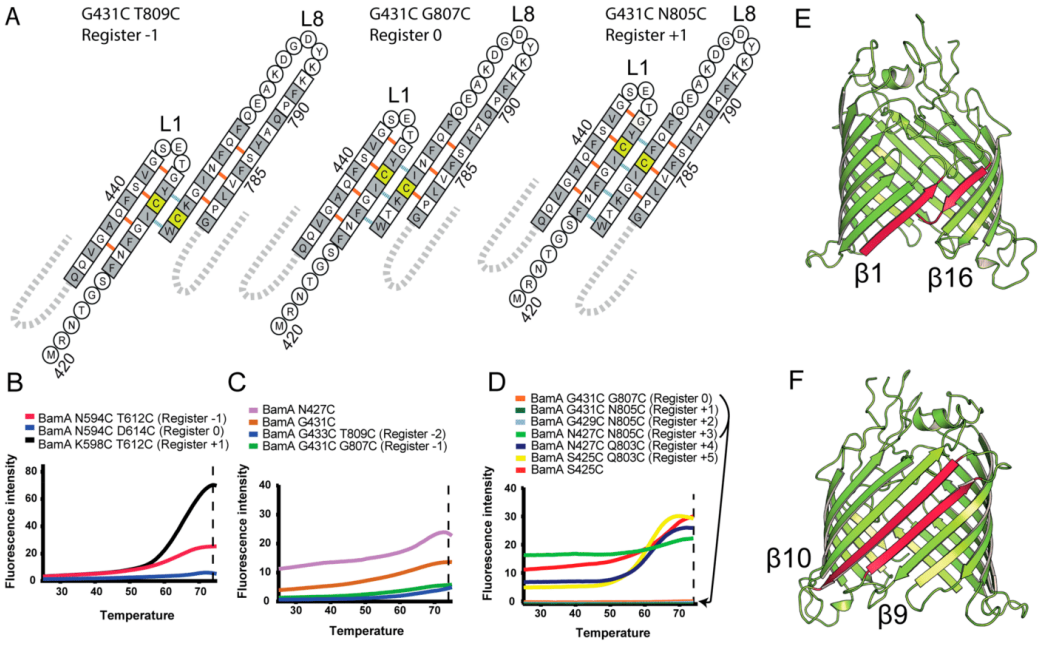

Figure 5. Thermoshift assay of BamA cysteine mutants. (A) Design schemes for the cross-linked BamA variants in registers +1, 0 and +1. (B–D) Thermoshift assay curves. (B) Double cysteine constructs from the strand pair 9–10. (C–D) Double cysteine constructs from the strand pair 1–16 and single cysteine controls, as indicated. A high 440 nm fluorescence signal at 74 °C indicates the presence of free cysteines, i.e., the absence of a disulfide bond. (E–F) Location of the strand pairs 9–10 and 1–16 region in the canonical register.

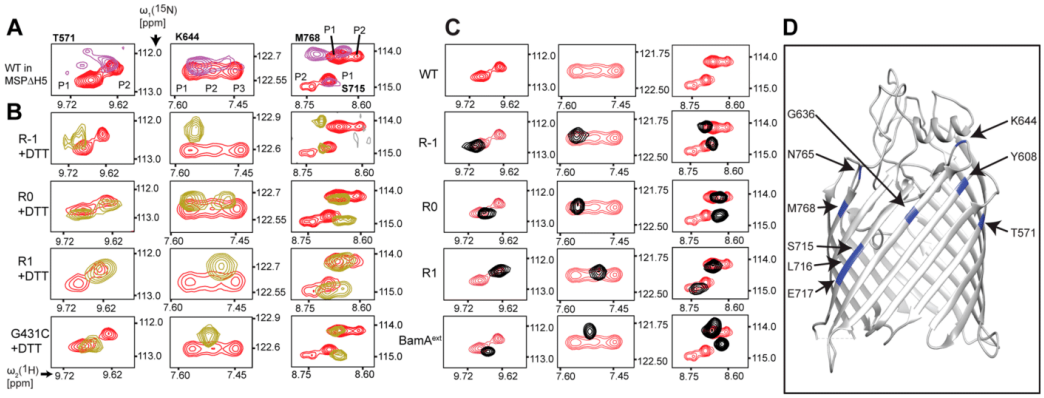

Figure 6. Selection of conformers from the BamA ensemble. For three selected residues, as indicated, the peak patterns in 2D [^{15}N,^{1}H]-TROSY-HSQC spectra are shown. In each row, the spectrum of 450 μM [U-^{2}H,^{15}N]-labeled wild-type BamA barrel in LDAO micelles (red) is overlaid with BamA β-barrel in different preparations: (A) 90 μM wild-type BamA barrel in MSPΔ*H5* nanodiscs (purple). (B) 630 μM BamA(G431C, T809C, register −1) under reducing conditions (gold), 280 μM BamA(G431C, G807C, register 0) under reducing conditions (gold), 200 μM BamA(G431C N805C, register +1) under reducing conditions (gold), 220 μM BamA(G431C) under reducing conditions (gold). (C) 450 μM wild-type BamA β-barrel (red), 250 μM cross-linked BamA(G431C, T809C, register −1, black), 200 μM cross-linked BamA(G431C, G807C, register 0, black), 220 μM cross-linked BamA(G431C N805C, register +1, black), and 700 μM BamA^{ext} (black). (D) Location of the residues that were singled out in the extended and locked constructs mapped on the structure (PDB 4N75).[31]

the other peak when locked in register +1 (Figure 6B). This observation indicates that shifting the register from 0 to −1 does not cause a conformational rearrangement of these residues at the opposite barrel side, while a shift to the +1 register triggers a strong conformational transition, leading to a population of the second peak. As a second example, for

DOI: 10.1021/jacs.8b03220
J. Am. Chem. Soc. XXXX, XXX, XXX−XXX

residue M768, registers −1, 0 and BamA^{ext} select the same state corresponding to the first peak, while register +1 selects the state corresponding to the second peak. Interestingly, in addition to the cross-linking, also the single point mutation G431C and the cysteine double mutants in their reduced forms single out doubled peaks from the wild-type spectrum, indicating that already slight changes in the amino acid composition at the gate region can have a significant effect on the conformational equilibrium (Figure 6B). For instance, when adding a second mutation toward the double mutant BamA (G431C,G807C), some peaks remain multiconformational (T571, K644, Y609, and L716), while others are singled out. Then, in the oxidized form of the same mutant, where the cross-links are formed, peaks T571, K644, and Y609 are singled out (Figure 6C). These data thus show that the mutation of the residue 431 from a glycine to a cysteine triggers a conformational rearrangement over the barrel circumference and that the addition of a second mutation, glycine 807 to cysteine, changes again the conformational equilibrium of the barrel. Finally, locking the barrel in register 0 selects a single state. Similarly, for the register +1 mutant BamA(G431C, N805C) in its reduced form, the peaks M768 and G636 are doubled while the other peaks are singled out as a consequence of the mutation (Figure 6B). After formation of the disulfide bridge, we observe single peaks for M768 and G636. Finally, for BamA(G431C, T809C) in the reduced form (register −1) all peaks but E717 were singled out, and this peak eventually singles out when the disulfide lock is formed (Figure 6)

Overall, these data show that multiple different modifications in the gating region of BamA, including single point mutations, chemical cross-links, and extensions of the strand 16 affect the backbone conformational equilibrium of the entire barrel circumference of BamA. In the wild-type protein, the gating region is not statically adopting a single state but populates a set of different conformations that are coupled to structural effects across the whole protein. The cross-linked constructs in register −1 and 0, as well as the stabilized BamA^{ext} favor the same conformation that is in turn different from the conformation of the +1 register. Notably, in the NMR spectra of the cross-linked gating regions, multiple peaks were missing compared to BamA^{ext}, suggesting that the β-strand extension makes the barrel more rigid than a single cysteine-lock.

■ DISCUSSION

Here, we have used solution NMR spectroscopy in combination with protein engineering and cysteine scanning experiments to characterize the conformational equilibrium of the *E. coli* BamA β-barrel gating region at the atomic level. The wild-type BamA barrel in detergent micelles and in MSPΔH5 nanodiscs populates a number of different conformational states in slow NMR equilibrium, i.e., with exchange rate constants $\lesssim 10\ s^{-1}$. By suitably engineered point mutations or disulfide bridge formations at the gating regions or by an extension of β-strand 16 (BamA^{ext}), we could stabilize single BamA-barrel conformations from this ensemble. In agreement with published data,[41] stable disulfide bonds could be formed for different registers between the first and last β-strand. By monitoring the barrel at the atomic level, we could now show that many residues are in slow exchange between several conformations in the unlocked barrel and that these can be singled out in the cysteine locked constructs. Notably, locking the gating region with a cysteine bond stabilizes the barrel less than forming additional hydrogen bonds between residues from the first and the last β-strand in the BamA^{ext} construct. Interestingly, the gate dynamics appear to depend in a sensitive way on the individual amino acids in the gate regions, and it will be interesting to determine the impact of individual residues in the gate region on the conformational ensemble and function of the BamA barrel on the basis of the assignments established here.

Structures of BamA solved by X-ray crystallography and cryo-EM[33−36] showed an open and a closed conformation of the barrel but could not give hints about other states of the protein. We have demonstrated here that the barrel conformations are modulated in response to modifications at the gating region. During the folding and insertion process, an unfolded Omp might interact with the first β-strand of the BamA barrel by forming additional hydrogen bonds. We can speculate that, upon the folding of the Omp, the BamA barrel could open to incorporate the forming hairpins. The stability of the BamA hybrid barrel would then fluctuate until the release of the Omp into the outer membrane.

Notably, with 400 residues, the BamA^{ext} protein studied here is the largest monomeric integral membrane protein for which extensive sequence-specific NMR resonance assignments have been obtained so far. Solid-state NMR spectroscopy in DLPC bilayers was previously used to assign a few residues from the sixth loop and transmembrane region of the BamA−POTRA4−POTRA5 construct.[55] When comparing the two assignments, some of the chemical shifts are similar, except for residues I601 and K793 which have significant differences (Table S3). As both residues are at the junction between a β-strand and a loop, the chemical shift differences might arise from the difference in membrane mimetic. Previous solution NMR assignment of large membrane proteins include 280-residues OmpG, 283-residue VDAC-1, and 303-residue UCP2.[56−58] By stabilization of the BamA barrel by β-strand extension and by making use of recent developments in auxotrophic strains, as well as by structure-based NOESY interpretation, we managed to assign a major portion of the transmembrane part of the extended BamA barrel. The assignment paves the way for future NMR studies of the BamA protein with substrates, ligands, or partner proteins and for mechanistic studies of BamA and the potentially also the Bam complex.

■ EXPERIMENTAL SECTION

Cloning, Mutagenesis, and Expression. The pET15b-based plasmid for expressing BamA(421−810, C690S, C700S) with N-terminal TEV-cleavable His_6 tag was described previously.[43] On this template, individual or pairwise cysteine mutations following the scheme in Figure S7 or the mutation G433A were introduced using the Quickchange protocol. C-terminal extensions were introduced using restriction free cloning. The BamA^{49} construct consists of the template extended by the nine residues MENVALDFS, while the BamA^{ext} construct contains the G433A mutation and is extended by the residues MENVALDFSYEQSRIRSVDVGTWIAGVGYRF. All BamA constructs were expressed into inclusion bodies in *E. coli* BL21 (k DE3) Lemo[59,60] cells in LB or M9 medium in the presence of 100 μg/mL ampicillin (pET15b). Cells were grown at 37 °C until an OD_{600} of 0.8 and then induced with 1 mM isopropyl β-D-1-thiogalactopyranoside (IPTG). Cells were harvested after 5 H of expression and resuspended in buffer A (50 mM Tris−HCl pH 8.0, 300 mM NaCl) in the presence of lysozyme, DNase I, and EDTA-free complete protease inhibitor (Roche). Cells were lysed by sonication on ice and centrifuged for 30 min at 16 000*g*. Inclusion bodies were

DOI: 10.1021/jacs.8b03220
J. Am. Chem. Soc. XXXX, XXX, XXX−XXX

solubilized in buffer A with 6 M guanidine hydrochloride. After 1 H of centrifugation at 16 000g, supernatant was mixed with 5 mL of Ni-beads (Genscript) for 1 H at room temperature. Protein was eluted with buffer A supplemented of 6 M Gdm-HCl and 200 mM imidazole. Eluate was dialyzed against Milli-Q H_2O overnight with a snakeskin membrane of 3.5 kDa cutoff, and the precipitate was resuspended in buffer A + 6 M Gdm-HCl. BamA was diluted to 5 mg/mL and DTT was added to a final concentration of 10 mM prior to refolding.

Refolding and Purification. Refolding was performed at 4 °C by dropwise addition of 20 mL of the BamA solution to a final concentration of 1 mg/mL into 80 mL of refolding buffer (50 mM Tris pH 8, 300 mM NaCl, 500 mM arginine, 0.5% LDAO, DTT 10 mM) while stirring the refolding solution. For the 3D-NOESY sample, [^{2}H]-LDAO was used in all of the buffers. The solution was stirred for another 24 h and dialyzed against 20 mM Tris pH 8.0. BamA was applied to a HiTrap Q HP ion exchange column (GE; Figure S11). Buffer A: Tris pH 8.0, LDAO 0.1%. Buffer B: Buffer A + 500 mM NaCl. The protein was eluted with a step gradient of buffer B (0% B, 40% B, 65% B, and 100% B). Well-refolded protein eluted between 40 and 65%B. When analyzed on a gel filtration column, the protein displayed a monodisperse profile (Figure S11). Fractions were concentrated using a 30 kDa Vivaspin concentrator and buffer exchanged to 0.1 M NaPi, 150 mM NaCl, LDAO 0.1% (thermoshift assay buffer) or 0.02 M NaPi, 150 mM NaCl, LDAO 0.1%, 5% D_2O (NMR Buffer). Samples were frozen at −80 °C and thawed prior to measurements. BamA (G431C, T809C) (register −1), BamA (G431C, G807C) (register 0), and BamA (G431C, N805C) (register +1) were transformed into LEMO(DE3) strains and expressed in LB or M9 minimal media.[59,60] Following a previously established protocol,[43] proteins were purified and refolded in the presence of 10 mM DTT. For the targeted formation of disulfide bonds, DTT was dialyzed out and 10 mM H_2O_2 were added.

Reconstitution in Nanodiscs. The plasmid pET-28a with the coding sequence of truncated apoA-I missing residues 1−54 and 121−142 (MSPΔH5), with an N-terminal TEV protease-cleavable histidine tag, was a gift of the Zerbe lab (University of Zurich) with permission from Gerhard Wagner (Harvard University). MSPΔH5 was expressed in *E. coli* strain BL21(DE3) Lemo and purified as described before.[61] For the reconstitution of BamA into MSPΔH5 nanodiscs with the lipid 1,2-dimyristoyl-*sn*-glycero-3-phosphocholine (DMPC), a molar ratio of 1:6:132:264 of BamA:MSPΔH5:DMPC:-sodium cholate was used (final sodium cholate concentration was 13.2 mM). In a first step MSPΔH5, then the DMPC lipids, and finally BamA was given in a glass vial and gently shaken for 1 h at 27 °C. Subsequently, 1 g of Biobeads SM-2 (Biorad) per mL of assembly solution was given to the mixture and shaken for 3−4 h at 27 °C. Separation of the Biobeads was obtained by slow speed centrifugation. The supernatant was centrifuged for 5 min at 13 000g and was purified using size exclusion chromatography (S200 10/300 GL) as reported previously.[61] The fractions were concentrated to a BamA concentration of around 100 μM using an Amicon Ultra-4 10 000 Da molecular weight cutoff (MWCO) concentrator (Millipore).

Thermoshift Assay. Cysteine mutants of the BamA barrel in the strand 9/10 region and gate region were measured by a thermal denaturation assay experiment with 7-diethylamino-3-((4′-iodoacetyl)amino)phenyl)-4-methylcoumarin (DCIA).[53,54] Samples were thawed, and the disulfide bond formation was catalyzed by addition of H_2O_2 to 10 mM final 1 h before measurement. For each construct, 50 μL of sample was prepared with final concentrations of 25 μM of protein and 50 μM of DCIA dye (Anaspec). Controls containing no protein, single cysteine, and cysteine-less BamA were prepared. A RotorGene Q RT-PCR instrument (Qiagen) was used to ramp the temperature from 20 to 95 °C, excite at λ_{350nm}, and measure the absorbance at λ_{440nm} of the conjugate between end the protein. As the protein unfolds, cysteines become accessible to react with DCIA. Fluorescence intensity was reported at 74 °C, at maximal intensity. Samples with intensity is similar to the sample containing no cysteines are identified as closed. Depending on their localization, the accessibility of the cysteines to the reagent differs. The fluorescence data were corrected with the values from the cysteine-less construct.

SDS-Gel/Mass Spectrometry. Samples were thawed, and the reaction of cysteine bond formation was catalyzed with 10 mM H_2O_2. As a control experiment, we recorded an NMR spectrum of BamA wild-type with and without H_2O_2 (Figure S15). H_2O_2 had no effect on BamA chemical shifts. Samples were run on a nonreducing SDS-gel and boiled for 30 min at 95 °C. Constructs found to contain the disulfide bridge by thermoshift assay displayed a second band that migrated lower on the gel (Figures S11C and S12−S15 and Table S2). For analysis of this band by mass spectrometry (MS), the bands were cut into small pieces and placed into *n*-propanol droplets. Destaining was performed by washing the gel pieces five times with a solution of 50% acetonitrile/0.1 M NH_4HCO_3. The gel pieces were dried completely, 10 μL of a solution of 12.5 ng/μL chymotrypsin in 50 mM NH_4HCO_3 was added, and the solution was incubated for 4 h at 37 °C. The supernatant was collected, and the gel pieces were further extracted with 40 μL of 50% acetonitrile/1% TFA. The pooled supernatant was dried and redissolved in 50 μL of 0.1% acetic acid. A total of 2 μL of samples were subjected to LC-MS analysis using a dual pressure LTQ-Orbitrap Elite mass spectrometer connected to an electrospray ion source (Thermo Fisher Scientific) as recently specified[62] and a custom-made column heater set to 60 °C. Peptide separation was carried out using an EASY nLC-1000 system (Thermo Fisher Scientific) equipped with a RP-HPLC column (75 μm × 30 cm) packed in-house with C18 resin (ReproSil-Pur C18−AQ, 1.9 μm resin; Maisch GmbH, Germany) using a linear gradient from 95% solvent A (0.1% formic acid, 99.9% water) and 5% solvent B (80% acetonitrile, 0.1% formic acid, 19.9% water) to 28% solvent B over 75 min to 40% solvent B over 15 min to 95% solvent B over 2 min and 95% solvent B over 18 min at a flow rate of 0.2 μL/min. The data acquisition mode was set to obtain one high resolution MS scan in the FT part of the mass spectrometer at a resolution of 60 000 full width at half-maximum (at 400 *m*/*z*, MS1) followed by MS/MS (MS2) scans in the linear ion trap of the 20 most intense MS signals. The charged state screening modus was enabled to exclude unassigned and singly charged ions and the dynamic exclusion duration was set to 30 s. The ion accumulation times were set to 200 ms (MS1) and 50 ms (MS2). MS1 and MS2 scans were acquired at a target setting of 1E6 ions and 10 000 ions, respectively. The collision energy was set to 30%, and one microscan was acquired for each spectrum. Peptide identification was carried out by peptide mass fingerprinting using the Skyline software (v4.1.0.11796, https://skyline.ms/) allowing all theoretical precursor ion masses with up to three missed cleavages and charge states +2 to +5. Mass tolerance was set to 10 ppm and the experimental isotope pattern were manually checked to match the expected values.

NMR Spectroscopy. Samples for NMR spectroscopy were expressed in M9 medium, supplemented with perdeuterated water and 1 g/L ^{15}N ammonium chloride. Additionally, the triple-labeled sample and 3D-NOESY sample were supplemented with 2 g/L of [^{2}H, ^{13}C]-glucose and 2 g/L of [^{2}H, ^{12}C]-glucose, respectively. The samples for specific labeling were supplemented according to Table S2. Samples were concentrated and buffer exchanged to 20 mM NaPi pH 7.5, NaCl 150 mM, LDAO 0.1%. 2D [^{15}N, ^{1}H]-TROSY[63] experiments of all samples were measured on 600, 700, and 900 MHz spectrometers equipped with a cryo-probes. The TROSY-HNCA experiment was recorded on a sample of 700 μM [*U*-^{15}N, ^{13}C, ^{2}H]-labeled BamA^{ext} in NMR buffer on a 900 MHz Bruker spectrometer equipped with a cryo-probe. 64 scans were acquired at 37 °C with 2048, 88, and 80 increments in the δ_3(^{1}H), δ_2(^{15}N), and δ_1(^{13}C) dimension, respectively, using deuterium decoupling (Figure S4). TROSY-HNCACB experiment was recorded on the same sample with a 900 MHz Bruker spectrometer equipped with a cryo-probe. A total of 52 scans were acquired at 37 °C with 2048, 80, and 148 increments in the δ_3(^{1}H), δ_2(^{15}N), and δ_1(^{13}C) dimension, respectively, using deuterium decoupling. The ^{15}N-TROSY-[^{1}H,^{1}H]-NOESY experiment was recorded on a sample of 700 μM [*U*-^{15}N,^{13}C,^{2}H]-labeled BamA^{ext} in NMR buffer on a 900 MHz Bruker spectrometer equipped with a cryo-probe. Sixteen scans were

DOI: 10.1021/jacs.8b03220
J. Am. Chem. Soc. XXXX, XXX, XXX−XXX

acquired at 37 °C with 2048, 100, and 320 increments in the $\delta_3(^1H)$, $\delta_2(^{15}N)$, and $\delta_1(^1H)$ dimension, respectively, with a NOESY mixing time of 100 ms (Figure S6). A figure containing a summary of the data available for the assigned residues is shown in the Supporting Information (Figure S8). The [^{15}N,^1H]-TRACT experiment[64] and bulk R_1 and R_2 experiments[65] were recorded at 37 °C, on a Bruker 600 MHz Avance III HD spectrometer equipped with a cryogenic probe. The number of scans was adjusted to achieve a satisfactory signal-to-noise ratio. From [^{15}N, ^1H]-TRACT the slow relaxing α-spin (R_α) and fast relaxing β-spin state (R_β) of ^{15}N were measured (incremental time was 600 μs). From single exponential fits the bulk relaxation rates R_α and R_β of the corresponding spin states were derived from an integral (^1H ppm range of 9.5 ppm to 8.5 ppm) and converted into the rotational correlation time τ_c.[64] Bulk R_1 (relaxation delays: 0, 200, 400, 600, 800, 1000, 1200, and 1400 ms) and R_2 (relaxation delays: 0, 4, 7, 10, 14, 17, 20, and 25 ms) relaxation rates were derived from single exponential fits (^1H ppm range of 9.5 to 8.5 ppm) using intensities.

Specific Labeling. Specific labeling/unlabeling of samples was performed on the BamA^{ext} construct using auxotrophic strains (Figure S5).[50] A summary of the strains and isotopes used for specific labeling is given in Table S1. Arginine, glycine, histidine, isoleucine, leucine, methionine, phenylalanine, threonine, tyrosine, or valine were specifically labeled. Lysine and tryptophan were specifically unlabeled. Lysine was additionally ^{13}C unlabeled and a 2D-TROSY HNCO was recorded.[66] Aspartic acid/asparagine were unlabeled together as well as glutamine and glutamic acid. Serine was labeled using a controlled scrambling strategy. Threonine was labeled and allowed to scramble to serine and glycine. Using the identities from individual samples of labeled threonine and glycine, serines were identified as the remaining unidentified residues.

Structure Determination of C-Terminally Extended BamA (BamA^{+9}). For the crystallization of the BamA-barrel including nine additional amino acids at the C-terminus (MENVALDFS), BamA^{+9}, the protein buffer was exchanged by gel-filtration into 20 mM Tris pH 7.5, 150 mM NaCl, 0.05% LDAO and 0.35% C_8E_4. Initial crystallization trials were performed at 293 K by sitting-drop vapor diffusion using MemGold- and MemGold2-Screen from Molecular Dimensions with a Gryphon robot (Art Robin Instruments). The initial hits were optimized by fine-screening with larger drops by hanging drop vapor diffusion. Crystals in space group $P2_12_12$ were grown in 22% (w/v) PEG 400, 0.07 M NaCl and 0.05 M sodium citrate pH 4.5. Crystals were directly flash-frozen in liquid nitrogen. A data set was collected at beamline X06DA (PXIII) at the Swiss Light Source (SLS, Paul Scherer Institute, Villigen, Switzerland). Data were integrated and scaled with XDS.[67] Phases for BamA^{+9} were obtained by molecular replacement (MR) using MOLREP[68] with PDB entry 4N75 as a search model. Model building was performed using COOT,[69] and the structure was refined with REFMAC.[70] The program MolProbity[71] was used to evaluate the final model and PyMOL[72] for the visualization of the protein structure.

In Vivo Complementation Assay. The in vivo functionality of all BamA β-barrel mutants and C-terminal elongations were tested in JCM166 cells which were transformed with a pET3b plasmid carrying the full length BamA versions with an N-terminal His_{10}-tag of the corresponding BamA barrel mutants. In JCM166 cells, the genomic gene of BamA is under control of an arabinose promotor. In the presence of 0.1% L-(+)-arabinose, the BamA gene is expressed and the cells show a normal phenotype. The absence of arabinose is lethal and cells only survive by transformation with a BamA plasmid which is able to complement native BamA function. Empty pET3b plasmid and pET3b with wild type BamA were used as negative and positive control, respectively. All transformations were streaked out on agar-plates without and with 0.1% L-(+)-arabinose and incubated at 37 °C overnight.

■ ASSOCIATED CONTENT

Supporting Information

The Supporting Information is available free of charge on the ACS Publications website at DOI: 10.1021/jacs.8b03220.

Data and collection statistics, labeling information, mass spectrometry of cross-linking patterns, arabinose assay, examples spectra of triple-resonance experiments and selective labeling, the sequence-specific resonance assignment of BamA^{ext}, a diagram with the available NMR data for each assigned residue, the design schemes for the cross-linked BamA variants, the purification profile and SDS-gel of cross-linked BamA variants, and additional BamA conformers spectra (PDF)

■ AUTHOR INFORMATION

Corresponding Author

*sebastian.hiller@unibas.ch

ORCID

Stefan Bibow: 0000-0003-1564-7045

Sebastian Hiller: 0000-0002-6709-4684

Present Address

‡Wallenberg Centre for Molecular and Translational Medicine and the Department of Psychiatry and Neurochemistry, University of Gothenburg, 405 30 Göteborg, Sweden.

Author Contributions

†J.-B.H. and M.Z. contributed equally.

Notes

The authors declare no competing financial interest.

■ ACKNOWLEDGMENTS

We thank Dario Dörig, Roman Jakob, Timm Maier, and the beamline staff at Swiss Light Source (Villigen, Switzerland) for technical support. The sequence-specific resonance assignment of BamA was deposited in the BMRB database with accession code 27431. The crystal structure of BamA^{ext} was deposited in the PDB with accession code 6FSU. This work was supported by the Swiss National Science Foundation via the NRP 72 (Grant 407240_167125 to S.H.) and the European Research Council (FP7 Contract MOMP 281746 to S.H.).

■ REFERENCES

(1) Nikaido, H.; Vaara, M. *Microbiol. Rev.* **1985**, *49*, 1−32.
(2) Nikaido, H. *Microbiol. Mol. Biol. Rev.* **2003**, *67*, 593−656.
(3) Koebnik, R.; Locher, K. P.; Van Gelder, P. *Mol. Microbiol.* **2000**, *37*, 239−253.
(4) Sjöström, M.; Wold, S.; Wieslander, A.; Rilfors, L. *EMBO J.* **1987**, *6*, 823−831.
(5) Korndörfer, I. P.; Dommel, M. K.; Skerra, A. *Nat. Struct. Mol. Biol.* **2004**, *11*, 1015−1020.
(6) Schiffrin, B.; Calabrese, A. N.; Higgins, A. J.; Humes, J. R.; Ashcroft, A. E.; Kalli, A. C.; Brockwell, D. J.; Radford, S. E. *J. Mol. Biol.* **2017**, *429*, 3776−3792.
(7) Zhong, M.; Ferrell, B.; Lu, W.; Chai, Q.; Wei, Y. *J. Bacteriol.* **2013**, *195*, 1061−1067.
(8) Thoma, J.; Burmann, B. M.; Hiller, S.; Müller, D. J. *Nat. Struct. Mol. Biol.* **2015**, *22*, 795−802.
(9) Voulhoux, R.; Bos, M. P.; Geurtsen, J.; Mols, M.; Tommassen, J. *Science* **2003**, *299*, 262−265.
(10) Knowles, T. J.; Scott-Tucker, A.; Overduin, M.; Henderson, I. R. *Nat. Rev. Microbiol.* **2009**, *7*, 206−214.
(11) Ricci, D. P.; Hagan, C. L.; Kahne, D.; Silhavy, T. J. *Proc. Natl. Acad. Sci. U. S. A.* **2012**, *109*, 3487−3491.

DOI: 10.1021/jacs.8b03220
J. Am. Chem. Soc. XXXX, XXX, XXX−XXX

(12) Sánchez-Pulido, L.; Devos, D.; Genevrois, S.; Vicente, M.; Valencia, A. *Trends Biochem. Sci.* **2003**, *28*, 523−526.
(13) Gentle, I. E.; Burri, L.; Lithgow, T. *Mol. Microbiol.* **2005**, *58*, 1216−1225.
(14) Bos, M. P.; Robert, V.; Tommassen, J. *EMBO Rep.* **2007**, *8*, 1149−1154.
(15) Robert, V.; Volokhina, E. B.; Senf, F.; Bos, M. P.; Gelder, P. V.; Tommassen, J. *PLoS Biol.* **2006**, *4*, e377.
(16) Wu, T.; Malinverni, J.; Ruiz, N.; Kim, S.; Silhavy, T. J.; Kahne, D. *Cell* **2005**, *121*, 235−245.
(17) Malinverni, J. C.; Werner, J.; Kim, S.; Sklar, J. G.; Kahne, D.; Misra, R.; Silhavy, T. J. *Mol. Microbiol.* **2006**, *61*, 151−164.
(18) Sklar, J. G.; Wu, T.; Gronenberg, L. S.; Malinverni, J. C.; Kahne, D.; Silhavy, T. J. *Proc. Natl. Acad. Sci. U. S. A.* **2007**, *104*, 6400−6405.
(19) Knowles, T. J.; McClelland, D. M.; Rajesh, S.; Henderson, I. R.; Overduin, M. *Biomol. NMR Assignments* **2009**, *3*, 203−206.
(20) Albrecht, R.; Zeth, K. *Acta Crystallogr., Sect. F: Struct. Biol. Cryst. Commun.* **2010**, *66*, 1586−1590.
(21) Knowles, T. J.; Sridhar, P.; Rajesh, S.; Manoli, E.; Overduin, M.; Henderson, I. R. *Biomol. NMR Assignments* **2010**, *4*, 179−181.
(22) Heuck, A.; Schleiffer, A.; Clausen, T. *J. Mol. Biol.* **2011**, *406*, 659−666.
(23) Warner, L. R.; Varga, K.; Lange, O. F.; Baker, S. L.; Baker, D.; Sousa, M. C.; Pardi, A. *J. Mol. Biol.* **2011**, *411*, 83−95.
(24) Rossiter, A. E.; Leyton, D. L.; Tveen-Jensen, K.; Browning, D. F.; Sevastsyanovich, Y.; Knowles, T. J.; Nichols, K. B.; Cunningham, A. F.; Overduin, M.; Schembri, M. A.; Henderson, I. R. *J. Bacteriol.* **2011**, *193*, 4250−4253.
(25) Kim, K. H.; Kang, H.-S.; Okon, M.; Escobar-Cabrera, E.; McIntosh, L. P.; Paetzel, M. *Biochemistry* **2011**, *50*, 1081−1090.
(26) Knowles, T. J.; Browning, D. F.; Jeeves, M.; Maderbocus, R.; Rajesh, S.; Sridhar, P.; Manoli, E.; Emery, D.; Sommer, U.; Spencer, A.; Leyton, D. L.; Squire, D.; Chaudhuri, R. R.; Viant, M. R.; Cunningham, A. F.; Henderson, I. R.; Overduin, M. *EMBO Rep.* **2011**, *12*, 123−128.
(27) Kim, K. H.; Paetzel, M. *J. Mol. Biol.* **2011**, *406*, 667−678.
(28) Rigel, N. W.; Ricci, D. P.; Silhavy, T. J. *Proc. Natl. Acad. Sci. U. S. A.* **2013**, *110*, 5151−5156.
(29) Dong, C.; Yang, X.; Hou, H.-F.; Shen, Y.-Q.; Dong, Y.-H. *Acta Crystallogr., Sect. D: Biol. Crystallogr.* **2012**, *68*, 1134−1139.
(30) Chen, Z.; Zhan, L.-H.; Hou, H.-F.; Gao, Z.-Q.; Xu, J.-H.; Dong, C.; Dong, Y.-H. *Acta Crystallogr. D* **2016**, *72*, 236−244.
(31) Ni, D.; Wang, Y.; Yang, X.; Zhou, H.; Hou, X.; Cao, B.; Lu, Z.; Zhao, X.; Yang, K.; Huang, Y. *FASEB J.* **2014**, *28*, 2677−2685.
(32) Noinaj, N.; Kuszak, A. J.; Gumbart, J. C.; Lukacik, P.; Chang, H.; Easley, N. C.; Lithgow, T.; Buchanan, S. K. *Nature* **2013**, *501*, 385−390.
(33) Bakelar, J.; Buchanan, S. K.; Noinaj, N. *Science* **2016**, *351*, 180−186.
(34) Gu, Y.; Li, H.; Dong, H.; Zeng, Y.; Zhang, Z.; Paterson, N. G.; Stansfeld, P. J.; Wang, Z.; Zhang, Y.; Wang, W.; Dong, C. *Nature* **2016**, *531*, 64−69.
(35) Han, L.; Zheng, J.; Wang, Y.; Yang, X.; Liu, Y.; Sun, C.; Cao, B.; Zhou, H.; Ni, D.; Lou, J.; Zhao, Y.; Huang, Y. *Nat. Struct. Mol. Biol.* **2016**, *23*, 192−196.
(36) Iadanza, M. G.; Higgins, A. J.; Schiffrin, B.; Calabrese, A. N.; Brockwell, D. J.; Ashcroft, A. E.; Radford, S. E.; Ranson, N. A. *Nat. Commun.* **2016**, *7*, 12865.
(37) Gruss, F.; Zähringer, F.; Jakob, R. P.; Burmann, B. M.; Hiller, S.; Maier, T. *Nat. Struct. Mol. Biol.* **2013**, *20*, 1318−1320.
(38) Schiffrin, B.; Brockwell, D. J.; Radford, S. E. *BMC Biol.* **2017**, *15*, 123.
(39) Noinaj, N.; Gumbart, J. C.; Buchanan, S. K. *Nat. Rev. Microbiol.* **2017**, *15*, 197−204.
(40) Konovalova, A.; Kahne, D. E.; Silhavy, T. J. *Annu. Rev. Microbiol.* **2017**, *71*, 539−556.
(41) Doerner, P. A.; Sousa, M. C. *Biochemistry* **2017**, *56*, 3142−3149.
(42) Noinaj, N.; Kuszak, A. J.; Balusek, C.; Gumbart, J. C.; Buchanan, S. K. *Structure* **2014**, *22*, 1055−1062.
(43) Morgado, L.; Zeth, K.; Burmann, B. M.; Maier, T.; Hiller, S. *J. Biomol. NMR* **2015**, *61*, 333−345.
(44) Gu, Y.; Zeng, Y.; Wang, Z.; Dong, C. *Biochem. J.* **2017**, *474*, 3951−3961.
(45) Kay, L. E.; Ikura, M.; Tschudin, R.; Bax, A. *J. Magn. Reson.* **1990**, *89*, 496−514.
(46) Salzmann, M.; Wider, G.; Pervushin, K.; Senn, H.; Wüthrich, K. *J. Am. Chem. Soc.* **1999**, *121*, 844−848.
(47) Grzesiek, S.; Bax, A. D. *J. Magn. Reson.* **1992**, *96*, 432−440.
(48) Marion, D.; Kay, L. E.; Sparks, S. W.; Torchia, D. A.; Bax, A. *J. Am. Chem. Soc.* **1989**, *111*, 1515−1517.
(49) Muchmore, D. C.; McIntosh, L. P.; Russell, C. B.; Anderson, D. E.; Dahlquist, F. W. *Methods Enzymol.* **1989**, *177*, 44−73.
(50) Lin, M. T.; Fukazawa, R.; Miyajima-Nakano, Y.; Matsushita, S.; Choi, S. K.; Iwasaki, T.; Gennis, R. B. *Methods Enzymol.* **2015**, *565*, 45−66.
(51) Talluri, S.; Wagner, G. *J. Magn. Reson., Ser. B* **1996**, *112*, 200−205.
(52) Shen, Y.; Bax, A. *Methods Mol. Biol.* **2015**, *1260*, 17−32.
(53) Alexandrov, A. I.; Mileni, M.; Chien, E. Y. T.; Hanson, M. A.; Stevens, R. C. *Structure* **2008**, *16*, 351−359.
(54) Branigan, E.; Pliotas, C.; Hagelueken, G.; Naismith, J. H. *Nat. Protoc.* **2013**, *8*, 2090−2097.
(55) Sinnige, T.; Houben, K.; Pritisanac, I.; Renault, M.; Boelens, R.; Baldus, M. *J. Biomol. NMR* **2015**, *61*, 321−332.
(56) Liang, B.; Tamm, L. K. *Proc. Natl. Acad. Sci. U. S. A.* **2007**, *104*, 16140−16145.
(57) Hiller, S.; Malia, T. J.; Garces, R. G.; Orekhov, V. Y.; Wagner, G. *Biomol. NMR Assignments* **2010**, *4*, 29−32.
(58) Berardi, M. J.; Shih, W. M.; Harrison, S. C.; Chou, J. J. *Nature* **2011**, *476*, 109−113.
(59) Wagner, S.; Klepsch, M. M.; Schlegel, S.; Appel, A.; Draheim, R.; Tarry, M.; Högbom, M.; Van Wijk, K. J.; Slotboom, D. J.; Persson, J. O.; de Gier, J.-W. *Proc. Natl. Acad. Sci. U. S. A.* **2008**, *105*, 14371−14376.
(60) Schlegel, S.; Löfblom, J.; Lee, C.; Hjelm, A.; Klepsch, M.; Strous, M.; Drew, D.; Slotboom, D. J.; de Gier, J.-W. *J. Mol. Biol.* **2012**, *423*, 648−659.
(61) Frey, L.; Lakomek, N.-A.; Riek, R.; Bibow, S. *Angew. Chem., Int. Ed.* **2017**, *56*, 380−383.
(62) Ahrné, E.; Glatter, T.; Viganò, C.; Schubert, C. v.; Nigg, E. A.; Schmidt, A. *J. Proteome Res.* **2016**, *15*, 2537−2547.
(63) Pervushin, K.; Riek, R.; Wider, G.; Wüthrich, K. *J. Am. Chem. Soc.* **1998**, *120*, 6394−6400.
(64) Lee, D.; Hilty, C.; Wider, G.; Wüthrich, K. *J. Magn. Reson.* **2006**, *178*, 72−76.
(65) Lakomek, N.-A.; Ying, J.; Bax, A. *J. Biomol. NMR* **2012**, *53*, 209−221.
(66) Takeuchi, K.; Ng, E.; Malia, T. J.; Wagner, G. *J. Biomol. NMR* **2007**, *38*, 89−98.
(67) Kabsch, W. *Acta Crystallogr., Sect. D: Biol. Crystallogr.* **2010**, *66*, 125−132.
(68) Vagin, A.; Teplyakov, A. *J. Appl. Crystallogr.* **1997**, *30*, 1022−1025.
(69) Emsley, P.; Cowtan, K. *Acta Crystallogr., Sect. D: Biol. Crystallogr.* **2004**, *60*, 2126−2132.
(70) Murshudov, G. N.; Skubák, P.; Lebedev, A. A.; Pannu, N. S.; Steiner, R. A.; Nicholls, R. A.; Winn, M. D.; Long, F.; Vagin, A. A. *Acta Crystallogr., Sect. D: Biol. Crystallogr.* **2011**, *67*, 355−367.
(71) Chen, V. B.; Arendall, W. B.; Headd, J. J.; Keedy, D. A.; Immormino, R. M.; Kapral, G. J.; Murray, L. W.; Richardson, J. S.; Richardson, D. C. *Acta Crystallogr., Sect. D: Biol. Crystallogr.* **2010**, *66*, 12−21.
(72) DeLano, W. L. *CCP4 Newsletter on Protein Crystallography* **2002**, *40*, 82−92.

DOI: 10.1021/jacs.8b03220
J. Am. Chem. Soc. XXXX, XXX, XXX−XXX

Supporting material

Sequence-specific solution NMR assignments of the β-barrel insertase BamA to monitor its conformational ensemble at the atomic level

Jean-Baptiste Hartmann, Michael Zahn, Irena Matečko Burmann, Stefan Bibow, Sebastian Hiller*

* Correspondance to sebastian.hiller@unibas.ch

This file contains:

- Supplementary Tables S1–S3
- Supplementary Figures S1–S15

Supplementary Tables

Table S1: Data collection and refinement statistics for $BamA^{+9}$. Values in parentheses refer to the highest-resolution shell.

Data Collection	
Beamline	SLS PXIII
Space Group	$P2_12_12$
Cell Dimensions	
a, b, c (Å)	122.7, 159.4, 55.9
α, β, γ (°)	90.0, 90.0, 90.0
Wavelength (Å)	1.0
Resolution (Å)	66.84 – 2.60 (2.72 – 2.60)
R_{merge} [%]	15.6 (107.2)
R_{pim} [%]	11.1 (76.8)
CC(1/2)	0.997 (0.647)
$<I/\sigma I>$	7.7 (1.4)
Completeness (%)	99.8 (99.8)
Redundancy	5.4 (5.5)
Refinement	
R_{work} / R_{free}	26.9/29.8
Ramachandran plot	
most favored [%]	89.6
allowed [%]	10.1
generously allowed [%]	0.0
disallowed [%]	0.3
No. atoms	
Protein	6142
Water	53
B-factors	
Protein	47.1
Water	35.8
R.m.s. deviations	
Bond lengths (Å)	0.020
Bond angles (°)	2.11
MolProbity clashscore	4.85
pdb-code	6FSU

Table S2. Expression conditions for specifically labeled NMR samples of $BamA^{ext}$

Amino acid	Strain (ref. 56)	Type	Label (/l)	Additional a.a (/l) for scrambling control, auxotrophy supplementation, or unlabeling	Remarks
A	Lemo	Labeling (^{15}N)	274 mg ^{15}N-alanine		
D+N	RF4	Unlabeling (^{15}N)	1 g $^{15}NH_4Cl$ + 1 g ^{15}N-Isogro as background	2 g ^{14}N-aspartic acid	D/N are both unlabeled as Isogro does not contain asparagine.
Q+E	ML17	Unlabeling (^{15}N)	1 g $^{15}NH_4Cl$ + 1 g ^{15}N-Isogro as background	2 g ^{14}N-glutamine	Q/E are both unlabeled as well as W. Isogro does not contain Q nor W. D and N were partially unlabeled.
G	RF1	Labeling (^{15}N)	390 mg ^{15}N-glycine	0.5 g ^{14}N-serine	
H	ML3	Labeling (^{15}N)	32 mg ^{15}N-histidine	all ^{14}N amino acids but histidine (molarity according to Lin, M.T (**52**)).	
F	RF4	Labeling (^{15}N)	130 mg ^{15}N-phenylalanine	1 g ^{14}N-tyrosine and 1 g ^{14}N-aspartic acid	
I	ML6	Labeling (^{15}N)	130 mg ^{15}N-isoleucine	1 g ^{14}N-leucine and 1g ^{14}N-valine	
L	ML6	Labeling (^{15}N)	260 mg ^{15}N-leucine	1 g ^{14}N-isoleucine and 1g ^{14}N-valine	
K	RF10	Unlabeling (^{15}N and ^{13}C)	1 g $^{15}NH_4Cl$ + 1 g ^{13}C-glucose as background	1 g ^{14}N-lysine	2D TROSY-HNCO was additionally measured on this sample.
M	RF11	Labeling (^{15}N)	20 mg ^{15}N-methionine	all ^{14}N amino acids but methionine (molarity according to Lin, M.T (**52**)).	
R	ML8	Labeling (^{15}N)	100 mg ^{15}N-arginine	all ^{14}N amino acids but arginine (molarity according to Lin, M.T (**52**)).	
S	RF2	Controlled scrambling Labeling (^{15}N)	162 mg ^{15}N-threonine	No amino acid added	Sample scrambled to serine and glycine. As glycines and threonines are identified from their respective samples, the remaining peaks are serines.
T	RF2	Labeling (^{15}N)	162 mg ^{15}N-threonine	1 g ^{14}N-serine and 1g ^{14}N-glycine	

W	RF12	Unlabeling (^{15}N)	1g $^{15}NH_4Cl$ as background	2 g ^{14}N-tryptophan	
Y	RF4	Labeling (^{15}N)	20 mg ^{15}N-tyrosine	1 g ^{14}N-phenylalanine and 1 g ^{14}N-aspartic acid	.
V	RF12	Labeling (^{15}N)	195mg ^{15}N-valine	1g ^{14}N-isoleucine and 1g ^{14}N-leucine	

Table S3. Chemical shift comparison between BamA–POTRA4–POTRA5 in lipid bilayers (**58**) and $BamA^{ext}$ in LDAO micelles.

Atom [1]	$\delta_{solid\text{-}state}$ [ppm] [2]	$\delta_{solution}$ [ppm] [3]
L581 N	121.3	122.3
L581 CA	54	53.8
T600 CA	61.7	61.2
I601 N	130.1	121.1
I601 CA	61.3	57.6
I601 CB	38.8	NA
V628 CA	60.2	59.9
V628 CB	37.9	36.5
V629 N	126.7	127.4
V629 CA	61.5	60.7
V629 CB	33.5	NA
L630 N	130.5	131.2
L630 CA	52.3	52
L630 CB	44	42.7
V733 CA	59.6	59.8
K792 CA	56.6	55.9
K793 N	122.2	119.7
K793 CA	54.8	58.2
K793 CB	36.2	NA

[1] from reference 58 (Sinnige et al., J. Biomol. NMR *61*, 321–332 (2015))

[2] this work

[3] atoms with matching assignment are indicated bold ($\Delta\delta$ < 1.0 ppm)

Suppplementary Figures

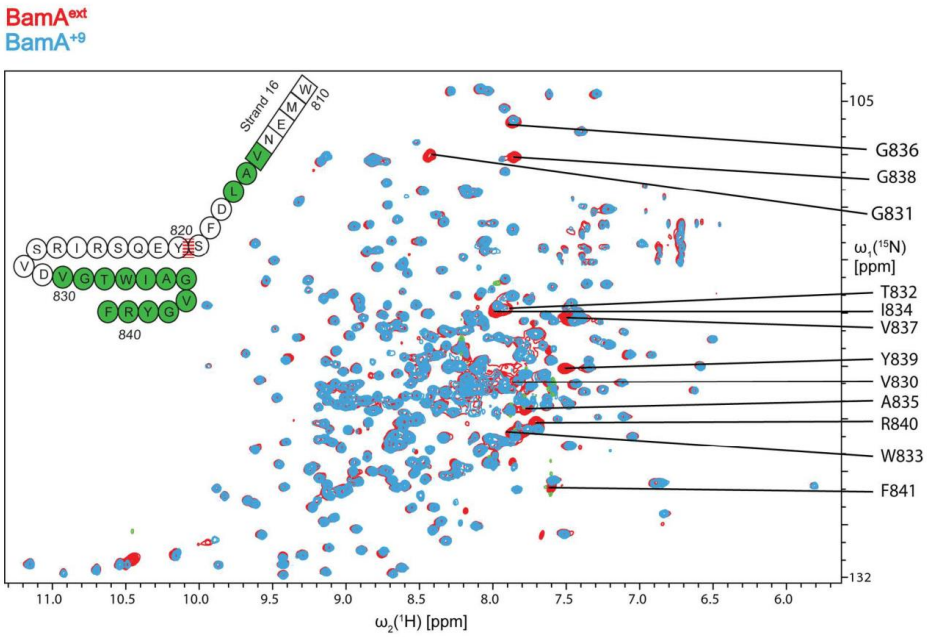

Figure S1. Overlay of 2D [^{15}N,^{1}H]-TROSY-HSQC spectra of BamA^{ext} (red) and BamA^{+9} (blue). The sequence-specific backbone amide resonance assignments of residues 830–841 are indicated. These are all located in the random coil region (7.5 ppm < $\delta(^{1}H^{N})$ < 8.5 ppm). A scheme of the C-terminal strand extension of BamA^{ext} is shown as an inset, with the assigned residues marked green. The construct BamA^{+9} ends after residue 819 (red dashed line).

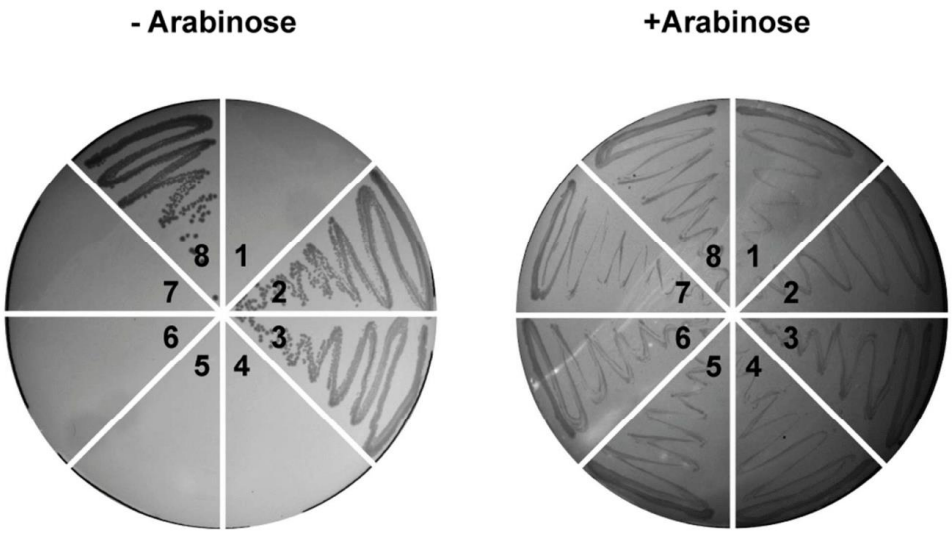

Figure S2. (A) *In vivo* functional assay of BamA β-barrel mutants and C-terminal extensions using JCM166 cells in the absence and presence of arabinose. (1) Empy vector and (2) *wt*-BamA serve as a negative and positive control, respectively. (3–6) Extension of the C-terminus of BamA by: +M (3), +ME (4), +MEN (5) and +MENVALDFS (6). Effect of the single amino acid mutations W810A (7) and G433A (8) on the background of *wt*-BamA.

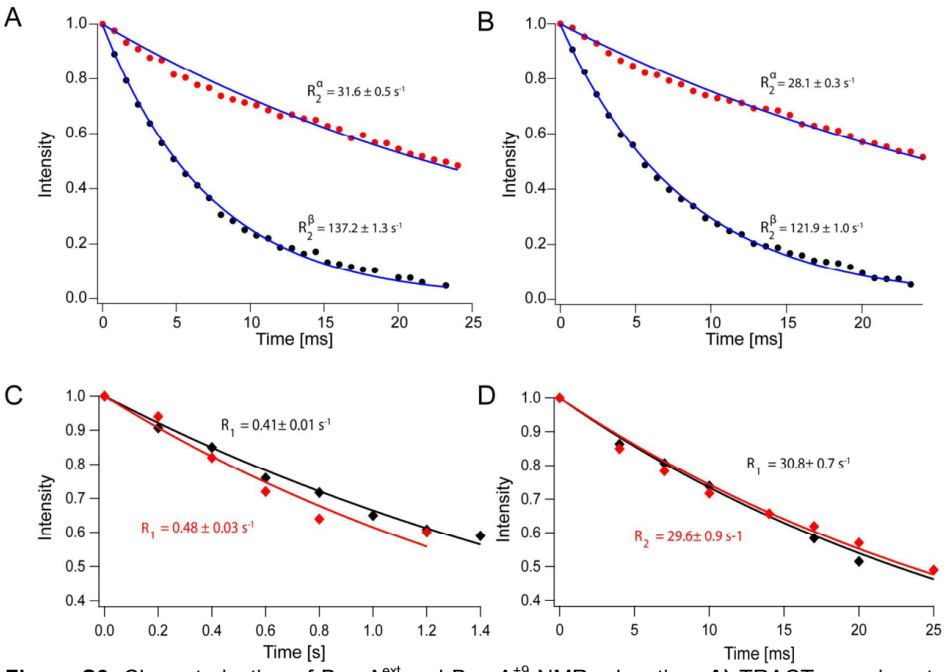

Figure S3. Characterization of BamA^{ext} and BamA^{+9} NMR relaxation. **A)** TRACT experiment of BamA^{ext} in LDAO micelles. The obtained R_2^{α} and R_2^{β} rates correspond to a rotational coorelation time τ_c of 55 ns. **B)** TRACT experiment of BamA^{+9} construct in LDAO. The obtained R_2^{α} and R_2^{β} rates correspond to a rotational correlation time τ_c of 49 ns. **C)** Longitudinal R_1 bulk relaxation rates of the downfield amide region (8.5–9.5 ppm) of BamA^{ext} (black) and BamA^{+9} (red) in LDAO micelles. **D)** Transverse R_2 bulk relaxation rates of the downfield amide region (8.5–9.5 ppm) of BamA^{ext} (black) and BamA^{+9} (red) in LDAO. All experiments were measured at 600 MHz field strength.

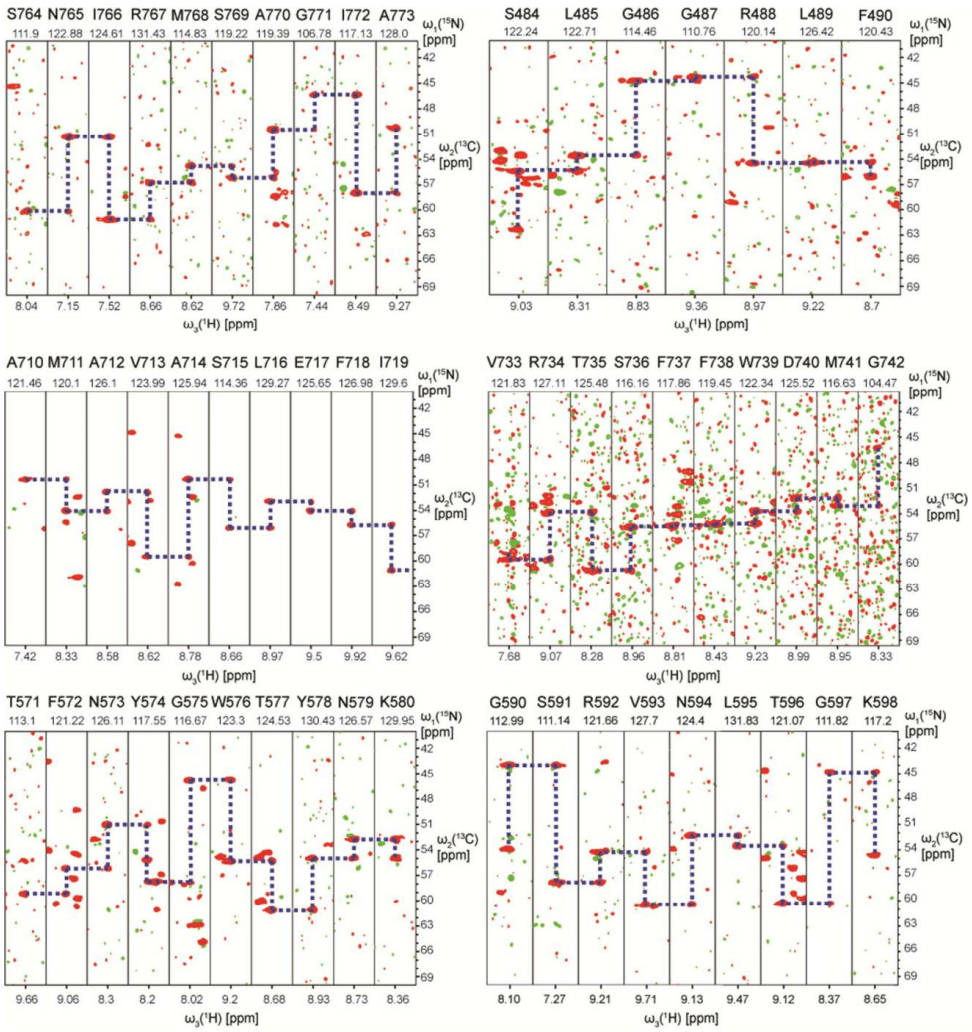

Figure S4. Backbone assignment of BamA^{ext}. Selected strips from a 3D TROSY-HNCA experiment recorded on a 700 µM sample of [*U*-^{2}H,^{13}C,^{15}N]-BamA^{ext} in LDAO detergent micelles in 20 mM NaPi, 150 mM NaCl at 37 °C on a 900 MHz Bruker spectrometer with cryogenic probe.

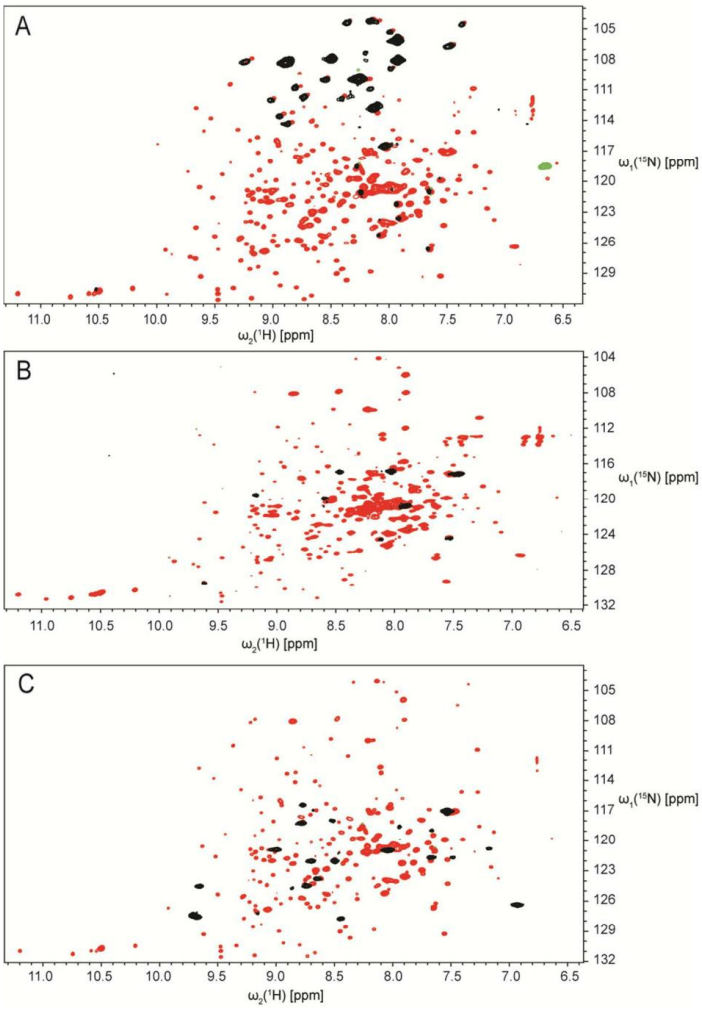

Figure S5. Selective labeling of BamA^{ext}. (A) [^{15}N,^{1}H]-TROSY-HSQC of a 100 µM sample of [*U*-^{2}H,^{15}N]-BamA^{ext} (red) and [Gly-^{1}H,^{15}N] BamA^{ext} (black) in LDAO detergent micelles, 20 mM NaPi, 150 mM NaCl. Minor scrambling is visible for high intensity ILV residues. (B) 2D [^{15}N,^{1}H]-TROSY-HSQC of a 100 µM sample of [*U*-^{2}H,^{15}N]-BamA^{ext} (red) and [Ile-^{1}H,^{15}N] BamA^{ext} in LDAO detergent micelles, 20 mM NaPi,150 mM NaCl. (C) [^{15}N,^{1}H]-TROSY-HSQC of a 100 µM sample of [*U*-^{2}H,^{15}N]-BamA^{ext} (red) and [Val-^{1}H,^{15}N]-BamA^{ext} in LDAO detergent micelles, 20 mM NaPi,150 mM NaCl.

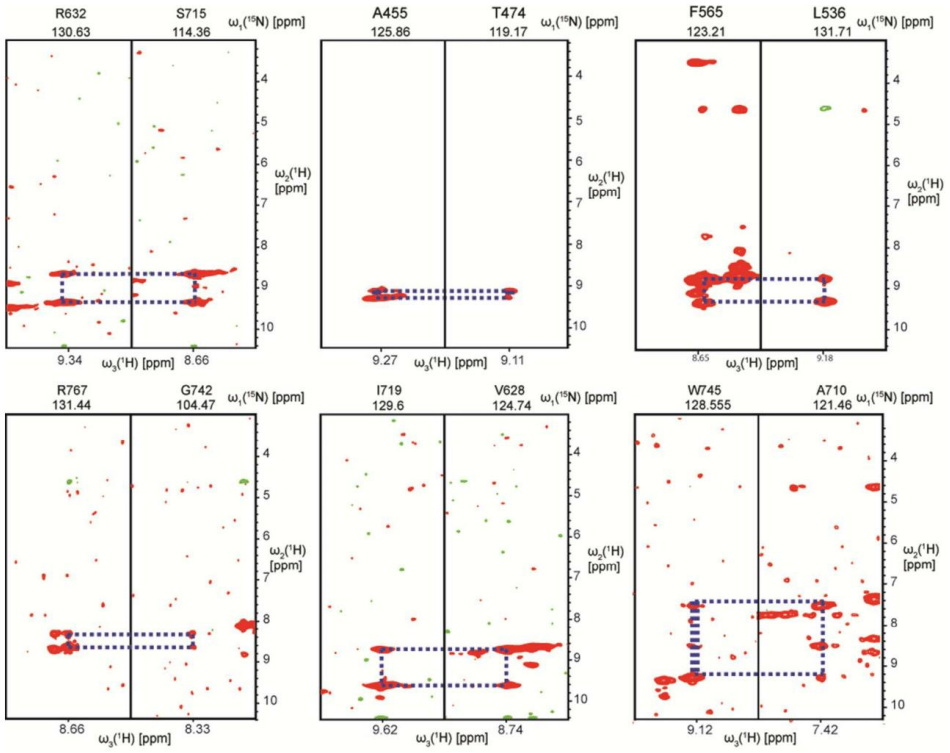

Figure S6. NOESY spectroscopy of BamA^{ext}. Selected strips from a 3D ^{15}N-TROSY-resolved-[^{1}H,^{1}H]-NOESY experiment recorded on a 700 µM sample of [*U*-^{2}H,^{13}C,^{15}N]-BamA^{ext} in [^{2}H]-LDAO micelles in 20 mM NaPi, 150 mM NaCl. Measured at 37 °C on a 900 MHz Bruker spectrometer with cryogenic probe.

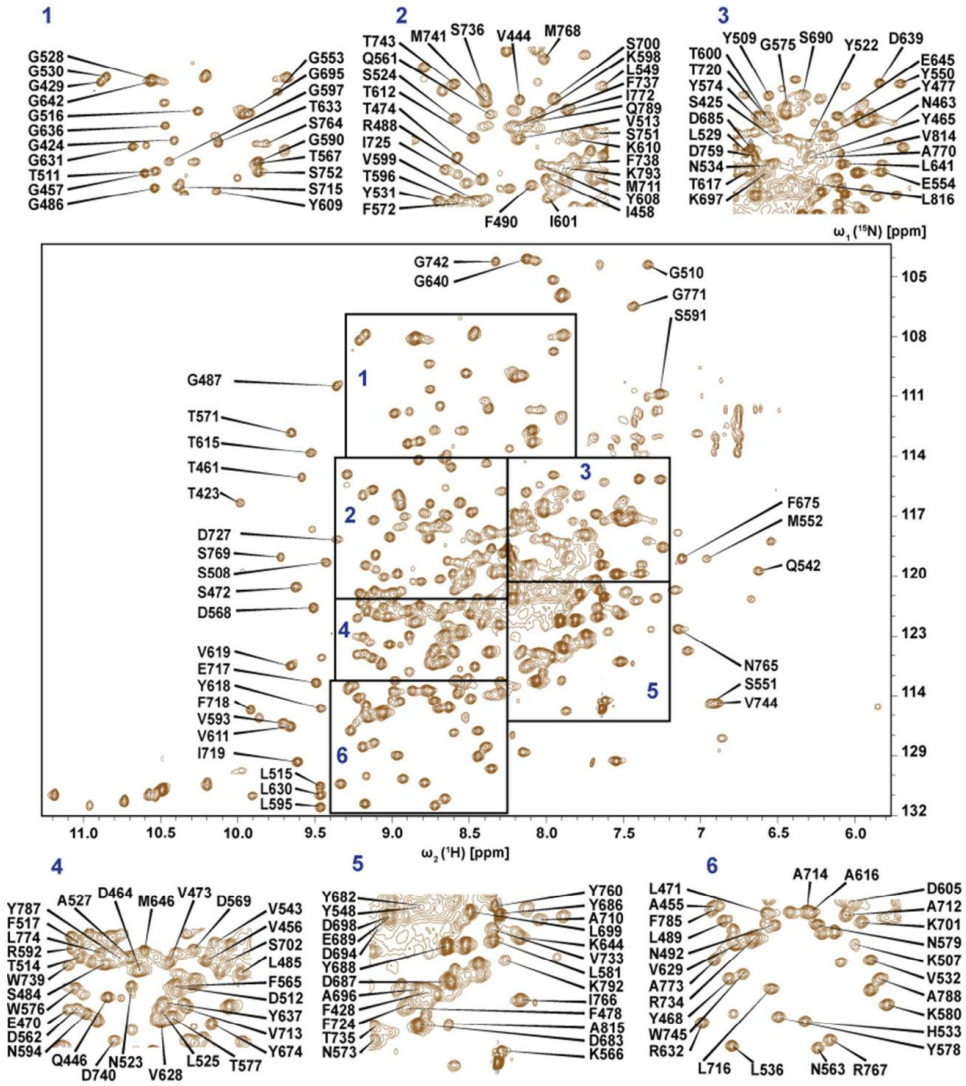

Figure S7. Sequence-specific resonance assignment of BamA^{ext}. 2D [^{15}N,^{1}H]-TROSY-HSQC spectra of 700 µM [*U*-^{2}H,^{15}N]-BamA^{ext}. The peaks are individually labelled with their backbone assignment. The crowded center region was extended into six side panels 1-6.

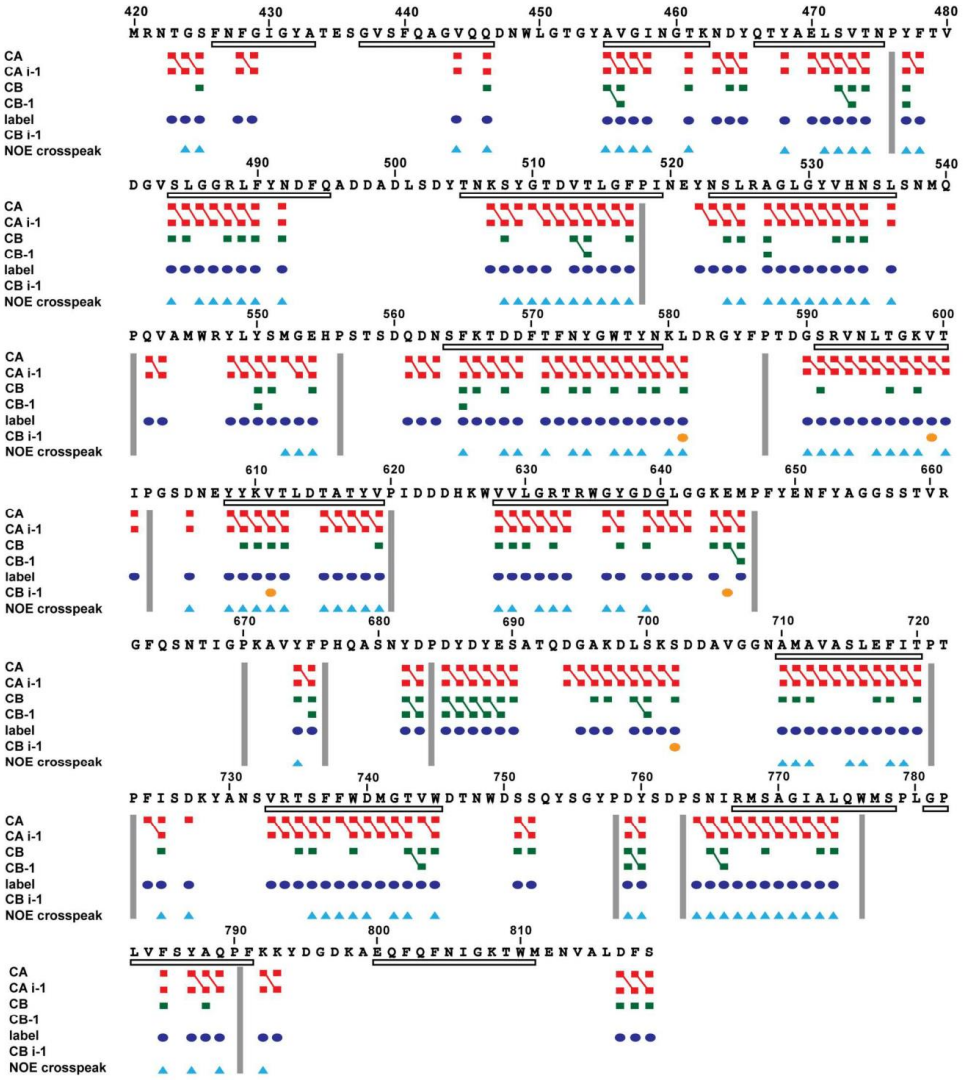

Figure S8. Connectivity diagram representing the experimental data available for the assignment of BamA^{ext}. Lines between $C_\alpha/C_{\alpha-1}$ and $C_\beta/C_{\beta-1}$ represent residues that are were connected together by their respective C_α and C_β. Residues which identity was confirmed using specific labeling or unlabeling are illustrated with a blue circle. Residues which were identified as successors of lysines are pictured with an orange circle. Residues for which one or more NOE proton-proton crosspeaks have been measured have a light blue triangle.

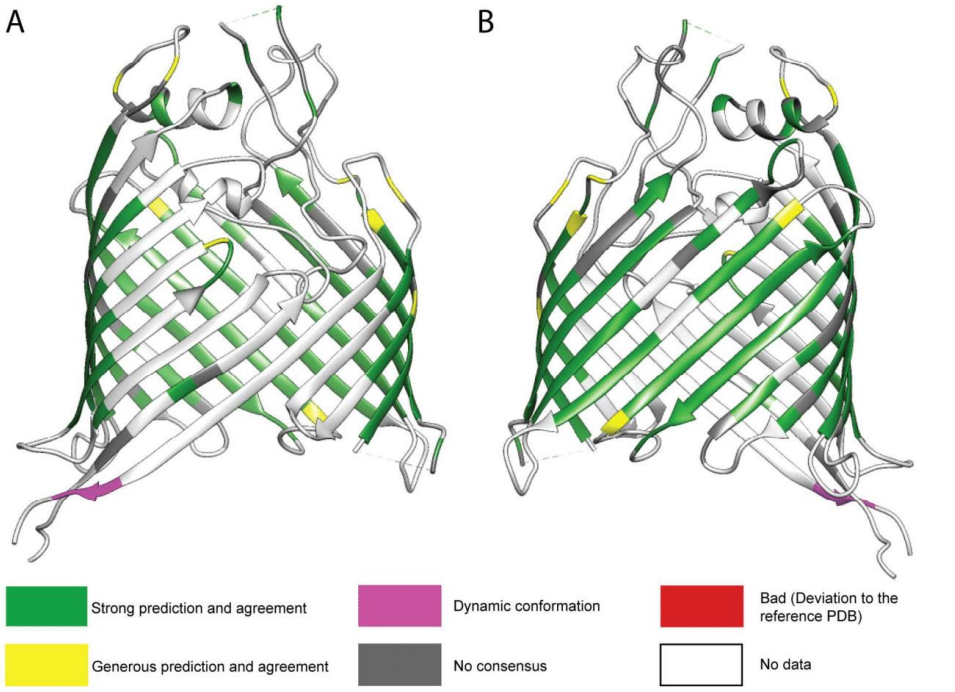

Figure S9. Secondary chemical shift analysis of BamA. Output of a chemical-shift-based dihedral angle prediction by Talos-N and its comparison with the crystal structure of $BamA^{+9}$. Residues where chemical shifts are in agreement with the structure are labeled green or yellow. Notably, for no residue a deviation between the prediction and the structure is obtained (would be shown in red color).

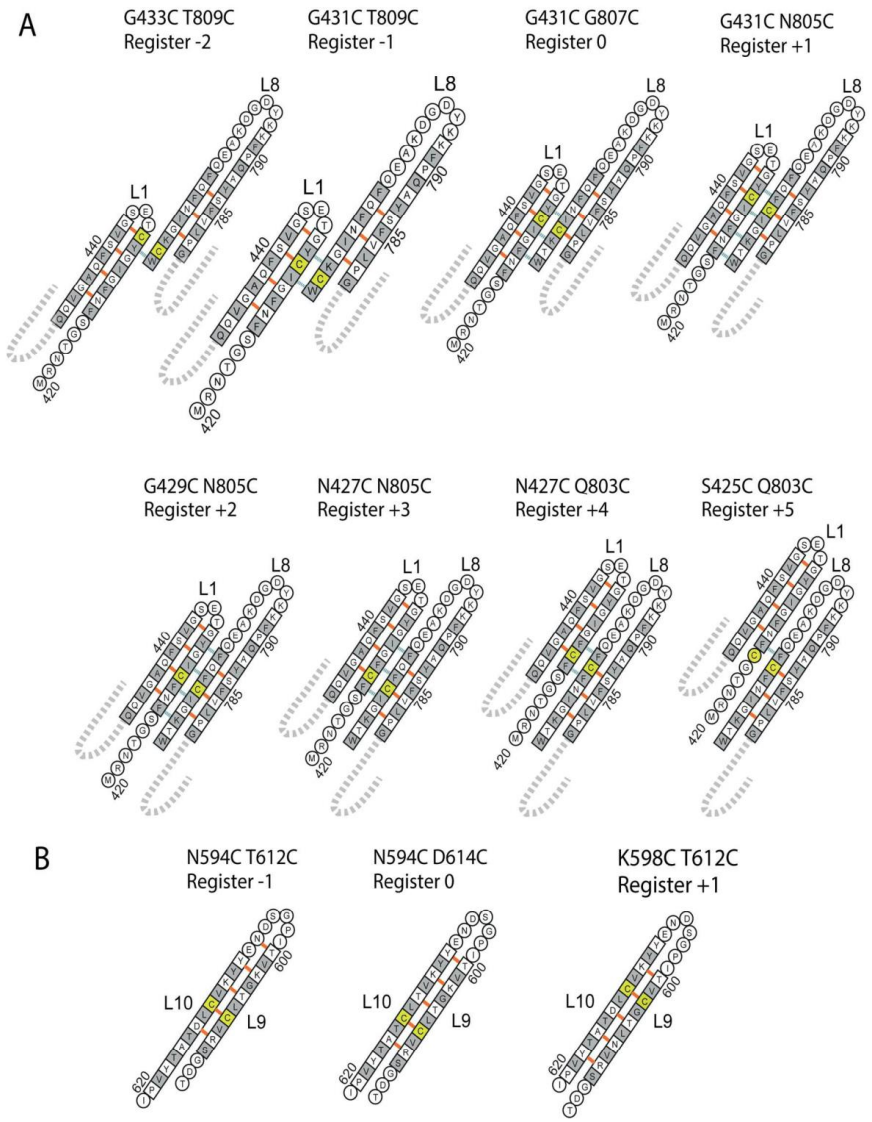

Figure S10. Design schemes for cross-linked BamA variants. The variants contain a pair of residues on two neighboring β-strands mutated to cysteines and resulting in the registers indicated. (A) the gate region strands 1–16 and (B) strands 9–10.

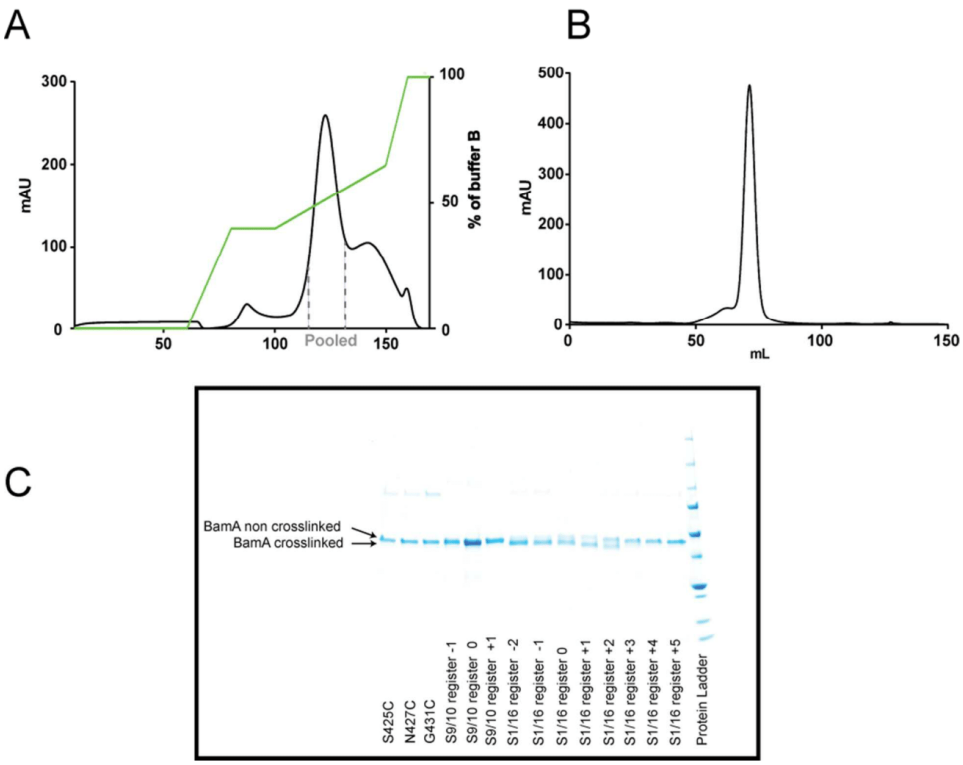

Figure S11. Purification of BamA constructs. (A) Elution profile of BamA(G431C,N805C) (register +1) from a HiTrap Q 5 mL HP column (GE). Buffer A: Tris 20 mM pH 8, LDAO 0.1%. Buffer B: BufferA + 500 mM NaCl. Well-folded protein elutes between 40%-65% of Buffer B. **(B)**. Size exclusion chromatogram of BamA(G431C,N805C) on a S200pg 16/600 column (GE). Buffer: Tris 20 mM, NaCl 150 mM, LDAO 0.1%. **(C).** SDS-PAGE of single and double cysteine mutants of the BamA barrel. Samples were boiled for 30 min at 95 °C in non-reducing conditions. For registers -2 to +2 of the gate region, a faster migrating band is present indicating successfully crosslinked BamA.

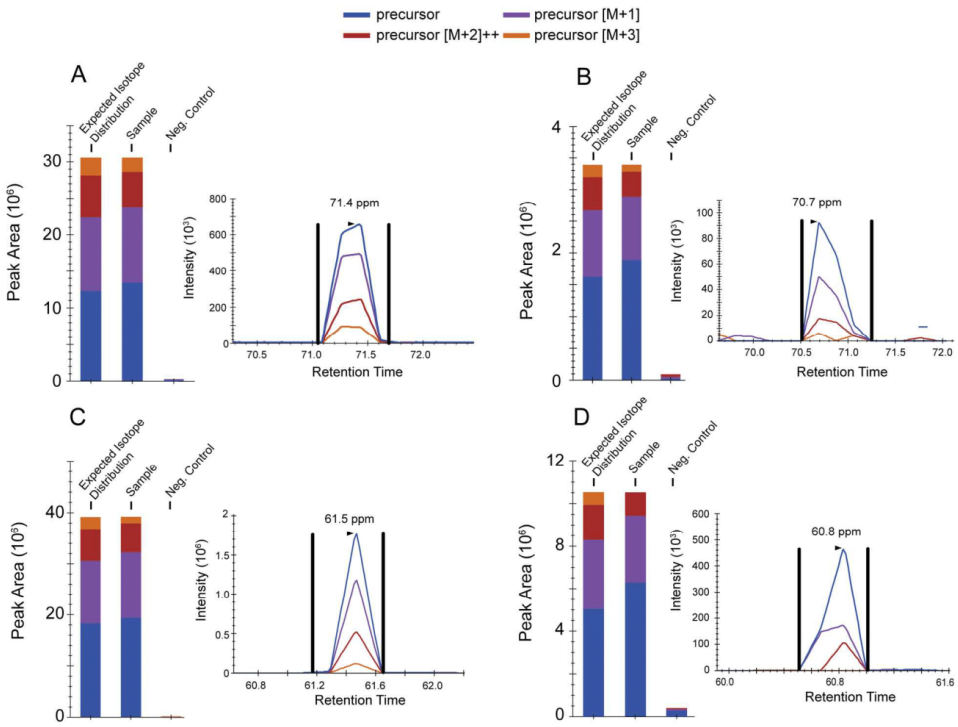

Figure S12. Identification of chemical cross-links in BamA by peptide mass fingerprinting. For each of four samples, the elution profile of the cross-linked peptide is shown together with a comparison of the resulting signal distribution with expected values and a negative control. **(A)** BamA(G433C, T809C), cross-linked in register -2. **(B)** BamA(G431, T809C), cross-linked in register -1. **(C)** BamA(G431, G807C), cross-linked in register 0. **(D)** BamA(G431, N805C), cross-linked in register 1.

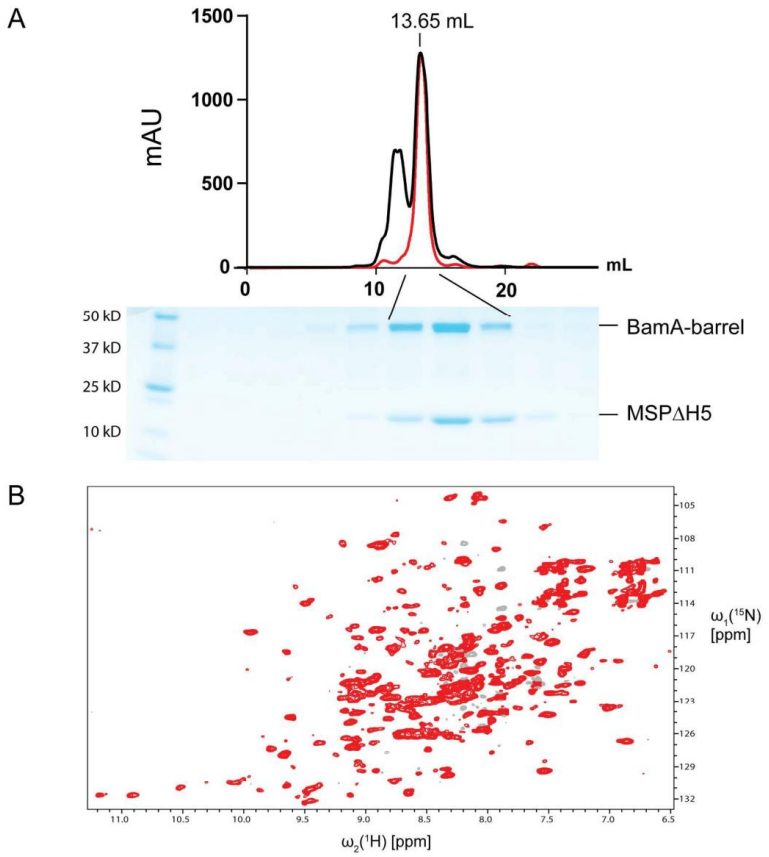

Figure S13. Reconstitution of wild-type BamA in lipid bilayer nanodiscs. (A) Size-exclusion chromatography profile (S200 10/300 GL) of wild-type BamA in MSPΔH5 lipid bilayer nanodiscs. From the initial chromatography run (black), the peak at 13.65 mL was pooled and re-run (red), demonstrating the stability of the assembly. The SDS-PAGE below shows the composition of the assembly. **(B)** 2D [^{15}N,^{1}H]-TROSY spectrum of 90 μM wild-type BamA reconstituted in MSPΔH5 nanodiscs in NMR buffer. The spectrum was recorded on a 600 MHz spectrometer.

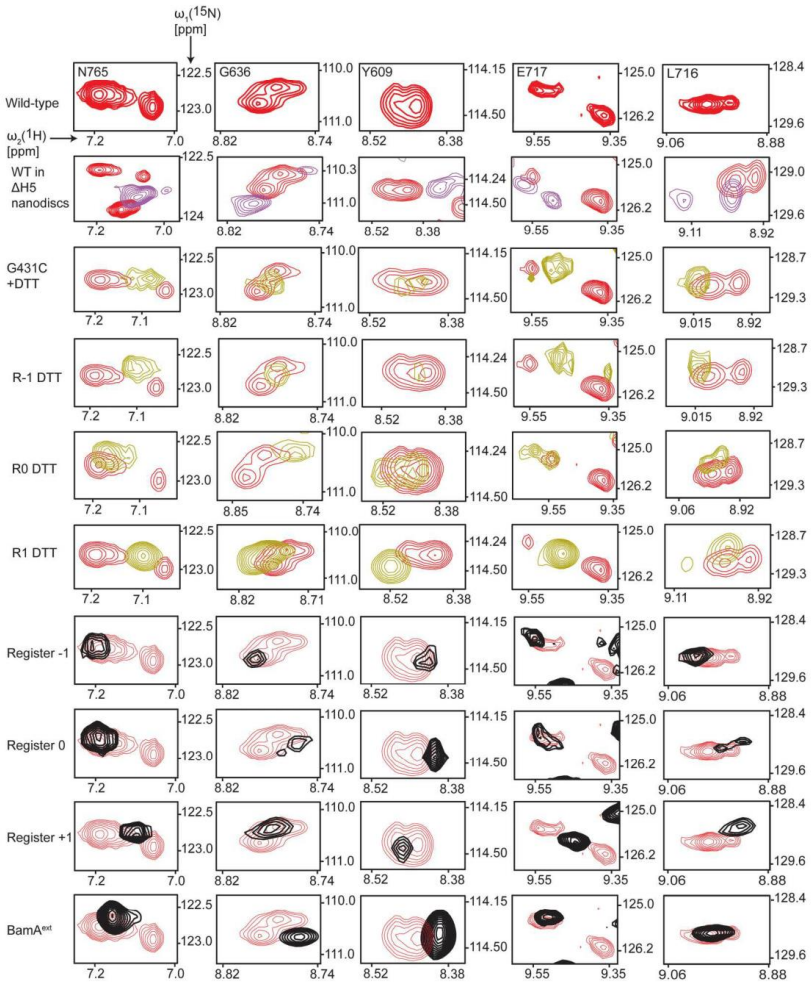

Figure S14. Selection of conformers from the BamA ensemble. For five selected residues, as indicated, the peak pattern in 2D [^{15}N,^{1}H]-TROSY-HSQC spectra is shown. The top row shows as a reference [*U*-^{2}H,^{15}N]-labeled wild-type BamA β-barrel in LDAO micelles. In subsequent rows, the wild spectrum (red) is overlaid with BamA β-barrel in different preparations, as indicated: BamA in MSPΔH5 lipid bilayer nanodiscs (purple); BamA(G431C) under reducing conditions (gold); BamA(G431C, T809C, register -1) under reducing conditions (gold), BamA (G431C, G807C, register 0) under reducing conditions (gold), BamA(G431C N805C, register +1) under reducing conditions (gold), cross-linked BamA(G431C, T809C, register -1, black), cross-linked BamA(G431C, G807C, register 0, black), cross-linked BamA(G431C N805C, register +1, black), BamA^{ext} (black).

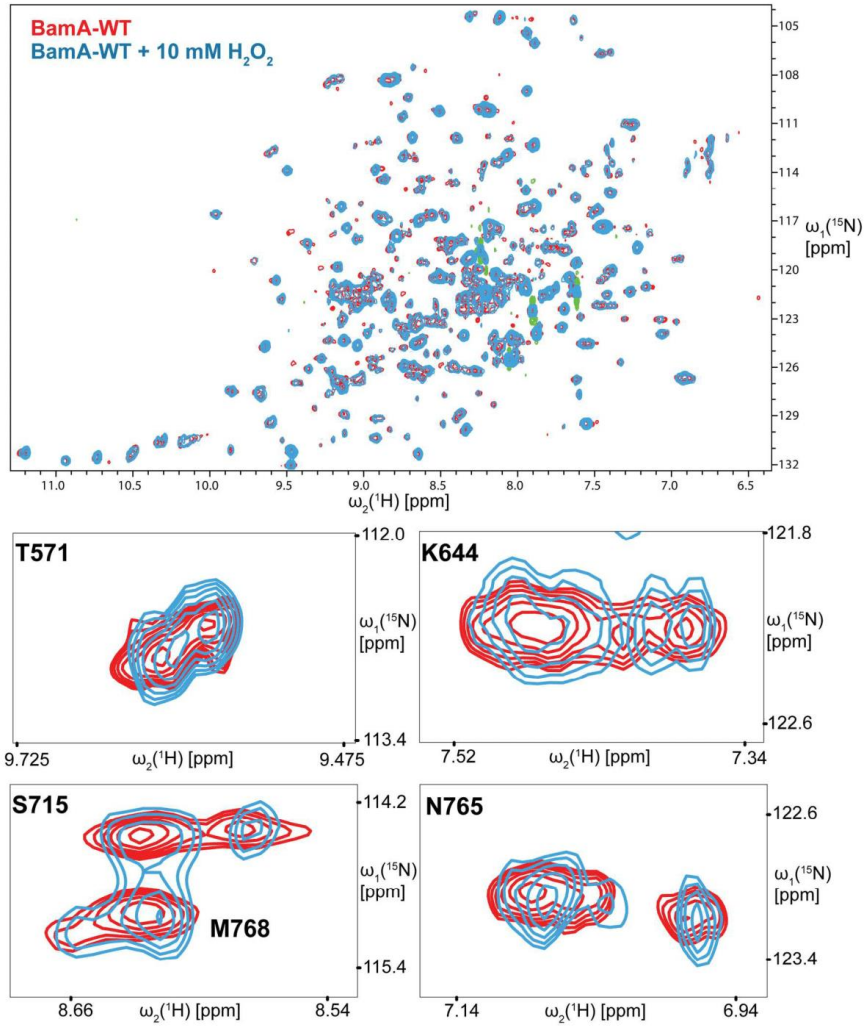

Figure S15. Effect of the oxidation agent H_2O_2 on the wild-type BamA conformational ensemble. Overlay of 2D [^{15}N,^{1}H]-TROSY-HSQC spectra of 200 μM [*U*-^{2}H,^{15}N]-labeled BamA before (red) and after (blue) 10mM H_2O_2. While the overall spectral quality is slightly different, the conformational ensemble appears not to be affected by the oxidation.

Chapter 5: Methyl side-chain labeling strategy, single-domain antibody interactions, and attempts at forming a BamA-hybrid barrel

Michael Zahn titrated the BamA samples with the nanobodies and NMR spectroscopy, and I analyzed the data. Michael Zahn crystallized and solved the structures of the BamA samples with the nanobodies. All other work was performed by me.

5.1 Summary

The backbone assignments of the BamA β-barrel are a valuable plateform to study the protein with NMR spectroscopy. However, the large size of the Bam complex, is beyond the limitations of what can offer TROSY-HSQC spectroscopy. In this scope, the methyl groups of a protein have different relaxations dynamics as the rest of the protein, due to the rotation of the methyl moiety around its axis. Hence, obtaining the methyl side-chain assignments of BamA could provide a basis to study the BamA β-barrel in a larger assembly. To this goal, we started to record methyl side-chain HMQC and methyl side-chain NOESY experiments of the BamA OmpX B7B8 G433A construct. With the help of available backbone assignments, those experiments will allow us to assign the methyl groups of the BamA β-barrel.

The discovery of new antibiotics is of critical importance in the pharmaceutical industry. The BamA β-barrel backbone assignment now provides a basis on which to perform screening, as a way to find potential binding sites on the surface of the protein. The NMR titration of the BamA-OmpX B7B8 G433A construct was performed with the nanobody F7, targeted against BamA. An interaction was observed between the extracellular loops of BamA and the nanobody. After crystallizing the nanobody F7 and other nanobodies with the BamA β-barrel, the structures were solved. They confirmed the binding site of the nanobodies to be located on the BamA extracellular loops. These findings show that a strategy to design new antibiotics, targeting BamA, could be designed, by mimicking the interactions between the nanobodies and the extracellular loops of BamA.

In order to understand the importance of the gate-region of the BamA β-barrel, and study the hypothetical hybrid barrel mechanism, several constructs were prepared, where BamA was C-terminally extended with strands from the outer membrane proteins OmpX, LamB and PhoE. NMR measurements of those hybrid proteins, could show the various effects of C-terminal extensions on the quality of the spectra and, indirectly, on the protein dynamics.

5.2 Results

Methyl side-chain HMQC and Methyl side-chain NOESY

In proteins, six amino acids have side chains containing methyl groups (alanine, valine, isoleucine, leucine, methionine and threonine). The peculiarity of the methyl group for liquid-state NMR is the fast rotation of this moiety around its axis (in the ps timescale). As such, experiments measuring the methyl side chains are much more sensitive than the one measuring the backbone (Tugarinov et al., 2003) and allow to study large complexes by solution NMR (Wiesner and Sprangers, 2015). Additionally, the side chain labeling of specific amino acids allows to reduce the spectral crowding but still permits to cover the protein with labeled probes. In the case of the BamA β-barrel, assigning the sidechains will open the door to study molecular mechanisms in various configurations of higher molecular weights. In example, one could measure the protein containing the POTRA domains, with associated proteins BamBCDE, and in different membrane mimetics such as nanodiscs as the molecular size-limitation for methyl side chain experiments is in the range of the mega Dalton. This method was applied to systems of high molecular weights such as in the peptidase TET2 study (Mas et al., 2013).

A 2D HMQC experiment was acquired to record the chemical shifts from the methyl sidechains of isoleucines, leucines, valines and methionines of the BamA-OmpXB7B8 G433A sample (**Figure 4.1**). Interestingly, for isoleucines and methionines, two peaks appeared for each residue. In the case of valines and leucines, the peaks for the two methyl groups are detected, but we detected twice the number of expected peaks. A 3D-HMQC NOESY was acquired to measure the correlations from the methyl groups of ILVA protons to the surrounding protons. Two peaks corresponding to isoleucines were identified as having cross-correlations with four peaks from the leucine region (**Figure 4.2**). Each of the isoleucine peak had correlations with two leucines peaks (one for each methyl group). Therefore, the BamA β-barrel populates at least two conformers in solution, each of them showing crosspeaks with residues from the same conformation. The intensity ratio between the peaks that could be identified as the same residue in two different conformations was approximatively 25%. This shows that there are two populations of the BamA-OmpXB7B8 G433A in solution, a main conformation and a secondary conformation with a 3:1 ratio. While the secondary conformation is invisible in 2D experiments performed on the backbone, the sensitivity of the methyl experiments, can explain its visibility in the 2D-HMQC experiment.

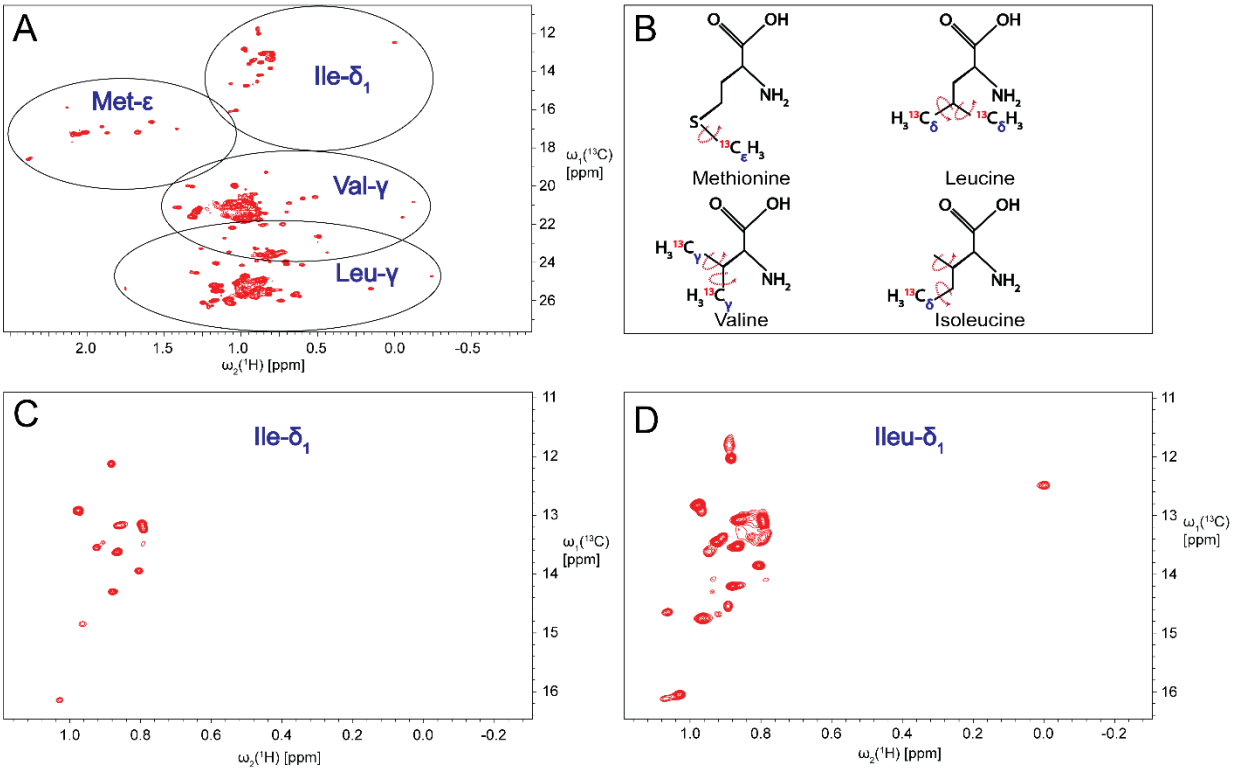

Figure 4.1 A) 2D [^{1}H, ^{13}C] HMQC spectrum of a sample of 700 µM [U-^{2}H, ^{15}N], [Ileu-^{2}HC$_{\gamma}$ -^{13}C$_{\delta}$], [Leu-^{13}C$_{\gamma}$], [Val-^{13}C$_{\gamma}$], [Met-^{13}C$_{\varepsilon}$] BamA-OmpXB7B8 G433A. **B)** Depiction of the methyl groups from Methionine, Leucine, Valine and Isoleucine residues. **C)** Thirteen peaks are expected from the methyl side-chains of isoleucines, at a high contour level, a set of peak corresponding to this number is visible. **D)** At a lower contour level, a second set of peak appear. The two sets represent two conformation of BamA which are only detected in the methyl side-chain experiment, due to its sensitivity. The [^{1}H, ^{15}N] TROSY-HSQC spectrum recorded afterwards on the same sample was exactly the same as the reference spectrum used for assignment, showing only one conformation.

Labeled methyl groups that are close in space yield a crosspeak in the 3D [^{1}H, ^{1}H, ^{13}C]-HMQC NOESY experiment. Combined with the structural information, this method will assist assignment of the sidechains. Because we know which methyl groups are neighbors from the crystal structure, we can reconstitute the interaction map and analyze the crosspeak network to establish the identity of the methyl groups and assign them. Another possible strategy for the assignment of the methyl sidechains, is to transfer the magnetization from the ^{13}C$_{\alpha}$ to the ^{13}C sidechains using an HCCH-COSY experiment (Bax et al., 1990). This method requires a specifically labeled sample where the entire side-chain is ^{13}C labeled.

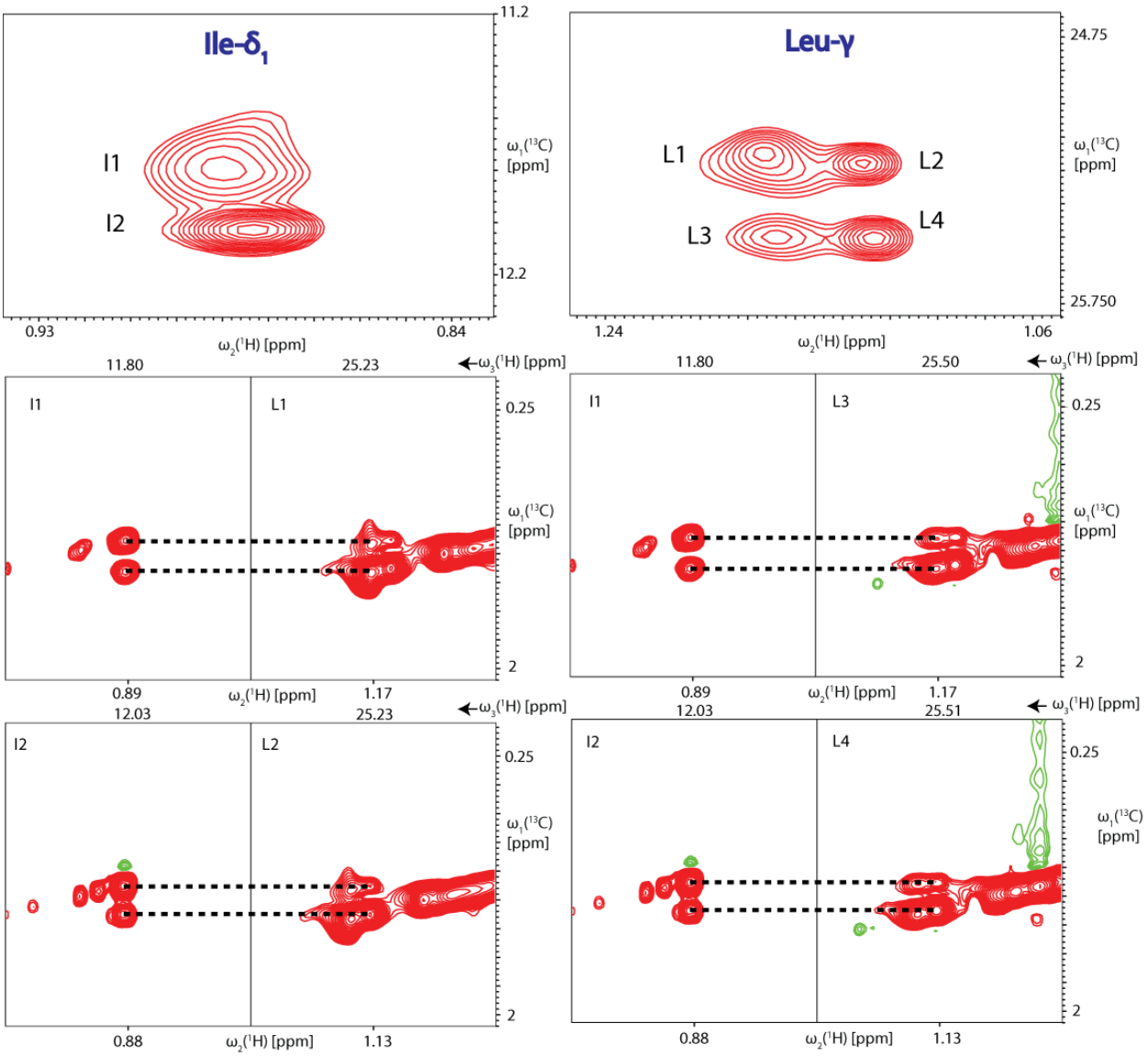

Figure 4.2 Strips from the 3D [^{1}H, ^{1}H, ^{13C}]-HMQC NOESY experiment recorded on a sample of 700 µM [U-^{2}H, ^{15}N], [Ileu-^{2}HC$_{\gamma}$ -^{13}C$_{\delta}$], [Leu-^{13}C$_{\gamma}$], [Val-^{13}C$_{\gamma}$], [Met-^{13}C$_{\varepsilon}$] BamA-OmpX B7B8 G433A. Two peaks are visible for the isoleucine δ-methyl, and four peaks for the leucine γ-methyl. Each of the isoleucine peaks correlate to two of the leucine peaks.

Interaction studies between BamA and nanobodies

A set of single-domain antibodies targeted against BamA, also known as nanobodies, were developed by Michael Zahn and collaborators. The interaction between those nanoparticles and the BamA β-barrel was studied with liquid-state NMR spectroscopy by titrating the wild-type as well as the stabilized BamA-OmpxB7B8 G433A protein with different nanobodies. The titration of BamA-OmpxB7B8 G433A with the nanobody F7 led to notice disappearing residues and important chemical shift differences for assigned residues of the extra-cellular loop regions **(Figure 4.3 A, B)**. Interestingly as well, the titration of the wild-type BamA β-barrel with the nanobody F7 triggered the apparition of new peaks as well as many chemical shift differences across the spectrum **(Figure 4.3 C)**. Then, Michael Zahn performed the crystallization of the complexes between the wild-type BamA β-barrel and three of those nanobodies **(Figure 4.4)**. As expected, the solved structures displayed interactions between the extracellular loops of the BamA β-barrel and the single-domain antibodies **(Figure 4.3 A, Figure 4.4)**. The crystal structure of BamA with F7 only displayed a single conformer, but the NMR spectra shows that F7 seems to stabilize the BamA β-barrel, in a comparable manner as the C-terminal addition of OmpX residues. Because the importance of the extracellular residues of BamA β-barrel to its dynamics are known, it is not surprising to observed that the binding of the nanobody F7 alters the conformational ensemble populated by the BamA β-barrel.

The structures of the BamA β-barrel with nanobody F7 (**Figure 4.4 A**) and B12 (**Figure 4.4 B**) are similar, as the nanobodies bind on the same side, involving loops 4, 5 and 6. However, the structure of the BamA β-barrel with the nanobody E6 shows an interaction involving only the loop 4 (**Figure 4.4 C**).

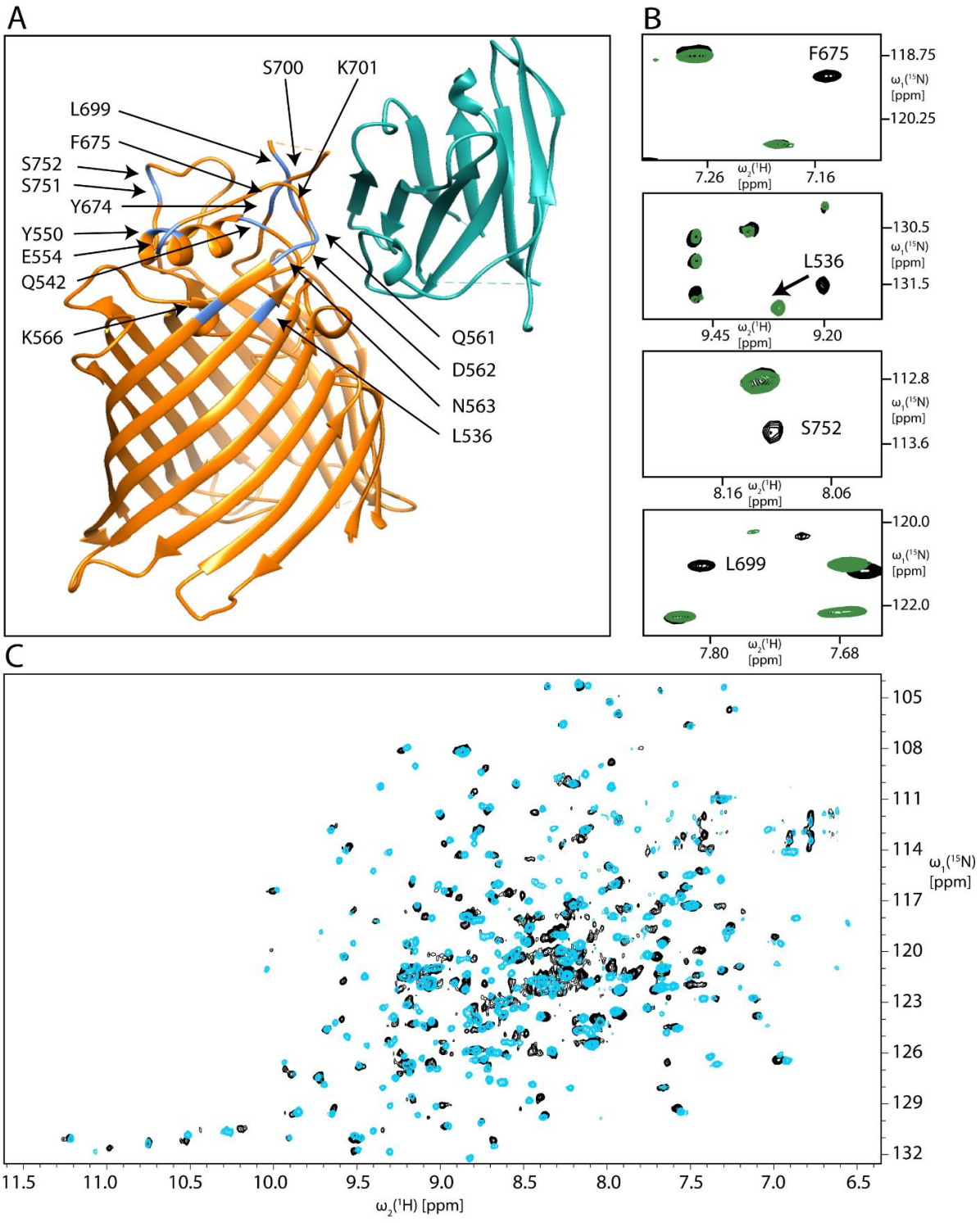

Figure 4.3 A) Structure of BamA β-barrel (orange) with the nanobody F7 (cyan). Assigned residues with the highest chemical shift difference, or that disappeared upon titration of BamA-Ompx B7B8 G433A with the nanobody F7, are mapped in blue. **B)** Portions of overlapped [^{1}H, ^{15}N] TROSY-HSQC of [U-^{2}H, ^{15}N] BamA-Ompx B7B8 G433A in black, with equimolar amount of nanobody F7 in green. **C)** [^{15}N, ^{1}H]-TROSY-HSQC of [U-^{2}H, ^{15}N] BamA β-barrel (black) with equimolar amount of nanobody F7 (blue).

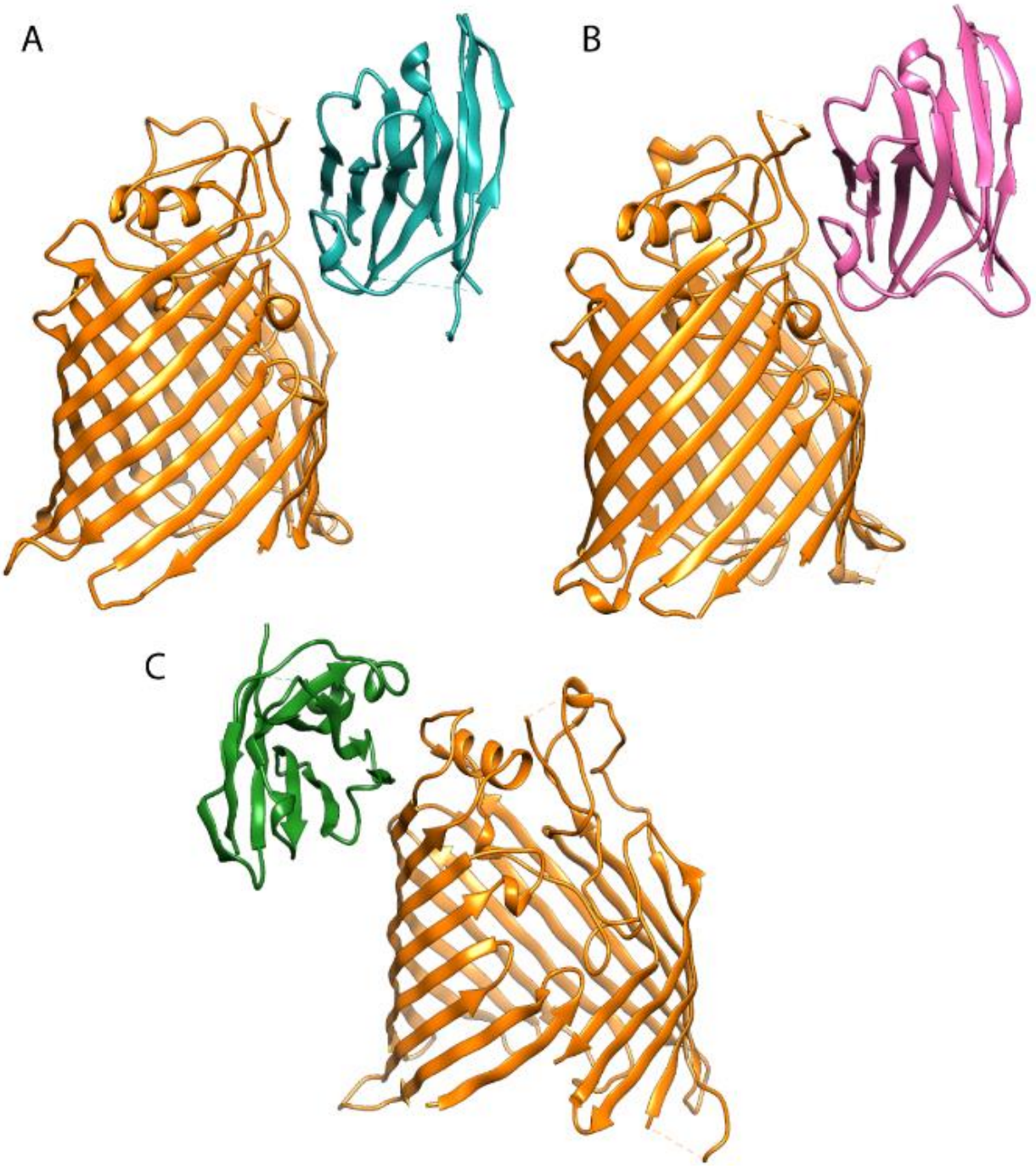

Figure 4.4 Structures of BamA β-barrel with various nanobodies. **A)** Nanobody F7 (blue). **B)** Nanobody B12 (pink). **C)** Nanobody E6 (green).

Attempts at forming a folded BamA-OMP hybrid

Additionally to the BamA-OmpX B7B8 hybrid protein, several constructs were prepared where the BamA β-barrel was extended with four (BamA-OmpX B5B8), six (BamA-OmpX B3B8), and eight hairpins of Ompx (BamA-OmpX B1B8) (**Figure 4.5**) in order to test the possibility of forming a hybrid barrel observable by NMR spectroscopy. The NMR spectra of BamA-OmpX B5B8 and BamA-OmpXB3B8 showed resonances in the 8 ppm region, where are localized the chemical shifts of the residues from unstructured regions. However, the number of residues visible in those spectra does not match the number of residues expected for the unfolded protein (468 residues for BamA-OmpX B5B8, 509 residues for BamA-OmpX B3B8). Therefore, it is not to exclude, that most of the residues of those constructs are in intermediate exchange conformational state, and not visible for HSQC experiments. The spectrum of the BamA-OmpX B1B8 protein displays a fully folded and stable OmpX protein (**Figure 4.5 C, D**), which shows that the OmpX β-barrel is capable of forming, despite having the full BamA β-barrel residues tethered at its N-terminus. However the state of the BamA-β barrel within this construct is not known.

Two construct encompassing the BamA β-barrel C-terminally extended with one hairpin from the outer membrane protein LamB were prepared. One with two cysteines in the BamA β-barrel and LamB portions that could hypothetically be in contact in case of the formation of a hybrid barrel (**Figure 4.6 A**), and one without. The objective was to increase the stability, and therefore the observability of such a construct in the timescale of measurement by NMR spectroscopy. After catalysis of the cysteine-bond formation using H_2O_2, the double-mutant was purified with IEX chromatography and SEC and measured with nano differential scanning fluorimetry (nanoDSF) in the same buffer condition and concentration that were used for the following NMR experiment. The protein transition mid-point temperature (T_M) was measured at 66°C and the scattering curve indicated that the protein starts aggregating at 63.7°C (**Figure 4.6 B, C)**. Both variants were measured by NMR spectroscopy (**Figure 4.6 D).** The spectra showed that resonances were mainly located in the 8 ppm region. While it is still required to measure whether the cysteine bond properly formed, the spectrum acquired by NMR spectroscopy at 37°C does not correspond to an aggregated or unfolded protein according to the nanoDSF experiment. Because the aggregation process starts at 63.7 °C and the protein is folded at 37 °C in this buffer condition it is then likely that most peaks of those hybrid constructs are invisible in the spectrum as a result of the peaks being in the intermediate exchange regime.

Another hybrid construct was prepared, where the BamA β-barrel was C-terminally extended with one hairpin from the outer membrane protein PhoE (BamA-PhoE B15B16. When measured by NMR spectroscopy, as compared to the BamA-OmpX B7B8 construct, the spectra missed resonances and had broader lines (**Figure 4.7).** However the spectrum was well dispersed and of much higher quality than the one of BamA-LamB B17B18.

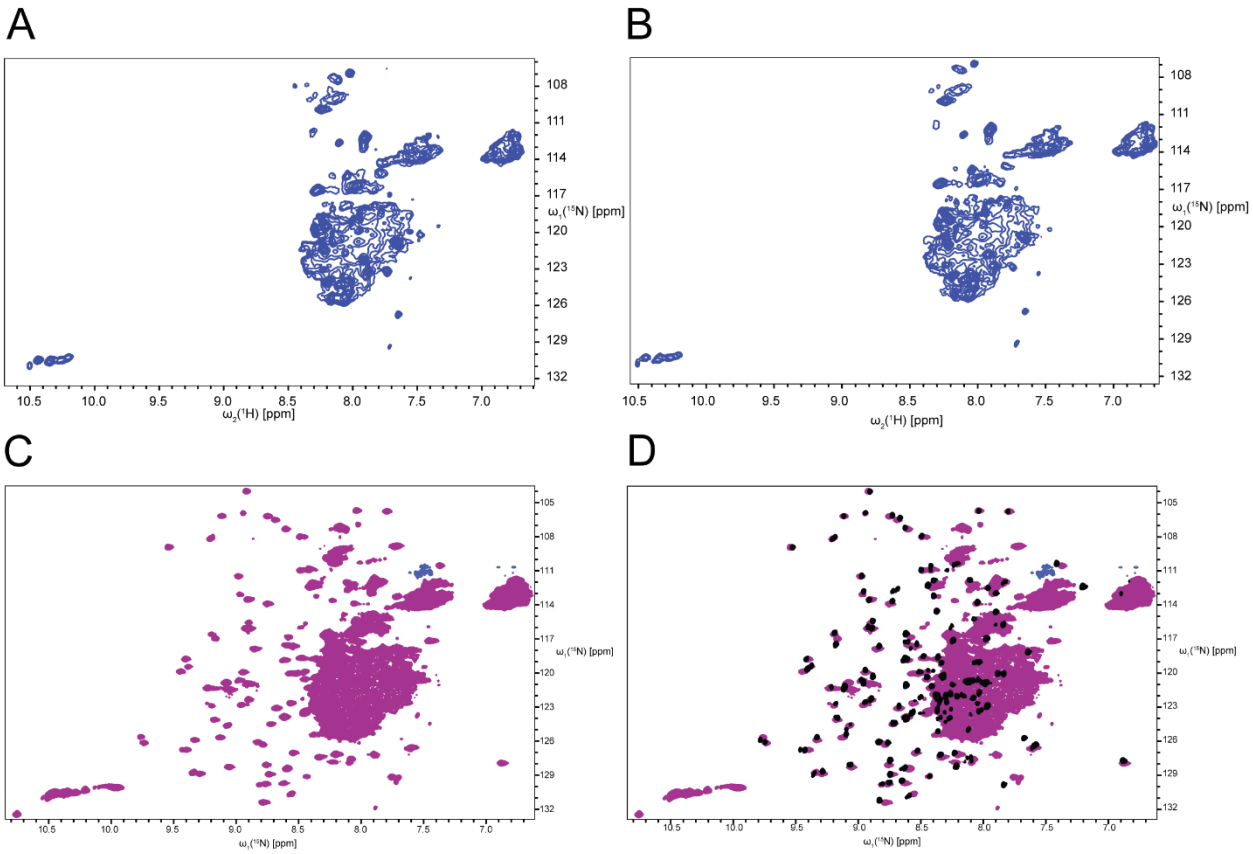

Figure 4.5 A) 2D-[^{15}N, ^{1}H]-TROSY-HSQC of [U-^{2}H, ^{15}N] BamA-OmpX B5B8. **B)** 2D-[^{15}N, ^{1}H]-TROSY-HSQC of [U-^{2}H, ^{15}N] BamA-OmpX B3B8. **C)** 2D-[^{15}N, ^{1}H]-TROSY-HSQC of [U-^{2}H, ^{15}N] BamA-OmpX B1B8. **D)** 2D-[^{15}N, ^{1}H]-TROSY-HSQC of [U-^{2}H, ^{15}N] BamA-OmpX B1B8 (purple), 2D-[^{15}N, ^{1}H]-TROSY-HSQC of 100 µM [U-^{2}H, ^{15}N] OmpX (black). Samples of BamA-hybrids at 500 µM measured at 37°C in buffer 20 mM NaPi pH 7.5, 150 mM NaCl, 0.1% LDAO. The spectrum of OmpX is a courtesy of Parthasarathi Rath.

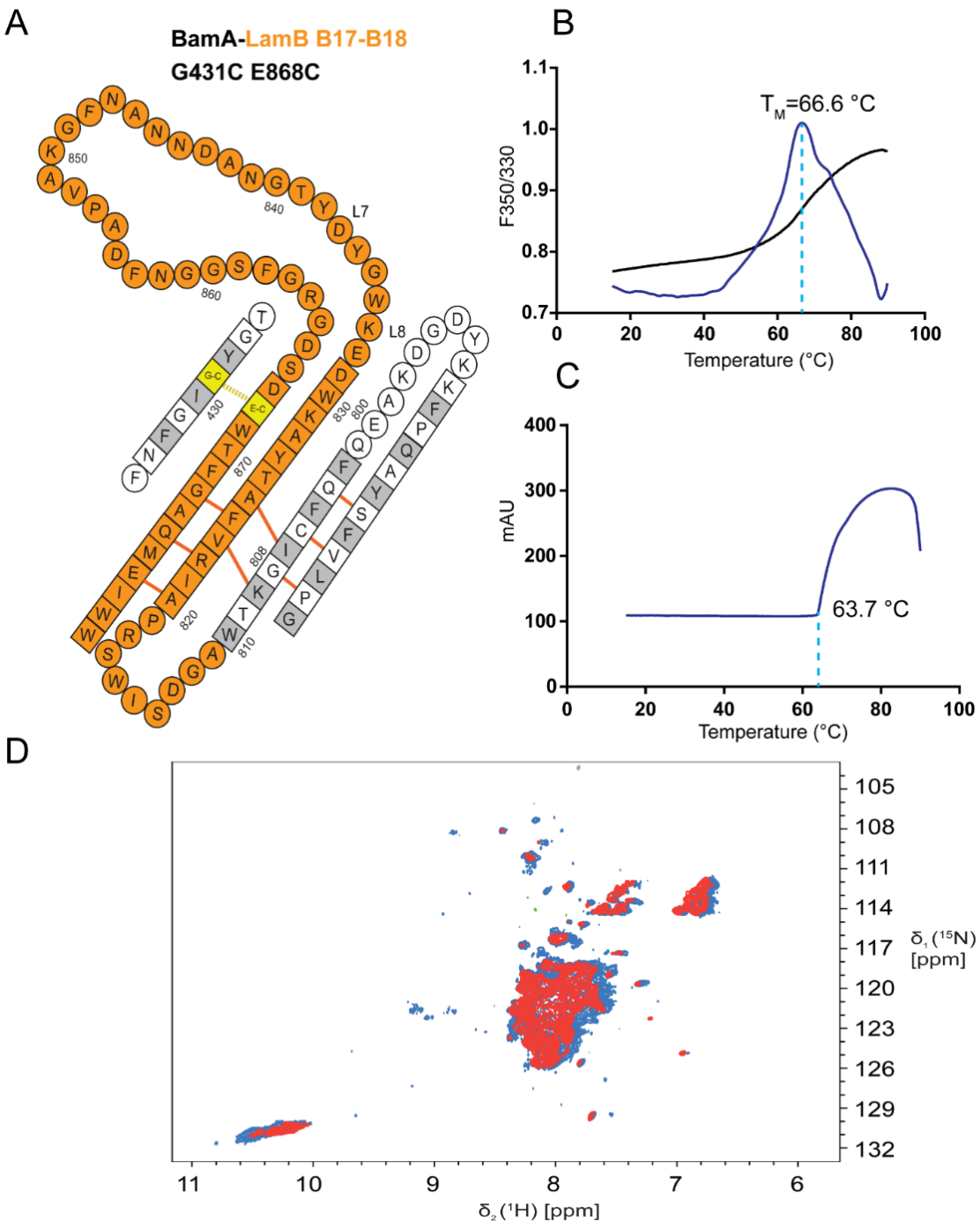

Figure 4.6 A) Scheme of the gate region from the BamA-LamB B17B18 hybrid construct. Two construct were prepared, one without mutations, and one with mutations G431C and E868C (in yellow). **B-C)** NanoDSF experiment measured on the BamA-LamB B17B18 G431C, E868C construct in the oxidized form. **B)** Intrinsic fluorescence ratio (350 nm/330 nm) over a temperature gradient. The first derivative shows the transition mid-point temperature (T_M) at which half of the protein population is unfolded. **C)** Scattering curve of the NanoDSF experiment. **D)** 2D-[^{15}N, ^{1}H]-TROSY-HSQC of [U-^{2}H, ^{15}N] BamA-OmpX-LamB B17B18 at 190 µM in red and 2D-[^{15}N, ^{1}H]-TROSY-HSQC of [U-^{2}H, ^{15}N] BamA-LamB B17B18 G431C E868C in the oxidized form at 320 µM in blue. Samples measured at 37°C in buffer 20 mM NaPi pH 7.5, 150 mM NaCl, 0.1% LDAO.

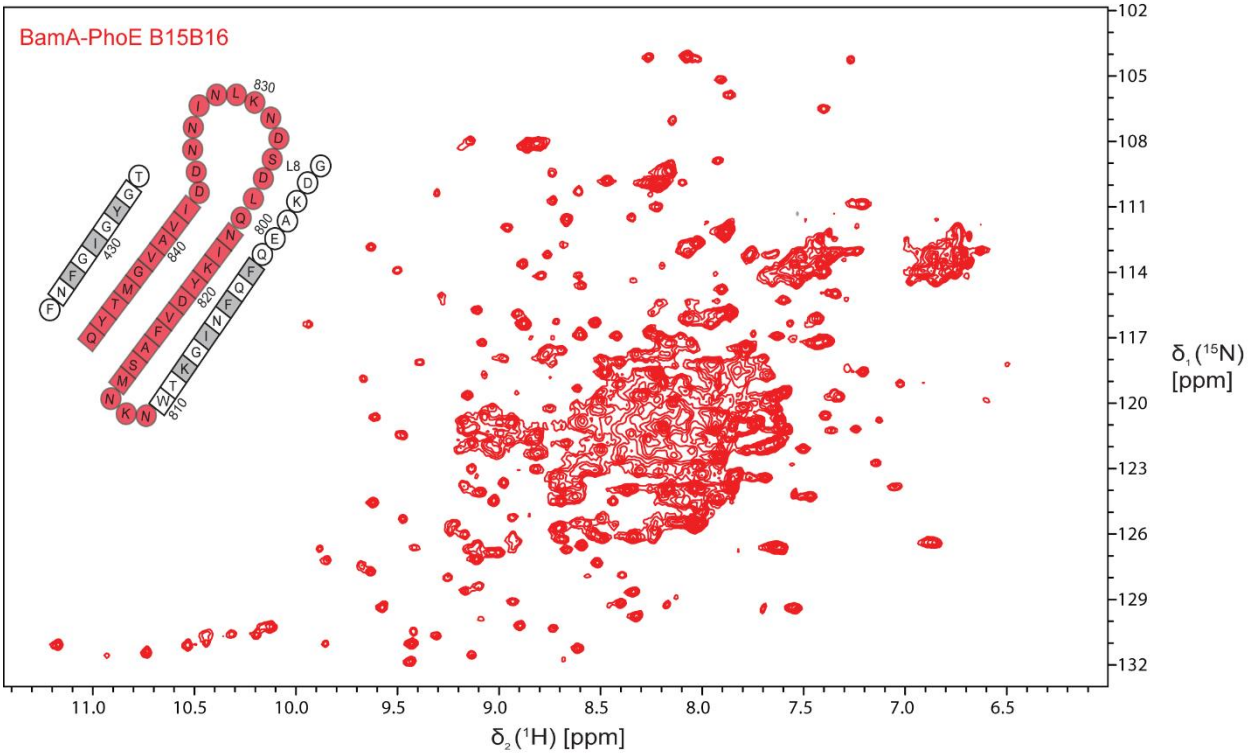

Figure 4.7 2D-[^{15}N, ^{1}H]-TROSY-HSQC of [U-^{2}H, ^{15}N] BamA-PhoE B15B16 at 100 µM in red. Scheme of the gate region from a hypothetical hybrid barrel between BamA and the B15B16 hairpin from PhoE. Sample measured at 30°C in buffer 20 mM NaPi pH 7.5, 150 mM NaCl, 0.1% LDAO.

5.3 Discussion

The methyl side-chain assignment strategy will allow to study the BamA protein, within its complex, by NMR spectroscopy. However it will be required to obtain a sample which only populate a single visible molecular conformation in solution. The NOESY/HMQC approach could be completed using COSY-type schemes to transfer magnetization from the $^{13}C_{\alpha}$ to the sidechains.

The NMR titration of the stabilized BamA with nanobody F7, revealed a binding site on the extracellular loops of BamA. Additionally, large differences were noticed in the spectra of the wild-type BamA in the presence and absence of nanobody F7. It is likely to think that the conformational ensemble populated by BamA was rearranged upon binding to the nanobody F7, which suggest the importance of the extracellular loops on the dynamics of the BamA β-barrel. The binding sites observed with NMR spectroscopy were confirmed in the crystal structures of BamA β-barrel with various nanobodies showing interactions with the extra cellular loops of the

BamA β-barrel. This approach exemplifies how NMR spectroscopy can be used to discover the molecular mechanisms of binding of potential antibiotics with BamA.

The attempts at measuring a stable hybrid protein between the BamA β-barrel and hairpins from OmpX, LamB and PhoE by NMR did not succeed, however we noticed great differences in the quality of the NMR spectra obtained depending on the length, and sequence of the C-terminal extension. While, one hairpin from OmpX helped to stabilized the barrel (**Chapter 2**), the addition of subsequent hairpins, yielded spectra of poor quality, presumably due to the destabilization of the protein. The addition of a hairpin from PhoE, did not permit to reach the same spectral quality as for the BamA-OmpX B7B8 construct, but did not destabilized the BamA β-barrel further. Extending the BamA β-barrel with a hairpin from LamB, yielded a low quality spectrum. The BamA-LamB B15B16 construct was mutated to attempt its stabilization by forming a cysteine bond between the first strand of BamA and the last strand of LamB. However, the quality of the NMR spectra did not improve. Measuring this construct with nanoDSF, the protein was found to be folded and non-aggregated, indicating that the low number of peaks visible in the spectrum are likely to be caused by the protein dynamics, sampling a range of conformations. It is reasonable to think that possible hybrid proteins formed in vivo between BamA and its substrates are not stable assemblies because there is no energy source in the periplasm to trigger the separation of the BamA/substrate hybrid. It is thinkable that the constructs measured by solution NMR are indeed sampling a dynamic conformational range that include hybrid barrels, but other strategies and methods will have to establish their existence and measure their properties.

5.4 Material and methods

Expression and purification

The 3D-HHN NOESY/3D-NOESY HMQC sample of BamA-OmPX B7B8 with the G433A mutation was expressed in 1 L of perdeuterated M9 minimal media supplemented with 2 g of ^{2}H, ^{12}C glucose and 1 g of ^{15}N NH_4Cl. The precursors for the ^{13}C labeling of the methyl side-chains of ILVM were added 1 H prior to induction: 100 mg of 2-keto-3-(methyl ^{13}C)-butyric-4-^{13}C for valine/leucine side-chain NOESY-type labeling, 100 mg of methyl ^{13}C alpha-ketobutyric acid for isoleucine side-chain NOESY-type labeling and 100 mg of ^{13}C CH_3-methionine. Refolding and following purification steps were performed in deuterated LDAO detergent with the same protocol as the Material and Methods section of **Chapter 3**. The final NMR buffer contained deuterated LDAO. BamA-LamB B17B18 G431C E868C was expressed and purified in the same manner as

in **Chapter 3**, but in the presence of 10 mM DTT during refolding. After refolding the DTT was dialyzed out and 10 mM of H_2O_2 was used to catalyze the formation of the cysteine bond. Other samples of BamA were prepared with the same protocol as in **Chapter 3**.

NMR Spectroscopy

The 2D-HMQC experiment of the 700 µM [U-^{2}H, ^{15}N], [Ileu-^{2}HC$_{\gamma}$ -^{13}C$_{\delta}$], [Leu-^{13}C$_{\gamma}$], [Val-^{13}C$_{\gamma}$], [Met-^{13}C$_{\varepsilon}$] sample of BamA-OmpXB7B8 G433A was recorded in the NMR buffer at 37 °C on a 900 MHz spectrometer with 4 scans. The transmitter frequency offset was set on 4.72 ppm for the proton and 17 ppm for the ^{13}C with spectral widths of 13.7 ppm and 24 ppm for the first proton dimension and ^{13}C respectively. The experiment was recorded with 2048, 184 and 300 points for the ^{1}H, ^{13}C and ^{1}H. The interscan delay was set to 0.8 s. The 3D-NOESY HMQC experiment of the 700 µM [U-^{2}H, ^{15}N], [Ileu-^{2}HC$_{\gamma}$ -^{13}C$_{\delta}$], [Leu-^{13}C$_{\gamma}$], [Val-^{13}C$_{\gamma}$], [Met-^{13}C$_{\varepsilon}$] sample of BamA-OmpX B7B8 G433A in the NMR buffer was recorded at 37 °C on a 900 MHz spectrometer with 8 scans. The transmitter frequency offset was set on 4.72 ppm for the proton and 19 ppm for the ^{13}C with spectral widths of 13.7 ppm, 18 ppm and 13.7 ppm for the first proton dimension, ^{13}C dimension and second proton dimension respectively. The experiment was recorded with 2048, 184 and 300 points for the ^{1}H, ^{13}C and ^{1}H. The interscan delay was set to 0.75 s. The NOE mixing time was set to 250 ms. The 100 µM sample of [U-^{2}H, ^{15}N]-BamA-PhoE B15B16 in buffer 20 mM NaPi pH 7.5, 150 mM NaCl, 0.1 % LDAO was recorded at 30 °C with a 2D [^{1}H,^{15}N]-TROSY HSQC experiment on a 700 MHz spectrometer with 32 scans. The transmitter frequency offset was set on 4.74 ppm for the proton and 117 ppm for the ^{15}N with spectral widths of 16 ppm and 32 ppm respectively and recorded with 256 points for the indirect dimension and 2048 points for the direct dimension. The interscan delay was set to 1 s. The 500 µM samples of [U-^{2}H, ^{15}N]-BamA-OmpX B5B8, [U-^{2}H, ^{15}N]-BamA-OmpX B3B8 and [U-^{2}H, ^{15}N]-BamA-OmpX B1B8 in buffer 20 mM NaPi pH 7.5, 150 mM NaCl, 0.1 % LDAO were recorded at 37 °C with a 2D [^{1}H,^{15}N]-TROSY HSQC experiment on a 700 MHz spectrometer with 128 scans. The transmitter frequency offset was set on 4.72 ppm for the proton and 117 ppm for the ^{15}N with spectral widths of 16 ppm and 32 ppm respectively and recorded with 256 points for the indirect dimension and 2048 points for the direct dimension. The interscan delay was set to 1 s. The 190 µM sample of [^{2}H, ^{15}N] BamA-OmpX-LamB B17B18 in buffer 20 mM NaPi pH 7.5, 150 mM NaCl, 0.1 % LDAO was recorded at 30 °C with a 2D [^{1}H,^{15}N]-TROSY HSQC experiment on a 700 MHz spectrometer with 192 scans. The transmitter frequency offset was set on 4.72 ppm for the proton and 117 ppm for the ^{15}N with spectral widths of 16 ppm and 32 ppm respectively and recorded with 256 points for the indirect dimension and 2048 points for the direct dimension. The interscan delay was set to 1 s. The 320

µM sample of the oxidized [U-^{2}H, ^{15}N] BamA-OmpX-LamB B17B18 G431C E868C in buffer 20 mM NaPi pH 7.5, 150 mM NaCl, 0.1 % LDAO was recorded at 37 °C with a 2D [^{1}H,^{15}N]-TROSY HSQC experiment on a 600 MHz spectrometer with 120 scans. The transmitter frequency offset was set on 4.72 ppm for the proton and 117 ppm for the ^{15}N with spectral widths of 16 ppm and 32 ppm respectively and recorded with 256 points for the indirect dimension and 2048 points for the direct dimension. The interscan delay was set to 1 s.

Michael Zahn performed the titration of BamA β-barrel and BamA-OmpX B7B8 G433A with the nanobody F7. The chemical shift difference $\Delta\delta_{NH}$ between the peaks of the apo and bound form of BamA was calculated using the following formula (Goldflam et al., 2012):

$$\Delta\delta_{NH} = \left(\sqrt{\Delta\delta_H^2 + \left(\frac{\Delta\delta_N}{5}\right)^2} \right)$$

Where δ_H is the proton chemical shift, δ_N the nitrogen chemical shift.

The OmpX spectrum was nicely provided by Parthasarathi Rath.

All the NMR samples contained 5 % D_2O. All spectrometers were equipped with a cryo-probe. All experiments were processed with TopSpin (Bruker BioSpin) and analyzed with CARA. (Keller, Rochus, 2004).

Crystallization

Michael Zahn performed the crystallization of the BamA β-barrel with the nanobodies F7, E6, B12. The protein buffer was exchanged by gel-filtration into 20 mM Tris pH 7.5, 150 mM NaCl, 0.05% LDAO and 0.35% C_8E_4. For BamA β-barrel + F7, crystals in the spacegroup $P2_12_12_1$ were grown in 22 % (w/v) PEG 400, 0.07 M NaCl and 0.05 M sodium citrate pH 4.5. For BamA β-barrel + E6, crystals in the spacegroup I2 were grown in 22 % (w/v) PEG 400, 0.1 M $MgCl_2$ and 0.1 M Tris pH 7.5. For BamA β-barrel + B12, crystals in the spacegroup P121 were grown in 32 % (w/v) PEG 400, 0.2 M $(NH_4)H_2PO_4$, 0.1 M $(NH_4)_2SO_4$ and 0.1 M Na Citrate pH 4.5. Crystals were directly flash-frozen in liquid nitrogen. A data set was collected at beamline X06DA (PXIII) at the Swiss Light Source (SLS, Paul Scherer Institute, Villigen, Switzerland). Phases were obtained by molecular replacement.

NanoDSF

The oxidized form of the BamA-OmpX-LamB B17B18 G431C E868C protein at 300 µM in buffer 20 mM NaPi pH 7.5, 150 mM NaCl, 0.1% LDAO was measured with a nanoTemper Prometheus instrument. The intrinsic fluorescence and scattering were measured at 330 nm and 350 nm over a temperature gradient of 15-90°C.

Appendix

List of protein sequences

1. **BamB (21-392), no signal-sequence with thrombine cleavable Nterm hexa His-Tag, plasmid pET 15b**:

MGSSHHHHHHSSGLVPRGSHMSLFNSEEDVVKMSPLPTVENQFTPTTAWSTSVGSGIGNFYS
NLHPALADNVVYAADRAGLVKALNADDGKEIWSVSLAEKDGWFSKEPALLSGGVTVSGGHVYI
GSEKAQVYALNTSDGTVAWQTKVAGEALSRPVVSDGLVLIHTSNGQLQALNEADGAVKWTVN
LDMPSLSLRGESAPTTAFGAAVVGGDNGRVSAVLMEQGQMIWQQRISQATGSTEIDRLSDVD
TTPVVVNGVVFALAYNGNLTALDLRSGQIMWKRELGSVNDFIVDGNRIYLVDQNDRVMALTIDG
GVTLWTQSDLLHRLLTSPVLYNGNLVVGDSEGYLHWINVEDGRFVAQQKVDSSGFQTEPVAA
DGKLLIQAKDGTVYSITR

2. **BamC (26-344), no signal-sequence with thrombine cleavable N-terminal hexa histidine tag, plasmid pET15b**:

MGSSHHHHHHSSGLVPRGSHMASSDSRYKRQVSGDEAYLEAAPLAELHAPAGMILPVTSGDY
AIPVTNGSGAVGKALDIRPPAQPLALVSGARTQFTGDTASLLVENGRGNTLWPQVVSVLQAKN
YTITQRDDAGQTLTTDWVQWNRLDEDEQYRGRYQISVKPQGYQQAVTVKLLNLEQAGKPVAD
AASMQRYSTEMMNVISAGLDKSATDAANAAQNRASTTMDVQSAADDTGLPMLVVRGPFNVV
WQRLPAALEKVGMKVTDSTRSQGNMAVTYKPLSDSDWQELGASDPGLASGDYKLQVGDLDN
RSSLQFIDPKGHTLTQSQNDALVAVFQAAFSK

3. **BamD (29-245), no signal-sequence with thrombine cleavable N-terminal hexa histidine tag, plasmid pET15b**:

MKGSSHHHHHHSSGLVPRGSHMDNPPNEIYATAQQKLQDGNWRQAITQLEALDNRYPFGPY
SQQVQLDLIYAYYKNADLPLAQAAIDRFIRLNPTHPNIDYVMYMRGLTNMALDDSALQGFFGVD
RSDRDPQHARAAFSDFSKLVRGYPNSQYTTDATKRLVFLKDRLAKYEYSVAEYYTERGAWVA
VVNRVEGMLRDYPDTQATRDALPLMENAYRQMQMNAQAEKVAKIIAANSSNT

4. **BamE (21-113), no signal-sequence with thrombine cleavable N-terminal hexa histidine tag, plasmid pET15b**:

MGSSHHHHHHSSGLVPRGSHMSTLERVVYRPDINQGNYLTANDVSKIRVGMTQQQVAYALGT
PLMSDPFGTNTWFYVFRQQPGHEGVTQQTLTLTFNSSGVLTNIDNKPALSGN

5. **BamC (26-217)-BamD(29-245) hybrid construct with a linker, without signal sequence, plasmid pET15b:**

MKGSSHHHHHHSSGLVPRGSASSDSRYKRQVSGDEAYLEAAPLAELHAPAGMILPVTSGDYAI
PVTNGSGAVGKALDIRPPAQPLALVSGARTQFTGDTASLLVENGRGNTLWPQVVSVLQAKNYT
ITQRDDAGQTLTTDWVQWNRLDEDEQYRGRYQISVKPQGYQQAVTVKLLNLEQAGKPVADAA

SMQRYSTEMMNVISAGLDKSATDAAGGGSGGDNPPNEIYATAQQKLQDGNWRQAITQLEALD
NRYPFGPYSQQVQLDLIYAYYKNADLPLAQAAIDRFIRLNPTHPNIDYVMYMRGLTNMALDDSA
LQGFFGVDRSDRDPQHARAAFSDFSKLVRGYPNSQYTTDATKRLVFLKDRLAKYEYSVAEYYT
ERGAWVAVVNRVEGMLRDYPDTQATRDALPLMENAYRQMQMNAQAEKVAKIIAANSSNT

6. **BamA β-barrel (421-810) C690S_C700S with TEV cleavable N-terminal hexa histidine tag, plasmid pET15b (established by Leonor Morgado):**

MGSSHHHHHHSSGENLYFQHMRNTGSFNFGIGYGTESGVSFQAGVQQDNWLGTGYAVGING
TKNDYQTYAELSVTNPYFTVDGVSLGGRLFYNDFQADDADLSDYTNKSYGTDVTLGFPINEYN
SLRAGLGYVHNSLSNMQPQVAMWRYLYSMGEHPSTSDQDNSFKTDDFTFNYGWTYNKLDRG
YFPTDGSRVNLTGKVTIPGSDNEYYKVTLDTATYVPIDDDHKWVVLGRTRWGYGDGLGGKEM
PFYENFYAGGSSTVRGFQSNTIGPKAVYFPHQASNYDPDYDYESATQDGAKDLSKSDDAVGG
NAMAVASLEFITPTPFISDKYANSVRTSFFWDMGTVWDTNWDSSQYSGYPDYSDPSNIRMSA
GIALQWMSPLGPLVFSYAQPFKKYDGDKAEQFQFNIGKTW

7. **BamA β-barrel (421-810) C690S_C700S + PhoE B15-B16 (315-351) with N-terminal TEV cleavable hexa histidine tag, plasmid pET15b (established by Leonor Morgado):**

MGSSHHHHHHSSGENLYFQHMRNTGSFNFGIGYGTESGVSFQAGVQQDNWLGTGYAVGING
TKNDYQTYAELSVTNPYFTVDGVSLGGRLFYNDFQADDADLSDYTNKSYGTDVTLGFPINEYN
SLRAGLGYVHNSLSNMQPQVAMWRYLYSMGEHPSTSDQDNSFKTDDFTFNYGWTYNKLDRG
YFPTDGSRVNLTGKVTIPGSDNEYYKVTLDTATYVPIDDDHKWVVLGRTRWGYGDGLGGKEM
PFYENFYAGGSSTVRGFQSNTIGPKAVYFPHQASNYDPDYDYESATQDGAKDLSKSDDAVGG
NAMAVASLEFITPTPFISDKYANSVRTSFFWDMGTVWDTNWDSSQYSGYPDYSDPSNIRMSA
GIALQWMSPLGPLVFSYAQPFKKYDGDKAEQFQFNIGKTWNKNMSAFVDYKINQLDSDNKLNI
NNDDIVAVGMTYQF

8. **BamA β-barrel (421-810) C690S_C700S + LamB B17-B18 (378-446) with N-terminal TEV cleavable hexa histidine tag, plasmid pET15b (established by Leonor Morgado):**

MGSSHHHHHHSSGENLYFQHMRNTGSFNFGIGYGTESGVSFQAGVQQDNWLGTGYAVGING
TKNDYQTYAELSVTNPYFTVDGVSLGGRLFYNDFQADDADLSDYTNKSYGTDVTLGFPINEYN
SLRAGLGYVHNSLSNMQPQVAMWRYLYSMGEHPSTSDQDNSFKTDDFTFNYGWTYNKLDRG
YFPTDGSRVNLTGKVTIPGSDNEYYKVTLDTATYVPIDDDHKWVVLGRTRWGYGDGLGGKEM
PFYENFYAGGSSTVRGFQSNTIGPKAVYFPHQASNYDPDYDYESATQDGAKDLSKSDDAVGG
NAMAVASLEFITPTPFISDKYANSVRTSFFWDMGTVWDTNWDSSQYSGYPDYSDPSNIRMSA
GIALQWMSPLGPLVFSYAQPFKKYDGDKAEQFQFNIGKTWAGDSIWSRPAIRVFATYAKWDEK
WGYDYTGNADNNANFGKAVPADFNGGSFGRGDSDEWTFGAQMEIWW

9. **BamA β-barrel (421-810) C690S_C700S G431C E868C + LamB B17-B18 (378-446) with N-terminal TEV cleavable hexa histidine tag, plasmid pET15b:**

MGSSHHHHHHSSGENLYFQHMRNTGSFNFGICYGTESGVSFQAGVQQDNWLGTGYAVGING
TKNDYQTYAELSVTNPYFTVDGVSLGGRLFYNDFQADDADLSDYTNKSYGTDVTLGFPINEYN
SLRAGLGYVHNSLSNMQPQVAMWRYLYSMGEHPSTSDQDNSFKTDDFTFNYGWTYNKLDRG
YFPTDGSRVNLTGKVTIPGSDNEYYKVTLDTATYVPIDDDHKWVVLGRTRWGYGDGLGGKEM
PFYENFYAGGSSTVRGFQSNTIGPKAVYFPHQASNYDPDYDYESATQDGAKDLSKSDDAVGG
NAMAVASLEFITPTPFISDKYANSVRTSFFWDMGTVWDTNWDSSQYSGYPDYSDPSNIRMSA
GIALQWMSPLGPLVFSYAQPFKKYDGDKAEQFQFNIGKTWAGDSIWSRPAIRVFATYAKWDEK
WGYDYTGNADNNANFGKAVPADFNGGSFGRGDSDCWTFGAQMEIWW

10. **BamA β-barrel (421-810) C690S_C700S + OmpX B7-B8 (141-171) with N-terminal TEV cleavable hexa histidine tag, plasmid pET15b (established by Leonor Morgado):**

MGSSHHHHHHSSGENLYFQHMRNTGSFNFGIGYGTESGVSFQAGVQQDNWLGTGYAVGING
TKNDYQTYAELSVTNPYFTVDGVSLGGRLFYNDFQADDADLSDYTNKSYGTDVTLGFPINEYN
SLRAGLGYVHNSLSNMQPQVAMWRYLYSMGEHPSTSDQDNSFKTDDFTFNYGWTYNKLDRG
YFPTDGSRVNLTGKVTIPGSDNEYYKVTLDTATYVPIDDDHKWVVLGRTRWGYGDGLGGKEM
PFYENFYAGGSSTVRGFQSNTIGPKAVYFPHQASNYDPDYDYESATQDGAKDLSKSDDAVGG
NAMAVASLEFITPTPFISDKYANSVRTSFFWDMGTVWDTNWDSSQYSGYPDYSDPSNIRMSA
GIALQWMSPLGPLVFSYAQPFKKYDGDKAEQFQFNIGKTWMENVALDFSYEQSRIRSVDVGT
WIAGVGYRF

11. **BamA β-barrel (421-810) C690S_C700S G433A + OmpX B7-B8 (141-171) with N-terminal TEV cleavable hexa histidine tag, plasmid pET15b:**

MGSSHHHHHHSSGENLYFQHMRNTGSFNFGIGYGTESGVSFQAGVQQDNWLGTGYAVGING
TKNDYQTYAELSVTNPYFTVDGVSLGGRLFYNDFQADDADLSDYTNKSYGTDVTLGFPINEYN
SLRAGLGYVHNSLSNMQPQVAMWRYLYSMGEHPSTSDQDNSFKTDDFTFNYGWTYNKLDRG
YFPTDGSRVNLTGKVTIPGSDNEYYKVTLDTATYVPIDDDHKWVVLGRTRWGYGDGLGGKEM
PFYENFYAGGSSTVRGFQSNTIGPKAVYFPHQASNYDPDYDYESATQDGAKDLSKSDDAVGG
NAMAVASLEFITPTPFISDKYANSVRTSFFWDMGTVWDTNWDSSQYSGYPDYSDPSNIRMSA
GIALQWMSPLGPLVFSYAQPFKKYDGDKAEQFQFNIGKTWMENVALDFSYEQSRIRSVDVGT
WIAGVGYRF

12. **BamA-POTRA3-5 (174-810) C690S_C700S + OmpX B7-B8 (141-171), plasmid pET15b:**

MKGSSHHHHHHSSGLVPRGSHMSAEIQQINIVGNHAFTTDELISHFQLRDEVPWWNVVGDRK
YQKQKLAGDLETLRSYYLDRGYARFNIDSTQVSLTPDKKGIYVTVNITEGDQYKLSGVEVSGNL
AGHSAEIEQLTKIEPGELYNGTKVTKMEDDIKKLLGRYGYAYPRVQSMPEINDADKTVKLRVNV
DAGNRFYVRKIRFEGNDTSKDAVLRREMRQMEGAWLGSDLVDQGKERLNRLGFFETVDTDT
QRVPGSPDQVDVVYKVKERNTGSFNFGIGYGTESGVSFQAGVQQDNWLGTGYAVGINGTKN
DYQTYAELSVTNPYFTVDGVSLGGRLFYNDFQADDADLSDYTNKSYGTDVTLGFPINEYNSLR

AGLGYVHNSLSNMQPQVAMWRYLYSMGEHPSTSDQDNSFKTDDFTFNYGWTYNKLDRGYFP
TDGSRVNLTGKVTIPGSDNEYYKVTLDTATYVPIDDDHKWVVLGRTRWGYGDGLGGKEMPFY
ENFYAGGSSTVRGFQSNTIGPKAVYFPHQASNYDPDYDYESATQDGAKDLSKSDDAVGGNAM
AVASLEFITPTPFISDKYANSVRTSFFWDMGTVWDTNWDSSQYSGYPDYSDPSNIRMSAGIAL
QWMSPLGPLVFSYAQPFKKYDGDKAEQFQFNIGKTWMENVALDFSYEQSRIRSVDVGTWIAG
VGYRF

13. BamA β-barrel (421-810) C690S_C700S + OmpX B7-B8 (139-171), plasmid pET15b:

MGSSHHHHHHSSGENLYFQHMRNTGSFNFGIGYGTESGVSFQAGVQQDNWLGTGYAVGING
TKNDYQTYAELSVTNPYFTVDGVSLGGRLFYNDFQADDADLSDYTNKSYGTDVTLGFPINEYN
SLRAGLGYVHNSLSNMQPQVAMWRYLYSMGEHPSTSDQDNSFKTDDFTFNYGWTYNKLDRG
YFPTDGSRVNLTGKVTIPGSDNEYYKVTLDTATYVPIDDDHKWVVLGRTRWGYGDGLGGKEM
PFYENFYAGGSSTVRGFQSNTIGPKAVYFPHQASNYDPDYDYESATQDGAKDLSKSDDAVGG
NAMAVASLEFITPTPFISDKYANSVRTSFFWDMGTVWDTNWDSSQYSGYPDYSDPSNIRMSA
GIALQWMSPLGPLVFSYAQPFKKYDGDKAEQFQFNIGKTWNPMENVALDFSYEQSRIRSVDV
GTWIAGVGYRF

14. BamA β-barrel (421-810) C690S_C700S + OmpX B5-B8 (95-171), plasmid pET15b:

MGSSHHHHHHSSGENLYFQHMRNTGSFNFGIGYGTESGVSFQAGVQQDNWLGTGYAVGING
TKNDYQTYAELSVTNPYFTVDGVSLGGRLFYNDFQADDADLSDYTNKSYGTDVTLGFPINEYN
SLRAGLGYVHNSLSNMQPQVAMWRYLYSMGEHPSTSDQDNSFKTDDFTFNYGWTYNKLDRG
YFPTDGSRVNLTGKVTIPGSDNEYYKVTLDTATYVPIDDDHKWVVLGRTRWGYGDGLGGKEM
PFYENFYAGGSSTVRGFQSNTIGPKAVYFPHQASNYDPDYDYESATQDGAKDLSKSDDAVGG
NAMAVASLEFITPTPFISDKYANSVRTSFFWDMGTVWDTNWDSSQYSGYPDYSDPSNIRMSA
GIALQWMSPLGPLVFSYAQPFKKYDGDKAEQFQFNIGKTWRINDWASIYGVVGVGYGKFQTTE
YPTYKHDTSDYGFSYGAGLQFNPMENVALDFSYEQSRIRSVDVGTWIAGVGYRF

15. BamA β-barrel (421-810) C690S_C700S + OmpX B3-B8 (54-171), plasmid pET15b:

MGSSHHHHHHSSGENLYFQHMRNTGSFNFGIGYGTESGVSFQAGVQQDNWLGTGYAVGING
TKNDYQTYAELSVTNPYFTVDGVSLGGRLFYNDFQADDADLSDYTNKSYGTDVTLGFPINEYN
SLRAGLGYVHNSLSNMQPQVAMWRYLYSMGEHPSTSDQDNSFKTDDFTFNYGWTYNKLDRG
YFPTDGSRVNLTGKVTIPGSDNEYYKVTLDTATYVPIDDDHKWVVLGRTRWGYGDGLGGKEM
PFYENFYAGGSSTVRGFQSNTIGPKAVYFPHQASNYDPDYDYESATQDGAKDLSKSDDAVGG
NAMAVASLEFITPTPFISDKYANSVRTSFFWDMGTVWDTNWDSSQYSGYPDYSDPSNIRMSA
GIALQWMSPLGPLVFSYAQPFKKYDGDKAEQFQFNIGKTWEEDNSPLGVIGSFTYTEKSRTAS
SGDYNKNQYYGITAGPAYRINDWASIYGVVGVGYGKFQTTEYPTYKHDTSDYGFSYGAGLQF
NPMENVALDFSYEQSRIRSVDVGTWIAGVGYRF

16. BamA β-barrel (421-810) C690S_C700S + OmpX B1-B8 (24-171), plasmid pET15b:

MGSSHHHHHHSSGENLYFQHMRNTGSFNFGIGYGTESGVSFQAGVQQDNWLGTGYAVGING
TKNDYQTYAELSVTNPYFTVDGVSLGGRLFYNDFQADDADLSDYTNKSYGTDVTLGFPINEYN
SLRAGLGYVHNSLSNMQPQVAMWRYLYSMGEHPSTSDQDNSFKTDDFTFNYGWTYNKLDRG
YFPTDGSRVNLTGKVTIPGSDNEYYKVTLDTATYVPIDDDHKWVVLGRTRWGYGDGLGGKEM
PFYENFYAGGSSTVRGFQSNTIGPKAVYFPHQASNYDPDYDYESATQDGAKDLSKSDDAVGG
NAMAVASLEFITPTPFISDKYANSVRTSFFWDMGTVWDTNWDSSQYSGYPDYSDPSNIRMSA
GIALQWMSPLGPLVFSYAQPFKKYDGDKAEQFQFNIGKTWATSTVTGGYAQSDAQGQMNKM
GGFNLKYRYEEDNSPLGVIGSFTYTEKSRTASSGDYNKNQYYGITAGPAYRINDWASIYGVVG
VGYGKFQTTEYPTYKHDTSDYGFSYGAGLQFNPMENVALDFSYEQSRIRSVDVGTWIAGVGY
RF

17. BamA β-barrel (421-810) C690S_C700S + OmpX B7-B8 (141-144) with N-terminal TEV cleavable hexa histidine tag, plasmid pET15b:

MGSSHHHHHHSSGENLYFQHMRNTGSFNFGIGYGTESGVSFQAGVQQDNWLGTGYAVGING
TKNDYQTYAELSVTNPYFTVDGVSLGGRLFYNDFQADDADLSDYTNKSYGTDVTLGFPINEYN
SLRAGLGYVHNSLSNMQPQVAMWRYLYSMGEHPSTSDQDNSFKTDDFTFNYGWTYNKLDRG
YFPTDGSRVNLTGKVTIPGSDNEYYKVTLDTATYVPIDDDHKWVVLGRTRWGYGDGLGGKEM
PFYENFYAGGSSTVRGFQSNTIGPKAVYFPHQASNYDPDYDYESATQDGAKDLSKSDDAVGG
NAMAVASLEFITPTPFISDKYANSVRTSFFWDMGTVWDTNWDSSQYSGYPDYSDPSNIRMSA
GIALQWMSPLGPLVFSYAQPFKKYDGDKAEQFQFNIGKTWMENV

18. BamA β-barrel (421-810) C690S_C700S + OmpX B7-B8 (141-149) with N-terminal TEV cleavable hexa histidine tag, plasmid pET15b:

MGSSHHHHHHSSGENLYFQHMRNTGSFNFGIGYGTESGVSFQAGVQQDNWLGTGYAVGING
TKNDYQTYAELSVTNPYFTVDGVSLGGRLFYNDFQADDADLSDYTNKSYGTDVTLGFPINEYN
SLRAGLGYVHNSLSNMQPQVAMWRYLYSMGEHPSTSDQDNSFKTDDFTFNYGWTYNKLDRG
YFPTDGSRVNLTGKVTIPGSDNEYYKVTLDTATYVPIDDDHKWVVLGRTRWGYGDGLGGKEM
PFYENFYAGGSSTVRGFQSNTIGPKAVYFPHQASNYDPDYDYESATQDGAKDLSKSDDAVGG
NAMAVASLEFITPTPFISDKYANSVRTSFFWDMGTVWDTNWDSSQYSGYPDYSDPSNIRMSA
GIALQWMSPLGPLVFSYAQPFKKYDGDKAEQFQFNIGKTWMENVALDFS

19. BamA β-barrel (421-810) C690S_C700S + OmpX B7-B8 (141-154) with N-terminal TEV cleavable hexa histidine tag, plasmid pET15b:

MGSSHHHHHHSSGENLYFQHMRNTGSFNFGIGYGTESGVSFQAGVQQDNWLGTGYAVGING
TKNDYQTYAELSVTNPYFTVDGVSLGGRLFYNDFQADDADLSDYTNKSYGTDVTLGFPINEYN
SLRAGLGYVHNSLSNMQPQVAMWRYLYSMGEHPSTSDQDNSFKTDDFTFNYGWTYNKLDRG
YFPTDGSRVNLTGKVTIPGSDNEYYKVTLDTATYVPIDDDHKWVVLGRTRWGYGDGLGGKEM
PFYENFYAGGSSTVRGFQSNTIGPKAVYFPHQASNYDPDYDYESATQDGAKDLSKSDDAVGG
NAMAVASLEFITPTPFISDKYANSVRTSFFWDMGTVWDTNWDSSQYSGYPDYSDPSNIRMSA
GIALQWMSPLGPLVFSYAQPFKKYDGDKAEQFQFNIGKTWMENVALDFSYEQSRIR

20. BamA β-barrel (421-810) C690S_C700S + OmpX B7-B8 (141-161) with N-terminal TEV cleavable hexa histidine tag, plasmid pET15b:

MGSSHHHHHHSSGENLYFQHMRNTGSFNFGIGYGTESGVSFQAGVQQDNWLGTGYAVGING
TKNDYQTYAELSVTNPYFTVDGVSLGGRLFYNDFQADDADLSDYTNKSYGTDVTLGFPINEYN
SLRAGLGYVHNSLSNMQPQVAMWRYLYSMGEHPSTSDQDNSFKTDDFTFNYGWTYNKLDRG
YFPTDGSRVNLTGKVTIPGSDNEYYKVTLDTATYVPIDDDHKWVVLGRTRWGYGDGLGGKEM
PFYENFYAGGSSTVRGFQSNTIGPKAVYFPHQASNYDPDYDYESATQDGAKDLSKSDDAVGG
NAMAVASLEFITPTPFISDKYANSVRTSFFWDMGTVWDTNWDSSQYSGYPDYSDPSNIRMSA
GIALQWMSPLGPLVFSYAQPFKKYDGDKAEQFQFNIGKTWMENVALDFSYEQSRIRSVDVG

Abbreviations and symbols

Å	Angstrom
α, β	Low and high-energy state of a half spin
B	Magnetic field
BAM	β-barrel assembly machinery
C8E4	Octyl Tetraethylene Glycol Ether
COSY	Correlation-spectroscopy
CPD	Composite pulse decoupling
Cryo-EM	Cryo-electron microscopy
CSA	Chemical shift anisotropy
CSP	Chemical shift perturbation
CW	Continuous wave
d_1	Interscan delay
Da	Dalton
DCIA	7-Diethylamino-3-[4'-(iodoacetamido)phenyl]-4-methylcoumarin
DD	Dipole-dipole
DLS	Dynamic light scattering
E. Coli	*Escherichia coli*
FT	Fourier transformation
Gdm-HCl	Guanidinium hydrochloride
NMR	Nuclear magnetic resonance
ħ	Planck constant divided by 2π
HSQC	Heteronuclear single quantum coherence
HMQC	Heteronuclear multiple quantum coherence
$^{n}J_{IS}$	Scalar coupling constant between spins I and S, separated by n covalent bonds
I, S	Nuclear spins
INEPT	Insensitive nuclei enhancement by polarization transfer
IM	Inner membrane
IPTG	Isopropyl β-D-1-thiogalactopyranoside

J(ω)	Spectral density function at the frequency ω
k	Chemical rate constant
K_D	Equilibrium dissociation constant
LamB	Maltoporine membrane protein
LB	Lysogeny broth medium
LDAO	N,N-Dimethyldodecylamine N-oxide
m	spin quantum number
M	Molar concentration (mole / L)
M9	M9 minimal media
MES	2-(N-morpholino)ethanesulfonic acid buffer
MST	Microscale thermophoresis
MWCO	Molecular weight cut-off
NaCl	Sodium chloride
nanoDSF	Nano differential scanning fluorimetry
NaPi	Sodium phosphate buffer
N-ter , C-ter	N-terminus, C-terminus
NOE	Nuclear overhauser effect
NOESY	Nuclear overhauser effect spectroscopy
OD	Optical density
O/N	Overnight
OM	Outer membrane
Omp	Outer membrane protein
OmpF	Outer membrane protein F
OmpG	Outer membrane protein G
OmpX	Outer membrane protein X
pH	Potential of hydrogen
PEG	Polyethylene glycol
POTRA	Polypeptide transport associated (domains)
δ	Chemical shift
γ	Gyromagnetic ratio

σ	Average shielding constant of the nucleus
σ_{IS}	Cross-relaxation rate constant between spins I and S
PDB	Protein databank
ppm	Part per million
v	Frequency (Hz)
Ω	Offset frequency
R_1	Longitudinal relaxation rate constant
$R_{I,} R_S$	Self-relaxation rate constants of spins I and S
RT	Room temperature
R_{IS}	Distance between two spins
S/N	Signal-to-noise ratio
SEC	Bacterial protein-secreting translocation complex
Skp	Seventeen-kilodalton protein chaperone
SurA	Survival factor A chaperone
T_1	Longitudinal relaxation time constant
T_2	Transversal relaxation time constant
TET	Tetrahedral aminopeptidase
T_m	Transition mid-point temperature
TROSY	Transverse relaxation-optimized spectroscopy
τ_c	Rotational correlation time
τ_m	NOE mixing time
μ	magnetic moment
ω_0	Larmor frequency
n_α, n_β	population of α and β state
W	rate constant of transition between energy levels

References

1. Albrecht, R., and Zeth, K. (2010). Crystallization and preliminary X-ray data collection of the *Escherichia coli* lipoproteins BamC, BamD and BamE. *Acta Crystallogr. F 66*, 1586–1590.

2. Albrecht, R., Schütz, M., Oberhettinger, P., Faulstich, M., Bermejo, I., Rudel, T., Diederichs, K., and Zeth, K. (2014). Structure of BamA, an essential factor in outer membrane protein biogenesis. *Acta Crystallogr. D 70*, 1779–1789.

3. Atreya, H.S., and Chary, K.V.R. (2001). Selective `unlabeling' of amino acids in fractionally ^{13}C labeled proteins: An approach for stereospecific NMR assignments of CH3 groups in Val and Leu residues. *J. Biomol. NMR 19*, 267–272.

4. Aue, W.P., Bartholdi, E., and Ernst, R.R. (1976). Two-dimensional spectroscopy. Application to nuclear magnetic resonance. *J. Chem. Phys. 64*, 2229–2246.

5. Bakelar, J., Buchanan, S.K., and Noinaj, N. (2016). The structure of the β-barrel assembly machinery complex. *Science 351*, 180–186.

6. Barnwal, R.P., Rout, A.K., Atreya, H.S., and Chary, K.V.R. Identification of C-terminal neighbours of amino acid residues without an aliphatic 13Cγ as an aid to NMR assignments in proteins. *J. Biomol. NMR 41*, 191–197.

7. Bax, A.D., Clore, G.M., Driscoll, P.C., Gronenborn, A.M., Ikura, M., and Kay, L.E. (1990). Practical aspects of proton-carbon-carbon-proton three-dimensional correlation spectroscopy of ^{13}C-labeled proteins. *J. Magn. Reson. 87*, 620–627.

8. Bayburt, T.H., Grinkova, Y.V., and Sligar, S.G. (2002). Self-Assembly of Discoidal Phospholipid Bilayer Nanoparticles with Membrane Scaffold Proteins. Nano Letters *2*, 853–856.

9. Berman, H.M., Westbrook, J., Feng, Z., Gilliland, G., Bhat, T.N., Weissig, H., Shindyalov, I.N., and Bourne, P.E. (2000). The Protein Data Bank. *Nucleic Acids Res*. *28*, 235–242.

10. Bloembergen, N., Purcell, E.M., and Pound, R.V. (1948). Relaxation Effects in Nuclear Magnetic Resonance Absorption. *Phys. Rev. 73*, 679–712.

11. Bloch, F. (1946). Nuclear induction. *Phys. Rev. 70*, 460.

12. Bodenhausen, G., and Ruben, D.J. (1980). Natural abundance nitrogen-15 NMR by enhanced heteronuclear spectroscopy. *Chem. Phys. Lett*. 69 (1), 185-189.

13. Bos, M.P., Robert, V., and Tommassen, J. (2007). Functioning of outer membrane protein assembly factor Omp85 requires a single POTRA domain. *EMBO Rep. 8*, 1149–1154.

14. Clubb, R.T., Thanabal, V., and Wagner, G. (1992). A constant-time three-dimensional triple-resonance pulse scheme to correlate intraresidue ^{1}HN, ^{15}N, and ^{13}C′ chemical shifts in ^{15}N-^{13}C-labelled proteins. *J. Magn. Reson. 97*, 213–217.

15. Danoff, E.J., and Fleming, K.G. (2015). Membrane defects accelerate outer membrane β-barrel protein folding. *Biochemistry 54*, 97–99.

16. Doerner, P.A., and Sousa, M.C. (2017). Extreme Dynamics in the BamA β-Barrel Seam. *Biochemistry 56*, 3142–3149.

17. Dong, C., Yang, X., Hou, H.-F., Shen, Y.-Q., and Dong, Y.-H. (2012). Structure of *Escherichia coli* BamB and its interaction with POTRA domains of BamA. *Acta Crystallogr. D 68*, 1134–1139.

18. Dubey, A., Kadumuri, R.V., Jaipuria, G., Vadrevu, R., and Atreya, H.S. (2016). Rapid NMR Assignments of Proteins by Using Optimized Combinatorial Selective Unlabeling. *ChemBioChem 17*, 334–340.

19. Duhr, S., and Braun, D. (2006). Why molecules move along a temperature gradient. *Proc. Natl. Acad. Sci. U.S.A. 103*, 19678–19682.

20. Ellman, J.A., Volkman, B.F., Mendel, D., Schulz, P.G., and Wemmer, D.E. (1992). Site-specific isotopic labeling of proteins for NMR studies. *J. Am. Chem. Soc. 114*, 7959–7961.

21. Ernst, R.R., and Anderson, W.A. (1966). Application of Fourier Transform Spectroscopy to Magnetic Resonance. *Rev. Sci. Instrum. 37*, 93–102.

22. Estrada Mallarino, L., Fan, E., Odermatt, M., Müller, M., Lin, M., Liang, J., Heinzelmann, M., Fritsche, F., Apell, H.-J., and Welte, W. (2015). TtOmp85, a β-Barrel Assembly Protein, Functions by Barrel Augmentation. *Biochemistry 54*, 844–852.

23. Fesik, S.W., and Zuiderweg, E.R.P. (1988). Heteronuclear three-dimensional nmr spectroscopy. A strategy for the simplification of homonuclear two-dimensional NMR spectra. *J. Magn. Reson. 78*, 588–593.

24. Fleming, K.G. (2015). A combined kinetic push and thermodynamic pull as driving forces for outer membrane protein sorting and folding in bacteria. *Phil. Trans. R. Soc. B* 370, 20150026.

25. Gardner, K.H., and Kay, L.E. (1998). The use of 2H, 13C, 15N multidimensional NMR to study the structure and dynamics of proteins. *Annu. Rev. Biophys. Biomol. Struct. 27*, 357–406.

26. Gentle, I., Gabriel, K., Beech, P., Waller, R., and Lithgow, T. (2004). The Omp85 family of proteins is essential for outer membrane biogenesis in mitochondria and bacteria. *J. Cell Biol. 164*, 19–24.

27. Goldflam, M., Tarragó, T., Gairí, M., and Giralt, E. (2012). NMR Studies of Protein–Ligand Interactions. *Protein NMR Techniques*, (Humana Press), pp. 233–259.

28. Gruss, F., Zähringer, F., Jakob, R.P., Burmann, B.M., Hiller, S., and Maier, T. (2013). The structural basis of autotransporter translocation by *TamA. Nat. Struct. Mol. Biol. 20*, 1318–1320.

29. Grzesiek, S., and Bax, A.D. (1992). Improved 3D triple-resonance NMR techniques applied to a 31 kDa protein. *J. Magn. Reson*. *96*, 432–440.

30. Gu, Y., Li, H., Dong, H., Zeng, Y., Zhang, Z., Paterson, N.G., Stansfeld, P.J., Wang, Z., Zhang, Y., Wang, W., et al. (2016). Structural basis of outer membrane protein insertion by the BAM complex. *Nature 531*, 64–69.

31. Gutowsky, H.S., McCall, D.W., and Slichter, C.P. (1951). Coupling among Nuclear Magnetic Dipoles in Molecules. *Phys. Rev. 84*, 589–590.

32. Hagan, C.L., Kim, S., and Kahne, D. (2010). Reconstitution of Outer Membrane Protein Assembly from Purified Components. *Science 328*, 890–892.

33. Hagan, C.L., Westwood, D.B., and Kahne, D. (2013). Bam Lipoproteins Assemble BamA *in Vitro*. *Biochemistry 52*, 6108–6113.

34. Hagan, C.L., Wzorek, J.S., and Kahne, D. (2015). Inhibition of the β-barrel assembly machine by a peptide that binds BamD. *Proc. Natl. Acad. Sci. U.S.A. 112*, 2011–2016.

35. Han, L., Zheng, J., Wang, Y., Yang, X., Liu, Y., Sun, C., Cao, B., Zhou, H., Ni, D., Lou, J., et al. (2016). Structure of the BAM complex and its implications for biogenesis of outer-membrane proteins. *Nat. Struct. Mol. Biol. 23*, 192–196.

36. Henke, K., Welte, W., and Hauser, K. (2016). Direct Monitoring of β-Sheet Formation in the Outer Membrane Protein TtoA Assisted by TtOmp85. *Biochemistry* 55, 4333–4343.

37. Higman, V.A. http://www.protein-nmr.org.uk

38. Höhr, A.I.C., Lindau, C., Wirth, C., Qiu, J., Stroud, D.A., Kutik, S., Guiard, B., Hunte, C., Becker, T., Pfanner, N., et al. (2018). Membrane protein insertion through a mitochondrial β-barrel gate. *Science 359*, eaah6834.

39. Iadanza, M.G., Higgins, A.J., Schiffrin, B., Calabrese, A.N., Brockwell, D.J., Ashcroft, A.E., Radford, S.E., and Ranson, N.A. (2016). Lateral opening in the intact β-barrel assembly machinery captured by cryo-EM. *Nat. Commun. 7*, 12865.

40. Ikura, M., Kay, L.E., and Bax, A. (1990). A novel approach for sequential assignment of proton, carbon-13, and nitrogen-15 spectra of larger proteins: heteronuclear triple-resonance three-dimensional NMR spectroscopy. Application to calmodulin. *Biochemistry 29*, 4659–4667.

41. Cavanagh, J., W.J. Fairbrother, A. G. Palmer III, M. Rance, N. J.Skelton, Protein NMR Spectroscopy, 2nd edition, Elsevier Academic Press, 2007.

42. Keeler, J., Understanding NMR Spectroscopy, 2002.

43. Jerabek-Willemsen, M., André, T., Wanner, R., Roth, H.M., Duhr, S., Baaske, P., and Breitsprecher, D. (2014). MicroScale Thermophoresis: Interaction analysis and beyond. *J. Mol. Struct. 1077*, 101–113.

44. Kaiser, R. (1963). Use of the Nuclear Overhauser Effect in the Analysis of High-Resolution Nuclear Magnetic Resonance Spectra. *J. Chem. Phys. 39*, 2435–2442.

45. Kay, L.E., Ikura, M., Tschudin, R., and Bax, A. (1990). Three-dimensional triple-resonance NMR spectroscopy of isotopically enriched proteins. *J. Magn. Reson.* 1969 *89*, 496–514.

46. Keller, R. Optimizing the Process of Nuclear Magnetic Resonance Spectrum Analysis and Computer Aided Resonance Assignment. Swiss Federal Institute of Technology. (2004/2005):

47. Kellogg, J.M.B., Rabi, I.I., Ramsey Jr, N.F., and Zacharias, J.R. (1939). The Magnetic Moments of the Proton and the Deuteron. The Radiofrequency Spectrum of H_2 in Various Magnetic Fields. *Phys. Rev. 56*, 728.

48. Kerfah, R., Plevin, M.J., Sounier, R., Gans, P., and Boisbouvier, J. (2015). Methyl-specific isotopic labeling: a molecular tool box for solution NMR studies of large proteins. *Curr. Opin. Struct. Biol. 32*, 113–122.

49. Kim, K.H., Aulakh, S., and Paetzel, M. (2011). Crystal Structure of β-Barrel Assembly Machinery BamCD Protein Complex. *J. Biol. Chem. 286*, 39116–39121.

50. Kim, K.H., and Paetzel, M. (2011). Crystal Structure of Escherichia coli BamB, a Lipoprotein Component of the β-Barrel Assembly Machinery Complex. *J. Mol. Biol. 406*, 667–678.

51. Kim, K.H., Aulakh, S., Tan, W., and Paetzel, M. (2011a). Crystallographic analysis of the C-terminal domain of the *Escherichia coli* lipoprotein BamC. *Acta Crystallogr. F 67*, 1350–1358.

52. Kim, K.H., Kang, H.-S., Okon, M., Escobar-Cabrera, E., McIntosh, L.P., and Paetzel, M. (2011). Structural Characterization of *Escherichia coli* BamE, a Lipoprotein Component of the β-Barrel Assembly Machinery Complex. *Biochemistry 50*, 1081–1090.

53. Kleckner, I.R., and Foster, M.P. (2011). An introduction to NMR-based approaches for measuring protein dynamics. *Biochim. Biophys. Acta 1814*, 942–968.

54. Knowles, T.J., Scott-Tucker, A., Overduin, M., and Henderson, I.R. (2009a). Membrane protein architects: the role of the BAM complex in outer membrane protein assembly. *Nat. Rev. Microbiol. 7*, 206–214.

55. Knowles, T.J., McClelland, D.M., Rajesh, S., Henderson, I.R., and Overduin, M. (2009b). Secondary structure and ^{1}H, ^{13}C and ^{15}N backbone resonance assignments of BamC, a component of the outer membrane protein assembly machinery in *Escherichia coli*. *Biomol. NMR Assign*. *3*, 203–206.

56. Knowles, T.J., Sridhar, P., Rajesh, S., Manoli, E., Overduin, M., and Henderson, I.R. (2010). Secondary structure and ^{1}H, ^{13}C and ^{15}N resonance assignments of BamE, a component of the outer membrane protein assembly machinery in Escherichia coli. *Biomol. NMR Assign*. *4*, 179–181.

57. Knowles, T.J., Browning, D.F., Jeeves, M., Maderbocus, R., Rajesh, S., Sridhar, P., Manoli, E., Emery, D., Sommer, U., Spencer, A., et al. (2011). Structure and function of BamE within the outer membrane and the β-barrel assembly machine. *EMBO Rep*. *12*, 123–128.

58. Koebnik, R., Locher, K.P., and Van Gelder, P. (2000). Structure and function of bacterial outer membrane proteins: barrels in a nutshell. *Mol. Microbiol. 37*, 239–253.

59. Korndörfer, I.P., Dommel, M.K., and Skerra, A. (2004). Structure of the periplasmic chaperone Skp suggests functional similarity with cytosolic chaperones despite differing architecture. Nat. Struct. Mol. Biol. *11*, 1015–1020.

60. Krishnarjuna, B., Jaipuria, G., Thakur, A., D'Silva, P., and Atreya, H.S. (2011). Amino acid selective unlabeling for sequence specific resonance assignments in proteins. *J. Biomol. NMR 49*, 39–51.

61. Lin, M.T., Sperling, L.J., Frericks Schmidt, H.L., Tang, M., Samoilova, R.I., Kumasaka, T., Iwasaki, T., Dikanov, S.A., Rienstra, C.M., and Gennis, R.B. (2011). A rapid and robust method for selective isotope labeling of proteins. *Methods 55*, 370–378.

62. Lin, M.T., Fukazawa, R., Miyajima-Nakano, Y., Matsushita, S., Choi, S.K., Iwasaki, T., and Gennis, R.B. (2015). *Escherichia coli* Auxotroph Host Strains for Amino Acid-Selective

Isotope Labeling of Recombinant Proteins. Methods in Enzymology 565, (Elsevier), pp. 45–66.

63. Malinverni, J.C., Werner, J., Kim, S., Sklar, J.G., Kahne, D., Misra, R., and Silhavy, T.J. (2006). YfiO stabilizes the YaeT complex and is essential for outer membrane protein assembly in *Escherichia coli*: YfiO assembles OMPs and stabilizes the YaeT complex. *Mol. Microbiol. 61*, 151–164.

64. Marion, D., Driscoll, P.C., Kay, L.E., Wingfield, P.T., Bax, A., Gronenborn, A.M., and Clore, G.M. (1989). Overcoming the overlap problem in the assignment of proton NMR spectra of larger proteins by use of three-dimensional heteronuclear proton-nitrogen-15 Hartmann-Hahn-multiple quantum coherence and nuclear Overhauser-multiple quantum coherence spectroscopy: application to interleukin 1.beta. *Biochemistry 28*, 6150–6156.

65. Mas, G., Crublet, E., Hamelin, O., Gans, P., and Boisbouvier, J. (2013). Specific labeling and assignment strategies of valine methyl groups for NMR studies of high molecular weight proteins. *J. Biomol. NMR 57*, 251–262.

66. McIntosh, L.P., and Dahlquist, F.W. (1990). Biosynthetic incorporation of 15N and 13C for assignment and interpretation of nuclear magnetic resonance spectra of proteins. *Q. Rev. Biophys*. *23*, 1–38.

67. Mielke, S.P., and Krishnan, V.V. (2009). Characterization of protein secondary structure from NMR chemical shifts. *Prog. Nucl. Magn. Reson. Spectrosc. 54*, 141–165.

68. Morgado, L., Zeth, K., Burmann, B.M., Maier, T., and Hiller, S. (2015). Characterization of the insertase BamA in three different membrane mimetics by solution NMR spectroscopy. *J. Biomol. NMR 61*, 333–345.

69. Mori, N., Ishii, Y., Tateda, K., Kimura, S., Kouyama, Y., Inoko, H., Mitsunaga, S., Yamaguchi, K., and Yoshihara, E. (2012). A peptide based on homologous sequences of the β-barrel assembly machinery component BamD potentiates antibiotic susceptibility of Pseudomonas aeruginosa. J. Antimicrob. Chemother. *67*, 2173–2181.

70. Morris, G.A., and Freeman, R. (1979). Enhancement of nuclear magnetic resonance signals by polarization transfer. J. Am. Chem. Soc. *101*, 760–762.

71. Muchmore, D.C., McIntosh, L.P., Russell, C.B., Anderson, D.E., and Dahlquist, F.W. (1989). Expression and nitrogen-15 labeling of proteins for proton and nitrogen-15 nuclear magnetic resonance. In Methods in Enzymology, (Elsevier), pp. 44–73.

72. Neer, E.J., Schmidt, C.J., Nambudripad, R., and Smith, T.F. (1994). The ancient regulatory-protein family of WD-repeat proteins. Nature *371*, 297.

73. Ni, D., Yang, K., and Huang, Y. (2014). Refolding, crystallization and preliminary X-ray crystallographic studies of the β-barrel domain of BamA, a membrane protein essential for outer membrane protein biogenesis. Acta Crystallogr. Sect. F Struct. Biol. Commun. *70*, 362–365.

74. Nikaido, H. (2003). Molecular basis of bacterial outer membrane permeability revisited. Microbiol. Mol. Biol. Rev. MMBR *67*, 593–656.

75. Nikaido, H., and Vaara, M. (1985). Molecular basis of bacterial outer membrane permeability. Microbiol. Rev. *49*, 1–32.

76. Noinaj, N., Fairman, J.W., and Buchanan, S.K. (2011a). The Crystal Structure of BamB Suggests Interactions with BamA and Its Role within the BAM Complex. J. Mol. Biol. *407*, 248–260.

77. Noinaj, N., Kuszak, A.J., Gumbart, J.C., Lukacik, P., Chang, H., Easley, N.C., Lithgow, T., and Buchanan, S.K. (2013). Structural insight into the biogenesis of β-barrel membrane proteins. Nature *501*, 385–390.

78. Noinaj, N., Kuszak, A.J., Balusek, C., Gumbart, J.C., and Buchanan, S.K. (2014). Lateral Opening and Exit Pore Formation Are Required for BamA Function. Structure *22*, 1055–1062.

79. Okuda, S., Yamada, T., Hamajima, M., Itoh, M., Katayama, T., Bork, P., Goto, S., and Kanehisa, M. (2008). KEGG Atlas mapping for global analysis of metabolic pathways. Nucleic Acids Res. *36*, W423–W426.

80. Overhauser, A.W. (1953). Polarization of Nuclei in Metals. Phys. Rev. *92*, 411–415.

81. Patel, G.J., and Kleinschmidt, J.H. (2013). The Lipid Bilayer-Inserted Membrane Protein BamA of *Escherichia coli* Facilitates Insertion and Folding of Outer Membrane Protein A from Its Complex with Skp. Biochemistry *52*, 3974–3986.

82. Pervushin, K., Riek, R., Wider, G., and Wüthrich, K. (1997). Attenuated T2 relaxation by mutual cancellation of dipole–dipole coupling and chemical shift anisotropy indicates an avenue to NMR structures of very large biological macromolecules in solution. Proc. Natl. Acad. Sci. *94*, 12366–12371.

83. Plummer, A.M., and Fleming, K.G. (2015). BamA alone accelerates outer membrane protein folding in vitro through a catalytic mechanism. Biochemistry *54*, 6009–6011.

84. Purcell, E.M., Torrey, H.C., and Pound, R.V. (1946). Resonance absorption by nuclear magnetic moments in a solid. Phys. Rev. *69*, 37.

85. Rabi, I.I., Millman, S., Kusch, P., and Zacharias, J.R. (1939). The Molecular Beam Resonance Method for Measuring Nuclear Magnetic Moments. The Magnetic Moments of Li 6 3 , Li 7 3 and F 19 9. Physical Review *55*, 526–535.

86. Reich, H. J. (2015). Structure Determination Using NMR. http://www.chem.wisc.edu/areas/reich/nmr/index.htm

87. Remaut, H., and Waksman, G. (2006). Protein–protein interaction through β-strand addition. Trends in Biochemical Sciences *31*, 436–444.

88. Ramsey, N.F., and Purcell, E.M. (1952). Interactions between Nuclear Spins in Molecules. Phys. Rev. *85*, 143–144.

89. Ricci, D.P., Hagan, C.L., Kahne, D., and Silhavy, T.J. (2012). Activation of the *Escherichia coli* β-barrel assembly machine (Bam) is required for essential components to interact properly with substrate. Proc. Natl. Acad. Sci. U. S. A. *109*, 3487–3491.

90. Rigel, N.W., Ricci, D.P., and Silhavy, T.J. (2013). Conformation-specific labeling of BamA and suppressor analysis suggest a cyclic mechanism for β-barrel assembly in *Escherichia coli*. Proc. Natl. Acad. Sci. *110*, 5151–5156.

91. Robert, V., Volokhina, E.B., Senf, F., Bos, M.P., Gelder, P.V., and Tommassen, J. (2006). Assembly Factor Omp85 Recognizes Its Outer Membrane Protein Substrates by a Species-Specific C-Terminal Motif. PLOS Biol. *4*, e377.

92. Rossiter, A.E., Leyton, D.L., Tveen-Jensen, K., Browning, D.F., Sevastsyanovich, Y., Knowles, T.J., Nichols, K.B., Cunningham, A.F., Overduin, M., Schembri, M.A., et al. (2011). The Essential β-Barrel Assembly Machinery Complex Components BamD and BamA Are Required for Autotransporter Biogenesis. J. Bacteriol. *193*, 4250–4253.

93. Saitô, H., Ando, I., and Ramamoorthy, A. (2010). Chemical shift tensor – The heart of NMR: Insights into biological aspects of proteins. Prog. Nucl. Magn. Reson. Spectrosc. *57*, 181–228.Salzmann, M., Wider, G., Pervushin, K., Senn, H., and Wüthrich, K. (1999). TROSY-type Triple-Resonance Experiments for Sequential NMR Assignments of Large Proteins. J. Am. Chem. Soc. *121*, 844–848.

94. Sánchez-Pulido, L., Devos, D., Genevrois, S., Vicente, M., and Valencia, A. (2003). POTRA: a conserved domain in the FtsQ family and a class of beta-barrel outer membrane proteins. Trends Biochem. Sci. *28*, 523–526.

95. Schiffrin, B., Calabrese, A.N., Higgins, A.J., Humes, J.R., Ashcroft, A.E., Kalli, A.C., Brockwell, D.J., and Radford, S.E. (2017). Effects of Periplasmic Chaperones and Membrane Thickness on BamA-Catalyzed Outer-Membrane Protein Folding. J. Mol. Biol. *429*, 3776–3792.

96. Schubert, M., Smalla, M., Schmieder, P., and Oschkinat, H. (1999). MUSIC in Triple-Resonance Experiments: Amino Acid Type-Selective ^{1}H–^{15}N Correlations. J. Magn. Reson. *141*, 34–43.

97. Sjöström, M., Wold, S., Wieslander, A., and Rilfors, L. (1987). Signal peptide amino acid sequences in Escherichia coli contain information related to final protein localization. A multivariate data analysis. EMBO J. *6*, 823–831.

98. Sklar, J.G., Wu, T., Gronenberg, L.S., Malinverni, J.C., Kahne, D., and Silhavy, T.J. (2007). Lipoprotein SmpA is a component of the YaeT complex that assembles outer membrane proteins in Escherichia coli. Proc. Natl. Acad. Sci. *104*, 6400–6405.

99. Solomon, I. (1955). Relaxation Processes in a System of Two Spins. Phys. Rev. *99*, 559–565.

100. Song, J. (2009). Insight into “insoluble proteins” with pure water. FEBS Lett. *583*, 953–959.Stetefeld, J., McKenna, S.A., and Patel, T.R. (2016). Dynamic light scattering: a practical guide and applications in biomedical sciences. Biophys. Rev. *8*, 409–427.

101. Takeuchi, K., Ng, E., Malia, T.J., and Wagner, G. (2007). 1-13C amino acid selective labeling in a $^{2}H^{15}N$ background for NMR studies of large proteins. J. Biomol. NMR *38*, 89–98.

102. Talluri, S., and Wagner, G. (1996). An optimized 3D NOESY-HSQC. J. Magn. Reson. B *112*, 200–205.

103. Thoma, J., Burmann, B.M., Hiller, S., and Müller, D.J. (2015). Impact of holdase chaperones Skp and SurA on the folding of β-barrel outer-membrane proteins. Nat. Struct. Mol. Biol. *22*, 795–802.

104. Thompson, P.M., Beck, M.R., and Campbell, S.L. (2015). Protein-Protein Interaction Analysis by Nuclear Magnetic Resonance Spectroscopy. In Protein-Protein Interactions,

105. Tugarinov, V., Hwang, P.M., Ollerenshaw, J.E., and Kay, L.E. (2003). Cross-Correlated Relaxation Enhanced $^{1}H-^{13}C$ NMR Spectroscopy of Methyl Groups in Very High Molecular Weight Proteins and Protein Complexes. J. Am. Chem. Soc. *125*, 10420–10428.

106. Vinogradova, O., and Qin, J. (2012). NMR as a Unique Tool in Assessment and Complex Determination of Weak Protein–Protein Interactions. Top. Curr. Chem. *326*, 35–45.

107. Voulhoux, R., Bos, M.P., Geurtsen, J., Mols, M., and Tommassen, J. (2003). Role of a highly conserved bacterial protein in outer membrane protein assembly. Science *299*, 262–265.

108. Warner, L.R., Varga, K., Lange, O.F., Baker, S.L., Baker, D., Sousa, M.C., and Pardi, A. (2011). Structure of the BamC Two-Domain Protein Obtained by Rosetta with a Limited NMR Data Set. J. Mol. Biol. *411*, 83–95.

109. Waugh, D.S. (1996). Genetic tools for selective labeling of proteins with α-^{15}N-amino acids. J. Biomol. NMR *8*, 184–192.

110. Wiesner, S., and Sprangers, R. (2015). Methyl groups as NMR probes for biomolecular interactions. Curr. Opin. Struct. Biol. *35*, 60–67.

111. Wu, T., Malinverni, J., Ruiz, N., Kim, S., Silhavy, T.J., and Kahne, D. (2005). Identification of a Multicomponent Complex Required for Outer Membrane Biogenesis in *Escherichia coli*. Cell *121*, 235–245.

112. Yu, Z., Reid, J.C., and Yang, Y.-P. (2013). Utilizing Dynamic Light Scattering as a Process Analytical Technology for Protein Folding and Aggregation Monitoring in Vaccine Manufacturing. J. Pharm. Sci. *102*, 4284–4290.

113. Zhong, M., Ferrell, B., Lu, W., Chai, Q., and Wei, Y. (2013). Insights into the Function and Structural Flexibility of the Periplasmic Molecular Chaperone SurA. J. Bacteriol. *195*, 1061–1067.

Acknowledgment

I am grateful to Prof. Dr. Sebastian Hiller for giving me the opportunity to work on this project and for his supervision of this PhD thesis. I would also like to thank Prof. Dr. Timm Maier for accepting to be the co-referee of this thesis and Prof. Dr. Torsten Schwede for his chairmanship. Thanks to Dario Dörig for helping with the specific labeling for assigning BamA, to Dr. Michael Zahn, Dr. Irena Burman, Dr. Leonor Morgado, Dr. Lichun He, Dr. Johannes Thoma, Dr. Thomas Raschle, Dr. Tim Sharpe, Dr. Hundeep Kaur, Dr Parthasarathi Rath, to the past and present members of the Hiller Group with who I had fruitful scientific discussions, to the staff of the Biozentrum, who provides a great plateform to perform high quality work, to the students and postdoctoral fellows of the third floor and also, thanks to Aude and T&L for cheerful support.